Development of an advanced drug delivery system to prevent and treat breast cancer bone metastasis

Shiva Shakori Poshteh

A thesis submitted in fulfilment of the requirements for the degree of Master of Philosophy

Sydney Pharmacy School
Faculty of Medicine and Health
The University of Sydney NSW, Australia
2025

THE UNIVERSITY OF SYDNEY

Abstract

Breast cancer (BC) remains the most prevalent malignancy among women globally, accounting for 12.5% of all new cancer cases, with an estimated 2.3 million diagnoses and 685,000 deaths in 2020 (WHO). Triple-negative breast cancer (TNBC), an aggressive and highly metastatic subtype, comprises 15–20% of BC cases. Due to the absence of estrogen, progesterone, and human epidermal growth factor receptor 2 (HER2) receptors, TNBC is unresponsive to hormone and HER2-targeted therapies, leaving chemotherapy—particularly doxorubicin (Dox)—as the mainstay treatment. However, Dox's efficacy is limited by systemic toxicity and multidrug resistance (MDR). Curcumin (Cur), a polyphenol from turmeric, exhibits anticancer properties but suffers from poor solubility, low bioavailability, and rapid metabolism. Nanocarrier-based co-delivery systems for Cur and Dox have been explored to address these limitations, yet precise tumor targeting remains a challenge. In this study, we developed a dual-drug delivery nanocarrier system co-delivering Cur and Dox, incorporating alendronate (ALN) for bone targeting and luteinizing hormone-releasing hormone (LHRH) peptide to exploit its receptor overexpression in breast cancer cells. Our primary goal was to optimize Pluronic F127-based micelles for Cur delivery and niosomes for co-delivery of Cur and Dox, aiming to enhance drug stability, bioavailability, and targeted delivery. Optimization identified Pluronic F127 as a crucial component in forming nanoparticles (NPs) with superior physicochemical properties. Incorporating F127 into niosomes at a molar ratio of Span 60:F127:Cholesterol (0.99:0.01:1) significantly improved encapsulation efficiency (EE%). Cur-Dox F127 niosomes (CDFN) achieved a Dox-equivalent EE% of 58.6%, compared to 18.3% in Cur-Dox niosomes (CDN) without F127. Similarly, Cur-equivalent EE% reached 98% in CDFN, markedly higher than the 30.1% in CDN. These results underscore F127's critical role in preventing ingredient adhesion to flask walls, thereby improving EE% and nanoparticle stability. To achieve targeted delivery, ALN and LHRH derivatives ([k^6]LHRH-Cur and [k^6(Amino-hexanoic acid (Ahx))]LHRH-Cur were successfully conjugated to F127 succinate/DSPE-PEG-COOH in the NP formulation. Fourier-transform infrared spectroscopy (FTIR) and X-ray photoelectron spectroscopy (XPS) confirmed successful conversion of F127 to F127-COOH and subsequent conjugation of ALN/LHRHD to F127-COOH/DSPE-PEG-COOH. Dynamic light scattering (DLS) and scanning electron microscopy (SEM) revealed all nanomicelles remained within the 10–100 nm range, with sizes of 20 ± 10.1 nm, 21 ± 8 nm, and 32 ± 10.6 nm for [k^6]LHRH-Cur, [k^6(Ahx)]LHRH-Cur, and Cur nanomicelles, respectively. Likewise, CDFN maintained a size of 244.6 ± 20.2 nm. Zeta potential analysis showed F127 increased negative charge (–26.2 mV), enhancing stability, while PEGylation reduced this negativity (–8.7 to –10.3 mV) due to steric shielding. These findings reinforce F127's role in improving nanoparticle stability and influencing cellular interactions. Comparative analysis of drug loading capacity (DL%)

revealed that LHRH-derivative Cur micelles achieved a DL% of 7.58 ± 0.7%, exceeding the 6.75 ± 0.2% observed in Cur micelles alone. The [k^6(Ahx)]-LHRH-Cur micelle exhibited the lowest half-maximal inhibitory concentration (IC_{50}) at 3.2 ± 0.5 μM, followed by [k^6]-LHRH-Cur micelle (6.3 ± 0.8 μM) and Cur micelle (7.9 ± 3.3 μM), demonstrating enhanced therapeutic efficacy through this derivative. CDFN showed the strongest cytotoxicity with an IC_{50} of 0.7671 μM, significantly surpassing free Dox (5.482 μM) and free Cur (124.6 μM). Additionally, [k^6]-LHRH-Cur and [k^6(Ahx)]-LHRH-Cur nanomicelles displayed improved cellular uptake and cytotoxic effects against MDA-MB-231 cells compared to Cur nanomicelles in confocal imaging. IC_{50} values reveal significantly greater cytotoxicity for nanoparticle-based formulations compared to free drugs, confirming enhanced anticancer effects of CFN, DFN, and especially CDFN. The CDFN showed markedly improved cytotoxicity (IC_{50} = 0.7671 μM) over DFN (2.096 μM) and CFN (4.364 μM) ($p < 0.0001$), with a combination index (CI) of 0.271 indicating strong synergistic effect between curcumin and doxorubicin in the co-delivery system. In the 3D spheroid model using IncuCyte S5 live-cell imaging, spheroid disintegration over time served as a functional measure of cytotoxicity. Near-complete disintegration by day 4 confirmed CDFN's superior cytotoxicity compared to free-Cur and free-Dox, highlighting its ability to effectively penetrate and disrupt tumor architecture. To assess bone-targeting potential, a calcium-binding assay using Ca-coated plates was conducted. ALN-functionalised niosomes (CDPAN) showed significantly higher binding to the Ca-mimicking surface ($p < 0.0001$), as indicated by lower supernatant absorbance (0.3938) compared to non-targeted niosomes (CDPN; 0.8963). These results highlight the promise of ALN-targeted niosomes for bone-specific drug delivery in breast cancer metastasis. Stability studies confirmed that CDFN remained stable in solution for up to seven days at room temperature, with enhanced preservation under refrigeration. Additionally, pH-responsive drug release profiling demonstrated controlled, sustained release of Cur and Dox, with significantly accelerated release at acidic pH (pH 4), in line with tumor-specific drug release requirements.

In conclusion, the optimized nanocarrier system achieved superior drug encapsulation and cytotoxicity against breast cancer cells compared to conventional systems. The inclusion of ALN enabled selective targeting of both tumor and bone sites, while CDFN exhibited favourable stability and release kinetics, representing a promising therapeutic platform for breast cancer treatment.

Statement of Authenticity

This research was conducted under the supervision of Dr. Pegah Varamini at the Sydney Pharmacy School and Dr. Michelle McDonald at the Charles Perkins Centre, University of Sydney, Australia.

I confirm that the intellectual content of this thesis is solely my own work, and all assistance received in its preparation, along with relevant sources, has been appropriately acknowledged.

Furthermore, this thesis has not been submitted for any other degree at any institution or for any other purpose.

Shiva Shakori Poshteh

February 2025

Published Material Included in this Thesis and Authorship Attribution Statement

S Shakori Poshteh, S Alipour, P Varamini. Harnessing curcumin and nanotechnology for enhanced treatment of breast cancer bone metastasis. Discover Nano, 2024 – Springer. I have conducted research and wrote the article. Pegah Varamini supervised the research project and Shohre Alipour critically reviewed the article.

Chapter 2 of this thesis is prepared for submission as a primary research article. I played a key role in designing, conducting, and analyzing a significant portion of the *in vitro* studies. Additionally, I authored the entire manuscript for this publication.

Shiva Shakori Poshteh

February 2025

Supervisor Statement

As the supervisor for the candidature upon which this thesis is based, I confirm that the authorship attribution statements provided above are accurate and reflect the contributions made to this research.

Pegah Varamini

March 2025

Contributions by Others

In Chapter 2, Pegah Varamini designed and synthesized the initial batch of LHRH peptide derivatives, while Nadeem Ahmad conducted part of cell viability assay . Farhana Mollah carried out confocal imaging. Elmer Austria also performed the FTIR and XPS experiments in Chapters 2 and 3.

In addition to the statements above, for any published work where I am not the corresponding author, I have obtained permission from the corresponding author to include the material.

Artificial intelligence

During the preparation of this thesis, Copilot was used to enhance the text, including proofreading and language refinement. Where generative AI contributed to modifying the text, the author carefully reviewed the output for any errors, inaccuracies, or biases, and made necessary adjustments. The author takes full responsibility for the content of the submitted thesis and affirms that the work is their own. Generative AI was used in accordance with the University of Sydney generative AI guide for researchers.

Financial Support

This work was supported by funding from Tour de Cure (RSP-030-19/19) and the Sydney Nano Kickstarter Grant 2021.

Acknowledgements

I extend my deepest gratitude to my supervisor, Dr. Pegah Varamini, for her unwavering support, exceptional mentorship, and invaluable guidance throughout my research journey. Her dedication to scientific excellence and passion for innovation have shaped me into the researcher I am today.

Beyond our weekly meetings, she was always available—day and night—offering insightful advice and encouragement. Despite her demanding schedule, she remained incredibly responsive, ensuring I had the support I needed at every stage. Her mentorship extended beyond research, instilling in me confidence, resilience, and a deep appreciation for scientific discovery.

I am truly fortunate to have had her guidance, and I will always be grateful for her belief in me, her patience, and the inspiration she has provided.

I am grateful to Dr. Michelle McDonald for her guidance and support in the bone metastasis aspect of my research, which greatly contributed to this thesis. I also extend my thanks to Dr. Behnam Akhavan for his support as my auxiliary supervisor.

I truly appreciate Farhana Mollah for training me on tissue lab-specific protocols and for being a wonderful friend throughout this journey.

I appreciate Elmer Austria for his contributions to the characterization work in my thesis and for being a great friend throughout this journey.

I would like to thank the Pharmacy Laboratory Support Team—Kaiser, Wilson, Trish, and Suley—for their invaluable assistance in training and maintaining the equipment essential to this research. Additionally, I appreciate Craig Jackson for inducting me on the Charles Perkins Centre equipment.

Many thanks to all my friends at the Sydney Pharmacy School and Sydney Engineering School—Niusha Nazemi, Srija Sur, Mona Mirzai, Rafia Ali, Ayu Lestari, Bashayr Ahmed Aldehaafeeri, Sophie Coolen, Waiting Tai, Hany Ghaly, Alireza Soltani, Parham Vatankhah, Ali Azargoonjahromi, Mohamad Nasri, Hamidreza Arash Araghi—who brightened my days with coffee breaks, shared laughter, and conversations about experimental wins and frustrations.

Massive thanks to my mom, dad, and siblings (Neda and Setayesh), as well as my brother-in-law (Ehsan) and niece (Adrina) for their unwavering support throughout my endless educational journey. Special gratitude to my older sister, Neda, who has been my pillar of strength, offering constant encouragement and understanding, especially during the most challenging moments of this journey.

Table of Contents

List of Figures

List of Tables

List of Abbreviations and Acronyms

2D	Two-dimensional
3D	Three-dimensional
ADA	Adapalene
ADCs	Antibody-drug conjugates
Ahx	Amino-hexanoic acid
ALN	Alendronate
ATCC	American Type Culture Collection
ATR-FTIR	Attenuated total reflectance Fourier transform infrared spectroscopy
Au NPs	Gold nanoparticles
BC	Breast cancer
BL1	Basal-like 1
BL2	Basal-like 2
BRCA1	Breast cancer gene 1
BRCA2	Breast cancer gene 2
CAR	Carvedilol
CDFAN	Cur-Dox F127 ALN niosomes
CDFLN	Cur-Dox F127 LHRH niosomes
CDFN	Cur-Dox F127 niosomes
CDKs	Cyclin-dependent kinases
CDN	Cur-Dox niosomes
CDPAN	Cur-Dox DSPE-PEG-COOH ALN niosomes
CDPLN	Cur-Dox DSPE-PEG-COOH LHRH niosomes
CDPN	Cur-Dox DSPE-PEG-COOH niosomes
CFN	Curcumin F127 niosomes
Chk2	Checkpoint kinase2
Chol	Cholesterol
CL	Claudin-low
CLSM	Confocal Laser Scanning Microscopy
CN	Curcumin niosomes
Cur	Curcumin
Da	Dalton

DCM	Dichloromethane
DDS	Drug Delivery System
DFN	Dox F127 niosomes
DL%	Drug loading%
DLS	Dynamic light scattering
DMAP	4-dimethylaminopyridine
Dox	Doxorubicin
DSPE-PEG-COOH	1,2-distearoyl-sn-glycero-3-phosphoethanolamine-polyethylene glycol-carboxylic acid
EDC· HCl	1-ethyl-3-(3-dimethylaminopropyl) carbodiimide hydrochloride
EE%	Encapsulation efficiency%
EGFR	Epidermal growth factor receptor
EMT	Epithelial-mesenchymal transition
EPR	Enhanced permeability and retention
ER	Estrogen Receptor
ESI-MS	Electrospray ionization mass spectrometry
FBS	Fetal bovine serum
FDA	Food and drug administration
FSH	Follicle-stimulating hormone
GCPQ	quaternary ammonium palmitoyl glycol chitosan
GnRH	Gonadotropin-releasing hormone
GTN	Glyceryl trinitrate
HER2	Human epidermal growth factor receptor2
HR	Hormone receptors
IC_{50}	Half-maximal inhibitory concentration
IHC	Immunohistochemistry
IM	Immunomodulatory
LAR	Luminal Androgen Receptor
LH	Luteinizing hormone
LHRH	Luteinizing hormone-releasing hormone
LHRHD	Luteinizing hormone-releasing hormone derivatives
M	Mesenchymal
MRI	Magnetic resonance imaging

NHEJ	Non-homologous end joining
NLCs	Nanostructured lipid carriers
NPs	Nanoparticles
P	DSPE-PEG-COOH
PARP	Poly ADP-ribose polymerase
PBS	Phosphate Buffered Saline
PDI	Poly dispersibility index
PDX	Patient-derived xenograft
PEG	polyethylene glycol
PEO	polyethylene oxide
PFA	Paraformaldehyde
PPO	polypropylene oxide
PR	Progesterone receptor
RES	Reticuloendothelial system
ROS	Reactive oxygen species
RP-HPLC	reverse-phase high-performance liquid chromatography
RPMI	Roswell Park Memorial Institute
SA	Succinic anhydride
SEM	Scanning electron microscopy
SD	Standard deviation
SLNs	solid lipid nanoparticles
SPPS	Solid-phase peptide synthesis
TNBC	Triple-negative breast cancer
VEGF	Vascular endothelial growth factor
VEGFR	Vascular endothelial growth factor receptor
WHO	World Health Organization
XPS	X-ray photoelectron spectroscopy

Introduction to the thesis

This thesis is comprised of six chapters.

Chapter 1 provides a comprehensive introduction to breast cancer (BC), with a focus on triple-negative breast cancer (TNBC). It outlines the epidemiology, subtypes, diagnosis, and current treatment strategies of TNBC, along with emerging nanotechnology-based therapeutic approaches. The chapter also highlights the challenges associated with conventional chemotherapy and introduces curcumin and doxorubicin as key therapeutic agents. It sets the stage for the experimental work that follows by discussing the potential of polymeric micelles and niosomes in improving drug delivery for TNBC treatment.

Chapter 2 presents the development and optimization of LHRH receptor-targeted curcumin-loaded polymeric micelles using Pluronic® F127. It details the synthesis of targeting ligands, their conjugation to F127, and the physicochemical and biological evaluation of the micelles. This chapter is written as a standalone manuscript intended for publication. Therefore, some repetition of background content from Chapter 1 may occur to ensure the manuscript is self-contained and suitable for independent reading.

Chapter 3 describes the design, fabrication, and evaluation of untargeted and targeted niosomal formulations co-loaded with curcumin and doxorubicin for the treatment of TNBC-associated bone metastasis. It includes optimization studies, characterization of nanoparticles, cytotoxicity assays, and bone-targeting assessments using alendronate. Like Chapter 2, this chapter is also structured as a manuscript prepared for publication and therefore contains some repetition of introductory material for clarity and completeness.

Chapter 4 presents an integrated discussion of the research findings from Chapters 2 and 3. It synthesizes the results and identifies key implications for future development of targeted therapies for TNBC and its metastases.

Chapter 5 contains the references cited throughout the thesis.

Chapter 6 includes the full version of a previously published review article: *S. Shakori Poshteh, S. Alipour, P. Varamini. Harnessing curcumin and nanotechnology for enhanced treatment of breast cancer bone metastasis*. Discover Nano, 2024 – Springer. This chapter also includes supplementary data related to the experimental work presented in earlier chapters.

Chapter 1. Introduction

Breast cancer (BC) is a malignant disorder of the breast epithelium, driven by genetic and molecular alterations. One classification of BC is based on the presence of hormone receptors (HR), including estrogen, progesterone, and human epidermal growth factor receptor 2 (HER2), which guide treatment options (1). Triple-negative breast cancer (TNBC) is an aggressive subtype lacking these receptors, making it resistant to hormonal and HER2-targeted therapies (2) The lung is the most common site for metastasis of TNBC, while other frequent sites include the brain, bone, and liver (3). In bone metastasis, TNBC cells disrupt the balance between osteoclasts and osteoblasts, promoting bone resorption and cancer progression through factors like TGF-β (4).

1.1 Epidemiology of BC

BC is the most common cancer among women worldwide, accounting for about 12.5% of all new cancer cases, with approximately 2.3 million new cases and 685,000 deaths reported in 2020, according to the World Health Organization (WHO) (5). The incidence of breast cancer is highest in high-income countries like the United States, Canada, and many European nations due to factors such as longer life expectancy, greater access to screening programs like mammography, and lifestyle factors including diet and reproductive behaviors. Meanwhile, low- and middle-income countries are seeing a rise in cases as life expectancy increases and westernized lifestyles become more prevalent (6). BC predominantly affects women over 50 and remains the leading cause of cancer-related deaths among women globally (7). However, in high-income countries, early detection, advanced treatments, and increased public awareness have led to declining mortality rates (8). In contrast, mortality remains high in low- and middle-income countries due to limited access to healthcare, insufficient early detection programs, and lower awareness of the disease, underscoring the need for improved healthcare access and education worldwide (9).

BC is the most frequently diagnosed cancer among females in Australia. In 2024, approximately 21,000 cases are expected to be identified in females, accounting for about 28% of all projected cancer diagnoses in this group. It ranks as the second most common cancer diagnosis among individuals aged 20 to 39 and 60 to 79, while being the most prevalent cancer in those aged 40 to 59 (10). Despite this large number of cases, the number of deaths from BC has been decreasing primarily because of early detection from regular screenings, better access to advanced treatments, and successful public awareness campaigns, which have increased the five-year survival rate for women diagnosed with BC to around 91.5% (11). This positive outcome results from various national healthcare initiatives and support from organizations like the

National Breast Cancer Foundation, which promotes early detection and comprehensive care. Overall, Australia's strategy emphasizes the importance of early detection and accessible healthcare in reducing deaths from BC.

1.2 BC Subtypes

BC is classified into several subtypes based on hormone receptor and HER2 status (1). A) Luminal A cancers, which are HR+ and HER2- with low proliferation rates (Ki-67), account for around 40% of cases and are less aggressive, treated mainly with hormone therapy (12). B) Luminal B cancers, which may be HR+ with either HER2 + or HER2 - and have higher Ki-67 levels, make up 10-20% and are treated with hormone therapy, chemotherapy and HER2-targeted therapy if HER2+ (13). C) HR+/HER2- cancers, which express estrogen and/or progesterone receptors but lack HER2 overexpression, account for around 70% of cases and are treated with hormone therapy and chemotherapy (14). D) HER2+ cancers, with or without HR expression, make up 15-20% of cases and are treated with HER2-targeted therapies, and hormone therapy (15). E) TNBC, lacking HR and HER2 expression, represents 10-15% of cases, primarily treated with chemotherapy, though immunotherapies are being explored (16).These subtypes help guide treatment and prognosis.

1.2.1 TNBC

At the cellular level, TNBC is often categorized as a "basal-like" cancer (17). These cells tend to have a high proliferative rate, as indicated by elevated levels of Ki-67, a marker for cell division (18). They also frequently express cytokeratin 5/6 and epidermal growth factor receptor (EGFR) , both of which are associated with aggressive cancer behavior (19). TNBC tumors are highly heterogeneous, meaning that there is considerable diversity among the cells within a single tumor (20). This heterogeneity complicates treatment, as different cell populations may respond differently to therapy (20). TNBC tumors are also often rich in cancer stem cells (CSCs), which can self-renew and drive tumor growth and metastasis (21).

Molecularly, TNBC is driven by several genetic and epigenetic alterations (22). One of the most common mutations found in TNBC is in the TP53 gene, which encodes the tumor suppressor protein p53 (22, 23). When p53 function is lost, cells can proliferate uncontrollably, leading to tumor formation (23). Mutations in the breast cancer gene 1 (BRCA1) and breast cancer gene 2 (BRCA2), which are involved in DNA repair, are also frequently associated with TNBC (24). These mutations make the cells more reliant on alternative DNA repair mechanisms, which can be targeted with therapies like Poly ADP-ribose polymerase (PARP) inhibitors (25). In addition to genetic mutations, TNBC is characterized by dysregulation of growth factor pathways, particularly those involving EGFR and vascular endothelial growth factor (VEGF), which

promote cancer cell survival, proliferation, and angiogenesis (26). TNBC also frequently exhibits immune evasion strategies, such as upregulating the PD-L1 protein, which allows cancer cells to suppress the immune response (2).

TNBC's aggressive biological behavior is further driven by its interactions with the tumor microenvironment (27). The tumor microenvironment includes not only cancer cells but also stromal cells, immune cells, and extracellular matrix components (27). Tumor-associated macrophages (TAMs) and cancer-associated fibroblasts (CAFs) play a significant role in promoting tumor growth and metastasis by releasing cytokines and growth factors that support cancer progression (28). Additionally, the process of epithelial-mesenchymal transition (EMT) is commonly observed in TNBC (29). EMT allows cancer cells to lose their adhesion properties and become more mobile, enabling them to invade surrounding tissues and spread to distant organs (30).

1.2.2 TNBC's subtypes

Recent research has revealed that TNBC is not a homogenous disease but consists of various molecular subtypes, each with distinct biological behaviors and treatment responses (31). Among the key subtypes of TNBC are Basal-like 1 (BL1), Basal-like 2 (BL2), Immunomodulatory (IM), Luminal Androgen Receptor (LAR), Mesenchymal (M), and Claudin-low (CL), which help define different pathways of progression and resistance mechanisms (32) (***Figure 1-1***).

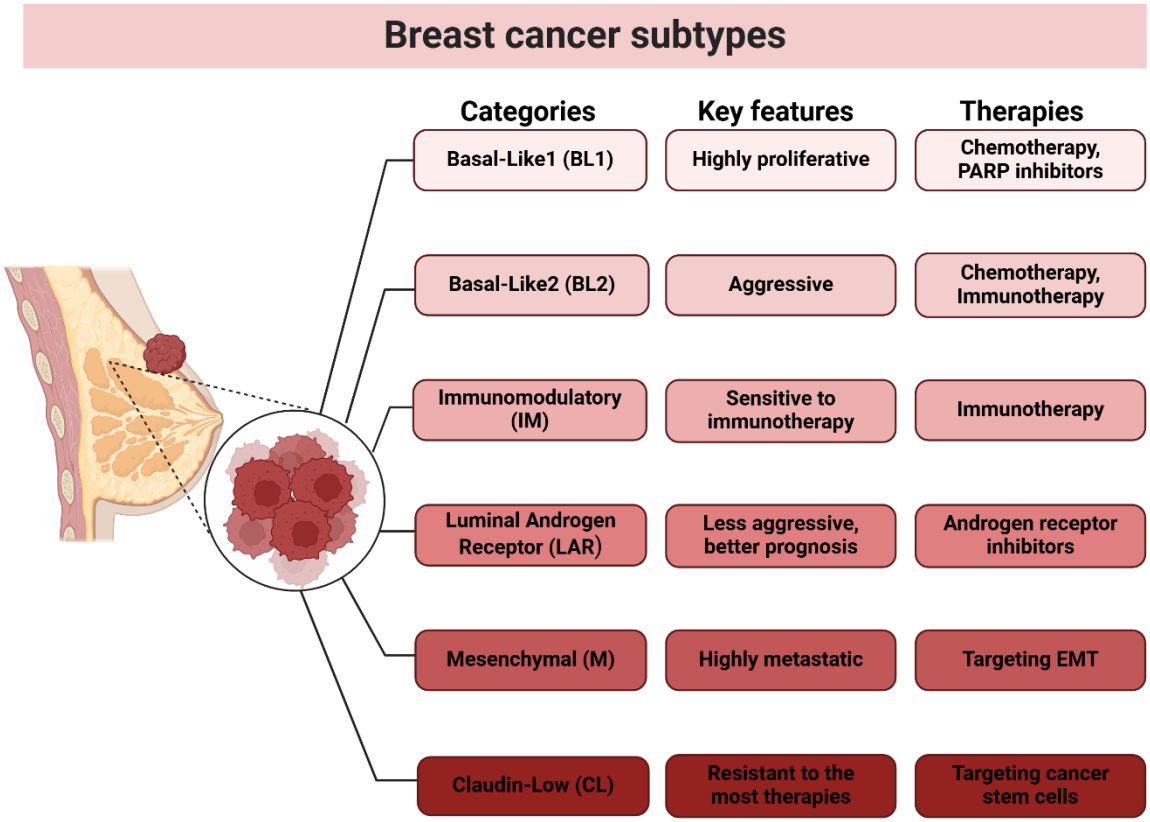

Figure 1-1. Breast cancer subtypes

1.2.3 TNBC's epidemiology

TNBC accounts for approximately 10-15% of all breast cancer cases, representing a particularly aggressive and challenging subtype (33). Also, patients with TNBC have a poorer prognosis and recurrence is common, particularly within the first 3 to 5 years after treatment (34).

TNBC disproportionately affects certain demographic groups (35). It is more commonly diagnosed in younger women, particularly those under the age of 50 (35). Additionally, African American and Hispanic women have a higher prevalence of TNBC compared to other racial and ethnic groups (35). Socioeconomic factors, limited access to healthcare, and genetic predispositions are believed to contribute to these disparities (35).

Despite the aggressive nature of TNBC, early detection and effective treatment can lead to long-term remission for many patients (35). Research has demonstrated that those who respond well to chemotherapy,

particularly anthracycline- or platinum-based regimens, can achieve favorable outcomes (36). However, the heterogeneity within TNBC means that responses to treatment can vary significantly among patients (37). While early-stage TNBC shows better outcomes with treatment, late-stage or recurrent disease is more difficult to manage (35).

1.2.4 TNBC's Diagnosis

TNBC is primarily diagnosed through immunohistochemistry (IHC), which analyzes protein expression in tumor tissue samples to detect the absence of key receptors: estrogen receptor (ER), progesterone receptor (PR), and HER2 (38). This absence confirms TNBC status, distinguishing it from other BC subtypes that may express these receptors and respond to hormone or HER2-targeted therapies (38). The IHC process begins with a biopsy, followed by staining the tissue with antibodies (39). If there is no significant receptor expression, the tumor is classified as TNBC, meaning hormone therapy and HER2-targeted treatments are ineffective. In such cases, chemotherapy remains the primary treatment option, while emerging therapies like immunotherapy are being actively developed and integrated as potential first-line treatments. (1, 40).

In addition to IHC, genetic testing for BRCA1 and BRCA2 mutations is recommended due to their strong association with TNBC (41).

1.2.5 Current TNBC Treatments

Chemotherapy remains the cornerstone of treatment for TNBC, utilized in both neoadjuvant and adjuvant settings (33). Neoadjuvant chemotherapy is administered before surgery, aiming to reduce the size of the tumor and thereby enhance the feasibility of breast-conserving surgery, while adjuvant chemotherapy is employed post-surgery to eliminate any remaining cancer cells (42). A positive response can indicate better prognosis and guide subsequent therapy decisions. However, challenges with chemotherapy include severe side effects, such as nausea, fatigue, and immune suppression, which can significantly impact patients' quality of life and complicate subsequent treatments (43).

Surgical options for TNBC typically include either lumpectomy, which preserves most of the breast tissue, or mastectomy, which involves the complete removal of one or both breasts, depending on the extent of the disease (16). The biggest challenge in surgery is removing all the cancerous tissue while keeping as healthy tissue intact as possible (44).

Radiation therapy often accompanies surgical treatment, especially after breast-conserving surgery, to target any remaining cancer cells and minimize the risk of local recurrence (45). This additional treatment modality is vital, as it significantly lowers the chances of cancer returning in the same area (46, 47).

Nevertheless, the challenge lies in the potential long-term side effects of radiation, which can include skin changes, fatigue, and, in some cases, an increased risk of developing secondary cancers (46, 47).

In recent years, immunotherapy has emerged as a promising avenue for treating TNBC, particularly the use of immune checkpoint inhibitors in conjunction with chemotherapy (48). These therapies enhance the immune system's ability to recognize and destroy cancer cells, offering new hope for cancerous patients (49). However, immunotherapy may not be effective for all TNBC patients, and potential immune-related adverse effects can complicate treatment (50). For patients carrying BRCA1 or BRCA2 mutations, PARP inhibitors present an effective treatment option by exploiting the impaired DNA repair mechanisms typical of these tumors, leading to increased cell death (50). The challenge here is that not all patients with BRCA mutations respond equally to these inhibitors, and resistance can develop (51).

Furthermore, EGFR inhibitors are being explored as potential treatments for cases of TNBC where EGFR is overexpressed (52). By targeting the EGFR protein, which plays a crucial role in tumor growth and survival, these inhibitors may help slow disease progression (52). However, challenges remain in identifying patients who would benefit most from this targeted therapy and managing potential side effects, such as skin rashes and diarrhea (53, 54).

Anti-angiogenic agents are another promising strategy, as they inhibit angiogenesis the process of new blood vessel formation that tumors rely on for growth (55). By disrupting the tumor's blood supply, these agents can help to hinder tumor growth and prevent metastasis (55). Nevertheless, the efficacy of these agents can be limited, and they may come with significant side effects, including hypertension and bleeding risks (56).

Antibody-drug conjugates (ADCs) represent a cutting-edge therapeutic approach that combines a cancer-targeting antibody with a potent cytotoxic drug (57). This strategy allows for the direct delivery of treatment to tumor cells while minimizing systemic toxicity, thus improving the safety profile of chemotherapy (58).

Also, in 2016, the Food and Drug Administration (FDA) approved sacituzumab govitecan-hziy, an ADC, as a breakthrough therapy for TNBC in patients who had undergone at least two prior treatments for metastatic disease (59). However, the complexity of ADC design, including the choice of appropriate antibodies, linkers, and drug payloads, can affect their efficacy and safety (58).

Nanotechnology has become a potentially transformative strategy in TNBC (60). One of the key advantages of nanotechnology in treating TNBC is its ability to enhance drug delivery to the tumor site (60). Engineered nanoparticles with certain targeting moieties can precisely target tumor sites, increasing the concentration of therapeutic agents directly at the cancerous tissues while minimizing damage to healthy cells (61). This

targeted approach improves treatment efficacy and reduces systemic toxicity commonly associated with traditional chemotherapy (62).

Nanotechnology also can enhances the solubility and stability of poorly water-soluble chemotherapeutic agents, increasing their bioavailability and allowing for lower doses with fewer adverse effects (63). Additionally, integrating imaging agents with nanoparticles enables real-time monitoring of tumor responses, facilitating dynamic adjustments to treatment plans (64). This capability not only optimizes patient care but also supports personalized medicine by tailoring therapies to individual patient responses (64).

1.3 Nanotechnology-based promising strategies for treating TNBC

One of the cornerstone principles of nanotechnology in cancer treatment is the enhanced permeability and retention (EPR) effect (65). Tumor tissues often exhibit leaky blood vessels, which allow nanoparticles to accumulate more effectively within the tumor microenvironment compared to normal tissues (65). Indeed, by taking the advantage of the EPR effect, nanoparticles can deliver higher doses of chemotherapeutic agents directly where they are needed most, improving patient outcomes and reducing side effects (65).

Another significant advancement in nanotechnology is the development of smart nanocarriers that can respond to specific stimuli within the tumor environment, such as variations in pH or the presence of certain enzymes (66). For example, nanoparticles engineered to release their drug payload in response to the acidic conditions typical of tumor tissues can improve treatment precision and help circumvent the resistance mechanisms that cancer cells often develop against conventional therapies (66). This responsive delivery system not only enhances drug release specificity but also minimizes off-target effects, thus improving the overall therapeutic index (66).

Immune modulation is another promising strategy that nanotechnology brings to the forefront of TNBC treatment (67). Nanoparticles can be designed to carry immune-modulating agents that enhance the immune system's ability to recognize and destroy TNBC cells (68). By delivering checkpoint inhibitors, nanoparticles can help "release the brakes" on the immune system, promoting a more robust anti-tumor response (67). Additionally, this strategy can involve recruiting immune cells to the tumor site, further amplifying the body's natural defenses against cancer (69).

The potential of nanoparticles extends to vaccine development as well (70). Researchers are exploring the use of nanoparticles to deliver tumor-specific antigens to immune cells, thereby triggering targeted immune

responses (70). Thus, by mimicking natural infection, these nanoparticle-based vaccines aim to enhance the immune system's memory against cancer cells, providing lasting protection against recurrence (71).

Active targeting is another important aspect of nanotechnology in TNBC treatment (71). By modifying nanoparticles with specific ligands, such as antibodies or peptides that bind to overexpressed receptors on TNBC , researchers can significantly enhance the specificity of drug delivery (72). This targeted approach not only ensures that therapeutic agents are delivered primarily to cancerous tissues but also reduces collateral damage to healthy cells, thereby improving the patient's quality of life during treatment (61).

Finally, nanotechnology facilitates combination therapy, enabling the simultaneous delivery of multiple therapeutic agents or modalities through a single nanoparticle platform (73). This integrative approach allows for a more comprehensive treatment strategy, tailoring therapy to the individual patient and their unique cancer profile (73). **Error! Reference source not found.** summarizes some of these strategies, including the EPR effect, smart nanocarriers, immune modulation, vaccine development, active targeting, and combination therapy, all of which contribute to improved drug delivery and therapeutic outcomes in TNBC.

Table 1-1. Examples of different nanotechnology-based strategies to enhance TNBC treatment efficiency.

Nanotechnology Strategy	Mechanism of Action	Targeting Method	Advantages	Ref.
EPR Effect	Nanoparticles accumulate in tumors via leaky vasculature	Passive	Increase drug concentration at the tumor site	(65)
Smart Nanocarriers	Respond to tumor-specific stimuli (pH, enzymes)	Active	Improves drug release precision and reduces resistance	(66)
Immune Modulation	Deliver immune-modulating agents or recruit immune cells	Active/Passive	Helps the immune system recognize and attack cancer cells	(68)
Vaccine Development	Delivers tumor-specific antigens to immune cells, triggering targeted immune responses.	Active/Passive	Promotes immune memory against cancer cells, providing lasting protection against recurrence.	(70)
Active Targeting	Nanoparticles modified with ligands (antibodies, peptides)	Active	Enhances specificity by targeting overexpressed receptors	(72)
Combination therapy	Co-delivery of multiple drugs or therapies (e.g., chemo and immunotherapy)	Active/Passive	Allows simultaneous treatment modalities	(73)

1.3.1 Different types of nanoparticles used in TNBC research

Nanoparticles have emerged as a vital tool in the treatment of TNBC by enhancing drug delivery and targeting capabilities (74). For instance, liposomes, which are lipid bilayer structures, effectively encapsulate both hydrophilic and hydrophobic drugs (74). This encapsulation not only improves drug solubility but also reduces systemic toxicity, making them a popular choice in formulations like liposomal Dox , which specifically targets tumor cells (75). Additionally, polymeric nanoparticles, made from biodegradable polymers, allow for controlled drug release (76). These nanoparticles can be engineered to actively target cancer cells through surface modifications, thus enhancing their therapeutic efficacy (75). Furthermore, gold nanoparticles (AuNPs) are recognized for their unique optical and electronic properties, which enable targeted drug delivery and photothermal therapy (77). Similarly, mesoporous silica nanoparticles, engineered for high surface area, can deliver drugs in response to specific stimuli, thus aiding in targeted therapy and imaging (78) Moreover, magnetic nanoparticles leverage external magnetic fields to improve drug accumulation in tumors while also facilitating imaging through magnetic resonance imaging (MRI) (79).

Also, solid lipid nanoparticles (SLNs) are a solid lipid core that enhances drug stability and controlled release. Their biocompatibility, improved drug bioavailability, and potential for targeted delivery make them significant in cancer therapy.

In addition to these, carbon nanotubes enhance photothermal therapy and serve as efficient drug carriers (80, 81). On the other hand, quantum dots, known for their bright fluorescence, are utilized in imaging TNBC cells, allowing for real-time monitoring of treatment responses (82). Furthermore, dendrimers can carry multiple drug molecules, enabling combination therapies, while exosomes, which are natural extracellular vesicles, hold promise as carriers for therapeutic agents due to their ability to specifically target cells and evade the immune system (83, 84). Lastly, polymeric micelles and niosomes provide versatile platforms for drug delivery, improving the solubility of poorly water-soluble drugs and prolonging therapeutic effects, thus enhancing the targeted treatment of TNBC (85, 86).

Together, these nanoparticles represent a diverse range of strategies that harness nanotechnology to improve drug delivery and therapeutic outcomes in the treatment of TNBC, addressing the significant challenges posed by this aggressive cancer subtype **(*Figure 1-2*).**

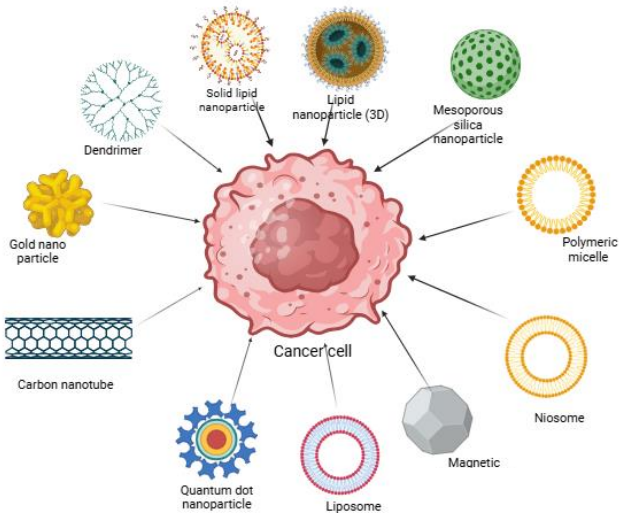

Figure 1-2. Different types of nanoparticles in TNBC research

1.3.1.1 *Polymeric micelles and niosomes*

These nanoparticles have emerged as promising nanocarriers for drug delivery, offering distinct advantages for therapeutic applications, including treatments for TNBC (60, 87). Polymeric micelles, formed by amphiphilic block copolymers, are particularly effective for solubilizing and delivering hydrophobic drugs such as Cur (88). Their small size and surface properties enable prolonged circulation, preferential accumulation at tumor sites via the EPR effect, and reduced systemic toxicity (88). These micelles can be multifunctional, incorporating targeting ligands and imaging agents to serve both therapeutic and diagnostic purposes (89).

Similarly, niosomes—vesicular systems composed of non-ionic surfactants and cholesterol (Chol)—are valued for their biocompatibility, structural flexibility, and ability to encapsulate both hydrophilic and hydrophobic drugs (90). They improve drug stability, prevent premature degradation, and enable controlled, prolonged release, which enhances therapeutic efficacy and patient compliance while minimizing side effects (90). Additionally, niosomes can be functionalized with targeting ligands to deliver drugs directly to tumor sites, further reducing systemic toxicity (87). Together, polymeric micelles and niosomes represent advanced strategies for enhancing the delivery and efficacy of hydrophobic drugs like Cur and chemotherapeutics such as Dox in TNBC therapy (60, 87, 91) . Together, micelles and niosomes are promising strategies for improving drug delivery in TNBC treatment.

1.4 Compounds under investigation in Breast Cancer therapy

Breast cancer, particularly TNBC, an aggressive subtype that lacks key hormone receptors, is primarily treated with chemotherapy agents such as anthracyclines, taxanes, and platinum-based drugs (2, 92). Immunotherapies, such as immune checkpoint inhibitors, and targeted therapies like PARP inhibitors are advancing treatment options (48, 50). Innovative drug delivery systems, such as nanoparticles, improve the precision and effectiveness of therapies while reducing toxicity (90). Additionally, natural compounds like Cur offer potential benefits due to their anti-inflammatory and anti-cancer properties, providing a complementary approach to conventional treatments (93) .

1.4.1 Curcumin as an anti-cancer agent

Curcumin is a bioactive yellow-orange polyphenol derived from the rhizome of *Curcuma longa* (turmeric), widely studied for its anti-inflammatory, antioxidant, and anticancer properties (94). Structurally, Cur consists of two aromatic rings connected by a conjugated dienone linkage, which is responsible for its stability in lipid-rich environments and its vibrant coloration (95). However, this hydrophobic nature limits its solubility in water to approximately 3.12 mg/L at 25°C, significantly restricting its bioavailability and therapeutic potential in aqueous environments (96).

The limited solubility of Cur is one of its primary challenges in medical applications, as poor solubility translates into low absorption and rapid elimination in the body (96). Additionally, Cur is sensitive to environmental factors such as light and heat, which can degrade its molecular structure and reduce its therapeutic efficacy (97). For instance, while Cur exhibits a shelf life of about two years in its solid form, it degrades within hours when in aqueous solutions at neutral PH. This instability poses challenges for developing formulations that maintain its bioactivity over time (***Table 1-2***).

Nevertheless, despite these physicochemical limitations, Curcumin continues to attract attention for its remarkable biological activity across multiple aspects of cancer progression**.** Curcumin has shown promising potential in modifying the tumor microenvironment by suppressing pro-inflammatory cytokines such as IL-6 and TNF-α (98). It also reduces the presence of immunosuppressive cells, including tumor-associated macrophages and regulatory T cells, thereby enhancing anti-tumor immune responses (98). Additionally, curcumin interferes with tumor-supportive stromal remodeling, including fibroblast activation and extracellular matrix stiffening, which play key roles in cancer progression (99). Beyond these immunomodulatory effects, curcumin can enhance the efficacy of conventional cancer therapies (100). It has been observed to sensitize tumors to chemotherapy and radiotherapy by promoting oxidative stress within cancer cells and inhibiting cell survival pathways that are often activated during treatment (100).This

dual action not only amplifies therapeutic outcomes but also helps to overcome resistance mechanisms (100).

Table 1-2. Physical properties of Cur

Property	Value/Description
UV Absorption	Maximum absorption at 425 nm, enabling easy spectrophotometric analysis.
Molecular Weight	368.4 g/mol, indicating moderate molecular size suitable for drug delivery systems.
Melting Point	179–182°C, suggesting thermal sensitivity.
Shelf Life (Solid Form)	Approximately 2 years, indicating stability under dry conditions.
Shelf Life in Solution	Rapid degradation within hours at neutral pH in aqueous solutions.

The instability and poor water solubility of Cur necessitate innovative approaches to enhance its therapeutic applicability (101). Nanocarriers such as polymeric micelles, niosomes, and liposomes are being explored to overcome these limitations (101). These delivery systems improve Cur's solubility, protect it from environmental degradation, and enhance its bioavailability, thereby maximizing its therapeutic benefits (101). Understanding Cur's physicochemical properties (***Figure 1-3***) is critical for optimizing its use in pharmaceuticals and designing effective drug delivery systems tailored to its unique challenges (***Table 1-3*** and ***Table 1-4***).

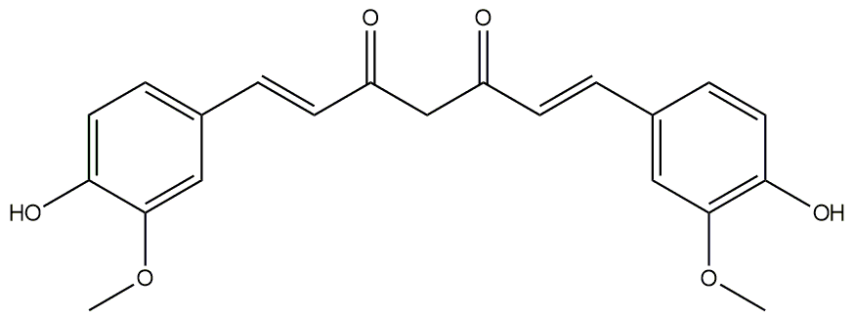

Figure 1-3. **The chemical structure of Curcumin.**

Table 1-3. Studies on Cur's anticancer mechanisms in breast cancer during the year 2024

Study Description	Outcome	Mechanism/Target	Challenges	Key Findings	References
Investigated curcumin's effects on miR-638-5p and its target genes in TNBC (MDA-MB-231 cells).	Curcumin increased miR-638-5p expression, decreased CFL1, SIX4, MAZ, inhibiting proliferation and migration.	miR-638-5p, CFL1, SIX4, MAZ	Poor cellular uptake and instability of miR-638-5p modulation limits curcumin's bioactivity in triple-negative breast cancer	Significantly inhibited cell proliferation and migration.	(102)
Curcumin’s effects on TNBC cells (Hs578T and MDA-MB-231), focusing on cell viability, apoptosis, and molecular pathways.	Curcumin reduced cell viability and induced apoptosis.	PI3K/Akt, mTOR, EMT	Limited ability to inhibit EMT and metastasis without targeted delivery in TNBC; systemic bioavailability remains a challenge	Induced apoptosis, G2/M arrest, downregulated key proteins like Akt and N-Cadherin.	(103)
Curcumin's epigenetic regulation via miR-15a-5p in MCF7 cells	Reduced cell viability and migration	miR-15a-5p	Epigenetic modulation via miR-15a-5p is effective but may lack clinical translatability due to low solubility and cellular targeting issues	Upregulation of tumor suppressor miRNA, inducing apoptosis	(104)
Modulation of signaling pathways by curcumin in breast cancer	Suppressed tumor growth and metastasis	PI3K/Akt/mTOR, MAPK, Wnt/β-catenin, NF-κB	Despite modulating multiple cancer pathways, curcumin’s clinical potential is hampered by poor solubility, instability, and rapid systemic elimination	Inhibition of key signaling pathways related to cancer progression	(105)

Table 1-4. Studies reporting the loading of Cur into different drug delivery systems during the years 2023 and 2024

Drug Delivery System Description	Outcome	Drug delivery system (DDS) /Mechanism	Challenges	Key Findings	References
Review of curcumin nano delivery systems for breast cancer treatment, including targeting strategies and imaging.	Addressed curcumin's poor solubility and bioavailability.	Liposomes, Nanoparticles	Clinical use of curcumin remains limited due to poor water solubility, chemical instability, and rapid metabolism	Improved cellular uptake, prolonged circulation, enhanced anticancer activity.	(106)
Nanotechnology-based DDS for curcumin in treating breast cancer bone metastasis (liposomes, nanoparticles).	Enhanced solubility, stability, and bioavailability.	Liposomes, Nanoparticles	Targeting ATM/Chk2/p53 pathways requires sufficient intracellular concentration, which is limited by curcumin's poor permeability and stability	Improved targeting, reduced side effects compared to free curcumin.	(101)
Development of chitosan/carbon quantum dots/Fe2O3 nanocomposite for curcumin delivery.	Improved solubility and controlled release in acidic cancer environments.	Carbon quantum dots, Fe2O3	Curcumin's thermal and photosensitivity make it unstable for direct use, requiring protective delivery platforms like CQD-Fe_2O_3-chitosan systems	Significant reduction in cell viability, induced apoptosis in MCF-7 cells.	(107)
Development of folic acid-conjugated curcumin-loaded bioMOF-101 for breast cancer therapy.	High encapsulation efficiency, selective targeting.	BioMOF-101, Folic acid	Passive targeting of curcumin via unfunctionalized MOFs results in low tumor selectivity and accumulation	Induced apoptosis and reduced lung metastasis.	(108)
Review on curcumin-based nano delivery systems for breast cancer.	Improved solubility, bioavailability, and therapeutic efficacy.	Nano delivery systems	Curcumin faces multiple barriers: poor solubility, rapid metabolism, low systemic bioavailability, and fast elimination limiting its therapeutic efficacy	Enhanced drug delivery, apoptosis induction, reduced multidrug resistance.	(109)
Comparison of curcumin-loaded niosomes and free curcumin in lung cancer cells.	Curcumin-loaded niosomes showed superior efficacy.	Niosomes, ROS, STAT3/NF-κB pathways	Free curcumin shows limited apoptosis induction and ROS generation due to poor cellular uptake and instability; nano-niosomal delivery significantly improves these effects	Induced apoptosis, enhanced ROS production, downregulated key pathways.	(110)

Studies on curcumin for treating BC face challenges related to its poor bioavailability, rapid metabolism, and short half-life (101). To improve its effectiveness, drug delivery systems like nanoparticles, liposomes, niosomes, and micelles, as well as combination therapies of Cur with Dox, have been developed (91). These

systems enhance Cur's solubility, stability, and targeted delivery, reducing toxicity and improving therapeutic outcomes (91) . However, issues with controlled release, stability, scalability, and potential drug-drug interactions remain (111). Additionally, challenges in dosing, timing, and clinical implementation, along with regulatory hurdles, emphasize the need for advanced drug delivery technologies and improved clinical methods to fully realize Cur's potential in cancer therapy (111).

Cur exerts its anticancer effects through a range of cellular mechanisms that collectively contribute to its potential as a therapeutic agent against various cancers (112). One of the key mechanisms is cell cycle arrest, which Cur induces at critical checkpoints within the cell cycle (112). Cur has been shown to arrest cells at the G1/S and G2/M phases (112). At the G1/S phase, Cur inhibits cyclin-dependent kinases (CDKs), which are necessary for the transition from the G1 phase to DNA replication in the S phase (112). Additionally, Cur increases the levels of p21 and cyclin-dependent kinase inhibitors that prevent the progression from G1 to S phase (112). In the G2/M phase, Cur induces the upregulation of checkpoint kinase 2 (Chk2) and the tumor suppressor protein p53, which halts the cell cycle to allow DNA repair or induces apoptosis in cells with damaged DNA (113). This inhibition of cell cycle progression prevents the uncontrolled proliferation characteristic of cancer cells (113).

Apoptosis induction is another critical mechanism through which Cur targets cancer cells (114). Cur activates pro-apoptotic proteins such as Bax, which promote mitochondrial outer membrane permeabilization, leading to the release of cytochrome c and the activation of caspases, particularly caspase-3, -8 and-9 (114, 115). This activation results in the dismantling of cellular structures and the initiation of programmed cell death (114). Concurrently, Cur inhibits anti-apoptotic proteins, most notably Bcl-2 and Bcl-xL, which are involved in maintaining mitochondrial integrity and preventing apoptosis (116). By disrupting this balance and favoring pro-apoptotic signals, Cur ensures that cancer cells with damaged DNA undergo controlled cell death rather than surviving and proliferating (114, 115) .

Inhibition of transcription factors plays a crucial role in Cur's anticancer properties. In many cancers, transcription factors like NF-κB, STAT3, and AP-1 are constitutively active and contribute to tumor growth, survival, and resistance to chemotherapy (117). Cur has been shown to inhibit the activation of NF-κB by preventing its phosphorylation and nuclear translocation (117). This reduces the expression of genes involved in inflammation, cell survival, and immune evasion, such as COX-2 and IL-6 (117). Similarly, Cur downregulates STAT3 signaling by inhibiting JAK2/STAT3 phosphorylation, which reduces the expression of anti-apoptotic and pro-inflammatory genes, thus limiting cancer cell survival and immune

suppression. AP-1, a transcription factor involved in regulating genes related to cell proliferation and migration, is also suppressed by Cur, further inhibiting cancer progression (117).

Another vital mechanism of Cur is its anti-angiogenesis and anti-metastasis properties. Cur inhibits tumor-induced angiogenesis by downregulating the expression of VEGF and inhibiting its receptor (VEGFR) (118). VEGF is essential for the formation of new blood vessels that supply nutrients to tumors, promoting their growth (118). Cur also decreases the activity of MMPs, particularly MMP-2 and MMP-9, which play a crucial role in the degradation of the extracellular matrix and facilitate the invasion of cancer cells into surrounding tissues (119). By inhibiting these processes, Cur prevents tumor growth and metastasis by limiting the ability of the cancer cells to invade adjacent tissues and spread to distant organs (119).

Furthermore, Cur addresses drug resistance mechanisms in cancer cells (120). One of the primary causes of chemotherapy failure is the overexpression of efflux pumps, such as P-glycoprotein (P-gp), which actively pump chemotherapeutic agents out of cancer cells, reducing their efficacy (120). Cur has been shown to inhibit P-gp expression and activity, leading to an increased intracellular concentration of chemotherapy drugs like Dox, which enhances their cytotoxic effects (121). Additionally, Cur modulates drug metabolism pathways by inhibiting enzymes such as cytochrome P450, which are involved in the metabolic degradation of chemotherapeutic agents (122). By interfering with these drug-resistance mechanisms, Cur enhances the sensitivity of cancer cells to treatment and may help overcome multi-drug resistance (MDR) (120) (***Table 1-5***).

Table 1-5. Key mechanisms of Cur's anti-cancer activity

Mechanism	Description	Ref.
Cell Cycle Arrest	Induces arrest at G1/S and G2/M checkpoints by inhibiting CDKs (e.g., CDK2, CDK4), increasing p21 and p27, and upregulating p53 and Chk2, preventing uncontrolled cell proliferation.	(112, 113)
Apoptosis Induction	Activates pro-apoptotic proteins (e.g., Bax), leading to mitochondrial dysfunction and caspase activation, while inhibiting anti-apoptotic proteins (e.g., Bcl-2, Bcl-xL).	(114-116)
Inhibition of Transcription Factors	Suppresses NF-κB, STAT3, and AP-1, reducing the expression of pro-inflammatory and survival genes (e.g., COX-2, IL-6), thereby limiting tumor growth and survival.	(117)
Anti-Angiogenesis/Metastasis	Downregulates VEGF and its receptor VEGFR, preventing new blood vessel formation and inhibiting MMPs (MMP-2, MMP-9) to limit tumor invasion and metastasis.	(118, 119)
Drug Resistance Modulation	Inhibits efflux pumps like P-gp, increasing the intracellular concentration of chemotherapeutic drugs and modulating drug metabolism to enhance treatment efficacy.	(120)

1.4.2 Doxorubicin (Dox)

Dox is a widely used chemotherapeutic agent from the anthracycline class, which was first discovered in the early 1960s. It is derived from *Streptomyces peucetius*, a bacterium that demonstrated significant cytotoxic activity against cancer cells. This discovery was pivotal, as it offered a promising treatment option for a variety of cancers (123). In 1970s, researchers identified and published the chemical structure of Dox, laying the foundation for its further development as a potent chemotherapy drug (123). The chemical structure, which is crucial for its biological activity, is shown in (***Figure 1-4***).

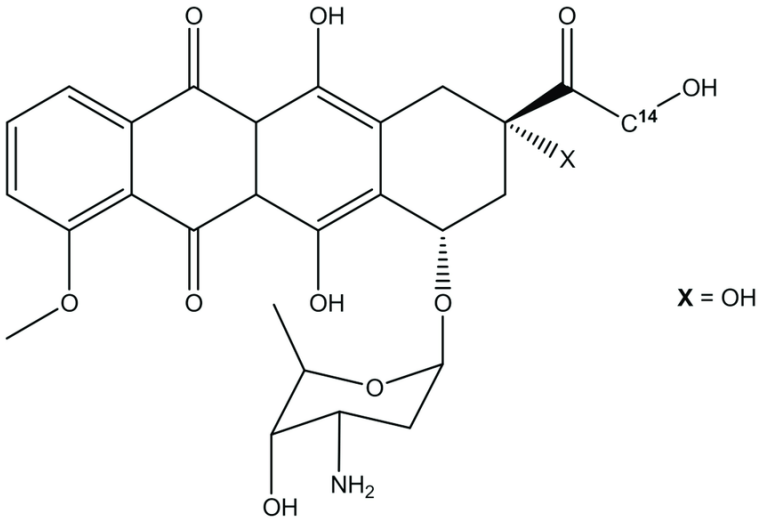

Figure 1-4. The chemical structure of Dox

Despite its effectiveness in cancer treatment, the clinical use of Dox is often limited by its dose-dependent cardiotoxicity, which can lead to long-term heart damage (123). As a result, researchers have focused on developing nanoparticle-based delivery systems to improve its therapeutic index and reduce systemic side effects (123) (***Table 1-6***).

Table 1-6. physical properties of Dox

Property	Value/Description
Water Solubility	1.23 mg/mL (at 25°C)
Stability	Unstable at room temperature; degrades in light and heat; best stored at 2-8°C in the dark
Molecular Weight	543.52 g/mol
Log P	1.27 (octanol/water partition coefficient, indicating moderate lipophilicity)
UV Absorption	Maximum absorption at 480-500 nm
Shelf Life (Solid Form)	Approximately 2 years
Shelf Life (Solution)	7 days

The pharmacokinetics of Dox are characterized by a triphasic plasma clearance profile (124). Upon intravenous (IV) administration, the drug initially distributes rapidly into highly perfused tissues, such as the heart, liver and kidneys (125). This is followed by a slower redistribution phase as the drug moves into peripheral tissues, and a prolonged terminal elimination phase (125). Dox exhibits extensive binding to tissues, particularly to the myocardium, which contributes to its relatively long half-life and slow clearance from the body (125, 126). The drug's mean terminal half-life is between 20 and 48 hours, which indicates that it persists in the system for a significant amount of time, thus providing prolonged therapeutic effects. (drug bank) This prolonged presence in the body is advantageous for the treatment of cancer but also poses a risk for cardiotoxicity, a major limitation of Dox therapy (drug bank) (***Table 1-7***).

Table 1-7. Studies reporting various strategies for Doxorubicin delivery during the years 2020–2024

(Note. Table includes both advanced drug delivery systems and conventional formulation strategies reported during the years 2020-2024)

Study Description	Strategy	Outcomes	Key Implications	Ref
Effect of Dox on TNBC cells focusing on gene expression alterations and drug resistance	Dox alone	Increased IC_{50} values; 196 upregulated and 115 downregulated genes; activation of DNA repair and EMT.	Identified biomarkers and therapeutic targets for overcoming drug resistance in TNBC.	(127)
Synergistic effects of adapalene (ADA) and Dox in TNBC, focusing on apoptosis and ROS induction	Drug combination of Dox and ADA	Enhanced apoptosis, ROS increase, disrupted mitochondria, and reduced migration and mammosphere formation.	Promotes combination strategies for improved therapeutic outcomes in TNBC.	(128)
Characterization of Dox -resistant MDA-MB-231 cells (DRM) and their EMT/CSC properties	Dox Resistance Model	Increased resistance, proliferation, EMT, and CSC traits with autocrine signaling-mediated transfer.	Highlights EGFR as a target to overcome Dox resistance in DRM cells.	(129)
Cytotoxic and anti-migratory effects of Caesalpinia sappan and Ficus septica extracts with Dox	Plant Extracts with Dox	Enhanced cytotoxicity, reduced NF-κB activation, and nephroprotective effects against Dox-induced ROS.	Suggests potential of plant extracts in combination therapies for TNBC with reduced toxicity.	(130)
Adrenergic blockade with carvedilol (CAR) combined with Dox under stress conditions in TNBC	Adrenergic Blocker (CAR) + Dox	Reduced CSC markers, tumor volume, and hypoxia; increased apoptosis and histopathological improvement.	Proposes adrenergic blockers as adjuvants to improve Dox efficacy in hypoxic TME.	(131)
Glyceryl trinitrate (GTN) as a nitric oxide donor enhancing Dox effects in TNBC	GTN + Dox	Increased CD8+ T cells, reduced PMN-MDSC immunosuppression, reprogrammed TME.	Suggests GTN as a potential immunomodulatory agent to enhance Dox efficacy.	(132)
Oncolytic alphavirus M1 combined with Dox for TNBC treatment	Oncolytic Virus (M1) + Dox	Amplified antitumor effect via necroptosis induction and interferon pathway inhibition.	Synergistic effects support the combination of oncolytic viruses with Dox.	(133)

Role of circRNA-CREIT in overcoming Dox resistance in TNBC	circRNA-CREIT + ISRIB	Increased chemosensitivity via stress granule reduction and PKR degradation.	Demonstrates circRNA-CREIT's potential in reversing Dox resistance in TNBC.	(134)
Development of nano-DDs for Dox in TNBC	Liposomes, micelles, nanogels, exosomes, etc.	Enhanced Dox targeting, solubility, stability, and tumor inhibition with reduced systemic toxicity.	Advocates for DDs to improve efficacy and minimize side effects in TNBC therapy.	(135)
Pluronic P123-modified nano-micelles for treating drug-resistant breast cancer	Pluronic P123 Nano-micelles	Increased apoptosis, reduced P-gp expression, and enhanced Dox efficacy in resistant cells.	Supports the use of nano-micelles to overcome multidrug resistance in TNBC.	(136)
Nano-curcumin supplementation against Dox-induced cardiotoxicity in breast cancer patients	Nano-curcumin	Reduced cardiotoxicity; preserved cardiac function (LVEF and LVEDV) with no symptomatic cardiomyopathy.	Confirms the cardioprotective potential of nano-curcumin in Dox-based therapies.	(137)

.

Dox is a widely used chemotherapeutic agent that exerts its anticancer effects through multiple cellular mechanisms (123). Its primary action involves intercalating into DNA, where it disrupts the structural integrity of the double helix (123). By inserting itself between the base pairs of the DNA, Dox inhibits the activity of topoisomerase II, an enzyme essential for DNA replication and repair (123). Normally, topoisomerase II creates temporary breaks in the DNA to allow the strands to unwind during replication (123). Dox interferes with this process, leading to the accumulation of DNA breaks (123). This disruption ultimately results in genomic instability and triggers the apoptotic pathways, promoting programmed cell death in rapidly dividing cancer cells (123).

In addition to DNA intercalation, Dox generates ROS, such as superoxide anion radicals, hydrogen peroxide, and hydroxyl radicals (138). The production of ROS induces oxidative stress, which further damages cellular components, including lipids, proteins, and DNA (138). This oxidative damage exacerbates the effects of DNA intercalation, enhancing the cell's susceptibility to apoptosis (138). Mitochondria are particularly vulnerable to ROS, and their dysfunction leads to mitochondrial membrane permeabilization and the release of cytochrome c, which activates the mitochondrial pathway of apoptosis (138). The combined effect of DNA damage and oxidative stress overwhelms the cancer cell's survival mechanisms, ultimately leading to cell death (123, 138).

Another critical mechanism through which Dox exerts its effects is by interfering with the cancer cell's DNA repair mechanisms (139). Dox inhibits the repair of double-strand DNA breaks, specifically by suppressing the non-homologous end joining (NHEJ) repair pathway (139). The failure to repair these breaks allows the accumulation of DNA damage, which activates cell cycle checkpoints and triggers

apoptosis (139). Dox-induced cell cycle arrest occurs predominantly in the G2/M phase, where the cell is prevented from entering mitosis with damaged DNA (140). This delay in cell cycle progression, combined with accumulated DNA damage, ensures that cancer cells either repair the damage or undergo apoptosis, thus preventing uncontrolled proliferation (139, 140) .

Dox also exerts effects on tumor angiogenesis, the process by which tumors recruit new blood vessels to supply their growing mass. By targeting endothelial cells, Dox interferes with their ability to form new capillaries, thereby limiting the tumor's access to nutrients and oxygen (141). This reduction in blood supply not only promotes cancer cell death but also inhibits metastasis, as the newly formed blood vessels are crucial for tumor cell dissemination to distant organs (142). By impeding angiogenesis, Dox further curtails the tumor's ability to expand and spread (141).

However, resistance to Dox can develop in cancer cells, primarily through mechanisms such as overexpression of P-gp, which acts as an efflux pump to remove Dox from the cell (121). This decreases the intracellular concentration of the drug, rendering it less effective (121) . Other mechanisms of resistance include alterations in the drug target (topoisomerase II), enhanced DNA repair capabilities, and the activation of anti-apoptotic signaling pathways (123) . To overcome these challenges, researchers are focusing on developing advanced drug delivery systems, such as liposomes and nanoparticles, which can bypass P-gp-mediated drug efflux and improve the accumulation of Dox in tumor cells (143). These innovative formulations aim to enhance the therapeutic efficacy of Dox while minimizing its systemic toxicity (143).

1.5 Co-delivery of Cur and Dox Using Various Nanocarriers

Numerous studies have explored the co-delivery of Cur and Dox using various nanocarriers, particularly niosomes, to improve breast cancer treatment by overcoming key challenges such as multidrug resistance MDR, systemic toxicity, and enhancing therapeutic efficacy. These studies offer valuable insights into the potential of nanocarriers but also highlight the existing gaps in understanding optimal formulations and clinical applicability.

One of the earliest studies developed a pH-responsive niosomal formulation for co-loading Dox and Cur. This formulation achieved high encapsulation efficiencies (77.06% for Dox and 79.08% for Cur) and demonstrated pH-sensitive drug release. The co-loaded niosomes exhibited synergistic effects, significantly reducing MCF-7 cell viability (to 26%) while sparing normal cells (L929). Compared to the co-administration of individually loaded niosomes, this formulation displayed superior therapeutic efficacy

(91). This study emphasizes the importance of pH sensitivity in targeting tumor tissues, which are often more acidic than normal tissues, thus enhancing drug release specifically at the tumor site.

In contrast, a comparative study of PEGylated and non-PEGylated niosomes revealed that PEGylation significantly improved stability and drug encapsulation efficiency (~95% for Cur and ~84% for Dox), resulting in prolonged drug release. The PEGylated formulation showed enhanced cytotoxicity against MCF-7 cancer cells (IC_{50} ~20.7 μg/mL) and better selectivity for cancer cells over normal cells. Non-PEGylated niosomes, while showing higher immediate cellular uptake, were less stable (144). This finding highlights the role of PEGylation in enhancing the pharmacokinetic properties of niosomal formulations, though non-PEGylated niosomes might be useful for applications where rapid drug uptake is crucial.

Further research focused on the synergistic effects of Cur and Dox co-loaded in niosomes demonstrated improved drug synergy and reduced drug resistance. One study found that this co-encapsulation enhanced cellular uptake, reduced drug resistance, and significantly improved cytotoxicity in MCF-7 breast cancer cells. The sustained release of drugs also improved therapeutic outcomes compared to single-drug-loaded niosomes (145, 146) These studies underscore the importance of drug synergy in overcoming the challenges posed by drug resistance and the potential of co-delivery systems in maximizing therapeutic efficacy.

Additionally, a study employing a quaternary ammonium palmitoyl glycol chitosan (GCPQ) nanocarrier for co-delivery of Dox and Cur demonstrated sustained drug release and high cytotoxicity (88%) in CAL-51 cells. The GCPQ nano micelles showed superior apoptosis induction (93%) compared to free drugs, and *in vivo* studies indicated targeted accumulation, reduced cardiotoxicity, and prolonged retention in the liver and spleen (147).This study demonstrates the potential of using more complex nanocarriers like GCPQ to enhance drug targeting and reduce toxicity.

Multifunctional niosomes incorporating Pluronic surfactants and targeting ligands, such as transferrin and folic acid, further enhanced cellular uptake in breast cancer cell lines (MCF-7 and MDA-MB-231). These formulations showed improved apoptosis induction and reduced cancer cell viability compared to single-drug formulations (148).This approach emphasizes the potential of combining active targeting with drug co-delivery to improve therapeutic selectivity and efficacy.

While all these formulations show promise, they have certain limitations. While *in vitro* results are encouraging, there is a lack of long-term data on the stability and clinical translation of these formulations. Moreover, the optimal balance between drug synergy, release kinetics, and toxicity remains unclear. For instance, while PEGylation improves stability, it may also limit the immediate cellular uptake observed in

non-PEGylated formulations. Additionally, while multifunctional systems like those incorporating targeting ligands show improved efficacy, their complexity may pose challenges in scalability and manufacturing for clinical use (***Table 1-8***).

Table 1-8. Nanocarrier-Based Co-Delivery of Cur and Dox in Cancer Therapy

Study Description	Nanocarrier Type	Key Features	Cell Lines Tested	Drug Release Characteristics	Outcome	Ref.
Development and evaluation of a pH-responsive niosomal formulation for co-loading Dox and Cur in breast cancer therapy.	pH-responsive niosomes	High encapsulation, pH-sensitive release	MCF-7, L929	pH-sensitive, high encapsulation efficiency	High encapsulation efficiencies (77.06% for DOX, 79.08% for Cur), pH-sensitive drug release, and synergistic effects reducing MCF-7 cell viability to 26%.	(91)
Comparative analysis of PEGylated and non-PEGylated niosomes for co-loading Cur and Dox.	PEGylated and non-PEGylated niosomes	Stability, encapsulation, prolonged release	MCF-7	Prolonged in PEGylated, immediate in non-PEGylated	PEGylated niosomes showed improved stability, higher drug encapsulation (~95% Cur, ~84% DOX), and prolonged release. Non-PEGylated niosomes showed higher immediate uptake but less stability.	(144)
Co-encapsulation of Cur and Dox in niosomes for enhanced cancer therapy.	Niosomes	High encapsulation, sustained release, synergistic effects	MCF-7	Sustained release, high encapsulation	High encapsulation (~90% Cur, ~85% DOX), sustained drug release, synergistic effects improving cellular uptake, reducing drug resistance, and enhancing cytotoxicity.	(145)
Co-encapsulation of Cur and Dox in niosomal nanocarriers for enhanced therapy.	Niosomal nanocarriers	Solubility improvement, apoptosis induction	MCF-7	Controlled, apoptosis induction	Enhanced cytotoxicity, improved Cur solubility, and doxorubicin's therapeutic index. controlled release and significant apoptosis induction in cancer cells.	(146)
Development of GCPQ nanocarrier for co-delivery of Dox and Cur to overcome MDR in breast cancer.	GCPQ Nanocarriers with self-targeting via EPR effect	Targeted delivery, reduced cardiotoxicity, validated by in vivo studies in Balb/c mice	CAL-51	Sustained release, reduced toxicity	Sustained release, high cytotoxicity (88%), superior apoptosis induction (93%) compared to free drugs. In vivo targeted accumulation with reduced cardiotoxicity	(147)

Co-delivery of Dox and Cur using multifunctional niosomes with Pluronic surfactants and targeting ligands.	Multifunctional niosomes	Targeting ligands (transferrin, folic acid), improved uptake	MCF-7, MDA-MB-231	Synergistic release, improved uptake	Enhanced cellular uptake in MCF-7 and MDA-MB-231 cells, synergistic effects improving apoptosis induction and reducing cancer cell viability compared to single-drug formulations.	(148)
Co-delivery of Dox and Cur using nanocarriers to enhance therapeutic efficacy in cancer therapy.	Nanocarriers	Synergistic effects, enhanced bioavailability	General cancer lines	Controlled release, reduced toxicity	Synergistic cytotoxic effects, enhanced bioavailability, controlled release, and reduced systemic toxicity, particularly minimizing Dox-induced cardiotoxicity.	(149)
Co-delivery of Cur and Dox using nanocarriers for various cancer therapies.	Nanocarriers	Multifunctional approach, therapeutic and diagnostic capabilities	Various cancer lines	Enhanced bioavailability, prolonged circulation	Enhanced therapeutic efficacy in gastric, prostate, and ovarian cancers, promoting apoptosis in lung cancer cells. Multifunctional approach with therapeutic and diagnostic capabilities.	(150)
Co-loading of Cur and miRNA-34a in niosomes for targeted breast cancer therapy.	Niosomes	Synergistic effects, overcoming drug resistance	MCF-7	Enhanced cellular uptake, cytotoxicity	Niosomes enhanced cytotoxicity and apoptosis induction in cancer cells. Synergistic effects overcoming drug resistance and reducing systemic toxicity.	(151)
Co-delivery of Cur and Dox using various nanocarriers for synergistic effects.	Various nanocarriers	Improved therapeutic efficacy, bioavailability	Various cancer lines	Prolonged circulation, enhanced bioavailability	Cur improved Dox's therapeutic efficacy by inhibiting MDR pathways (e.g., P-gp), enhancing apoptosis, reducing toxicity. The formulation improved bioavailability and prolonged circulation.	(152)
Niosomes (Span 60, Tween) for dual delivery of Cur and Dox to HeLa cells.	Niosomes (Span 60, Tween)	Dual-phase release, synergistic effects	HeLa	Two-phase release, synergistic effects	Two-phase drug release, with Dox released early and Cur over an extended period. Synergistic cytotoxic effects, enhancing anti-cancer effectiveness.	(153)

This research focuses on overcoming critical barriers in cancer treatment by designing advanced drug delivery systems that specifically target cancer cells while minimizing harm to healthy tissues. By

integrating LHRHD and alendronate into the formulations, this targeted approach enhances therapeutic precision, reducing systemic toxicity and improving treatment outcomes.

A key innovation in this work was optimizing drug delivery for both hydrophilic Dox and hydrophobic Cur compounds. These nanoparticles demonstrated high drug loading (DL%) and EE%, ensuring effective delivery and sustained release of therapeutic agents. Comprehensive characterization techniques, including FTIR for chemical modification, X-ray photoelectron spectroscopy (XPS) for conjugation confirmation, HPLC for drug encapsulation metrics, and DLS for particle size and uniformity, ensured the robustness and reliability of the formulations. This systematic approach addressed common issues of instability and inconsistency in nanoparticle preparation.

To evaluate efficacy, I conducted *in vitro* studies using MDA-MB-231 cancer cells. Cell viability assays confirmed the nanoparticles' ability to reduce cancer cell proliferation, while live-cell imaging provided insights into cellular uptake and therapeutic impact. Importantly, 3D spheroid models were employed to replicate the tumor microenvironment, offering a more realistic assessment of the nanoparticles' anticancer potential. These studies validated the synergistic effects of co-delivering Cur and Dox, which enhanced cytotoxicity and addressed multidrug resistance—a significant challenge in cancer therapy.

Additionally, my research tackled technical challenges in nanoparticle preparation. Incorporating F127 into the formulation improved stability and prevented adhesion issues, making the process more efficient and reproducible. These enhancements not only refined the nanoparticle design but also advanced the scalability of the system for potential clinical applications.

This work offers a comprehensive strategy to address major limitations in cancer therapy, including poor drug targeting, multidrug resistance, and short drug half-life. Future studies will focus on *in vivo* testing and fine-tuning drug release profiles to further bridge the gap between lab-based research and clinical translation. Ultimately, this research contributes to the growing field of nanomedicine, providing a pathway toward safer and more effective cancer treatments.

Chapter 2. LHRH Receptor-Targeted Curcumin Nanomicelles for Enhanced TNBC Therapy

2.1 Introduction

BC is a prevalent cancer among women, marked by the uncontrolled proliferation of breast tissue cells (154, 155). Its classification depends on the expression of hormone receptors, including estrogen, progesterone, and HER2, which help determine therapeutic strategies (1). TNBC, a highly aggressive form, lacks these receptors, rendering it unresponsive to hormonal and HER2-targeted treatments (2).

Additionally, there is currently no highly effective targeted therapy for TNBC based on tumor biology and all current modalities have significant shortcomings. Plant-derived compounds, including Cur, a bioactive yellow-orange polyphenol derived from turmeric, have been reported to modulate dysregulated signaling pathways in TNBC (94), (156, 157). Cur has also shown promising applications in pharmacology and cancer therapy through preclinical research (158, 159), in TNBC (MDA-MB-231) cells, Cur suppresses growth and proliferation, diminishes cell viability, lowers the mitotic index, and promotes apoptosis (160).

Beyond its direct antitumor effects, Cur has been shown to enhance TNBC patients' responsiveness to conventional chemotherapy. Clinical trials indicated that when Cur is co-administered with paclitaxel or FOLFOX-based chemotherapy, overall response rates improve compared to chemotherapy alone (161, 162). However, Cur's poor solubility and bioavailability have hindered its clinical application. To overcome these limitations, novel Cur formulations—particularly nanoparticle-based delivery systems such as nanomicelles—are being investigated to improve its pharmacokinetic properties by increasing its solubility, circulation time, and tumor accumulation, ultimately enhancing its therapeutic impact (163, 164) .

Nanomicelles are self-assembling colloidal structures, typically ranging in size from 10 to 100 nm, characterized by a hydrophobic core surrounded by a hydrophilic shell (165).

Here, we present the development of a polymeric-based nanomicelle formulation, surface-functionalized with two distinct luteinizing hormone-releasing hormone (LHRH) analogs and loaded with Cur. gonadotropin-releasing hormone (GnRH), also known as LHRH, is a decapeptide (pGlu-His-Trp-Ser-Tyr-Gly-Leu-Arg-Pro-Gly-NH2) synthesized in the hypothalamus, playing a pivotal role in stimulating the ovaries and testes to produce and release estrogen and testosterone, respectively. Apart from the physiological role of LHRH receptors, they have been shown to be highly expressed in certain tumors. The differential expression levels of peptide hormone receptors in healthy and cancerous tissues provide a

unique opportunity for targeted treatment strategies (166-170). Previous studies have demonstrated that approximately 50% of human TNBC specimens express LHRH receptors (171). Moreover, recent findings highlight that LHRH peptides or their analogs can serve as effective carriers for targeted delivery of drugs, selectively delivering therapeutic agents to cancer cells with high LHRH receptor expression while sparing healthy cells with minimal or no receptor expression (172).

To overcome Cur's poor water solubility, low systemic bioavailability, rapid metabolism, and insufficient tumor accumulation, this study utilized Pluronic® F127-based micelles conjugated with two LHRH derivative peptides. Pluronic® F127 (**Figure 2-1**), a triblock copolymer composed of hydrophilic polyethylene oxide (PEO) and hydrophobic polypropylene oxide (PPO) blocks, was chosen for its biocompatibility, superior drug-loading capacity, and ability to form stable micelles with a hydrophobic core (173). This polymer also improves the solubility and stability of hydrophobic drugs like Cur (174). Furthermore, the hydrophilic corona of F127 reduces opsonization by the immune system, prolonging circulation time *in vivo* (173). By incorporating F127 into the NPs formulation, an optimal environment for drug encapsulation and delivery was created, enhancing therapeutic efficacy due to potentially improving Cur delivery and pharmacokinetics in the body (173).

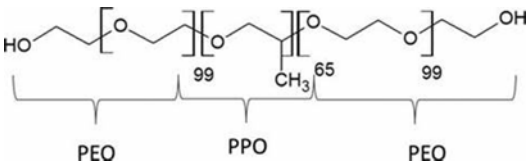

***Figure 2-1*. Structure of Pluronic® F127**

To further improve peptide stability and facilitate efficient conjugation with the F127 polymer, structural modifications were made to the original LHRH peptide. Specifically, Gly at position 6 (Gly6) in LHRH sequence was replaced with D-Lys^6 to yield [k^6]LHRH (***Figure 2-2*.A**), while an Ahx group was added to D-Lys^6 achieving [k^6(Ahx)]LHRH (***Figure 2-2*.B**). These modifications not only allowed the mi-sequence conjugation of the peptides to the polymer but also increased their binding affinity to LHRH receptors [unpublished data]. The formulation was evaluated using TNBC cell line, providing a promising approach for targeted cancer therapy.

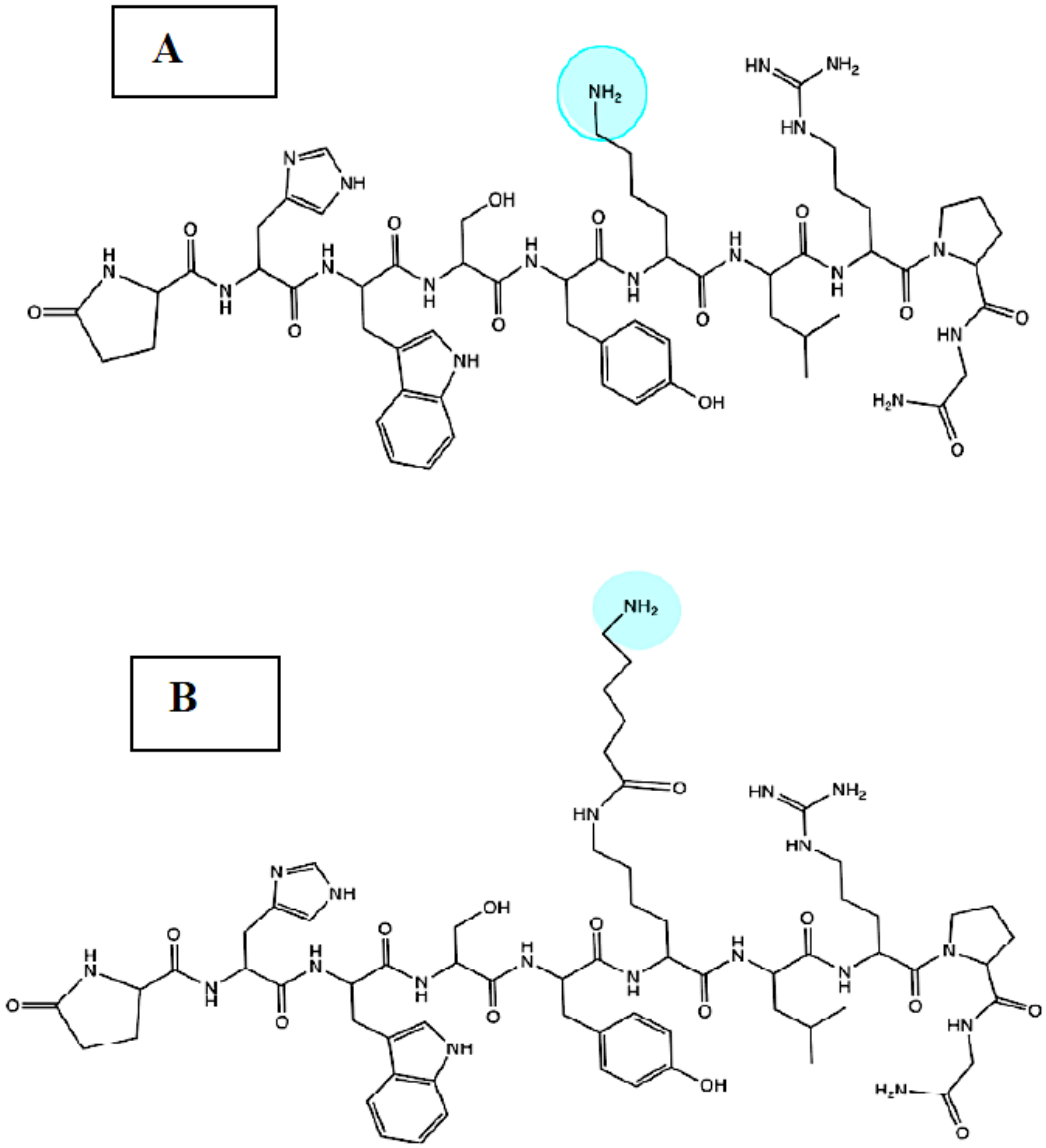

Figure 2-2. Chemical structure of the two LHRH peptides used for targeting.

A) [K⁶]LHRH: Glp-His-Trp-Ser-Tyr-D-Lys-Leu-Arg-Pro-Gly-NH_2
B) [K⁶(Ahx)]LHRH: Glp-His-Trp-Ser-Tyr-D-Lys(Ahx)-Leu-Arg-Pro-Gly-NH_2

2.2 Material and Instruments

Material

Succinic anhydride (SA), 1-ethyl-3-(3-dimethylaminopropyl) carbodiimide hydrochloride (EDC· HCl), 4-dimethylaminopyridine (DMAP), 1,4-dioxane, dichloromethane (DCM), curcumin (purity >65%), Pluronic® F127, Roswell Park Memorial Institute (RPMI)-1640 medium, fetal bovine serum (FBS), trypsin, and Phosphate Buffered Saline (PBS) were obtained from Sigma-Aldrich, Australia. Hexane was sourced from Chemical Reagents, Australia, while alendronate sodium trihydrate was kindly provided by Alcon Biosciences, India. Human breast cancer cells (MDA-MB-231) were acquired from the American Type Culture Collection (ATCC) and maintained at 37°C in a humidified atmosphere containing 5% CO_2, using RPMI medium supplemented with 10% FBS. Additionally, LHRH analogues, [k^6]LHRH and [k^6(Ahx)]LHRH, were synthesized via Fmoc solid-phase peptide synthesis (SPPS) following previous studies (175, 176) by our previous members (177, 178).

Instruments

Freeze-drying of the formulated micelles was carried out at 50°C using an Alpha 2-4 LD plus freeze dryer from Christ (Osterode am Harz, Germany). Initially, the micelle solution was frozen at -70°C for 2 hours, then transferred to a pre-equilibrated freeze dryer chamber at 40°C and depressurized to 5 Pa. Primary drying was conducted at 40°C for 18 hours, followed by secondary drying at 20°C for 6 hours.

Particle size and zeta potential of Cur-loaded micelles were measured using dynamic light scattering (DLS) with a Nano Series ZS Zetasizer from Malvern Instruments (Malvern, UK). Analytical reverse-phase high-performance liquid chromatography (RP-HPLC) was performed on a Shimadzu Prominence system (Kyoto, Japan) equipped with a C18 column (Nova Pak, 150 × 4.6 mm) and a diode array detector (Shimadzu SPD-M20A) to determine the DL% and EE%. Centrifugation was performed using an Allegra X-30R centrifuge (Beckman Coulter, USA). Live cell imaging was conducted using the IncuCyte® S3 Live Cell Analysis System (Essen Bioscience, Michigan, USA), while plate readings for *in vitro* cytotoxicity assessments were obtained using a VICTOR X4 plate reader (PerkinElmer, U.S.)

Functional group analysis of the NPs was performed using attenuated total reflectance Fourier transform infrared spectroscopy (ATR-FTIR) on a Bruker Alpha spectrometer equipped with a germanium crystal (Bruker, MA, USA). Both the background and the sample were scanned 128 times with a spectral resolution

of 4 cm^{-1} across a range of 400–4000 cm^{-1}. Data analysis was conducted using OPUS software (version 8.7.31).

The surface chemical composition of the NPs were evaluated using XPS with the Thermo Fisher K-Alpha XPS system (Thermo Fisher Scientific, E. Grinstead, UK).

Additionally, cellular uptake and distribution of the formulations were visualized with Leica SPE-II Confocal Laser Scanning Microscopy (CLSM).

Also, rotary evaporator (Rotavapor® R-300, Büchi, Switzerland) was used for solvent evaporation during the preparation of thin films and the hydration of NPs.

2.3 Methods

2.3.1 Converting the terminal hydroxyl groups of Pluronic® F127 to carboxyl groups (Pluronic®F127-succinate)

The terminal hydroxyl groups of Pluronic® F127 were modified to carboxyl groups to enable subsequent conjugation (179). In summary, 10 g of Pluronic® F127 was dissolved in 45 mL of anhydrous DCM. Succinic anhydride (1 g) and DMAP (100 mg) were then added to the solution, and the reaction was carried out under reflux at 60°C with continuous stirring overnight (***Figure 2-3***). The resultant product, Pluronic® F127 succinate, was isolated by precipitation using an excess of hexane. To eliminate residual succinic anhydride, the polymer underwent dialysis against methanol for 24 hours, followed by freeze-drying. The successful conversion of Pluronic® F127 to Pluronic® F127 succinate was confirmed by FTIR.

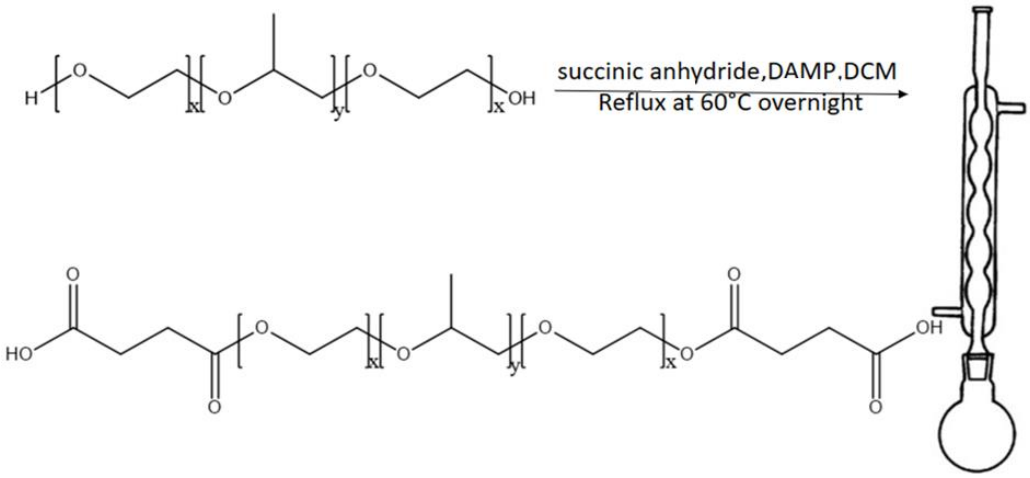

Figure 2-3. Synthesis of F127-Succinate.

Synthesis of Pluronic® F127 functionalized with carboxyl groups (F127-Succinate) with x = 101 and y = 56.

2.3.2 Conjugation and characterization of LHRH peptide analogs to F127-Succinate (F127-COOH)

As outlined in a previous study conducted by our group (180), two derivatives of LHRH peptides, [k^6]LHRH and [k^6(Ahx)]LHRH, were synthesized on a Rink amide resin using the in situ neutralization method via Fmoc SPPS and characterized by high resolution electrospray ionization mass spectrometry (ESI-MS) and HPLC. The peptides were then conjugated to F127-COOH using carbodiimide coupling chemistry. To begin with, F127-COOH (0.02 mmol, 270 mg) was dissolved in 10 mL of Milli-Q water and ultrasonicated for 10 minutes. After stirring the solution for 30 minutes, NHS (MW: 115.09, 0.026 mmol, 2.3 mg) and EDC (MW: 191.70, 0.026 mmol, 4.6 mg) were added to activate the carboxyl groups of F127-COOH. The solution was then divided into two portions, and each was separately combined with a LHRH derivative: [k^6]LHRH (12.5 mg) or [k^6(Ahx)]LHRH (13.5 mg), added dropwise. The reaction mixtures were stirred continuously at room temperature for 24 hours. To eliminate unbound peptides and EDC, the conjugated polymers were purified via dialysis against water for 24 hours using a dialysis bag with a 12 k Da cut-off. Finally, the purified products, [k^6] and [k^6(Ahx)]LHRH polymeric nanomicelles (**Figure 2-4 A** and **B**), were freeze-dried for further material characterization. To confirm the success of the conjugation XPS was performed to verify surface elemental composition and confirm successful conjugation. The conjugated peptide-polymer powder was mounted on the XPS sample holder by adhering them to indium

foil fixed onto carbon tape. High-resolution spectra for carbon (C 1s), nitrogen (N 1s), and oxygen (O 1s) were collected along with survey scans. Data was analyzed using Advantage software.

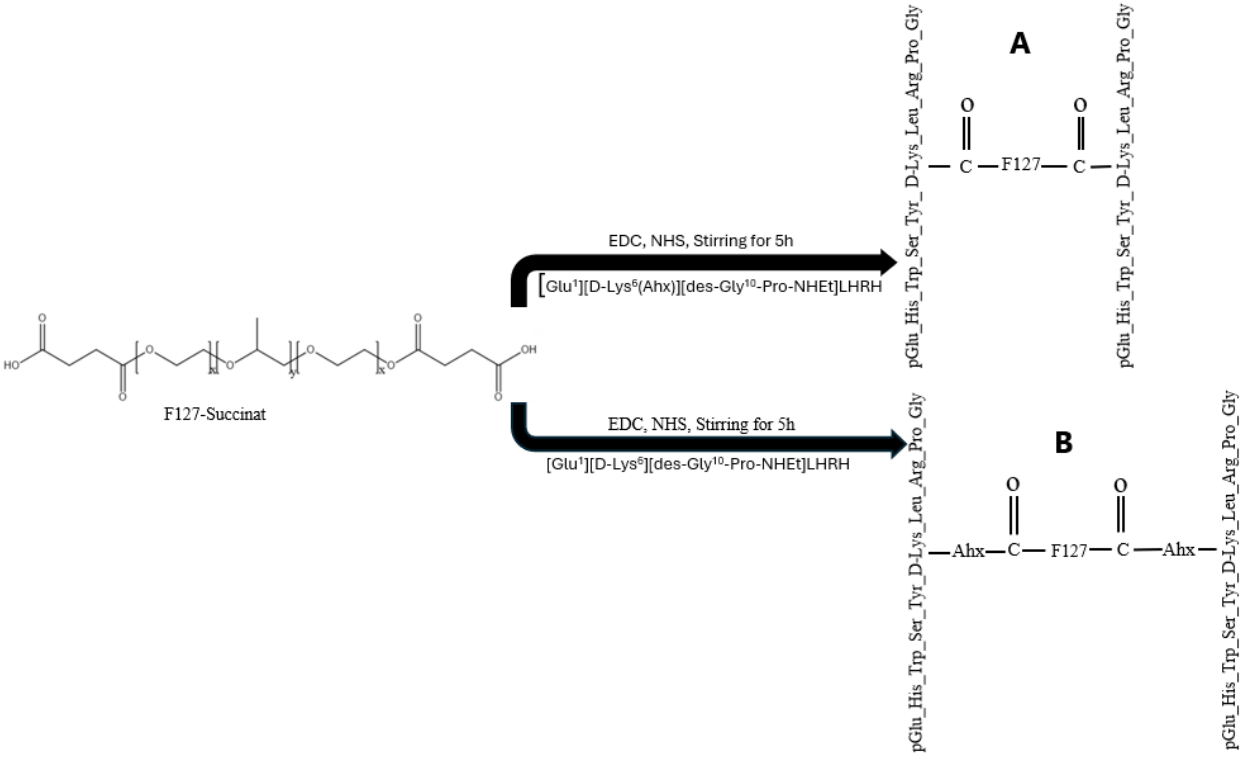

Figure 2-4. Conjugation of LHRH Peptides to F127-Succinate.

[k^6]LHRH (A) and [k^6(Ahx)]LHRH (B) functionalized Pluronic® F127

2.3.3 Loading of curcumin into [k^6] and [k^6(Ahx)]LHRH polymeric nanomicelles

Curcumin was encapsulated into the [k^6] and [k^6(Ahx)]LHRH polymeric nanomicelles using the thin-film hydration method(180). To prepare the nanoparticles, Cur was also incorporated into Pluronic® F127. Briefly, 4 mg of Cur dissolved in 5 mL of methanol was combined with 40 mg of Pluronic® F127, [k^6], or [k^6(Ahx)]LHRH-F127 separately. The mixtures of organic solvents were vacuum evaporated at 40°C to form polymer thin films. The films were then vacuum-sealed and left at room temperature overnight to eliminate any residual solvent. To prepare the micellar suspensions, 3 mL of Milli-Q water was added to each film, followed by hydration for 1 hour at 50°C with constant stirring at 200 rpm. Any large particles or free-Cur in the suspensions were removed using a 0.22 µM membrane filter (181). Finally, the resulting

polymeric nanomicelles F127-Cur, [k^6]LHRH-Cur, and [k^6(Ahx)]LHRH-Cur were lyophilized at -20°C and stored at -80°C for future use.

2.3.4 Physicochemical characterizations of the produced nanomicelles

2.3.4.1 Dynamic light scattering (DLS)

The particle size, zeta potential, and polydispersity index (PDI) of the NPs were measured using DLS at room temperature. In brief, 1 mg of NPs was dissolved in 1 mL of Milli-Q water, and the dispersion was homogenized using a vortex mixer to ensure uniform distribution of micelles.

2.3.4.2 Drug loading (DL%) and encapsulation efficiency (EE%)

The drug loading of Cur-loaded NPs was quantified using HPLC. To remove free-Cur, 5 mg of freeze-dried polymer was dissolved in water, centrifuged at 7379 g for 10 mins, and the supernatant was lyophilized. The dry residue was dissolved in DCM, and the evaporated DCM residue was reconstituted in the HPLC solvent to prepare a 1 mg/mL solution. Standard curves of free-Cur were used to calculate DL% and EE%.

DL% =Loaded Curcumin/Weight of NPs×100

EE% =Actual drug loading/Theoretical drug loading×100

2.3.5 *In vitro* experiments

2.3.5.1 Alamar Blue cell viability assay

The viability and proliferation of MDA-MB-231 cells were evaluated using the Alamar Blue assay. Cells were seeded into a 96-well plate and allowed to adhere overnight. Then, 10 µL of [K^6(Ahx)]LHRH-Cur, [K^6]LHRH-Cur, and Cur nanomicelles were added in eight serial dilutions (50, 16.66, 5.55, 1.85, 0.61, 0.2, 0.06, and 0.02 µM). For void nanoparticles (F127-based without drug), additional concentrations of 100 and 200 µM were tested to ensure that their IC50 exceeded 100 µM. PBS was used as a negative control, while Sodium Dodecyl Sulphate (SDS) served as a positive control. The cells were incubated for 72 hours. After incubation, 10 µL of Alamar Blue reagent was added to each well, and the plate was incubated for an additional four hours. Living cells metabolized the reagent, causing a color change from blue to pink, with the intensity of the color change directly corresponding to the number of viable cells. The absorbance of the pink supernatant was measured at 570 nm using a Victor X plate reader.

2.3.5.2 *In vitro* cytotoxicity assessment

In a flat-bottom 96-well plate, 5000 MDA-MB-231 cells per well were seeded and allowed to adhere for 24 hours. Nanomicelles of [k^6]LHRH-Cur, [k^6(Ahx)]LHRH-Cur, and F127-Cur were applied at concentrations of 5.5, 16.6, and 50 µM. Time-lapse images (4 per well every two hours) were captured over 48 hours using the IncuCyte® S3 Live-Cell Analysis System (Essen Bioscience, USA) at 20x magnification. The imaging system was configured to detect green fluorescence with a phase-contrast background and a laser set to excitation/emission at 480/550 nm. The green fluorescence signal arises from the intrinsic fluorescence of curcumin, allowing real-time monitoring of its cellular uptake and distribution. For each well, the IncuCyte captured four images from different regions, and representative images in the result section were selected from different areas of the same well to better illustrate differences between conditions.

2.3.5.3 Cellular uptake

MDA-MB-231 cells were seeded onto coverslips placed in a 24-well plate, with 50,000 cells per well and allowed to grow for an overnight. After removing the existing media, 180 µL of fresh media was added to each well. The cells were then treated with [k^6]LHRH-Cur, [k^6(Ahx)]LHRH-Cur, and F127-Cur, followed by incubation at 37°C for 24 hours. After incubation with LHRH-Cur, Cur-loaded nanomicelles, free-Cur, and PBS, the coverslips were washed with PBS.

Cells were fixed for 30 minutes using 200 µL of 4% paraformaldehyde (PFA), either fresh or frozen. The coverslips were then washed three times with PBS. Next, 2 µL of mounting media was applied to microscope slides, and the coverslips were carefully placed cell-side down onto the mounting media. The edges were sealed with nail polish. Finally, the prepared slides were wrapped in foil, stored at 4°C, and analyzed using an X filter on a Confocal Microscope.

2.3.6 Statistical analysis

All statistical analyses in this chapter were performed using GraphPad Prism (version 7). Data are expressed as mean ± standard deviation (SD) from three independent experiments (n = 3). The IC_{50} values were determined by fitting non-linear regression curves (log[inhibitor] vs. normalized response – variable slope). One-way analysis of variance (ANOVA) followed by Tukey's multiple comparison test was

employed to assess statistical significance among different nanoformulations. A *p*-value of less than 0.05 ($p < 0.05$) was considered statistically significant.

2.4 Results

2.4.1 Converting the terminal hydroxyl groups of Pluronic® F127 to carboxyl groups (Pluronic®F127-succinate)

FTIR spectroscopy was used to confirm the chemical modification of Pluronic® F127 to F127-COOH (F127 succinate). The FTIR spectrum of unmodified Pluronic® F127 (Figure 2-5) does not exhibit a peak in the carbonyl region (~1700 cm^{-1}). In contrast, the FTIR spectrum of F127-COOH shows a distinct absorption band at 1720 cm^{-1}**,** corresponding to the C=O stretching vibration of carboxylic acid groups. This confirms the successful introduction of terminal carboxyl groups. Additionally, a broad absorption band observed between 2700-3100 cm^{-1} is attributed to the O–H stretch of the carboxylic acid, further supporting the successful synthesis of F127-COOH.

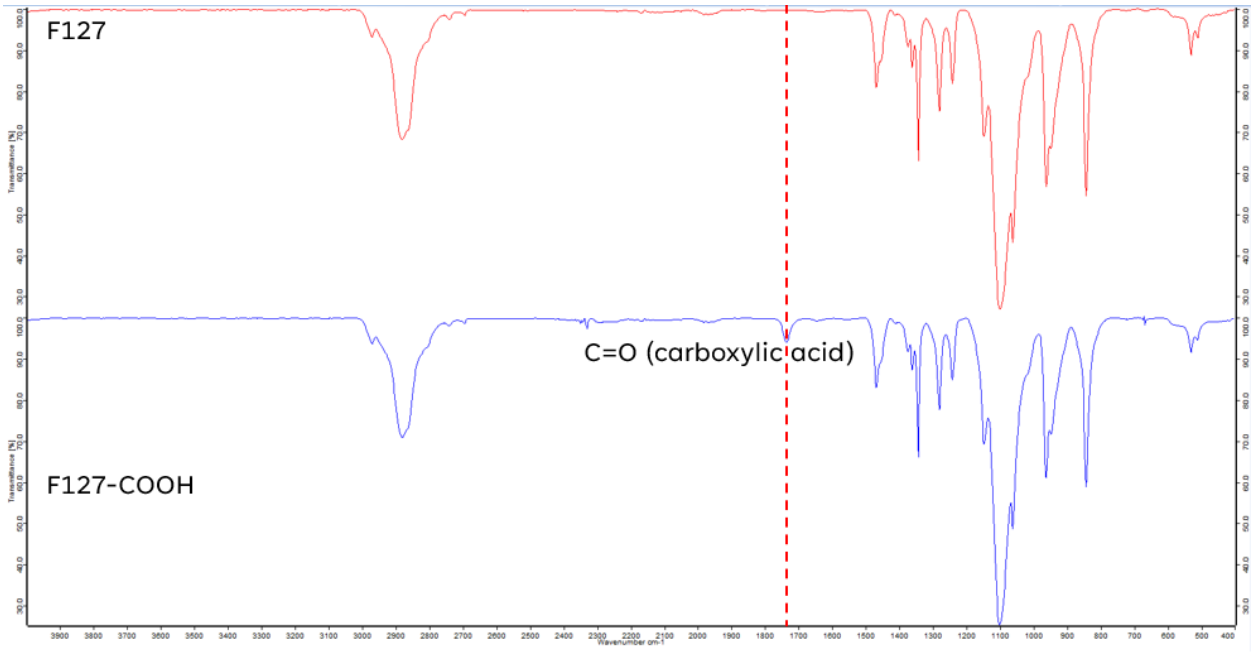

Figure 2-5. FTIR Analysis of Pluronic® F127 and F127-COOH.

The appearance of a characteristic peak in the 1720 cm^{-1} region in F127-COOH, absent in F127, confirms the successful conversion of hydroxyl groups to carboxyl groups in Pluronic® F127.

2.4.2 Conjugation and Characterization of LHRH Peptide Analogs to F127-Succinate via XPS and FTIR Spectroscopy

XPS analysis confirmed the elemental composition which revealed the presence of nitrogen (N) in the final conjugated products, [k^6]LHRH-F127 (1.80%) and [k^6(Ahx)]LHRH-F127 (0.79%), an element that is absent in F127-COOH (

Table 2-1). The detected nitrogen originates from the peptide derivatives, confirming successful conjugation.

The observed differences in nitrogen content between the two conjugates can be attributed to the presence of Ahx with an extra nitrogen group. During the preparation of LHRH-F127-Succinate, 135 mg of polymer and around 13 mg of peptides were used. Since nitrogen is present only in the peptide and not in the polymer, the overall nitrogen content in the final product remains relatively low. Given that the polymer amount is approximately ten times greater than the peptide amount, the resulting nitrogen percentage is expected to be minimal. However, the presence of even this small amount of nitrogen serves as strong evidence of successful peptide conjugation.

To further confirm the success of the peptide–polymer conjugation, FTIR spectroscopy was performed on both [K^6]LHRH-F127 and [K^6(Ahx)]LHRH-F127 conjugates and their corresponding controls. The FTIR spectrum of [K^6]LHRH-F127 (**Figure 2-6 A**) exhibited two distinct peaks around 1638 cm^{-1} and 1520 cm^{-1}, corresponding to the amide I (C=O stretching) and amide II (N–H bending) vibrations, respectively. These characteristic peaks were absent in both the [K^6]LHRH and F127-succinate spectra, confirming the formation of new amide bonds due to covalent linkage between the peptide and polymer.

Similarly, the FTIR spectrum of [K^6(Ahx)]LHRH-F127 (**Figure 2-6 B**) showed a strong absorption band near 1638 cm^{-1} (amide I), indicating successful amide bond formation. While the amide II peak at ~1520 cm^{-1} appeared less pronounced—likely due to overlapping bands or the structural influence of the Ahx spacer—the presence of the amide I band alone provides substantial evidence of conjugation. These features were not observed in the spectra of the unmodified peptide or the F127-COOH control, supporting the covalent attachment of [K^6(Ahx)]LHRH to the F127 backbone.

Together, the XPS and FTIR results confirm the successful conjugation of both LHRH peptide analogs to F127-succinate through stable amide bond formation.

Table 2-1. XPS analysis of [k^6]LHRH and [k^6(Ahx)]LHRH conjugated to Pluronic® F127.

Sample	Elemental composition (%)		
	C	**O**	**N**
F127-COOH	68.4	31.6	-
[K^6]LHRH	63.0	21.7	15.3
[K^6(Ahx)] LHRH	62.1	21.2	16.7
[K^6]LHRH-F127	65.7	32.5	1.80
[K^6(Ahx)]LHRH-F127	70.0	29.2	0.79

A

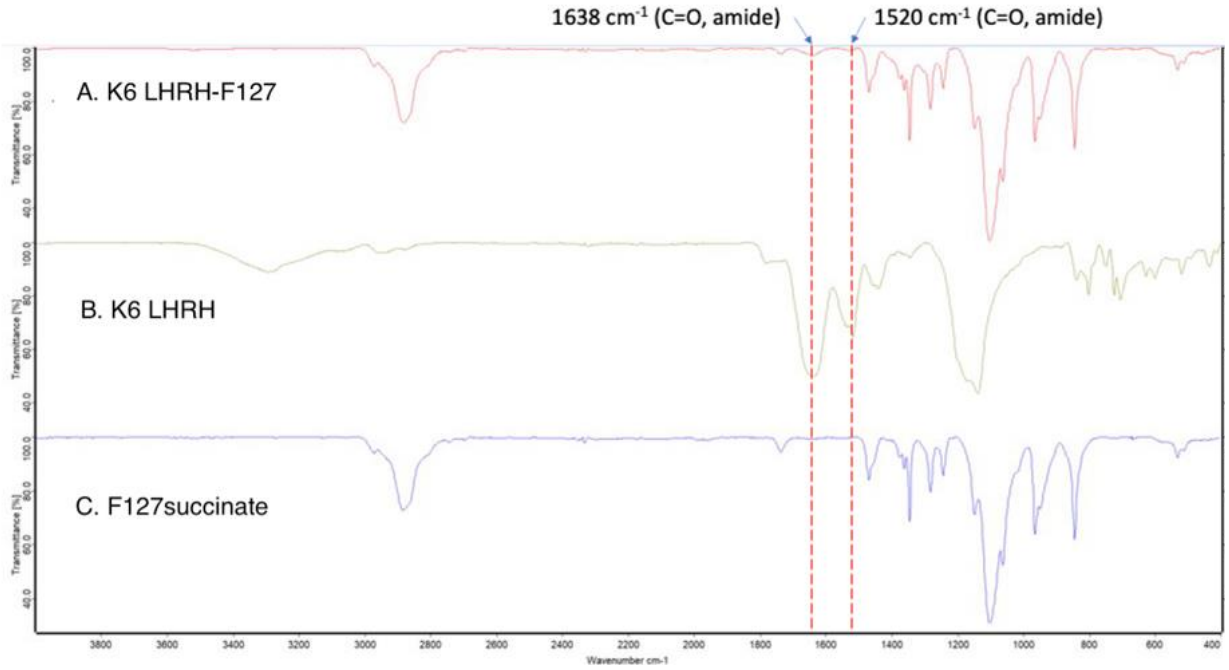
1638 cm-1 (C=O, amide)
1520 cm-1 (C=O, amide)
A. K6 LHRH-F127
B. K6 LHRH
C. F127succinate
Transmittance [%]
Wavenumber cm-1

B

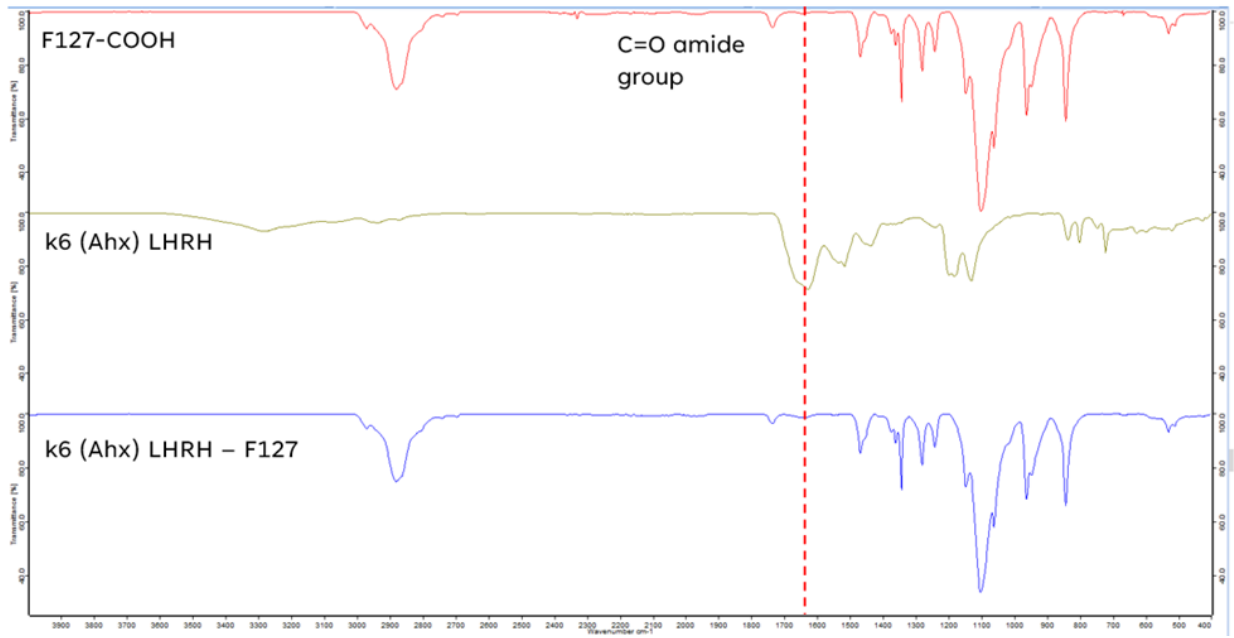

Figure 2-6. FTIR analysis of [K^6]LHRH-F127, [K^6]LHRH, [K^6(Ahx)]LHRH-F127, [K^6(Ahx)]LHRH, and F127-succinate.

A). FTIR spectra of [K^6]LHRH-F127, [K^6]LHRH, and F127-succinate.
Distinct peaks at ~1638 cm^{-1} (amide I) and ~1520 cm^{-1} (amide II) in [K^6]LHRH-F127—absent in controls—confirm successful peptide–polymer conjugation. **B).** FTIR spectra of [K^6(Ahx)]LHRH-F127, [K^6(Ahx)]LHRH, and F127-COOH. The C=O stretch at ~1638 cm^{-1} (amide I) in the conjugated sample—absent in controls—indicates amide bond formation. Amide II (~1520 cm^{-1}) is less prominent, possibly due to Ahx spacer effects.

2.4.3 Physicochemical characterizations of the produced nanomicelles: DLS, DL%, and EE% Measurements

According to DLS size measurements, all nanomicelles were within the low nanoscale range, with sizes of 20 nm, 21 nm, and 32 nm for [k^6]LHRH-Cur, [k^6(Ahx)]LHRH-Cur, and Cur nanomicelles, respectively.

DL% of peptide-conjugated Cur nanomicelles was determined using HPLC based on a standard curve. As shown in (***Table 2-2***), the DL% of [k^6]LHRH-Cur nanomicelles (7.58%) was slightly higher than that of [k^6(Ahx)]LHRH-Cur nanomicelles (7.5%) and Cur nanomicelles (6.75%). All nanoformulations achieved an EE% of over 70%. Also, [K^6]LHRH-Cur micelles was excluded from subsequent optimisation based on preliminary outcomes

Table 2-2. Physicochemical characterizations of LHRH-conjugated Cur-loaded nanomicelles and Cur- loaded nanomicelles (n = 3). (Note: Zeta potential was not measured for [K^6]LHRH-Cur micelles due to early consumption of peptide batch prior to full characterisation.)

Nano-formulation	Drug loading (%)	Encapsulation Efficiency (%)	Z-Average (d.nm)	PDI	Zeta potential (mV)
[K^6]LHRH-Cur micelles	7.5±0.7	82.5±7.21	20.86±10.1	0.22	-
[K^6(Ahx)]LHRH-Cur micelles	7.58±0.74	87.53±8.53	21.01±8	0.25	-12.43±3.95
Cur micelles	6.75±0.2	74.22±2.30	32.24±10.6	0.13	-12.21±5.42

2.4.4 *In vitro* experiments

2.4.4.1 Alamar Blue cell viability assay

The Alamar Blue cell viability assay demonstrated a cytotoxic effect of the formulated nanomicelles against MDA-MB-231 cells. As shown in **Table 2-3**, [K^6(Ahx)]LHRH-Cur nanomicelles exhibited the lowest IC50 value (3.2 ± 0.5 μM), significantly lower than [K^6]LHRH-Cur nanomicelles (6.3 ± 0.8 μM, *$p < 0.05$) and Cur nanomicelles (7.9 ± 3.3 μM, #$p < 0.05$), which were tested in the 0.02–50 μM range.

Void nanoparticles, composed of F127 without any active drug, were tested separately at higher concentrations (up to 200 μM) and showed no significant cytotoxicity, confirming an IC50 value greater than 100 μM. This indicates that the observed cytotoxic effects were attributable to the active agents and not the nanoparticle vehicle.

Statistical analysis indicated (*$p < 0.05$ compared to [K^6]LHRH-Cur-NPs and Cur-NPs; #$p < 0.05$ compared to Cur-NPs; n = 3).

Table 2-3. IC_{50} values of two derivatives of LHRH-Cur-NPs, curcumin NPs and void NPs against MDA-MB-231 cells.

NPs or control	IC_{50} (μM)
[k^6]LHRH-Cur-NPs	6.3±0.8#
[k^6(Ahx)]LHRH-Cur-NPs	3.2±0.5*, #
Cur-NPs	7.9±3.3
Void	>100

2.4.4.2 *In vitro* cytotoxicity assessment

The IncuCyte live-cell imaging analysis at 2, 24, and 48 hours demonstrated a time- and concentration-dependent cellular response to different nanomicelle formulations. At 2 hours, [K^6(Ahx)]LHRH nanomicelles showed early interaction, with noticeable fluorescence at higher concentrations, while [K^6]LHRH nanomicelles exhibited weaker fluorescence and retained an elongated morphology, suggesting lower uptake. Cur nanomicelles displayed fluorescence with minimal morphological changes, and PBS-treated cells remained unaffected (***Figure 2-7*** **A**). By 24 hours, [K^6(Ahx)]LHRH nanomicelles induced significant cell rounding and detachment, with intensified fluorescence, indicating increased uptake and cytotoxicity. [K^6]LHRH nanomicelles caused moderate changes, while Cur nanomicelles maintained cell integrity with visible fluorescence (***Figure 2-7*** **B**). At 48 hours, [K^6(Ahx)]LHRH nanomicelles further increased cell detachment, while [K^6]LHRH nanomicelles showed delayed but progressive cytotoxic effects. Cur nanomicelles remained stable with limited toxicity, and PBS-treated cells retained normal morphology. Overall, [K^6(Ahx)]LHRH nanomicelles exhibited the strongest cytotoxic effect over time, followed by [K^6]LHRH nanomicelles, whereas Cur nanomicelles showed minimal toxicity (***Figure 2-7*** **C**).

A

Time	2 h		
Concentration / Nanomicelle	50 µM	16.66 µM	5.55 µM
K6(Ahx) LHRH nanomicelle	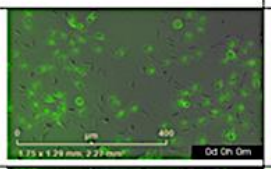	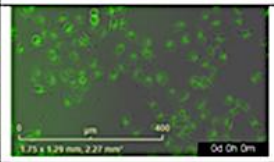	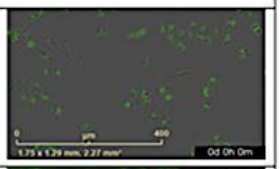
K6 LHRH nanomicelle	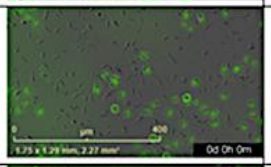	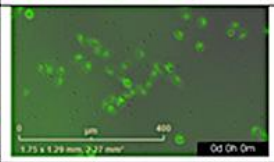	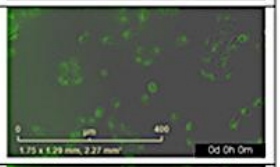
Cur nanomicelle	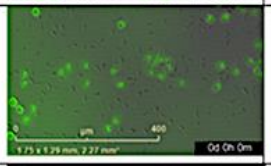	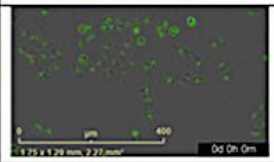	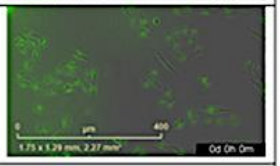
PBS	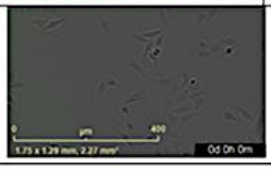		

B

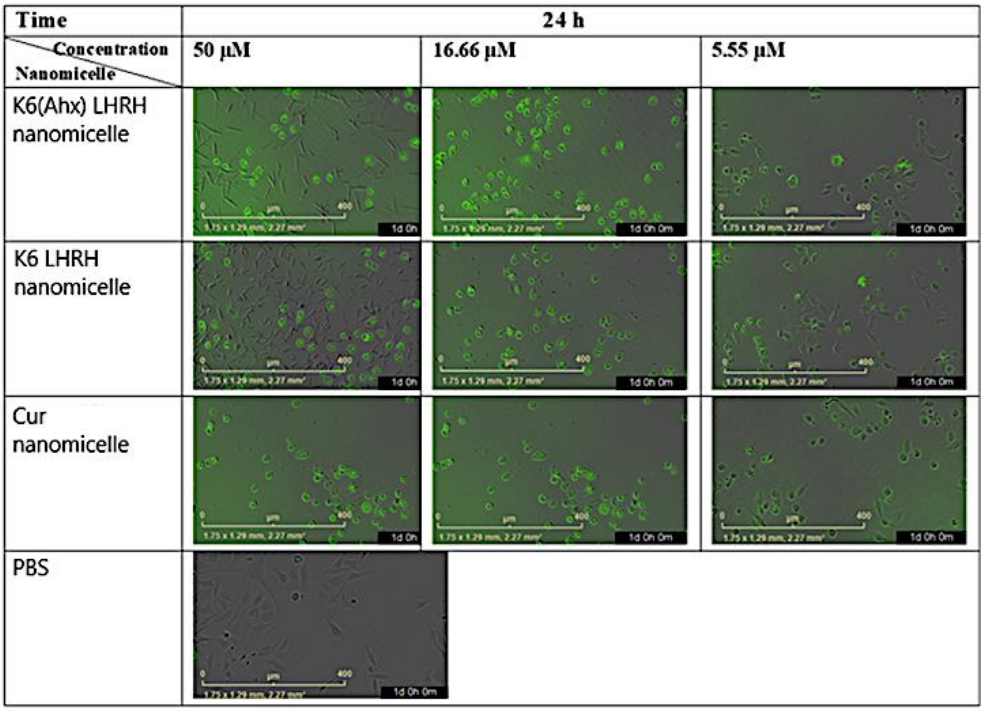

C

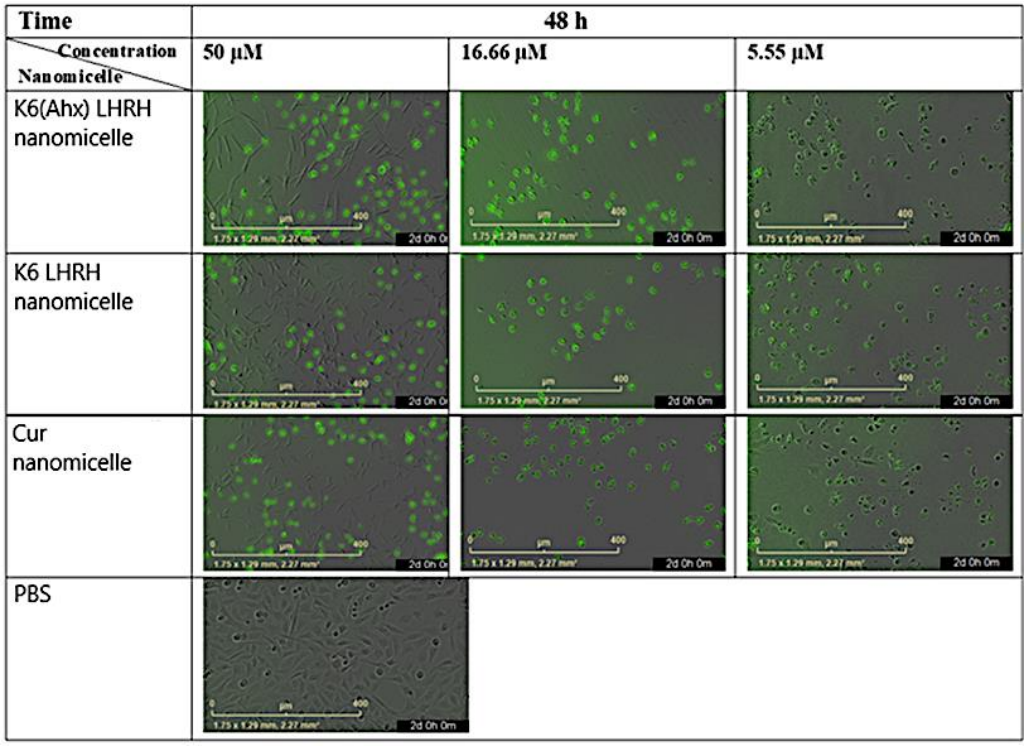

Figure 2-7. Time-Dependent cellular uptake of NPs formulations.

Representative fluorescence microscopy images of MDA-MB 231 cells treated with [K^6(Ahx)LHRH], [K^6]LHRH, and Cur nanomicelles at three concentrations (50, 16.66 and 5.55 μM) at three different incubation times: **(A)** after 2 hours, **(B)** after 24 hours, and **(C)** after 48 hours. PBS were included as negative control.

2.4.4.3 Cellular uptake

The confocal microscopy analysis (**Figure *2-8***) demonstrated a significant increase in fluorescence intensity following the uptake of LHRH-targeted Cur nanomicelles compared to non-targeted Cur nanomicelles and the PBS control in MDA-MB-231 cells. Among the formulations, [K^6(Ahx)] LHRH-Cur nanomicelles exhibited the highest level of cellular uptake, as indicated by the strongest green fluorescence signal, suggesting efficient internalization. [K^6]LHRH-Cur nanomicelles also display enhanced uptake relative to Cur nanomicelles, but at a lower intensity than the [K^6(Ahx)]LHRH-Cur formulation. In contrast, cells treated with Cur nanomicelles alone exhibited weaker fluorescence, indicating reduced cellular uptake in the absence of LHRH targeting. PBS control showed negligible fluorescence, confirming the specificity of nanomicelles internalization.

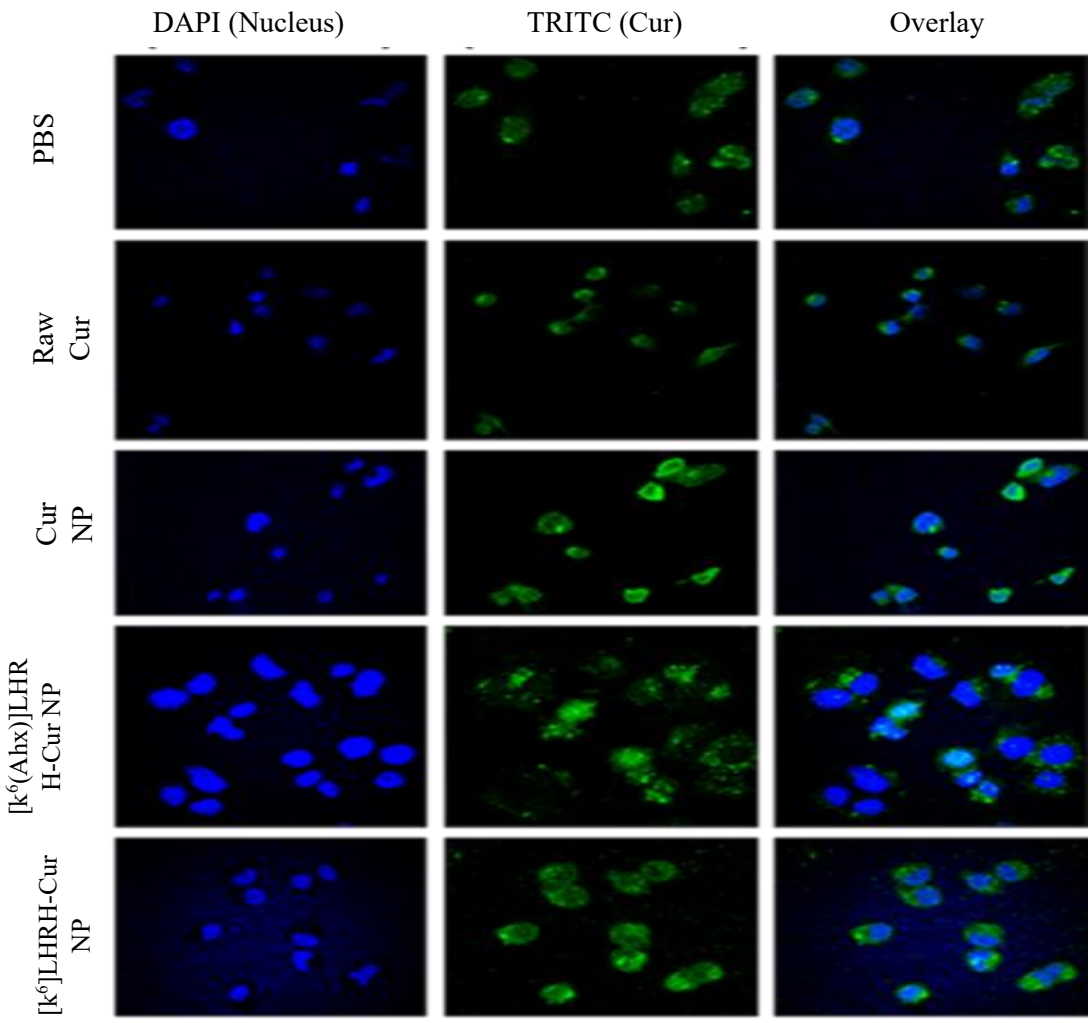

Figure 2-8. **Cellular uptake of targeted and non-targeted NPs in MDA-MB-231 Cells.**

Uptake of formulated nanomicelles compared to vehicle control and PBS in MDA-MB-231 cells. The cells were treated with10 μM of raw Cur, [k^6]LHRH-Cur NP, [k^6(Ahx)]LHRH-Cur NP, and Cur NPs and free-Cur for 24 hours before fixation. The uptake of the compounds appears green, and nuclei are stained with DAPI (blue).

2.5 Discussion

TNBC is a subtype of breast cancer characterized by the absence of ER, PR, and HER2 expression (182). Due to these biological features, TNBC is often more aggressive than other breast cancer subtypes, presents limited treatment options, and is associated with a poorer overall prognosis (183). Chemotherapy, particularly Dox, remains the standard treatment for TNBC (184) In metastatic cases, additional therapies such as PARP inhibitors, including Olaparib (Lynparza), are frequently required (185). Curcumin, a polyphenolic compound extracted from turmeric, has been shown to effectively inhibit TNBC tumor progression. Its therapeutic effects are partly attributed to its ability to target SIK3 (SIK

Family Kinase 3), a protein that is overexpressed in TNBC and plays a crucial role in tumor progression. In a patient-derived xenograft (PDX) model, curcumin treatment significantly suppressed tumor growth, highlighting its potential as a targeted therapeutic agent for TNBC. *In vitro* studies demonstrated that Cur at concentrations exceeding 25 μM could inhibit SIK3-mediated cyclin D upregulation, thereby halting the cell cycle and impeding TNBC cell proliferation (93). Furthermore, Cur has been observed to reduce epithelial-mesenchymal transition (EMT) and tumor migration by downregulating SIK3-mediated expression of mesenchymal markers such as vimentin, α-SMA, MMP3, and Twist (186).

In this study, we incorporated Pluronic® F127 to improve Cur's solubility and delivery. Pluronic F127, a biocompatible and biodegradable block copolymer, facilitates the solubilization and delivery of hydrophobic drugs like Cur. The micellar nanoformulation strategy enhances Cur's stability, bioavailability, and tumor-targeting capabilities (187). Research has demonstrated that Pluronic F127 in Cur nanoformulations can effectively circumvent MDR in TNBC cells, a crucial finding given TNBC's aggressive nature and common resistance to treatment via MDR pumps (188-190). Pluronic F127 sensitizes cancer cells to chemotherapeutic agents by inhibiting P-glycoprotein, a key efflux pump involved in MDR (191).

Pluronic F127 and F68 are amphiphilic triblock copolymers with different hydrophilic-lipophilic balances (HLB), influencing their self-assembly into micelles. Compared to more hydrophilic Pluronics like F68 (HLB 29), Pluronic F127 (HLB 22) has a larger hydrophobic PPO core, making it more suitable for encapsulating hydrophobic drugs like curcumin. This was confirmed in a study by Sripetthong et al. compared Cur encapsulation within Pluronic F68 and F127 micelles, reporting that Pluronic F127 exhibited a higher EE% of 67.61% at a Cur concentration of 0.3 mg/mL. The maximum DL% of the Pluronic F127 nano-micelles was determined to be 6.15 ± 0.41% (192).

Several studies employing Pluronic F127 micelles loaded with Cur have also demonstrated improved antiproliferative activity and higher efficacy, aligning with our findings (193, 194).

To further enhance Cur's efficacy, stability, and selectivity, we developed three distinct Pluronic F127-based nanomicelles in this study: Cur nanomicelles, [k^6(Ahx)]LHRH-Cur nanomicelles, and [k^6]LHRH-Cur nanomicelles. *In vitro* studies demonstrated that Cur-loaded Pluronic F127 micelles significantly enhanced Cur's anti-proliferative effects in MDA-MB-231 breast cancer cell line. Furthermore, we showed that the LHRH receptor, a biomarker highly expressed in TNBC, could have therapeutic potential in targeted drug delivery.

This study highlights the potential of LHRH-functionalized curcumin nanomicelles as an effective therapeutic strategy for triple-negative breast cancer (TNBC). The combined evidence from live-cell imaging (Incucyte), cell viability assays (Alamar Blue), and confocal microscopy confirms that LHRH-conjugated nanomicelles enhance cellular uptake and exhibit stronger cytotoxic effects compared to non-targeted formulations.

Live-cell imaging revealed that LHRH-functionalized nanomicelles induce time- and concentration-dependent morphological changes in TNBC cells, with notable increases in fluorescence intensity over time, suggesting efficient cellular uptake and sustained cytotoxicity. The Alamar Blue assay further supported these findings, demonstrating that LHRH-targeted nanomicelles significantly reduce cell viability compared to their non-targeted counterparts. The incorporation of LHRH peptides is known to facilitate receptor-mediated endocytosis, thereby enhancing intracellular drug accumulation and improving therapeutic efficacy, as previously reported for peptide-targeted drug delivery systems (195, 196).

The confocal microscopy analysis provided further confirmation of enhanced uptake, with LHRH-conjugated nanomicelles exhibiting the strongest intracellular fluorescence, while non-targeted curcumin formulations showed comparatively lower cellular internalization. This underscores the role of ligand-receptor interactions in facilitating selective uptake, consistent with studies demonstrating that peptide-functionalized nanocarriers improve drug delivery efficiency in TNBC (197).

Collectively, these results reinforce the importance of targeted nanomedicine approaches in enhancing the therapeutic potential of curcumin for TNBC treatment. The ability of LHRH-functionalized nanomicelles to improve cellular uptake, intracellular retention, and cytotoxicity suggests their potential as a promising drug delivery platform for overcoming the limitations of previously explored curcumin formulateons. Further studies, particularly *in vivo* evaluations, will be essential to assess their pharmacokinetic properties, biodistribution, and therapeutic efficacy in preclinical TNBC models. Additionally, exploring combination strategies with existing chemotherapies or immunotherapies could further enhance treatment outcomes.

2.6 Conclusion

The formulation of curcumin into micelles improved its solubility, stability, and overall physicochemical profile, effectively addressing key limitations of the free drug. Building on this foundation, the incorporation of the LHRH-targeting ligand enhanced specificity toward TNBC cells, leading to increased cellular uptake and improved in vitro cytotoxicity. While these results are encouraging, further studies are

required to validate the selectivity and therapeutic advantage of this targeted system in more complex biological models. The current findings justify continued development and in vivo evaluation of LHRH-targeted curcumin micelles and support the integration of this targeting approach into more advanced delivery platforms. Chapter 3 builds upon these outcomes by introducing a niosome-based co-delivery system for curcumin and doxorubicin.

Chapter 3. Development of niosomes as drug delivery systems to prevent and treat breast cancer bone metastasis

3.1 Introduction

TNBC is a highly aggressive subtype characterized by the absence of estrogen, progesterone, and HER2 receptors, rendering it unresponsive to targeted therapies (2). As a result, treatment primarily relies on chemotherapy, which is often limited by systemic toxicity, multidrug resistance, and non-specific action (46). Cur, a bioactive compound with anti-cancer properties such as apoptosis induction and pathway modulation, shows promise but suffers from poor bioavailability (94, 103). Similarly, Dox, a widely used chemotherapeutic agent, is effective but constrained by cardiotoxicity and resistance (198). Nanotechnology-based drug delivery systems offer a promising solution by improving drug solubility, while surface functionalization enables targeted delivery, enhancing cellular uptake and reducing off-target toxicity, thereby optimizing therapeutic outcomes (199). These challenges underscore the urgent need for innovative nanotechnology-based drug delivery systems to enhance therapeutic efficacy while minimizing adverse effects (63).

Integrating Cur and Dox within a single delivery system can potentially present a synergistic strategy to overcome key challenges in TNBC treatment (91). Cur enhances chemosensitivity by modulating resistance pathways, complementing Dox's DNA-damaging effects to improve therapeutic efficacy while potentially lowering the required dosage and reducing toxicity (91). The co-delivery of doxorubicin (Dox) and curcumin (Cur) via nanocarriers offers a promising strategy to overcome key therapeutic challenges in TNBC, including poor bioavailability, off-target toxicity, and drug resistance. Nanocarriers improve drug solubility, stability, and circulation time, while surface functionalization enables targeted delivery, reducing systemic toxicity (66). The synergistic effect of Cur enhances Dox-induced apoptosis and inhibits drug resistance mechanisms, such as efflux pumps and oncogenic signaling pathways. Additionally, Cur modulates the tumor microenvironment (TME) by reducing inflammation and increasing tumor sensitivity to Dox. By ensuring controlled, tumor-specific co-delivery, nanocarriers enhance therapeutic efficacy, making this approach a viable strategy for improving TNBC treatment outcomes (66).

This chapter explores the design, development, optimization and characterization of advanced nanocarrier systems for the dual delivery of Cur and Dox, with a specific focus on targeting BC and its associated bone metastases.

Niosomes, vesicular nanocarriers composed of non-ionic surfactants, serve as the foundation of this delivery system. Although niosomes can exhibit a wide size distribution ranging from 10 and 1000 nm (200) , it is generally reported that nanoparticles within the 50–200 nm range demonstrate enhanced tumor penetration and accumulation via the EPR effect. However, slightly larger niosomes, such as those developed in this study, may still offer therapeutic advantages, particularly in terms of drug loading capacity, and targeted delivery performance.

These versatile carriers can encapsulate both hydrophilic and hydrophobic drugs, enhance drug stability, and enable controlled release, making them particularly well-suited for overcoming the therapeutic challenges of TNBC (201, 202). As an aggressive and heterogeneous breast cancer subtype lacking hormone receptors and HER2 expression, TNBC is resistant to targeted therapies, leaving systemic chemotherapy as the primary treatment—an approach often limited by severe toxicity and drug resistance (2, 203).

A key factor in niosome formulation is the careful selection of components to optimize drug encapsulation, stability, and release profiles. Span 60 (Sorbitan monostearate), a non-ionic surfactant, and Chol, a lipid stabilizer, play essential roles in maintaining the structural and functional integrity of the niosomes, ensuring effective drug delivery (204). Span 60 (***Figure 3-1***) is a non-ionic surfactant widely used in pharmaceutical and cosmetic formulations (204). It is composed of sorbitol and stearic acid, making it a hydrophobic emulsifier with a hydrophilic-lipophilic balance (HLB) value of approximately 4.7 (205). Due to its amphiphilic nature, span 60 is commonly employed in the preparation of vesicular drug delivery systems such as niosomes, where it aids in stabilizing the bilayer structure and enhancing encapsulation efficiency. Its ability to improve drug solubility and sustain release makes it a valuable component in nanoparticle-based formulations (204).

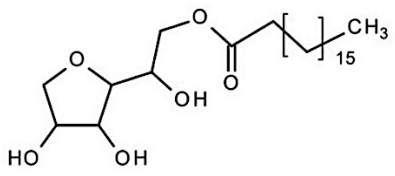

Figure 3-1. Chemical structure of span 60

Cholesterol **(Figure 3-2**) is an essential lipid that contributes significantly to the stability and flexibility of cell membranes (206). It acts as a key precursor in the production of steroid hormones, bile acids, and

vitamin D (206). In drug delivery systems, Chol is commonly used to enhance the stability and rigidity of lipid-based nanoparticles (207).

Cholesterol complements Span 60 by modulating the fluidity and permeability of the niosomal bilayer (204). By integrating into the membrane, it enhances structural stability while maintaining flexibility, thereby minimizing drug leakage and ensuring a controlled release profile (204). This balance is crucial for sustained therapeutic efficacy, particularly for Cur and Dox, which require precise delivery to maximize effectiveness while reducing systemic toxicity (91). Additionally, Chol plays a vital role in stabilizing niosomes under physiological conditions, preserving vesicle integrity during circulation and enhancing their potential for targeted drug delivery (208).

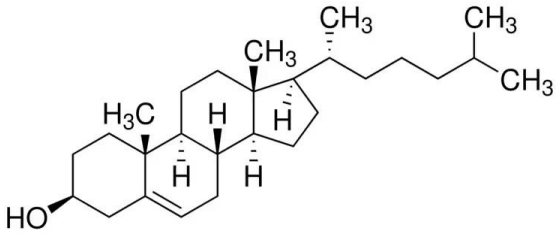

Figure 3-2. Cholesterol chemical structure.

Niosome formulation also necessitates a hydration medium, with phosphate buffer being commonly used due to its effectiveness in supporting both niosome formation and the encapsulation of drugs or natural compounds. Factors such as size, distribution, entrapment efficiency, and the release profile of the drug or natural molecule are influenced by the composition of the medium and hydration parameters (209, 210)

Pluronic® F127 (**Figure 2-1**), a triblock copolymer consisting of hydrophilic polyethylene oxide (PEO) and hydrophobic polypropylene oxide (PPO), was incorporated into the formulation to enhance the biological performance of NPs (173). Pluronic® F127 serves multiple roles, it stabilizes the NPs structure, reduces aggregation, and forms a protective corona around the vesicles (173). This protective layer minimizes protein adsorption and immune recognition, prolonging the circulation time of the NPs and improving their pharmacokinetic profile (173). Additionally, Pluronic® F127 enhances the solubility of the nanocarriers and prevents premature destabilization, ensuring that the vesicles remain intact until they reach their target site (174). Notably, targeted drug delivery was achieved by functionalizing the niosomes with different targeted agents (211).

GnRH, also known as LHRH, is a decapeptide hormone that regulates the secretion of luteinizing hormone (LH) and follicle-stimulating hormone (FSH) from the pituitary gland (212). Beyond its physiological role in the reproductive system, LHRH and its analogs have gained attention in cancer therapy due to the overexpression of LHRH receptors in various malignancies, including BC (213). LHRH analogs exploit the overexpression of LHRH receptors in TNBC cells, enabling receptor-mediated endocytosis of the drug-loaded NPs (214). This targeting mechanism enhances drug accumulation in the tumor microenvironment while minimizing off-target effects on healthy tissues (214). Among the two LHRH derivatives we worked on, K^6(Ahx) LHRH (Figure 2.2 B) was selected for continued study as it demonstrated superior targeting efficiency and therapeutic potential in the previous study (Chapter 2). LHRH-based targeting is particularly advantageous due to its ability to selectively bind to LHRH receptors, which are highly expressed in various hormone-related or unrelated cancers (214). This approach not only improves drug delivery but also reduces systemic toxicity, making it a promising strategy for enhancing treatment efficacy (214).

Alendronate (ALN) (***Figure 3-3***), a member of the bisphosphonate family, has emerged as a powerful bone-targeting agent with significant implications for BC bone metastasis (211). Bisphosphonates are synthetic analogs of pyrophosphate, characterized by their high affinity for hydroxyapatite in bone tissue (211). This bone-seeking property makes alendronate an ideal candidate for targeting cancer cells within the bone microenvironment (211).

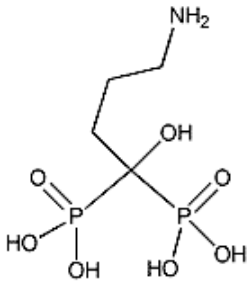

Figure 3-3. Alendronate chemical structure

In this study, alendronate was utilized as a targeting ligand to enhance the specificity of nanocarriers for BC bone metastases. By leveraging its high affinity for hydroxyapatite, the nanoparticles were designed to preferentially accumulate in metastatic bone sites, improving drug localization and therapeutic efficacy (215).

DSPE-PEG-COOH (1,2-distearoyl-sn-glycero-3-phosphoethanolamine-polyethylene glycol-carboxylic acid) (***Figure 3-4***) was employed as a polymer to integrate the two targeting ligands (216). DSPE-PEG-

COOH plays a pivotal role in the design of advanced nanocarriers for cancer therapy (216). As an amphiphilic molecule, DSPE-PEG-COOH combines a hydrophobic lipid moiety with a PEG chain, terminating in a reactive carboxylic acid group (217). This structure enables its dual functionality as both a stabilizing agent and a platform for surface modifications (217).

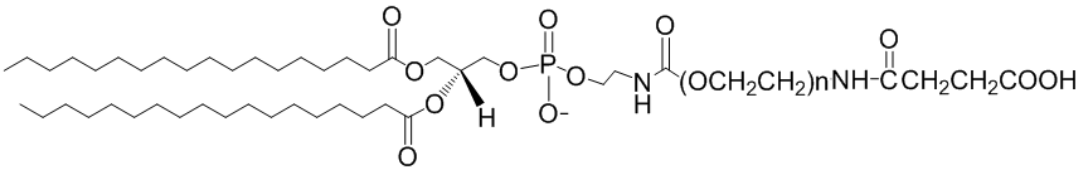

Figure 3-4. DSPE-PEG-COOH chemical structure

In dual-drug delivery systems, DSPE-PEG-COOH plays a crucial role in stabilizing nanoparticles by forming a steric barrier around their surface (217). The PEG chains reduce protein adsorption and opsonization, thereby prolonging circulation time *in vivo* and minimizing premature clearance by the reticuloendothelial system (RES) (217-219). Additionally, the carboxyl (-COOH) group provides a versatile conjugation site for ligands such as peptides, antibodies, or small molecules, facilitating targeted drug delivery to cancer cells (220).

In this study, DSPE-PEG-COOH was employed to functionalize the surface of niosomes. FTIR analyses confirmed successful conjugation. This modification enhanced the targeting specificity of the NPs.

Overall, this dual-drug niosomal system presents a robust strategy for breast cancer therapy by incorporating structural stability from Span 60 and cholesterol, along with functional enhancements from Pluronic® F127 and DSPE-PEG-linked targeting using LHRH and alendronate ligands. This design lays the foundation for future comparative evaluations of these delivery systems.

3.2 Material and Instruments

Materials: Succinic anhydride (SA), 4-dimethylaminopyridine (DMAP), 1,4-dioxane, dichloromethane (DCM), methanol, acetonitrile (ACN), Cur (purity >65%), Pluronic® F-127, and 1-ethyl-3-(3-dimethylaminopropyl) carbodiimide hydrochloride (EDC. HCl) and MES buffer were sourced from Sigma-

Aldrich, Australia. Span 60, D-mannitol, cholesterol, sucrose and 2-(N-morpholino) ethane sulfonic acid (MES, Sodium salt, ULTROL® Grade) were obtained from Merck Life Science Pty Ltd, Australia. Dox hydrochloride was procured from Focus Bioscience Pty Ltd, Australia, while alendronate sodium trihydrate was generously provided by Alcon Biosciences, India. Human BC cells (MDA-MB-231) were purchased from the American Type Culture Collection (ATCC) and cultured in RPMI-1640 medium with 10% fetal bovine serum (FBS) under a humidified atmosphere (37°C, 5% CO_2).

Instruments: The particle size and zeta potential of Cur-loaded micelles were analyzed using dynamic light scattering (DLS) on a Nano Series ZS Zetasizer (Malvern Instruments, UK). Drug loading (DL%) and encapsulation efficiency (EE%) and release study were determined via reverse-phase high-performance liquid chromatography (RP-HPLC) on a Shimadzu Prominence system (Kyoto, Japan) with a C18 column (Nova Pak, 150 × 4.6 mm) and a diode array detector (Shimadzu SPD-M20A). Centrifugation was performed using an Allegra X-30R centrifuge (Beckman Coulter, USA).

Live cell imaging was conducted with the IncuCyte® SX5 Live Cell Analysis System (Essen Bioscience, USA), while *in vitro* cytotoxicity was assessed using a VICTOR X4 plate reader (PerkinElmer). Functional group characterization of NPs was performed using attenuated total reflectance Fourier-transform infrared spectroscopy (ATR-FTIR) on a Bruker Alpha spectrometer (Bruker, MA, USA), with OPUS software (version 8.7.31) for data analysis. Surface morphology and structural analysis were carried out using scanning electron microscopy (SEM) on a JEOL JSM-7600F (JEOL Ltd., Japan) at an accelerating voltage of 5 kV. Samples were sputter-coated with a thin gold layer to enhance conductivity.

Solvent evaporation during thin-film preparation and NPs hydration was achieved using a rotary evaporator (Rotavapor® R-300, Büchi, Switzerland). For the formulation and size reduction of nanoparticles, probe sonication was employed using a sonicator (Branson Ultrasonics, USA) to deliver controlled energy for efficient dispersion, while bath sonication (Elmasonic S series, Elma Schmidbauer, Germany) was used for uniform mixing and removal of air bubbles in the dispersion.

3.3 Methods

3.3.1 Preparation and optimization of drug loaded niosomes

Initially, niosomes were prepared using a modified version of a previously reported method (221, 222). Span, Chol (in a molar ratio of 1:1), and Cur (1 mg/mL) were dissolved in a chloroform: methanol mixture (2:1 v/v) with a lipid-to-drug ratio of 10:1. The solvents were evaporated at 60 °C and 120 rpm to form a

thin lipid film, which was then hydrated for 1 hour with 10 mL of phosphate-buffered saline (PBS, pH 7.2). The formulations were sonicated and stored at 4 °.

Due to the lack of detailed specifications in the literature for reproducible niosome preparation, we systematically optimized key parameters, including solvent volume, flask size, component ratios, and rotary evaporator settings (pressure, temperature, and speed) during drying and hydration. We tested variations in these parameters, along with lipid-to-drug ratios and sonication durations, to evaluate their impact on particle size, polydispersity index (PDI), drug encapsulation efficiency, and overall stability, ensuring a robust and reproducible method. The schematics of all prepared niosome types are illustrated in

Figure 3-6.

3.3.1.1 Fabrication of Cur niosomes (CN)

The modifications implemented to optimise the physicochemical properties of Cur-niosomes are summarized in **Table 3-1**. These modifications were carefully designed to enhance parameters such as particle size, polydispersity index (PDI), drug encapsulation efficiency, and stability.

All centrifugation steps were conducted at 4400 rpm (1000 × g) for 10 minutes to ensure efficient separation of niosomes. Additionally, during probe sonication, the sample was maintained in an ice bath to prevent thermal degradation, with a duty cycle of 20 and an output control setting of 5 to achieve effective nanoparticle dispersion.

Table 3-1. Experimental Conditions for Niosome Preparation and Processing Parameters

Experiment	Curcumin (mg)	Cholesterol (mg)	Span 60 (mg)	Solvent volumes (mL): Chloroform: Methanol (2:1)	Flask Volume (mL)	Thin film processing	Hydration	Additional Steps
CN1	10	47.3	52.6	6.6:3.3	50	60°C, 120 rpm, 500 mbar for 1h	10 mL PBS at 60°C, 120 rpm, 500 mbar for 1h	Sample divided: two portions refrigerated (one sonicated for 7 min, one not), two freeze-dried (one sonicated before freezing, one not)
CN2	5	23.65	26.3	3.3:1.6	25	Same as CN1	10 mL PBS at	Probe sonicated for 7 min

							same condition	
CN3	10	47.3	52.6	6.6:3.3	50	Same as CN1	-	No additional steps
CN4	5	23.65	26.3	3.3:1.6	25	40°C, 120 rpm, 200 mbar for 1 h	-	No additional steps
CN5	10	47.3	52.6	13.2:6.6	100	Same as CN1	10 mL PBS at same condition	Centrifugation, sonication
CN6	10	100	111.4	6.6:3.3	50	Same as CN1	10 mL PBS at same condition	Centrifugation, sonication
CN7	5	50	55.6	6.6:3.3	25	Same as CN6	10 mL PBS at same condition	Increased lipid: drug ratio (20:1)
CN8	5	23.6	26.3	33.3:16.6	500	Same as CN6	10ml PBS at same condition	Large-scale processing
CN9	10	47.3	52.6	13.3:6.6	100	40°C, 200 rpm, 200 mbar for 1h	10 mL PBS at 60°C, 200 rpm, 200 mbar for 1h	No additional steps
CN10	10	47.3	52.6	13.3:6.6	100	Same as CN9	10 mL PBS, same as CN9	Mannitol & sucrose added as cryoprotectants, freeze-drying after DLS analysis

3.3.1.2 Incorporating F127 in Cur niosomes (CFN)

While working with micelles using F127, its surfactant properties were observed to prevent ingredients from adhering to the flask walls. However, F127 has a high hydrophilic-lipophilic balance (HLB) value of approximately 22, which exceeds the typical range (4–8) for surfactants used in niosomes and can destabilize bilayer formation, promoting micelle formation instead (223). To address this, a small amount of F127 was incorporated at a molar ratio of Span 60:F127:Chol of 0.99:0.01:1. Based on the optimal particle size and polydispersity index (PDI) observed in CN9, the same preparation steps were repeated in subsequent experiments, incorporating F127 into the formulation.

Experiment CFN1: A formulation consisting of Span 60 (44.7 mg), F127 (14.6 mg), Chol (40.6 mg), and curcumin (10 mg) was prepared by dissolving the components in 13.2 mL of chloroform and 6.6 mL of methanol in a 100 mL round-bottom flask. The solution was stirred at 40°C, 200 rpm, and 200 mbar pressure for 5 hours, as the addition of F127 necessitated a longer drying time. The sample was then left to evaporate the residual solvent overnight before being hydrated with 10 mL of PBS for 1 hour under the same conditions. Subsequently, the niosomal solution was kept at room temperature overnight to allow for complete annealing and drug distribution between the lipid bilayer and the aqueous phase (224), then the suspension was sonicated for 14 minutes and centrifuged.

Experiment CFN2: This experiment was built on CFN1 and aimed to explore the effect of prolonged sonication. The 14-minute sonication was compared to an extended sonication time of 21 minutes. The samples were labeled CNF2 (14 minutes) and CFN2' (21 minutes).

Experiment CFN3: Building on CFN1, this experiment examined the impact of freeze-drying with cryoprotectants. Mannitol and sucrose were added to the niosomal suspension before freeze-drying. The procedure included:

1. Mixing 2 mL of suspension with 29.6 mg of sucrose (1:2.5 surfactant: sucrose ratio (225)).
2. Combining 2 mL of suspension with 120 mg of mannitol (6 g/100 mL concentration (226)).
3. Keeping 2 mL of suspension without cryoprotectants as a control. DLS was performed before and after freeze-drying to assess the suspension's characteristics.

Experiment CFN4: This experiment followed the protocol from CFN1 with the only modification being an increase in flask volume to 250 mL to investigate its effect on ingredient detachment from the flask walls.

3.3.1.3 Incorporating Dox in F127 niosome (DFN)

A previous study (91) indicated that 2 mg of Dox in the niosomes formulation was sufficient to achieve the optimal physicochemical properties for the nanoparticles. To achieve this, various ratios of Dox were experimented in the formulation to determine the most optimal quantity for improving encapsulation efficiency, particle size, and drug release profile.

DFN1: Span 60 (44.7 mg), F-127 (14.6 mg), and Chol (40.6 mg) were dissolved in 13.3 mL of chloroform and 6.6 mL of methanol (molar ratio of Span 60: F-127: Chol, 0.99: 0.01: 1). The solution was processed

in a 250 mL round-bottom flask for 5 hours at 40°C, 200 rpm, and 200 mbar pressure, then left overnight at room temperature to ensure complete drying. Following this, 2 mg of Dox dissolved in PBS was added and briefly sonicated in a bath sonicator at 40°C for complete dissolution. The niosomal thin film was hydrated with 10 mL of PBS containing Dox for 1 hour at 60°C, 200 rpm, and 200 mbar pressure. After resting overnight at room temperature, the sample was sonicated for 14 minutes and then centrifuged.

DFN2: This experiment followed the same steps as DFN1, except that the amount of Dox was increased to 5 mg. Additionally, seven different sonication methods and durations were tested to determine the optimal conditions for the best results (labelled as sample 1-7).

Table 3-2. Sonication conditions applied in DFN2 formulations with 5 mg Dox

Sample ID	Sonication method	Details
1	Bath sonication	7 minutes
2	Probe sonication	7 minutes
3	Bath + Probe sonication	7 min bath followed by 7 min probe
4	Bath + Probe sonication	7 min bath followed by 14 min probe
5	Bath sonication	14 minutes
6	Probe sonication	14 minutes
7	Probe + Bath sonication	14 min probe followed by 14 min bath

DFN3: All steps were the same as in DFN1, except that the amount of Dox was increased to 8 mg to assess the impact on the formulation. DFN4: Similar to DFN3, but with the Dox amount increased to 10 mg to further evaluate the effects.

3.3.1.4 Fabrication of Cur-Dox F127 niosomes (CDFN)

Dual-drug delivery system of Cur-Dox niosomes were prepared using two different Dox quantities (2 mg and 5 mg) to assess their impact on physicochemical properties and identify the optimal formulation. Additionally, a formulation analogous to CDFN but without F127 was prepared to evaluate EE% in the presence and absence of F127. This formulation was designated as CDN.

3.3.2 Fabrication and optimization of targeted niosomes

3.3.2.1 Fabricating targeted niosomes by Implication of conjugated F127-succinate to LHRH (CDFLN)/ALN (CDFAN)

3.3.2.1.1 Fabrication of CDFLN

As explained in Sections 2.3.1 and 2.3.2, the conversion of F127 to F127-succinate and the conjugation of LHRH to F127-succinate were described. F127-[k^6(Ahx)]LHRH was used for targeting CDFN to produce CDFLN. The molar ratio of Span 60: F127-LHRH: Chol was set at 0.99:0.01:1, corresponding to 44.19 mg of Span 60, 15.87 mg of F127-LHRH, and 40.00 mg of Chol. The other preparation steps were the same as those used for CDFN, except F127-LHRH was used instead of F127.

3.3.2.1.2 Fabrication CDFAN

As detailed in sections 2.3.1and 3.3.2.1.2.1, the processes for converting F127 to F127-succinate and subsequently conjugating alendronate to F127-succinate were outlined. F127-Alendronate was employed to produce targeted CDFAN. The molar ratio of Span 60, F127-LHRH-D, and Chol was adjusted to 0.99:0.01:1, which corresponds to 44.4 mg of Span 60, 15.3 mg of F127-LHRH and 40.3 mg of Chol. All other preparation steps were consistent with those used for CDFN, except F127-Alendronate replaced F127.

3.3.2.1.2.1 Conjugation of Alendronate to carboxyl terminals of Pluronic®F127-succinate

To summarize, Pluronic® F127 succinate (2 g) was dissolved in a solution containing Milli-Q water (70 mL) and 1,4-dioxane (4 mL). Subsequently, EDC· HCl (600 mg) and alendronate sodium (500 mg) were introduced into the mixture and stirred continuously at room temperature for 24 hours. The resulting alendronate-Pluronic® F127-alendronate (ALN-F127) conjugate was subjected to dialysis against water for 24 hours to eliminate any unreacted alendronate and EDC· HCl. The purified conjugate was then freeze-dried and analyzed using FTIR. The conjugation of alendronate to Pluronic® F127 succinate was achieved using carbodiimide chemistry (***Figure 3-5***).

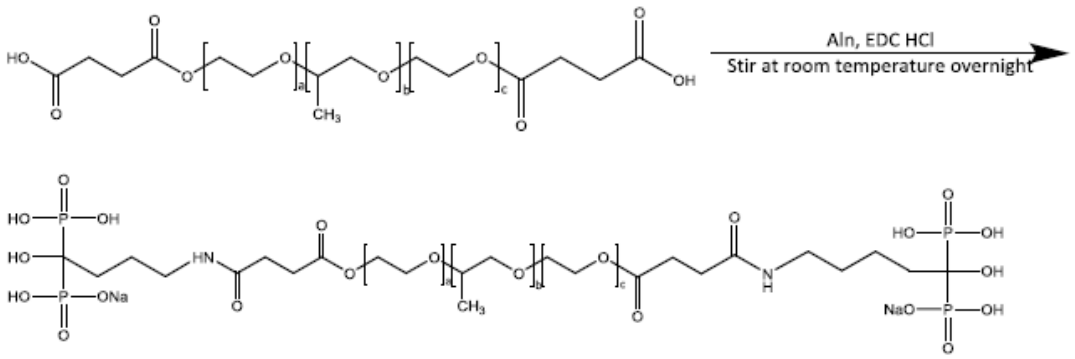

Figure 3-5. Conjugation of Alendronate to the carboxyl group of Pluronic®F127-succinate

3.3.2.2 Fabricating targeted niosomes by using DSPE-PEG-COOH as a linker for LHRH (CDPLN)/Alendronate (CDPAN)

The niosomes' surface was modified using carbodiimide chemistry, enabling the covalent attachment of the targeting agents (LHRH/ALN) via EDC-NHS activation, with DSPE-PEG-COOH2000 serving as the linker. PEGylated niosomes (CDPN) were prepared by dissolving Span 60 (43 mg), CHOL (39.5 mg), Cur (10 mg), and DSPE-PEG-COOH (7.5 mg) in a 20 mL mixture of chloroform and methanol within a 250 mL round-bottom flask. The solvent was removed under reduced pressure at 60°C using a rotary evaporator to create a thin lipid film. This film was then hydrated with PBS containing Dox at 60°C for 60 minutes to obtain CDPN. The process was modified from previously reported protocols (91) to optimize targeting efficiency. In this study, two separate niosomal formulations were prepared—one targeted with LHRH (CDPLN) and the other with alendronate (CDPAN)— as shown in

Figure *3-6*.

To facilitate conjugation, the carboxyl groups on PEGylated niosomes were linked to the amine groups of LHRH and ALN. Initially, EDC (2.2 mg) dissolved in MES buffer (0.1 M, pH 5) was added to the optimized PEGylated niosomes, followed by stirring for 30 minutes. After this activation step, NHS (1.11 mg) was introduced in a 2:1 EDC:NHS ratio to generate an amine-reactive intermediate, with continuous stirring at room temperature (RT) for 12 hours. Unreacted EDC and NHS were eliminated via dialysis against PBS using a pre-wetted 12,000 Da MWCO dialysis membrane, kept under stirring for 6 hours.

Subsequently, a fivefold excess of LHRH and ALN (relative to DSPE-PEG-COOH2000) dissolved in MES buffer (0.1 M, pH 5) was added to the niosomal dispersion separately, and the mixtures were gently rotated for 24 hours to ensure effective conjugations. Excess unreacted LHRH and ALN were then removed by dialysis, ensuring the purity of the targeted niosomes. The conjugation processes were modified from previously reported protocols (227) to enhance efficiency and stability.

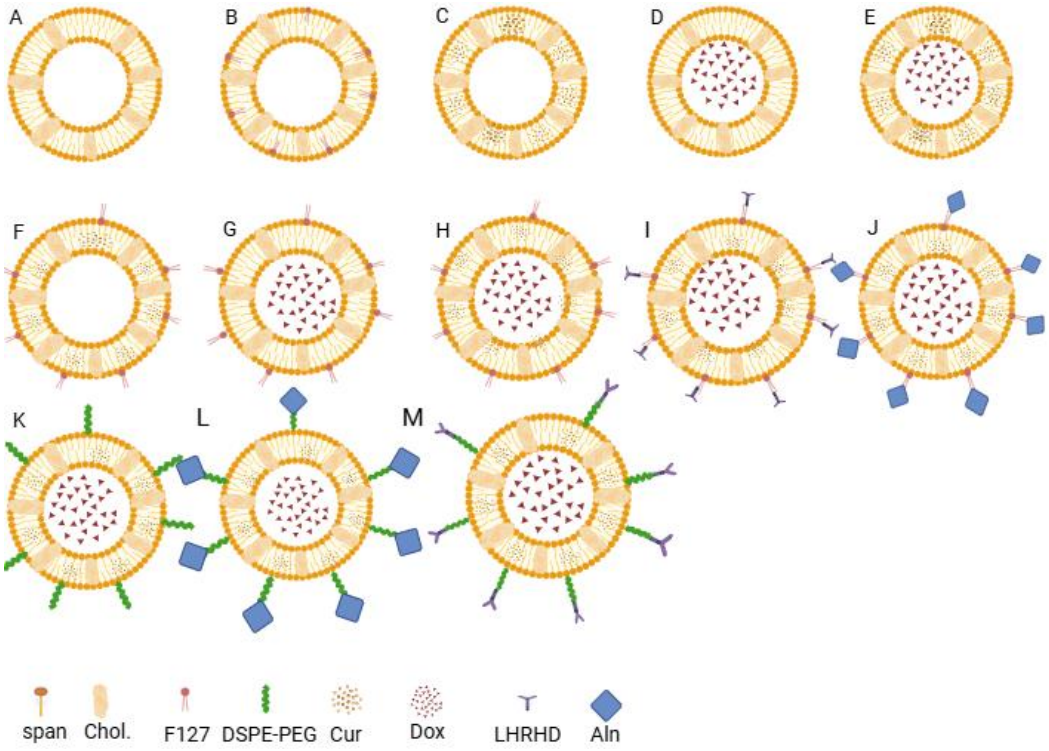

Figure 3-6. Schematic Representation of Various Niosomal Formulations.

Void niosomes (span60 and Chol) (A) , Void-F127 niosomes (B), CN (C), DN (D) , CDN (E), CFN (F), DFN (G), CDFN (H), CDFLN (I), CDFAN (J), CDPN (K), CDPAN (L), CDPLN (M)

3.3.3 Physicochemical characterization of the NPs

3.3.3.1 Particle size, zeta potential and polydispersity index

The particle size, zeta potential, and PDI of the NPs were analyzed using DLS at room temperature. In summary, 100 µL of NPs were diluted with 900 µL of PBS, and the DLS measurements were conducted in triplicate.

3.3.3.2 Encapsulation efficiency (EE%)

The prepared niosomal formulations were ultra-filtered using an Amicon Ultra-15 membrane (30K Da) (221) at 4400 rpm (1000×g) for 30 minutes at 4°C to remove any unloaded drugs. Subsequently, the supernatant was resuspended in PBS, and 0.5 mL of it was freeze-dried in Eppendorf tubes, after which 1 mL of DCM was added. Following evaporation of DCM under a fume hood, a RP-HPLC solvent mixture (30% acetonitrile and 70% water) was added to the residue. A 10 µL aliquot of the resulting solution was

injected into the RP HPLC system and analyzed using a UV detector at 480 nm for Dox and 420 nm for Cur.

EE (%) =Actual drug loading/Theoretical drug loading* 100

3.3.3.3 Assessing the conjugation of targeting agents to niosomes

The functional groups of niosomes were characterized using attenuated total reflectance Fourier-transform infrared spectroscopy (ATR-FTIR) on a Bruker Alpha spectrometer (Bruker, MA, USA), with data analysis conducted using OPUS software (version 8.7.31). The measurements were performed within the 400-4000 cm^{-1} wavenumber range.

3.3.4 *In vitro* experiments

3.3.4.1 Alamar Blue cell viability

In a flat-bottom 96-well plate, 5000 MDA-MB-231 cells per well were seeded and allowed to adhere for 24 hours

The cytotoxicity evaluation was conducted using the resazurin viability assay. MDA-MB-231 cells were seeded at a density of 5000 cells per well in 90 µL of media in 96-well flat-bottom plates and allowed to adhere overnight. Drug solutions were prepared in PBS through serial dilutions to achieve varying concentrations equivalent to Cur or Dox. PBS and SDS served as the negative and positive controls, respectively. Cells were then treated with 10 µL of drug solutions and controls and incubated for 72 hours.

At the end of the 72 hours, 10 µL of a 1.25 mM resazurin solution was added to each well, and after an additional 4 hour of incubation, absorbance measurements of the labelled cells were taken at 480/550 nm using a Victor X microplate reader. Data analysis and determination of half-maximal inhibitory concentration (IC_{50}) values were performed using GraphPad Prism software (version 7).

3.3.4.2 *In vitro* cytotoxicity assessment

The prepared plate for Alamar Blue assay was incubated for 72 hours, during which images were captured every 2 hours using the IncuCyte® SX5 system.

3.3.4.3 Anticancer studies using IncuCyte in 3D models

The cytotoxicity and tumor disintegration ability of the drug formulations were evaluated using a spheroid viability assay. Spheroids of MDA-MB-231 cells were formed by seeding 13,500 cells per well in 96-well U-bottom plates, followed by centrifugation to facilitate cell aggregation and incubation for two days to allow spheroid formation. Drug solutions and vehicles were prepared equivalent to 50 µM Cur or Dox. PBS and SDS were used as the negative and positive controls, respectively. Spheroids were then treated with 10

μL of the drug solutions and controls. Monitoring was continued using the IncuCyte®SX5 imaging system for 4 days.

3.3.4.4 Bone affinity assay

The Bone affinity assay was conducted to compare the affinity of ALN-targeted niosomes (Cur-Dox-DSPE PEG COOH-ALN niosomes (CDPAN)) to Ca on a bone-mimicking plate with the non-targeted niosomes (Cur-Dox-DSPE PEG COOH niosomes (CDPN)). A calcium phosphate (CaP)-coated 24-well plate (CSR-BRA-24P, Cosmo Bio Co., Japan) was used for this assay (exact calcium quantity per well is not disclosed by supplier (228)). The plate is coated with a synthetic CaP (carbonate apatite), which closely resembles natural apatite in bone. Both targeted and non-targeted niosomes at three different molar ratios (500, 250, and 125 μM, equivalent to Cur) were added in triplicate to the plate. At time point 0 and 1 hour, the absorbance was measured using a Victor X plate reader at 570 nm with photometry measurement technology. Data analysis was performed using GraphPad Prism software (version 7).

3.3.4.5 Stability studies

The stability study was conducted over a four-week period, with weekly evaluations. CDFNs were sonicated as described earlier and analyzed using DLS to determine their hydrodynamic size as an indicator of nanoparticle stability. Additionally, the niosomes were stored at room temperature. At time points of 0, 72 hours and 7 days samples were taken, and the hydrodynamic size of the dispersed nanoparticles was measured via DLS following repeated sonication.

3.3.4.6 Release study

To evaluate the release profile, 2 mL of CDFN were placed in dialysis bags (12 kDa cut-off) and submerged in 200 ml PBS at three different pH levels (4.0, 6.5, and 7.4), representing the pH of the lysosome, cancer tissue, and normal tissue, respectively. The samples were incubated at 37 °C while stirring at 100 rpm. Drug release was quantified by measuring the absorbance of the external solution at 420 nm for Cur and 480 nm for Dox at predetermined time intervals (8, 12, 24, 48, 72, and 96 hours) using HPLC. To maintain sink conditions, the volume of the withdrawn sample was replaced with an equal volume of fresh PBS.

3.3.4.7 Scanning electron microscopy (SEM)

The prepared niosomal formulations were ultrafiltered using an Amicon Ultra-15 membrane (30 kDa) at 4400 rpm (1000 × g) for 30 minutes at 4°C (221). Subsequently, the supernatant was resuspended in Milli-Q water instead of PBS, as PBS interferes with SEM imaging. A drop of the niosomal suspension was placed on a serialized SEM specimen stub with a Leit carbon tab, ensuring proper adhesion and stability of

the sample. The sample was then dried under a vacuum hood. To enhance conductivity and improve imaging quality, a thin layer of gold was sputter-coated onto the sample using the Safematic CCU-010 Compact Coating Unit. The surface morphology and structural characteristics of the NPs were then analyzed using the Zeiss Sigma HD VP SEM at an accelerating voltage of 3.00 kV and a magnification of 18.00-300.00 KX, ensuring high-resolution imaging of the nanoparticles' surface features.

3.3.5 Synergy analysis

To evaluate the synergistic effect of the co-delivered curcumin and doxorubicin formulation (CDFN), the Combination Index (CI) was calculated using the Chou–Talalay method. The IC_{50} values for the individual formulations—Cur F127 niosomes (CFN), Dox F127 niosomes (DFN), and the combined formulation (CDFN)—were obtained from cell viability assays. Assuming a 1:1 ratio of curcumin and doxorubicin in the combined formulation, CI was determined using the following equation:

$$\mathrm{CI} = \frac{D_1}{D_{x1}} + \frac{D_2}{D_{x2}}$$

Where D1 and D2 are the concentrations of Dox and Cur in combination required to achieve 50% inhibition, and Dx1 and Dx2 are the concentrations of each drug alone that produce the same effect. CI values were interpreted as follows: CI < 1 indicates synergy, CI = 1 indicates an additive effect, and CI > 1 indicates antagonism.

3.3.6 Statistical analysis

Statistical analyses were performed using GraphPad Prism (version 7). Data are presented as mean ±SD from a minimum of three independent experiments (n = 3). Two-way analysis of variance (ANOVA) was used to evaluate the interaction and main effects of formulation type, concentration, time, and pH in cytotoxicity, bone mineral affinity, and release studies. For cytotoxicity assays, IC_{50} values were determined by non-linear regression using a sigmoidal dose–response (variable slope) model. Two-way ANOVA was also employed to assess the statistical significance of drug release at different pH levels and time points. For the stability study, including changes in particle size and PDI under varying storage conditions and durations, data visualization and trend analysis were performed using Python programming language with the Matplotlib package. This approach enabled the generation of time-course plots to assess patterns of aggregation and formulation stability over the 28-day period.

3.4 Results

3.4.1 Physicochemical characterization of the NPs

3.4.1.1 Z-average size and PDI of Cur niosomes (CN)

Table 3-3 summarises the various formulations of Curcumin-loaded niosomes, which were systematically optimised by varying the concentrations of Chol and Span 60, as well as adjusting the volumes of the organic solvent and the rotary evaporation flask. These modifications were implemented to enhance the physicochemical properties of the niosomes, particularly their particle size, polydispersity index (PDI), stability, and uniformity.

Particle size and PDI values were measured to assess the stability and homogeneity of each formulation, as smaller, uniformly dispersed nanoparticles tend to exhibit better colloidal stability and drug encapsulation efficiency. Among the tested formulations, CN9 demonstrated the most favourable particle size and PDI, indicating a well-optimized formulation with optimal size distribution and minimal aggregation. This suggests that the specific combination of Chol, Span 60, and solvent conditions in CN9 contributed to the formation of stable and homogeneous niosomes, making it the preferred formulation for further studies. Due to significant adhesion of formulation components to the flask walls in samples lacking Pluronic F127, reliable EE% data could not be obtained. As a result, EE% was not reported for the CN formulation.

Table 3-3. Summary of CN Experiment Results: Composition, Processing Conditions, and Outcomes

Experiment	Cur (mg)	Chol (mg)	Span 60 (mg)	Chloroform: Methanol (2:1) (mL)	Flask (mL)	PDI	Z-average size	Observations
CN1	10	47.3	52.6	6.6:3.3	50	0.232 (sonicated)	183.9 (sonicated), 4382 (non-sonicated)	Significant precipitation, adhesion to flask walls, low drug loading and freeze-drying caused loss of peaks
CN2	5	23.65	26.3	3.3:1.6	25	0.487	202.9	Significant precipitation and adhesion, poor efficiency
CN3	10	47.3	52.6	6.6:3.3	50	N/A	N/A	Thin film did not form due to high ingredient concentration and insufficient solvent volume
CN4	5	23.65	26.3	3.3:1.6	25	N/A	N/A	Thin film formation failed due to high ingredient concentration relative to flask capacity
CN5 (Figure *3-7* A)	10	47.3	52.6	13.2:6.6	100	0.371	188.1	Reduced adhesion compared to CN1 and CN2
CN6	10	100	111.4	6.6:3.3	50	0.587	442.4	Increased lipid: drug ratio to 20:1, resulting in larger size and no significant improvement
CN7	5	50	55.6	6.6:3.3	25	0.596	469.9	Reduced ingredient quantities, but size increased, indicating unfavorable outcomes
CN8	5	23.6	26.3	33.3:16.6	500	0.083	174.9	Achieved smaller size, but significant flask adhesion remained
CN9	10	47.3	52.6	13.3:6.6	100	0.32	144.7±9.3	Improved outcomes, but adhesion to flask walls persisted
CN10	10	47.3	52.6	13.3:6.6	100	0.331 (before freeze-drying), 1.000 (post-freeze-drying)	149.9 (before freeze-drying), 2478 (sucrose), 3877 (mannitol)	Freeze-drying with sucrose and mannitol led to unsatisfactory results

3.4.1.2 Z-average size, PDI, Zeta potential and EE% of CFN

CFN are curcumin-loaded niosomes incorporating F127 to enhance stability, particle size control, and encapsulation efficiency.

CFN1 nanoformulations

Figure *3-7* B): The Z-average size and PDI in comparison with CN9 increased to 213.2 nm and 0.393, respectively, with a significant improvement in ingredient detachment from the flask walls. The inclusion of F127 enhanced component solubility, encapsulation efficiency, and drug loading, although a small fraction of the ingredients remained adhered to the flask walls.

CFN2 and CFN2' nanoformulations: Extending the sonication time resulted in an increase in Z-average size and PDI, from 216.4 nm and 0.35 in CNF2 to 255.8 nm and 0.436 in CNF2', respectively. This increase suggests that prolonged sonication led to niosome aggregation.

CFN3 nanoformulations: The pre-freeze-drying Z-average size was 184.5 nm with a PDI of 0.359. After freeze-drying, the control sample showed no detectable peaks, while the sucrose-supplemented sample exhibited a Z-average size of 6702 nm (PDI 0.53). The mannitol-supplemented sample displayed a Z-average size of 3284 nm (PDI 1.000). Cryoprotectant-containing samples were deemed unacceptable, highlighting the need for further optimization of the freeze-drying process.

CFN4 nanoformulations: Utilizing a larger flask resulted in a Z-average size of 212.9 nm, a PDI of 0.289, and an EE% of 89.3±9.5. Complete detachment of ingredients from the flask walls was observed, as illustrated in (

Figure *3-7* C).

A B C

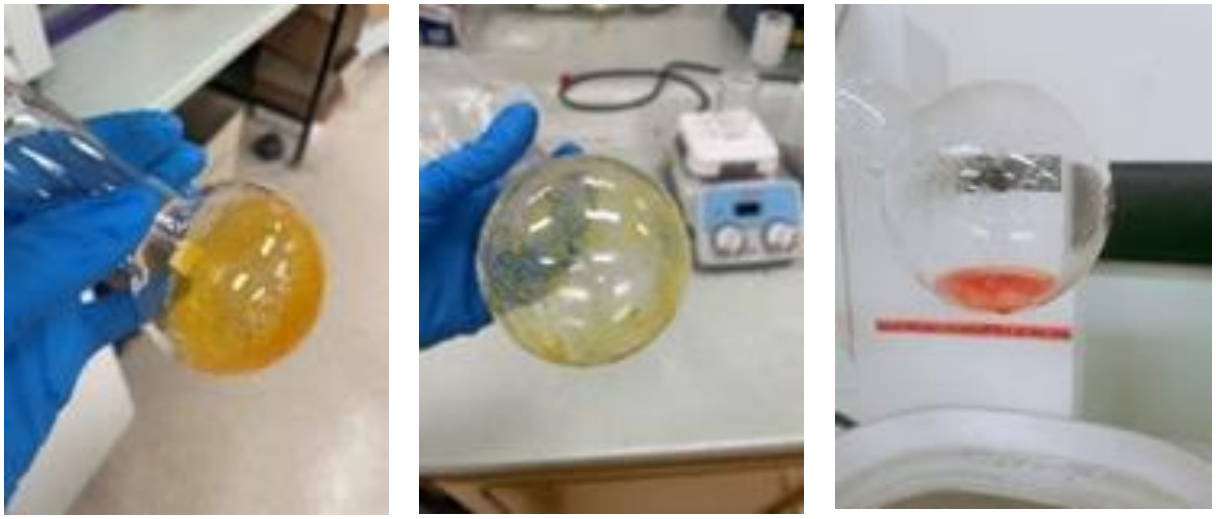

Figure 3-7. Visual appearance of samples after hydration.

(A) Flask containing sample CN5. (B) Flask containing sample CNF1 and (C) Flask containing sample CNF4 (in image C, the sample has not been removed yet).

3.4.1.3 Z-average size, PDI and EE% of DFN

In this study, doxorubicin was encapsulated into F127-niosomes. The formulations were optimized to achieve stable nanoparticles with favorable size, PDI, and encapsulation efficiency.

DFN1 nanoformulations: The DFN1 formulation exhibited a Z-average particle size of 209.2 nm and a PDI of 0.243, indicating a relatively uniform particle distribution.

DFN2 nanoformulations: Since DFN2 exhibited better PDI and particle size compared to the other DFN formulations, different probe sonication durations were investigated to further optimise this formulation. The results for the DFN2 samples (1–7) are summarised in **Table 3-4**, which presents their Z-average particle size and PDI values.

Table 3-4. Average Size and PDI for DFN2 Formulations with Different Sonication Conditions

Sample ID	Sonication Method	Sonication Details	Z-Average (d.nm)	PDI
1	Bath sonication	7 minutes	1384	0.666
2	Probe sonication	7 minutes	282.5	0.379
3	Bath + Probe sonication	7 min bath followed by 7 min probe	457.2	0.658
4	Bath + Probe sonication	7 min bath followed by 14 min probe	361.2	0.507
5	Bath sonication	14 minutes	1195	0.387
6	Probe sonication	14 minutes	194.1	0.258
7	Probe + Bath sonication	14 min probe followed by 14 min bath	422.8	0.410

Among these samples, Sample 6 demonstrated the most favourable results, with a Z-average size of 194.1 nm and a PDI of 0.258, indicating a well-dispersed and stable formulation. This sample underwent 14 minutes of probe sonication only, which appeared to be the optimal processing condition. Due to its superior size and PDI values, Sample 6 was selected for further analysis, and its EE% was measured at 63% ± 5.3, confirming its potential as an optimised formulation.

DFN3 nanoformulations: The DFN3 formulation exhibited a Z-average particle size of 607.5 nm and a PDI of 0.658, suggesting a higher degree of polydispersity and larger particle size, which may compromise stability.

DFN4 nanoformulations: The DFN4 formulation showed a Z-average particle size of 6658 nm with a PDI of 0.432. This exceptionally large particle size, indicating poor formulation stability and particle aggregation.

These findings highlight the importance of probe sonication time and formulation conditions in achieving optimal particle size and stability.

The results suggest that DFN2 Sample 6 provides the best characteristics for further investigation and potential application.

3.4.1.4 Size measurement, EE% of CDFN and EE% of CDN

Based on the results in 3.3.4.3, which showed better PDI, size and EE% with CDFN2, subsequent studies, including fabrication of targeted niosomes and *in vitro* analyses, were conducted using CDFN2.

EE% was evaluated for the formulations CDFN2 and CDN. For CDFN2, the EE% equivalent to Dox was 58.6%, while the Dox-equivalent EE% for CDN was only 18.3%. Similarly, the EE% equivalent to Cur was 98% for CDFN2, whereas the Cur-equivalent EE% for CDN was only 30.1%. These results indicated that the inclusion of F127 in the CDFN2 formulation significantly enhanced efficient loading of Dox and Cur compared to CDN, highlighting its critical role in improving the EE% and stability of the nanoparticles (***Table 3-5***). Results are presented as mean ±SD, n=3.

Table 3-5. Characterization of Cur and Dox co-loaded niosomes (CDFN1 and CDFN2).

(Note. The CDN formulation exhibited poor recovery; therefore, its PDI and particle size were not measured, and the experiment was not repeated; the %EE value of CDN was obtained from a single run.)

Formulation	Dox (mg)	PDI	Size	Cur-EE%	Dox-EE%
CDN	2	-	-	30.1	18.3
CDFN1	2	0.323±0.02	260.2±15.7	91±9.5	40.3±4.8
CDFN2	5	0.314±0.05	244.6±20.2	98±1.8	58.6±6.4

3.4.1.5 Z-average size and PDI of LHRH- and ALN-targeted niosomes

The results in the table below show the Z-average size and PDI of different LHRH- and ALN-targeted niosomal formulations, including CDFLN, CDFAN, CDPAN, and CDPLN. Variations in size and PDI

indicate the influence of different targeting ligands on nanoparticle characteristics, affecting their stability and uniformity (**Table 3-6**).

Table 3-6. Summary of Z-Average Size and PDI of targeted niosomal formulations

Formulation	Z-average size	PDI
CDFLN	277.7	0.374
CDFAN	291.4	0.264
CDPLN	260.6	0.398
CDPAN	271.3	0.346

3.4.1.6 Comparison of Zeta potential of different niosomes

The zeta potential measurements highlight the influence of different components on surface charge and stability **(Table 3-7**). CN9 with a Zeta potential of -19.7 ± 1.5 mV showed moderate negativity due to Span 60 and cholesterol, while CFN4 had increased negativity from F127 (-26.2 ± 8.3 mV), enhancing charge exposure and stability. CDFN2 (-22.2 ± 5.4 mV) exhibited slightly reduced negativity potentially due to doxorubicin's partial charge neutralization.

The addition of LHRH further reduced negativity reaching -17.8 mV in CDFLN, indicating neutral or slightly positive charge interactions. CDFAN remained more negative with a Zeta poteintial of -19.9 mV due to positive alendronate's phosphate groups. However, DSPE-PEG-COOH exhibited significantly decreased zeta potential (CDPLN, -8.7 mV; CDPAN, -10.3 mV)

Table 3-7. Zeta potential of different targeted niosomal formulations

Formulation	Zeta potential
CN9	-19.7±1.5
CFN4	-26.2±8.3
CDFN2	-22.2±5.4
CDFLN	-17.8
CDFAN	-19.9
CDPLN	-8.7
CDPAN	-10.3

3.4.1.7 Conjugation of Alendronate with F127-succinate

Comparing the three spectra (F127–COOH, ALN–F127–COOH, and ALN) clearly demonstrates successful conjugation of alendronate to the polymer. The F127–COOH spectrum exhibits the expected

carboxylic acid O–H and C=O signals, while pure ALN shows its unique bisphosphonate fingerprint (multiple P–O/P=O bands in 1200–1000 cm^{-1} and a marker at ~1544 cm^{-1}). The conjugate's FTIR spectrum contains hallmarks of both components**:** the broad carboxyl O–H and C=O features of F127–COOH are replaced/shifting to amide bands (new amide I at ~1645 cm^{-1} and amide II at ~1540 cm^{-1}), and the distinctive phosphonate peaks of ALN (~1050 cm^{-1} and ~1540 cm^{-1}) are present. This combination of spectral changes – loss of the original acid carbonyl, emergence of amide bonds, and appearance of ALN's phosphonate vibrations – confirms that ALN has been covalently attached to F127–COOH. In conclusion, the FTIR analysis provides strong evidence that the conjugation reaction was successful, yielding an ALN–F127–COOH conjugate where alendronate's functional groups are integrally linked via newly formed amide bonds. (***Figure 3-8***)**.**

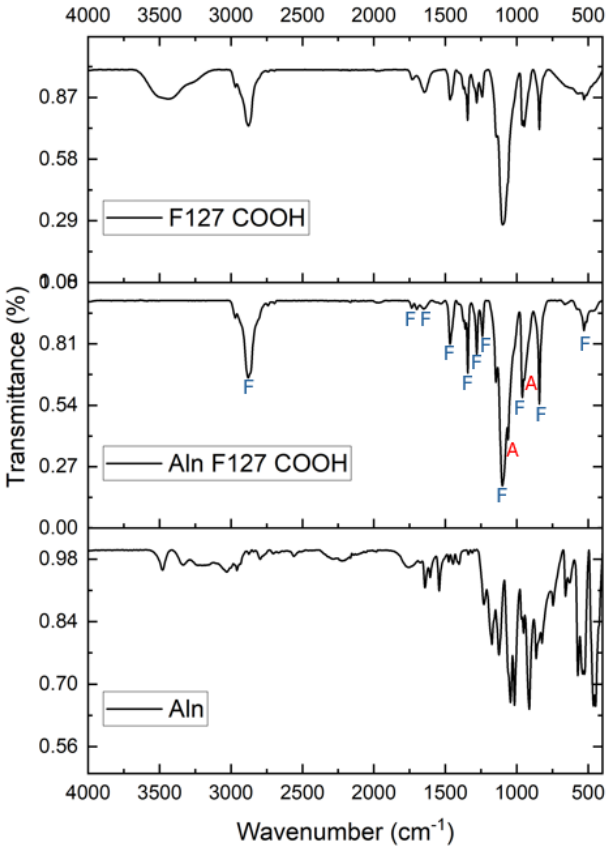

Figure 3-8. FTIR spectra of F127-COOH, ALN-F127-COOH, and ALN.

The ALN-F127-COOH spectrum shows characteristic phosphate peaks (1200–900 cm^{-1}) and amide bond signals, confirming successful conjugation of ALN to F127-COOH.

3.4.1.8 Assessing the conjugation of targeting agents to niosomes

FTIR spectroscopy was used to confirm the successful conjugation of [K^6(Ahx)]LHRH and ALN to CDFN, forming CDFLN and CDFAN, respectively. Key spectral shifts and new peaks provided direct evidence of covalent bond formation. The FTIR spectrum of CDFN exhibits a broad O–H stretching band (2500–3300 cm^{-1}) and a C=O stretching peak (~1700 cm^{-1}), confirming the presence of carboxyl (-COOH) groups, which are essential for conjugation. Upon conjugation with LHRH, the C=O stretching peak shifts (~1700 cm^{-1} → ~1640–1650 cm^{-1}), indicating amide bond formation, while a new amide II band (~1540 cm^{-1}) appears, confirming N–H bending coupled with C–N stretching, characteristic of peptide bond formation. Additionally, the disappearance of the free amine band (~1545 cm^{-1}) further supports LHRH conjugation (**Figure 3-9 A**). After conjugation of CDFN with ALN, the C=O peak shift (~1700 cm^{-1} → ~1640–1650 cm^{-1}) and the appearance of the amide II band (~1540 cm^{-1}) confirm amide bond formation between CDFN and ALN. Phosphate-related peaks (1200–1000 cm^{-1}) and a distinct phosphonate marker (~1544 cm^{-1}), absent in CDFN, validate the incorporation of ALN's phosphonate groups. FTIR spectral comparisons confirm the successful conjugation of LHRH and ALN to CDFN through amide bond formation, while phosphonate peaks uniquely validate ALN attachment (**Figure 3-9 B)**.

The spectra of linkers, such as F127_COOH, have been added in Section 2.4.1, while the DSPE-PEG spectrum was not obtained due to it being a commercial material.

The FTIR spectrum of CDPN confirmed the presence of key functional groups such as hydroxyl, carboxylate, and ether linkages, indicative of a suitable carrier for further conjugation. These characteristic features established the chemical foundation necessary for successful functionalization and targeting.

In the case of CDPLN, the FTIR spectrum revealed the emergence of distinct amide I and amide II bands around 1650 cm^{-1} and 1540 cm^{-1}, respectively—hallmark indicators of peptide bond formation. These findings, coupled with the broad N–H/O–H stretching region and additional peptide-associated vibrations in the fingerprint region, provide strong evidence for the successful conjugation of the LHRH decapeptide onto the CDPN carrier. The presence of these characteristic amide bands confirms the formation of covalent linkages between the carrier and the peptide, resulting in a structurally modified system optimized for receptor-targeted delivery (**Figure 3-9 C**).

For CDPAN, the FTIR spectrum similarly demonstrated successful conjugation of ALN through clear spectral shifts and the appearance of new peaks. Notably, strong phosphate-related absorptions between 1200–1000 cm^{-1} and a distinct peak around 1044 cm^{-1} confirmed the incorporation of ALN's phosphonate groups. Furthermore, the appearance of amide I and II bands in the regions of approximately 1650 cm^{-1} and 1540 cm^{-1} confirmed the formation of amide bonds between ALN and CDPN, indicating successful covalent attachment. These spectral features collectively confirm the effective functionalization of the niosomal surface with ALN, enabling bone-targeting potential (**Figure 3-9 D**).

In conclusion, the FTIR analysis confirmed that all CDFLN, CDFAN, CDPLN and CDPAN were successfully synthesized through covalent attachment of their respective targeting ligands. The observed spectral signatures provide strong evidence of chemical modification and validate these formulations for further targeted therapeutic applications.

A

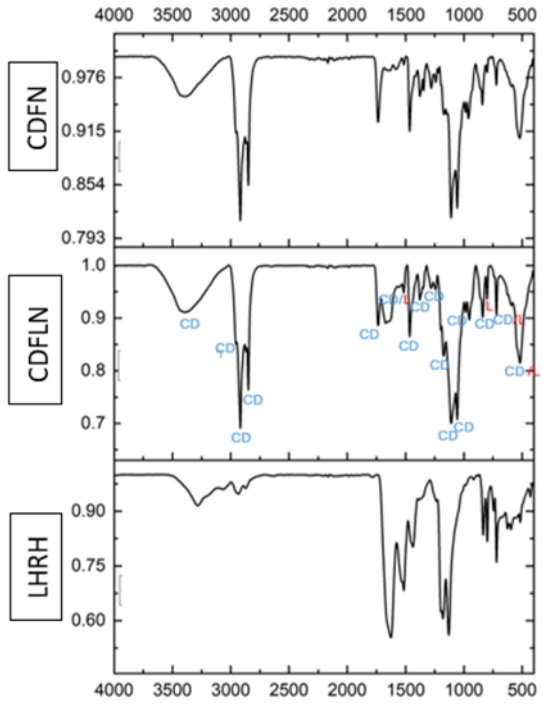

B

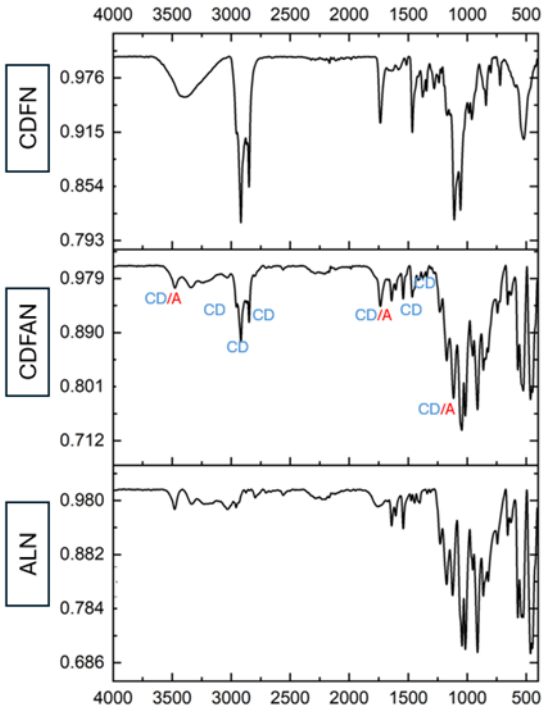

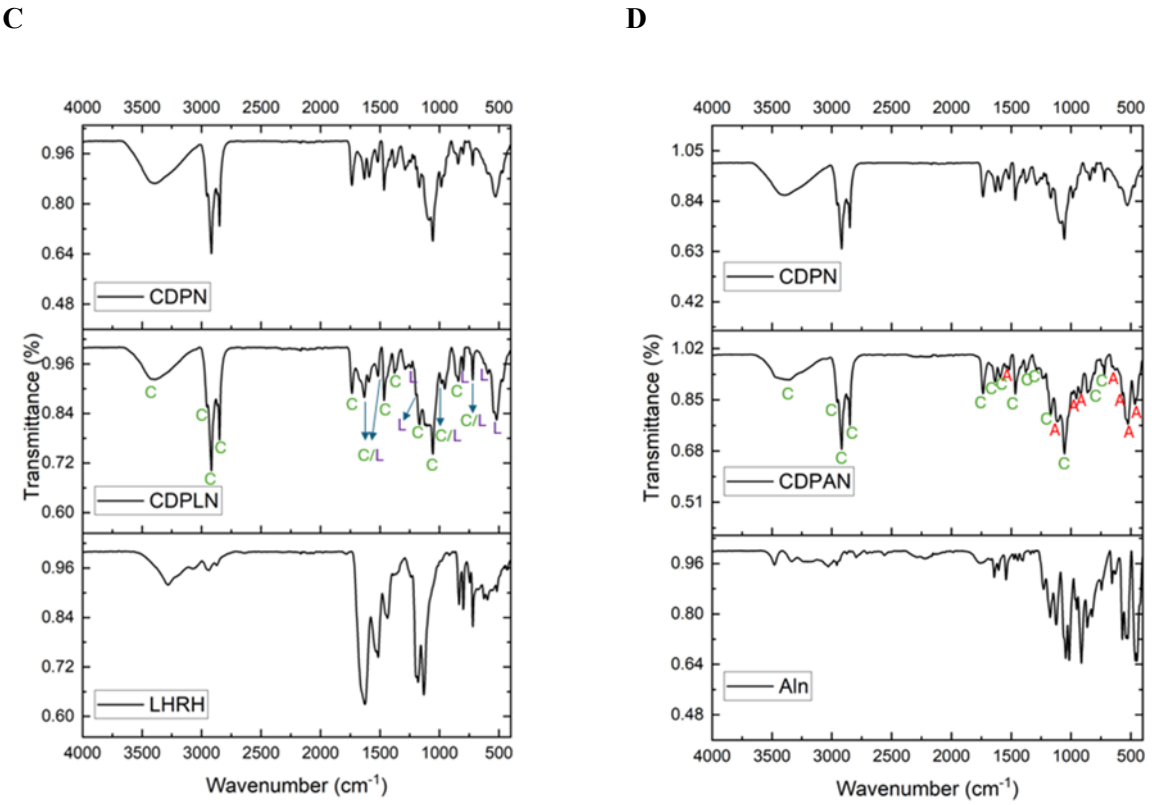

Figure 3-9. FTIR Spectra Confirming targeting agents Conjugation to CDFN.

The successful conjugation of CDFN with [K^6(Ahx)]LHRH to form CDFLN (A) .The successful conjugation of CDFN with ALN to form CDFAN (B). The successful conjugation of CDPN with [K^6(Ahx)]LHRH to form CDPLN (C). The successful conjugation of CDPN with ALN to form CDPAN (D).

3.4.2 *In vitro* experiments

3.4.2.1 Alamar Blue cell viability

The *in vitro* cytotoxicity of the fabricated niosomes were evaluated using the Alamar Blue (resazurin) viability assay on MDA-MB-231 cells. Viability of cells exposed to Void, free-Cur, free-Dox, CFN, DFN, and CDFN at an equivalent concentration of 50 µM Cur/Dox. Data are expressed as mean ± SD (n = 3), with $p < 0.0001$ indicating statistical significance (***Figure 3-10***A).

IC_{50} values show a significant reduction in cytotoxicity for nanoparticle-based formulations compared to their free payloads, confirming the improved anticancer effects of CFN, DFN, and particularly CDFN. The combined curcumin-doxorubicin formulation (CDFN) exhibited significantly enhanced cytotoxicity (IC_{50} = 0.7671 µM) compared to Dox F127 niosomes (DFN; IC_{50} = 2.096 µM) and Cur F127 niosomes (CFN; IC_{50} = 4.364 µM) ($p < 0.0001$). Based on the Chou–Talalay method, the calculated Combination Index (CI = 0.271) indicates a strong synergistic effect between curcumin and doxorubicin in the co-delivery system (***Figure 3-10*** **B**).

Two-way ANOVA analysis confirms significant differences between groups, with interaction, row, and column factors all yielding $p < 0.0001$. These findings support the superior cytotoxicity of CDFN compared to other formulations particularly DFN and CFN.

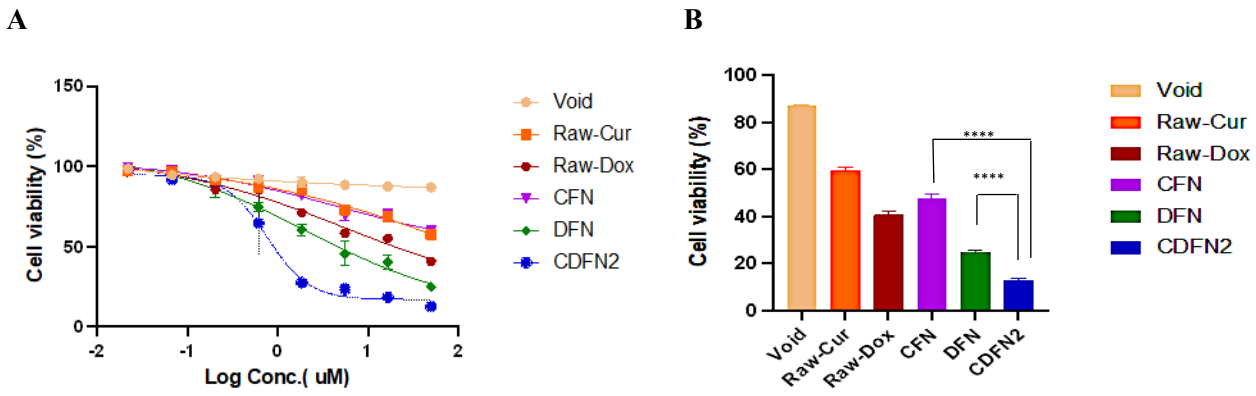

Figure 3-10. Cytotoxicity evaluation of free drug and NPs-based drug formulations in MDA-MB-231 Cells.

(A) Cell viability dose-response curve of MDA-MB-231 cells after exposure with void, free-Cur, free-Dox, CFN, DFN, and CDFN, demonstrating the enhanced cytotoxicity of nanoparticle-based formulations. **(B)** Comparative cell viability at a fixed concentration of 50 µM Cur/Dox. Statistically significant differences were observed between CDFN2 and both DFN and CFN (****p < 0.0001). Combination Index (CI) was calculated using the Chou–Talalay method based on IC_{50} values, with CI = 0.271 indicating a strong synergistic interaction between curcumin and doxorubicin in the co-loaded formulation. Data are expressed as mean ± SD (n = 3).

3.4.2.2 *In vitro* cytotoxicity assessment

The cellular uptake and cytotoxic effects of CFN, DFN and CDFN nanoparticles on MDA-MB-231 breast cancer cells were monitored over a 24 h period using IncuCyte SX5 live-cell imaging, with PBS-treated cells. In the initial 0–2 h after treatment, CFN- and DFN-treated cells exhibited only faint green

fluorescence and minimal morphological changes, indicating limited nanoparticle uptake and negligible early cytotoxic effects. In contrast, cells treated with CDFN showed bright green fluorescence within the first 2 h (reflecting rapid uptake) accompanied by the onset of mild cytotoxic changes such as slight cell rounding, while PBS-treated cells displayed no fluorescence or morphological alterations. By 4 h, differences between formulations were more pronounced: CDFN-treated cells presented further intensified intracellular green fluorescence and more notable morphological deterioration (e.g. increased cell shrinkage and membrane blebbing), whereas cells in the CFN and DFN groups showed only moderate increases in fluorescence with minor changes in cell shape. At 12 h, CDFN's superiority became even more evident, as CDFN-treated cells exhibited widespread intense fluorescence and significant cytotoxic effects (many cells rounding up and detaching), whereas cells in the CFN and DFN groups showed only modest fluorescence and much milder morphological changes. By 24 h, CDFN demonstrated the highest cytotoxic impact, with CDFN-treated cells displaying maximal green fluorescence and extensively disrupted morphology (most cells rounded and non-viable), underscoring CDFN's superior uptake and cytotoxicity (***Figure 3-11***). In comparison, CFN and DFN treatments caused only moderate fluorescence accumulation and partial cell damage by 24 h, with many cells still attached and viable, whereas PBS-treated cells remained completely unaffected, showing no fluorescence and healthy morphology throughout the experiment

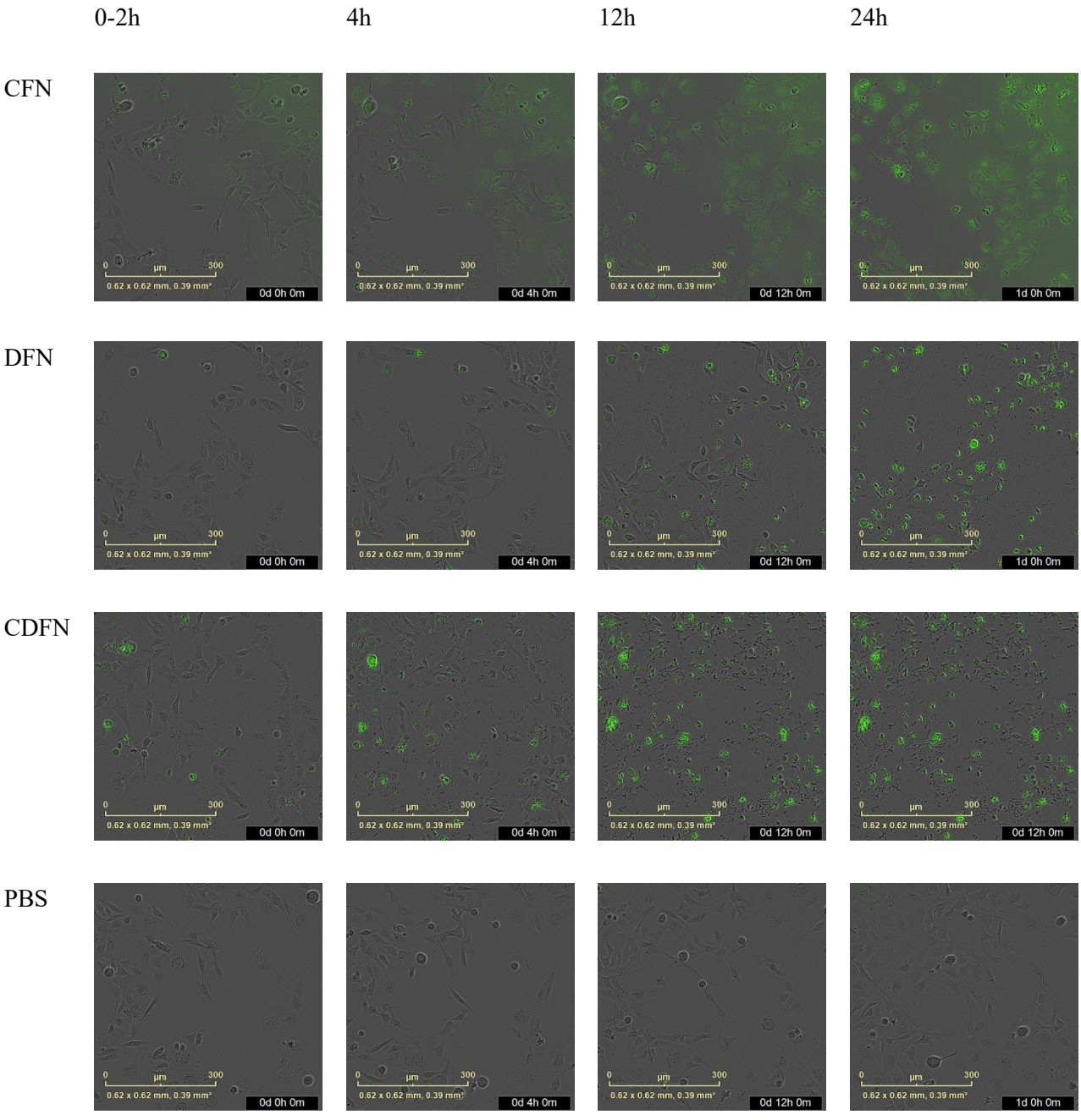

Figure 3-11. **Time-dependent cellular uptake of niosomes monitored by IncuCyte® Imaging.**

IncuCyte® images at time points 0–2, 4, 12, and 24 hours from MDA-MB-231 TNBC cells exposed to CFN, DFN, CDFN, and PBS at a concentration of 10 µM. Green fluorescence indicates drug uptake, with a noticeable increase over time in CFN, DFN, and CDFN groups. The highest fluorescence was observed in the CDFN group at 24 hours, while the PBS control showed no fluorescence.

3.4.2.3 Anticancer studies using IncuCyte in 3D models

The spheroid disintegration measurement was performed to evaluate the cytotoxic effects of PBS (control), Void, free-Cur, free-Dox, and CDFN formulations on MDA-MB-231 tumor spheroids over a 4-day period. The total area, representing the spheroid core and disintegrated material, was quantified using the IncuCyte analysis module with spheroid-specific masks (***Figure 3-12***). A larger total area indicates greater disruption of the spheroid structure. The results were visualized in a line graph to show the extent of disintegration over time (***Figure 3-13***), and representative images were captured to reflect structural changes at each time point (***Figure 3-14***).

At Day 0, all spheroids across treatment groups maintained compact morphology with no signs of disintegration. By Day 2, spheroids treated with free-Cur and free-Dox began showing early signs of disintegration, with a slight increase in total area compared to Void and PBS. free-Cur–treated spheroids exhibited partial loosening of the outer cell layers, while free-Dox caused mild expansion of the spheroid perimeter. In contrast, PBS- and Void-treated spheroids remained morphologically intact with minimal change in total area.

By Day 4, disintegration became more evident in the free-Cur and free-Dox groups. The free-Cur group showed moderate spheroid breakup and scattered cell material, while free-Dox resulted in more extensive spreading, indicating greater cytotoxicity. However, both groups were less effective than CDFN.

Spheroids treated with CDFN demonstrated the most significant disruption, as indicated by the largest total area in the red line of the graph. CDFN-treated spheroids exhibited near-complete structural collapse, with disaggregated cells spreading outward into the surrounding matrix. These changes were clearly visible in the captured images, showing extensive structural breakdown by Day 4 (***Figure 3-13***). In comparison, spheroids in the PBS and Void groups retained their dense, compact morphology with no visible signs of disintegration throughout the experiment.

Overall, the results confirm that CDFN nanoparticles induce the highest degree of spheroid disintegration.

Representative time-lapse videos for each treatment group, captured using the IncuCyte SX5 system to monitor cell viability over time, can be found in Appendix 1 (Section 6.1).

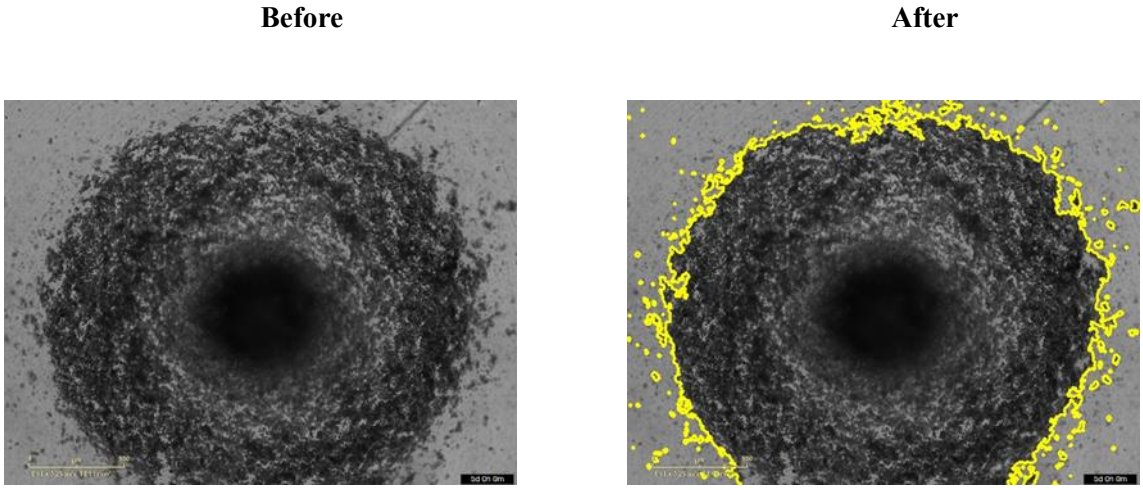

Figure 3-12. **Spheroid Disintegration Before and After Masking**

The images represent MDA-MB-231 spheroids treated with the CDFN formulation. The "After" image highlights disintegrated areas (yellow) detected by masking, confirming treatment-induced breakdown of the spheroid structure.

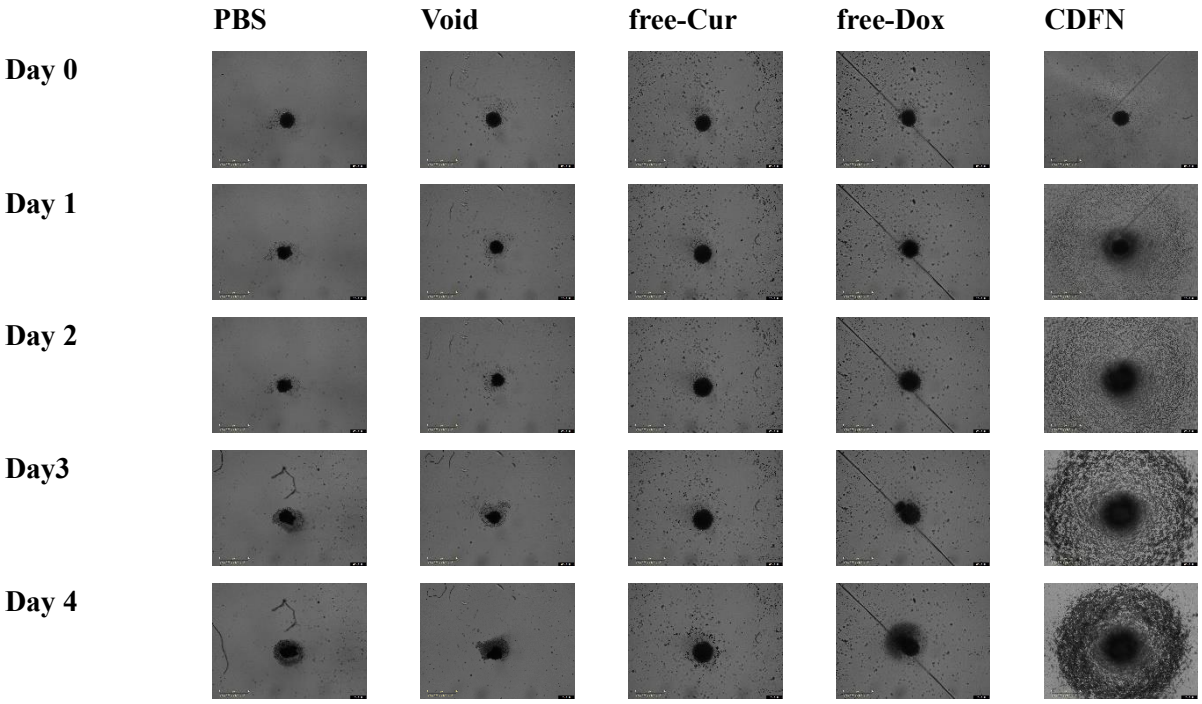

Figure 3-13. Spheroid integrity over time following treatment.

Representative images of spheroid integrity over four days for different treatments, including PBS (control), Void, free-Cur, free-Dox, and CDFN. Spheroid disintegration was assessed using the IncuCyte® analysis module.

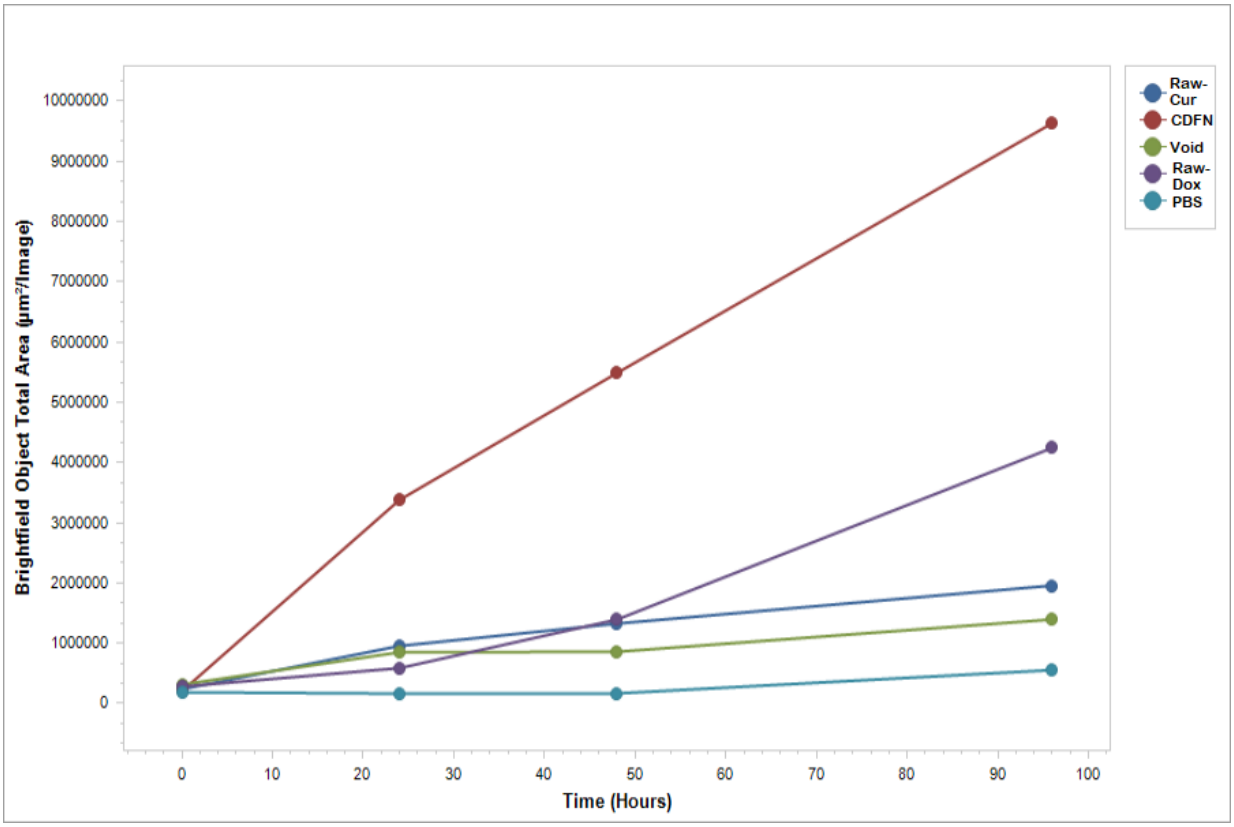

Figure 3-14. Quantitative Analysis of Spheroid Disintegration Over Time.

Quantification of total disintegrated spheroid areas over time using image analysis. Spheroids were treated with CDFN, and the total disintegrated area was measured at multiple time points to assess the extent of spheroid disruption.

3.4.2.4 Bone mineral affinity study

The Ca-coated plate assay was used to assess the binding affinity of niosome formulations to a calcium-rich surface, simulating potential interactions with biological mineralized environments. The results demonstrated that at 0 h, the absorbance values for both CDPAN and CDPN were similar across all concentrations (500, 250, and 125 µM), indicating that both niosome formulations were initially present

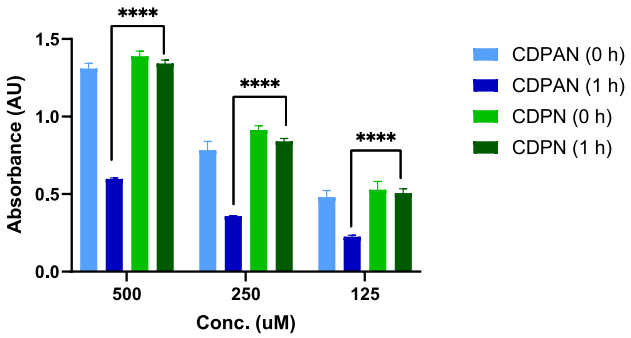

in comparable amounts in solution (

Figure 3-15). After 1 h, a significant difference was observed, with CDPAN showing a markedly lower absorbance than CDPN across all concentrations. This decrease in absorbance for CDPAN suggests a stronger binding affinity to the bone-mimicking calcium surface, resulting in a greater reduction of free-floating niosomes in solution. In contrast, CDPN maintained higher absorbance over time, indicating its weaker interaction with the surface.

A two-way ANOVA analysis was performed to evaluate the independent and interactive effects of targeting (ALN conjugation), concentration, and time on calcium binding efficiency. This analysis determines how these factors contribute to variations in absorbance, providing insights into the differences in niosome attachment to the bone-mimicking surface. A two-way ANOVA confirmed statistically significant differences ($p < 0.0001$) between alendronate targeted nanoparticles (CDPAN) and untargeted niosomes (CDPN) following one hour incubation demonstrating the influence of targeting (ALN conjugation), concentration, and time on binding affinities to the Ca coating of the plates. The significant p values ($p < 0.0001$) indicate that ALN conjugation and time-dependent changes are the primary contributors to calcium binding. These findings strongly support that ALN-conjugated niosomes (CDPAN) exhibit significantly higher binding affinity to bone-mimicking surfaces compared to non-targeted CDPN, highlighting their potential for targeted drug delivery in bone-related conditions.

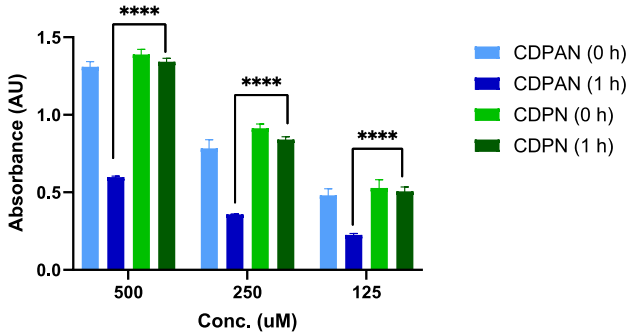

Figure 3-15. Binding the affinity of CDPAN and CDPN to a Calcium-coated surface.

Absorbance measurements were taken at 0 h and 1 h across different concentrations using a Victor X plate reader at 570 nm (photometry technology). Data are presented as mean ± SD, with statistical significance confirmed by two-way ANOVA, n=3, showing differences between CDPAN and CDPN following one hour incubation (****$p < 0.0001$).

3.4.2.5 Stability studies

The stability of CDFN niosomes was assessed under various storage conditions over a period of 28 days Table 6-2, with size measurements using DLS analysis to monitor changes in particle size, indicating potential aggregation or structural stability.

At the initial time point (0 days), the niosomes exhibited a particle size of 244.6±20.2 nm with a PDI of 0.314±0.05, indicating a relatively uniform size distribution and high stability. After 3 days, niosomes stored in the fridge showed an increase in particle size to 383.3±18.2 nm and a PDI of 0.385±0.03. Conversely, samples stored at room temperature exhibited slightly larger particle sizes of 391.6 ±14.8nm and a higher PDI of 0.418±0.04, indicating greater instability under ambient conditions. By day 7, the particle size of niosomes stored in the fridge increased further to 1114±203 nm with a PDI of 0.436±0.03. Samples stored at room temperature showed more significant changes, with the particle size reaching 1560±312 nm and a PDI of 0.645±0.06, suggesting severe aggregation and instability.

Longer-term storage revealed a continued increase in particle size and PDI, even under refrigerated conditions. By day 14, the particle size reached 1431±110 nm with a PDI of 0.536±0.04. By day 21, a marked aggregation was observed with a particle size of 6312±500 nm and a PDI of 0.843±0.01. Finally, after 28 days of refrigerated storage, the particle size was recorded as 1849 nm with a PDI of 1.000. This does not indicate an actual reduction in size but rather reflects the limitation of the DLS technique, as particles larger than 10,000 nm are not detected and thus contribute to a distorted size distribution (**Figure 3-16**).

Overall, these results highlight the time-dependent and storage condition-dependent instability of CDFN niosomes, with refrigeration providing better stability compared to room temperature but still leading to significant aggregation over extended periods.

A

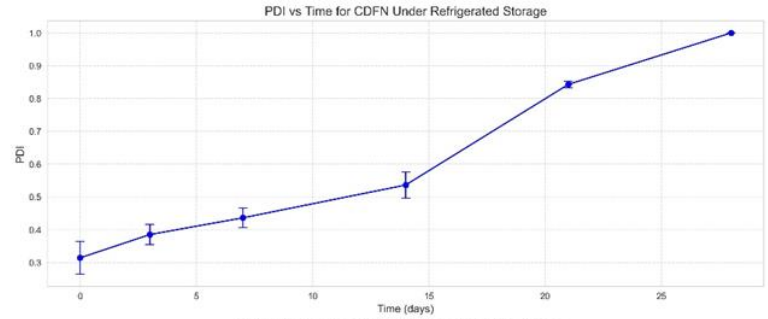
PDI vs Time for CDFN Under Refrigerated Storage
PDI
Time (days)

B

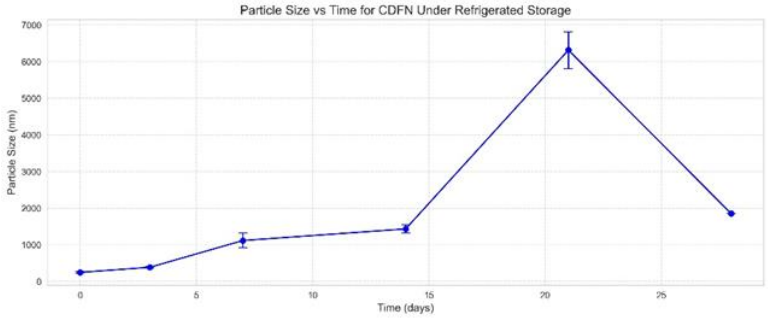
Particle Size vs Time for CDFN Under Refrigerated Storage
Particle Size (nm)
Time (days)

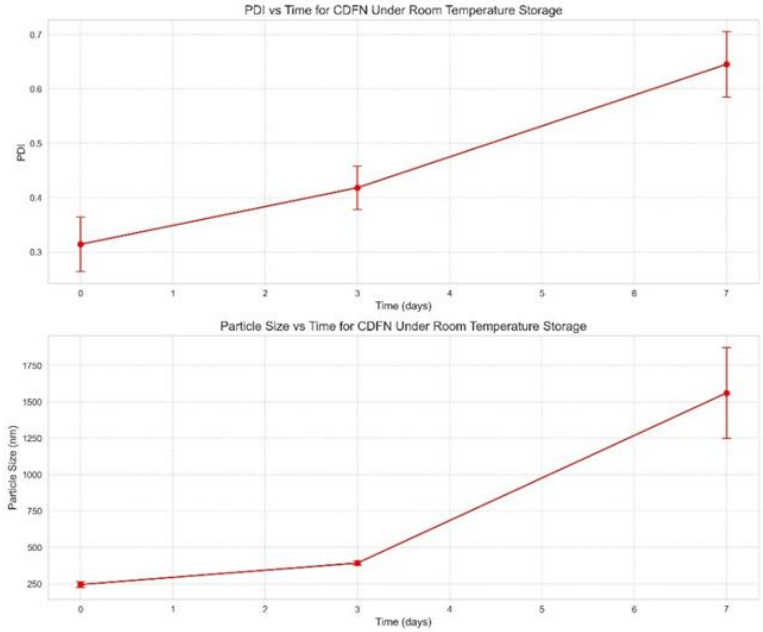

Figure 3-16. Stability profile of CDFN niosomes under different storage conditions.

Graphs A and B illustrate the time-dependent changes in PDI and particle size, respectively, for CDFN niosomes stored at fridge and room temperature, respectively.

3.4.2.6 Release study

The release profile of Dox and Cur from CDFN was evaluated at three different pH conditions (4.0, 6.5, and 7.4), representing the lysosomal environment, tumor microenvironment, and normal physiological conditions, respectively. The cumulative release of Dox and Cur was monitored over five times (8, 24, 48, 72, and 96 hours) **(Figure 3-17, Figure 3-18).**

At pH 4.0, Dox release was rapid, with 39.6% released within the first 8 hours, followed by a sustained increase to 63.1% at 24 hours and 82.4% at 96 hours, indicating enhanced drug release in acidic conditions. At pH 6.5, the release was slower, with 17.5% released at 8 hours, gradually increasing to 51.6% at 96 hours, suggesting that while Dox remains more stable in the tumor microenvironment, it still undergoes controlled diffusion over time. At pH 7.4, simulating normal physiological conditions, the release was the slowest, with only 9.6% at 8 hours and 43.2% at 96 hours, demonstrating that the formulation effectively retains Dox under physiological pH, which may help minimise off-target effects and enhance drug delivery specificity.

Two-way ANOVA analysis confirmed that both time and pH significantly affected Dox release (time: $\boldsymbol{p}$ = 0.0004; and pH: $\boldsymbol{p} < 0.0001$, respectively), with a significant interaction between the variables (***Figure 3-17***). These results strongly support the pH- and time-dependent release behavior of Dox from CDFN.

Overall, the pH-dependent release profile confirms that CDFN facilitates a controlled and sustained release of Dox, with a notably faster release in acidic environments, aligning with the expected behavior for effective drug delivery.

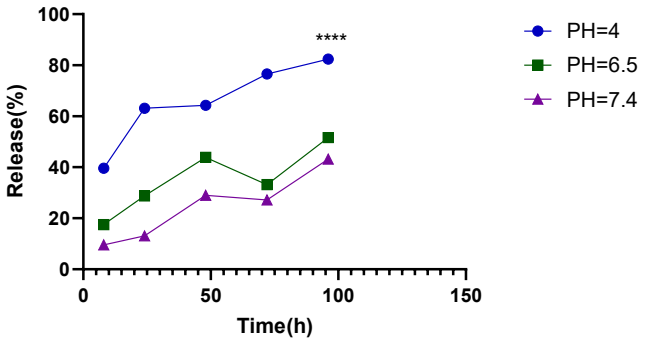

Figure 3-17. PH-dependent release profile of Dox from CDFN.

In vitro, release Dox from CDFN at pH 4.0, 6.5, and 7.4 over 96 hours. The release was highest at pH 4.0, indicating pH-dependent controlled drug release. Data are presented as mean ± SD, with statistical significance confirmed by two-way ANOVA, n=3, showing differences between the release of Dox in pH 4 compared to pH=6.5 and 7.4 (****$p < 0.0001$).

The Cur release profile from CDFN was evaluated at three different pH conditions (4.0, 6.5, and 7.4) over a period of 96 hours to simulate the lysosomal environment, tumor microenvironment, and normal physiological conditions, respectively. The data revealed a pH-responsive release behavior, with significantly enhanced Cur release observed in acidic conditions. At pH 4.0, the release was rapid and sustained, with 12.0% of Cur released within the first 8 hours, followed by a steep increase to 67.0% at 24 hours. The release continued to rise, reaching 93.9% at 96 hours, indicating a strong responsiveness to the lysosomal environment.

At pH 6.5, mimicking the tumor microenvironment, the release was slower than at pH 4.0, with 7.9% released at 8 hours and 30.0% at 24 hours. Over time, the cumulative release increased, reaching 55.0% at 96 hours, suggesting moderate but sustained Cur diffusion under these conditions. At pH 7.4, representing normal physiological conditions, Cur exhibited the slowest release, with only 5.0% released at 8 hours and 21.0% at 24 hours. The cumulative release gradually increased to 44.0% at 96 hours, demonstrating the formulation's ability to limit premature Cur release in neutral conditions, which could help reduce off-target effects.

A two-way ANOVA confirmed that both time and pH had statistically significant effects on Cur release (time: $p = 0.0016$; and pH: $p = 0.0006$, respectively), with a significant interaction between the two variables (***Figure 3-18***). These findings support observed time- and pH-dependent release behavior.

These results confirm that CDFN provides a controlled and sustained release of Cur, with preferential release in acidic environments, making it a promising formulation for drug delivery where pH-sensitive drug release is beneficial.

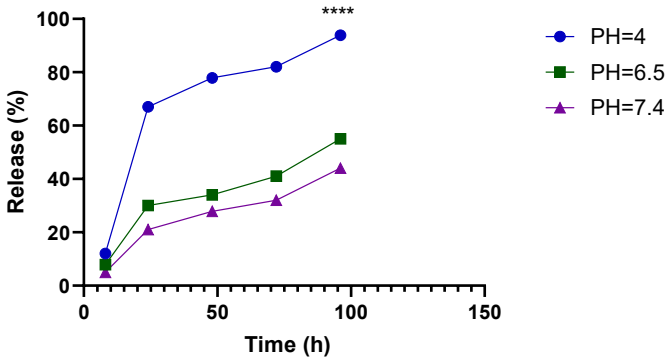

Figure 3-18. pH-Dependent Release Profile of Cur from CDFN.

In vitro, the release of Cur from CDFN at pH 4.0, 6.5, and 7.4 over 96 hours, showing enhanced release in acidic conditions. Data are presented as mean ± SD, with statistical significance confirmed by two-way ANOVA, n=3, showing differences between the release of Cur in pH 4 compared to pH=6.5 and 7.4 (****$p = 0.0006$).

3.4.2.7 Scanning electron microscopy (SEM)

The morphological characteristics of CDFN niosomes were analyzed using SEM. The images revealed well-defined, spherical structures with smooth surfaces and uniform size distribution, confirming the successful fabrication of niosomes. High-magnification SEM images (18.00KX) (**Figure 3-19A)** demonstrated individual niosomes with distinct morphology, while lower magnification images (10.93KX) (**Figure 3-19 B)** displayed an even distribution of nanoparticles across the substrate. The absence of significant aggregation suggests the robustness and stability of the formulation. These findings further support the suitability of CDFN niosomes for targeted drug delivery applications, as their controlled size and shape can facilitate efficient cellular uptake and sustained drug release. The average particle size was consistent with approximately 200-300 nm, aligning with the intended nanoparticle size from DLS.

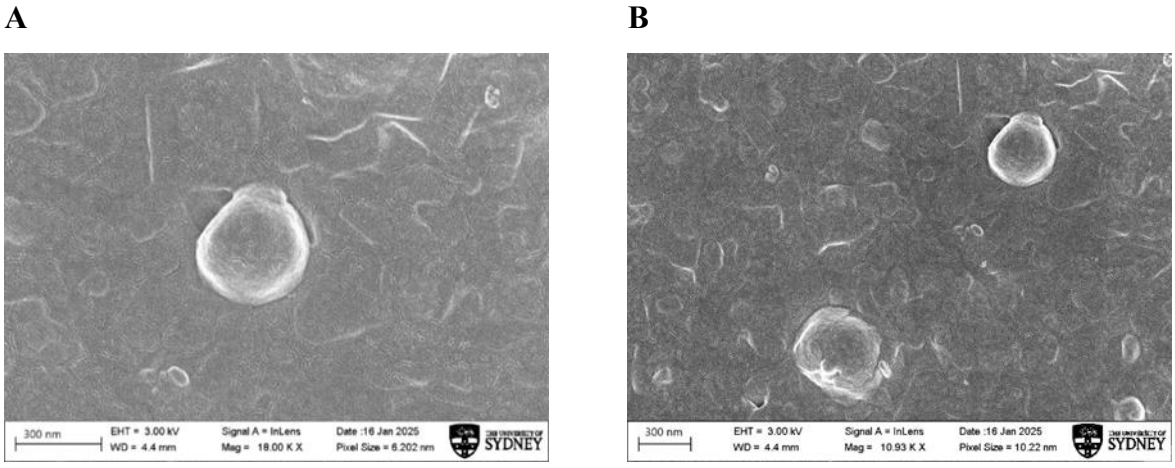

Figure 3-19. SEM characterization of CDFN at high magnification.

High-magnification images (A = 18.00KX, B = 10.93KX) depict the spherical morphology, smooth surfaces, and uniform size distribution of CDFN niosomes. The images confirm the successful fabrication of well-defined structures with minimal aggregation.

3.5 Discussion

This study presents the successful development of a dual-drug delivery niosomal system (CDFN) for enhanced TNBC therapy and bone metastasis targeting. Designed to co-deliver curcumin and doxorubicin, the formulation was optimized to improve encapsulation EE%, cellular uptake, pH-responsive release, and bone targeting.

CDFN niosomes exhibited uniform nano-scale morphology with enhanced stability due to the incorporation of Pluronic F127. This co-surfactant significantly increased EE%, particularly by reducing drug loss during formulation, resulting in higher curcumin and doxorubicin loading compared to non-F127 systems. SEM confirmed spherical nanoparticles with average sizes within the optimal range. Zeta potential analysis revealed that F127 contributed to a more negative charge, enhancing dispersion stability, while PEGylation provided stealth properties by reducing opsonization (200, 229). Although short-term stability was confirmed under refrigeration, long-term storage resulted in aggregation, highlighting the need for future optimization through strategies like lyophilization using cryoprotectants such as trehalose ((208, 230, 231),

In vitro studies showed that CDFN exhibited superior cytotoxicity against TNBC cells compared to mono-drug niosomes (CFN, DFN) or free drugs, with significantly lower IC50 values. This effect could be attributed to synergistic interaction between Cur and Dox. Curcumin's ability to sensitize cancer cells to doxorubicin through inhibition of resistance pathways such as NF-κB and P-gp pumps further contributed to this enhanced efficacy (91).

CDFN also demonstrated high therapeutic performance in a 3D spheroid model, simulating in vivo tumors more realistically. Treatment led to near-complete spheroid disintegration by day four, outperforming free drugs and non-targeted formulations. This performance was likely due to optimized nanoparticle size that enables deep tumor penetration and sustained release throughout the spheroid.

The pH-responsive behavior of CDFN further enhanced specificity. Drug release was minimal at physiological pH but significantly accelerated in acidic environments, particularly at pH 4.0 and 6.5, which simulate the lysosomal and tumor microenvironments, respectively. This selective release pattern is

aligned with prior pH-sensitive nanoformulation strategies (91, 232), and is intended to maximize drug activity in the tumor milieu while minimizing off-target toxicity in normal tissues.

However, the high release observed at pH 4.0—representing the lysosomal environment—also suggests that a significant portion of the drug may be released intracellularly within acidic vesicles following endocytosis (233). Since both doxorubicin and curcumin primarily exert their therapeutic effects in the cytosol or nucleus, premature drug release inside lysosomes may lead to reduced efficacy due to sequestration or degradation. To address this, future studies could incorporate endosomal escape mechanisms into the CDFN design, such as pH-responsive membrane-disruptive peptides (e.g., HA2) and proton sponge polymers (e.g., polyethylenimine) that facilitate drug release after cytosolic entry (234). These enhancements may help ensure effective intracellular drug delivery and optimize therapeutic performance.

The pH-responsive behavior of CDFN further enhanced specificity. Drug release was minimal at physiological pH but significantly accelerated in acidic environments mimicking tumor conditions. This selective release mechanism aligns with prior pH-sensitive nanoformulation strategies (91, 232), ensuring that the therapeutic effect is concentrated at tumor sites while sparing healthy tissues.

LHRH ligand functionalization was also successfully confirmed via FTIR, and bone-targeting was achieved via ALN conjugation, confirmed through calcium-coated plate assays. ALN-functionalized niosomes (CDPAN) showed significantly higher binding to bone-like surfaces compared to non-targeted formulations, indicating functional ligand retention after conjugation. This strategy provides a potential therapeutic avenue for preventing or treating bone metastasis, a frequent complication in TNBC (3, 235)). By directing drug payloads to bone, CDFAN may achieve high local drug concentrations while limiting systemic toxicity.

Overall, this work demonstrates that a dual-drug nanoparticle system can overcome key challenges in TNBC treatment by improving delivery, enhancing cytotoxicity, and reducing off-target effects. The formulation’s co-delivery strategy enhances the pharmacological synergy between curcumin and doxorubicin while the engineered stability and targeting features ensure optimal delivery to BC cells. Translational work ahead includes enhancing long-term storage stability, evaluating biodistribution and immune responses in vivo, and validating targeting efficiency in animal models.

In the context of clinical translation, the application of dual-targeted delivery systems such as LHRH- and ALN-functionalized niosomes requires careful consideration of pharmacokinetic compatibility, ligand stability, and potential regulatory challenges. LHRH-targeting offers specificity toward tumor cells expressing LHRH receptors (214), while ALN provides bone-targeting capability (211), making their combination particularly attractive for treating metastatic TNBC in bone. However, integrating both targeting ligands into a single dosage form raises questions regarding steric hindrance, receptor competition, and the balance of targeting efficiency (236). While a co-functionalized single formulation may enhance synergistic delivery (237) to bone metastases expressing both receptors, separate administration of LHRH- and ALN-targeted niosomes could allow for more precise temporal or site-specific targeting, potentially minimizing off-target interactions and allowing for dose adjustment of each moiety independently (214). Further preclinical studies and clinical pharmacology assessments are necessary to determine the most effective and clinically viable strategy for dual-ligand delivery.

3.6 Conclusion

In conclusion, the findings of this study highlight the potential of CDFN niosomes as a promising drug delivery system for enhancing the efficacy of anticancer treatments. The results demonstrated that CDFN niosomes significantly disrupted tumor spheroid structures, indicating their ability to improve drug penetration and efficacy in 3D tumor models, which better replicate *in vivo* conditions. Both LHRH- and ALN-targeted niosomes were successfully fabricated. ALN-targeted niosomes exhibited a strong affinity for calcium in the bone-mimicking plate, reinforcing their potential for site-specific drug delivery in breast cancer bone metastases. This targeted approach could enhance drug retention at metastatic bone sites, reducing systemic toxicity and improving treatment precision. Furthermore, the pH-sensitive release profiles observed for Dox and Cur suggest that CDFN niosomes provide targeted and controlled drug delivery, maximizing therapeutic effects while minimizing off-target toxicity. However, the study also identified stability challenges, particularly with particle aggregation over time, underscoring the need for further optimization to achieve improved its shelf stability. Future research should focus on addressing these stability concerns, evaluating the *in vivo* therapeutic potential of CDFN niosomes, and exploring their application in combination therapies to improve treatment outcomes and overcome drug resistance in cancer therapy. Overall, CDFN niosomes represent a significant advancement in nanomedicine,

offering a versatile and efficient platform for enhancing the delivery and effectiveness of anticancer agents.

Chapter 4. Overall discussion and Conclusion

4.1 Discussion

This thesis explored two strategic nanocarrier systems designed to address key therapeutic challenges in triple-negative breast cancer (TNBC), a highly aggressive and treatment-resistant subtype of breast cancer. Through the development of LHRH-targeted curcumin micelles (Chapter 2) and curcumin–doxorubicin dual-drug niosomes, separately functionalized with tumor-targeting (LHRH) and bone-targeting (ALN) ligands (Chapter 3), this research offers an integrated approach to improving drug delivery, tumor specificity, and therapeutic outcomes in TNBC. The overarching goal was to design and optimize nanoparticle-based formulations that could overcome the intrinsic limitations of conventional chemotherapy—such as poor drug solubility, off-target toxicity, multidrug resistance, and ineffective targeting of metastasis, particularly in bone. This thesis expanded the therapeutic strategy from single-drug delivery to combination therapy and broadened the targeting scope by developing separate systems for tumor-targeted and bone-targeted delivery. This final section synthesizes the findings from both systems, reflects on their broader scientific and clinical relevance, and outlines future directions for translation.

4.2 Integrated evaluation of the two delivery systems

The targeted micellar system developed in Chapter 2 demonstrated that a natural compound like curcumin, which typically suffers from poor aqueous solubility and limited bioavailability, can be effectively delivered to TNBC cells when encapsulated in a Pluronic F127-based polymeric micelle and functionalized with LHRH peptides. This targeted design not only enhanced curcumin's uptake in LHRH receptor-overexpressing TNBC cells, but also translated into improved cytotoxicity, confirming that receptor-mediated endocytosis can significantly increase intracellular drug accumulation. These findings emphasize the therapeutic potential of curcumin when its pharmacokinetic limitations are resolved and it is directed specifically toward tumor cells. The work also provided early validation of the LHRH ligand as a targeting mechanism, offering a non-hormonal approach to engage a receptor that is upregulated in a significant proportion of TNBC tumors.

Building on this success, Chapter 3 introduced a more complex but synergistic niosomal platform co-loaded with curcumin and doxorubicin. This system expanded the scope of therapy from single-drug delivery to combination therapy and from tumor targeting alone to both tumor and bone targeting. The optimized formulation incorporated Pluronic F127 for enhanced encapsulation efficiency. The result was

a smart delivery system capable of releasing its payload preferentially in acidic environments—mimicking the tumor microenvironment—and accumulating at bone metastatic sites. Cellular studies demonstrated that this system outperformed both free drugs and non-targeted controls in terms of uptake, cytotoxicity, and 3D tumor spheroid disintegration, offering strong in vitro evidence of its therapeutic promise.

Together, the findings from both chapters show a deliberate progression in nanomedicine design—from enhancing the delivery of a single compound to creating a multifunctional, targeted, and pH-responsive therapeutic platform. The micellar system provided proof-of-concept for receptor-mediated targeting using LHRH, while the niosomal system applied that principle to a dual-drug carrier that more closely aligns with the complex nature of metastatic TNBC.

4.3 Relevance to TNBC therapy

TNBC remains one of the most challenging breast cancer subtypes to treat, owing to its heterogeneity, absence of common molecular targets, and high rates of metastasis and recurrence. Standard chemotherapies often fail to provide durable responses due to systemic toxicity and acquired resistance. Nanomedicine offers a compelling solution by improving drug solubility, enhancing tumor accumulation, and enabling targeted delivery to reduce harm to healthy tissues. The research presented here contributes to this evolving field by designing nanoparticle systems tailored specifically to the biological features of TNBC—namely, LHRH receptor expression and bone metastatic behavior.

The niosomes developed in Chapter 3 provide a blueprint for reaching bone metastases, which are common in advanced breast cancer. This is particularly significant in the TNBC population, where systemic control is difficult, and targeted options are limited.

In the broader context of targeted cancer therapy, this research affirms the value of modular, ligand-functionalized delivery systems. It also demonstrates the potential of combining synthetic chemotherapeutics with plant-derived compounds like curcumin to leverage synergistic cytotoxic effects while mitigating toxicity. Such strategies align with current trends in personalized and precision oncology, which aim to tailor treatments to tumor biology and patient-specific features.

4.4 Limitations and future perspectives

While the findings are promising, several limitations must be acknowledged. The results presented here are primarily based on in vitro studies, including 2D and 3D models. These systems provide valuable

insights into cellular behavior and nanoparticle performance, but they cannot fully replicate the complexity of living organisms. Therefore, the next critical step is comprehensive in vivo evaluation. Future studies should assess biodistribution, pharmacokinetics, therapeutic efficacy, and safety in animal models, including orthotopic and metastatic TNBC models.

Another limitation is the absence of internalization studies in healthy (non-cancerous) cells. While selective uptake in TNBC cells was demonstrated, evaluating the potential off-target internalization in normal cells is essential to confirm targeting specificity and minimize systemic toxicity. This reflects the broader challenge of designing a single formulation that achieves both high therapeutic precision and safety. Future work should include parallel uptake assays in non-cancerous cells to better characterize the safety profile and inform clinical translation.

Future work also could explore dual-targeting with ALN and LHRH to combine LHRH-mediated cellular uptake with alendronate-driven bone localization—representing a next-generation therapeutic concept that not only targets primary tumor cells with precision but also reaches the metastatic microenvironment where they thrive.

Another area for development is the long-term stability and scalability of the formulations. While the micelles and niosomes showed good short-term stability under laboratory conditions, maintaining performance during storage, transport, and clinical preparation will require further optimization. Lyophilization and the use of cryoprotectants may offer solutions here. Additionally, ligand density and spatial orientation on the nanoparticle surface may affect binding efficiency and pharmacokinetics and supports systematic study.

Importantly, micelles' release kinetics is a critical regulatory and functional parameter that should be prioritised in the next study phase, as it plays a vital role in determining therapeutic performance and clinical acceptability.

Finally, the heterogeneity of TNBC tumors poses a translational challenge. While LHRH is a promising target, its expression is variable, and patient selection will be essential in any clinical application. Similarly, bone-targeting via alendronate may not benefit patients without bone metastases. For these reasons, future research should consider imaging-based pre-selection strategies (e.g., PET imaging of LHRH expression or bone lesions) to guide patient eligibility in clinical trials.

4.5 Conclusion

This thesis has demonstrated that the rational design of nanocarrier systems—integrating active targeting, combination therapy, and stimulus-responsive release—can offer significant advantages in the treatment of TNBC. The LHRH-targeted curcumin micelles improved cellular uptake and cytotoxicity by selectively engaging TNBC cells. Building on this foundation, the dual-drug niosomes further enhanced therapeutic potential by co-delivering synergistic agents. Together, these systems represent a flexible and effective approach to overcoming the limitations of conventional TNBC treatment. Although LHRH-targeted (CDFLN, CDPLN) and alendronate-targeted (CDFAN, CDPAN) niosomes were successfully synthesized, they were not fully characterized alongside the non-targeted CDFN formulation. Future studies will focus on detailed physicochemical characterization and in vitro evaluation of these targeted systems before progressing to in vivo or clinical investigations.

The results not only affirm the potential of ligand-functionalized nanocarriers in precision oncology but also pave the way for future in vivo validation and clinical translation. With further optimization and comprehensive biological testing, the nanocarrier systems developed in this thesis could evolve into viable therapeutic platforms for managing both localized and metastatic TNBC—ultimately contributing to improved outcomes and quality of life for patients facing this aggressive disease.

Chapter 5. References

1. Walsh EM, Smith KL, Stearns V. Management of hormone receptor-positive, HER2-negative early breast cancer. Semin Oncol. 2020;47(4):187-200.
2. Won KA, Spruck C. Triple-negative breast cancer therapy: Current and future perspectives (Review). Int J Oncol. 2020;57(6):1245-61.
3. Al-Mahmood S, Sapiezynski J, Garbuzenko OB, Minko T. Metastatic and triple-negative breast cancer: challenges and treatment options. Drug Deliv Transl Res. 2018;8(5):1483-507.
4. Wu Z, Li W, Jiang K, Lin Z, Qian C, Wu M, et al. Regulation of bone homeostasis: signaling pathways and therapeutic targets. MedComm (2020). 2024;5(8):e657.
5. Lei S, Zheng R, Zhang S, Wang S, Chen R, Sun K, et al. Global patterns of breast cancer incidence and mortality: A population-based cancer registry data analysis from 2000 to 2020. Cancer Communications. 2021;41(11):1183-94.
6. Liu S, Tang Y, Li J, Zhao W. Global, regional, and national trends in the burden of breast cancer among individuals aged 70 years and older from 1990 to 2021: an analysis based on the global burden of disease study 2021. Archives of Public Health. 2024;82(1):170.
7. Health AIo, Welfare. BreastScreen Australia monitoring report 2024. Canberra: AIHW; 2024.
8. Murthy SS, Trapani D, Cao B, Bray F, Murthy S, Kingham TP, et al. Premature mortality trends in 183 countries by cancer type, sex, WHO region, and World Bank income level in 2000–19: a retrospective, cross-sectional, population-based study. The Lancet Oncology. 2024;25(8):969-78.
9. Olufadewa I, Adesina M, Ayorinde T. Global health in low-income and middle-income countries: a framework for action. The Lancet Global Health. 2021;9(7):e899-e900.
10. Cancer data in Australia Australian Institute of Health and Welfare2024 [Available from: https://www.aihw.gov.au/reports/cancer/cancer-data-in-australia/contents/overview.
11. Survival Rate BC [Available from: https://ncci.canceraustralia.gov.au/outcomes/relative-survival-rate/5-year-relative-survival-diagnosis.
12. Health central [Available from: https://www.healthcentral.com/condition/breast-cancer/luminal-a-breast-cancer.
13. Breast cancer trials [Available from: https://www.breastcancertrials.org.au/luminal-b-breast-cancer/.
14. Health line [Available from: https://www.healthline.com/health/breast-cancer/understanding-managing/understanding-hr-breast-cancer-diagnosis.
15. MD Anderson [Available from: https://www.mdanderson.org/cancerwise/her2-positive-breast-cancer--what-it-is--diagnosis-and-treatment.h00-159542112.html.
16. Mastectomy [Available from: https://www.premiersurgicalnetwork.com/mastectomy-vs-lumpectomy/.
17. Yin L, Duan JJ, Bian XW, Yu SC. Triple-negative breast cancer molecular subtyping and treatment progress. Breast Cancer Res. 2020;22(1):61.
18. Zhu X, Chen L, Huang B, Wang Y, Ji L, Wu J, et al. The prognostic and predictive potential of Ki-67 in triple-negative breast cancer. Scientific Reports. 2020;10(1):225.
19. Zhu Y, Li K, Zhang J, Wang L, Sheng L, Yan L. The prognostic and predictive significance of cytokeratin 5/6 and epidermal growth factor receptor in metastatic triple-negative breast cancer treated with maintenance capecitabine. Transl Cancer Res. 2021;10(3):1193-203.
20. Zagami P, Carey LA. Triple negative breast cancer: Pitfalls and progress. npj Breast Cancer. 2022;8(1):95.

21. Park SY, Choi JH, Nam JS. Targeting Cancer Stem Cells in Triple-Negative Breast Cancer. Cancers (Basel). 2019;11(7).
22. Karim AM, Eun Kwon J, Ali T, Jang J, Ullah I, Lee Y-G, et al. Triple-negative breast cancer: epidemiology, molecular mechanisms, and modern vaccine-based treatment strategies. Biochemical Pharmacology. 2023;212:115545.
23. Xiao G, Annor GK, Fung K, Keinänen O, Zeglis BM, Bargonetti J. Targeting Triple Negative Breast Cancer with a Nucleus-Directed p53 Tetramerization Domain Peptide. Mol Pharm. 2021;18(1):338-46.
24. Arun B, Couch FJ, Abraham J, Tung N, Fasching PA. BRCA-mutated breast cancer: the unmet need, challenges and therapeutic benefits of genetic testing. British Journal of Cancer. 2024.
25. Singh DD, Parveen A, Yadav DK. Role of PARP in TNBC: Mechanism of Inhibition, Clinical Applications, and Resistance. Biomedicines. 2021;9(11).
26. Sukumar J, Gast K, Quiroga D, Lustberg M, Williams N. Triple-negative breast cancer: promising prognostic biomarkers currently in development. Expert Rev Anticancer Ther. 2021;21(2):135-48.
27. Hachey SJ, Hatch CJ, Gaebler D, Mocherla A, Nee K, Kessenbrock K, Hughes CCW. Targeting tumor–stromal interactions in triple-negative breast cancer using a human vascularized micro-tumor model. Breast Cancer Research. 2024;26(1):5.
28. Yu S, Wang S, Wang X, Xu X. The axis of tumor-associated macrophages, extracellular matrix proteins, and cancer-associated fibroblasts in oncogenesis. Cancer Cell International. 2024;24(1):335.
29. Grasset EM, Dunworth M, Sharma G, Loth M, Tandurella J, Cimino-Mathews A, et al. Triple-negative breast cancer metastasis involves complex epithelial-mesenchymal transition dynamics and requires vimentin. Sci Transl Med. 2022;14(656):eabn7571.
30. Ribatti D, Tamma R, Annese T. Epithelial-Mesenchymal Transition in Cancer: A Historical Overview. Transl Oncol. 2020;13(6):100773.
31. Yang Z, Luo, Y., Luo, J., Fang, Q., Miao, J., & Zhang, L. Influencing Factors and a Predictive Nomogram of Frailty in Chinese Patients with Cancer: A Single-Center Retrospective Study. European Journal of Cancer Care. 2024.
32. Bou Zerdan M, Ghorayeb T, Saliba F, Allam S, Bou Zerdan M, Yaghi M, et al. Triple Negative Breast Cancer: Updates on Classification and Treatment in 2021. Cancers (Basel). 2022;14(5).
33. Han HS, Vikas P, Costa RLB, Jahan N, Taye A, Stringer-Reasor EM. Early-Stage Triple-Negative Breast Cancer Journey: Beginning, End, and Everything in Between. American Society of Clinical Oncology Educational Book. 2023(43):e390464.
34. Reddy SM, Barcenas CH, Sinha AK, Hsu L, Moulder SL, Tripathy D, et al. Long-term survival outcomes of triple-receptor negative breast cancer survivors who are disease free at 5 years and relationship with low hormone receptor positivity. Br J Cancer. 2018;118(1):17-23.
35. Prakash O, Hossain F, Danos D, Lassak A, Scribner R, Miele L. Racial Disparities in Triple Negative Breast Cancer: A Review of the Role of Biologic and Non-biologic Factors. Front Public Health. 2020;8:576964.
36. Ghafouri SN, Nayeri RW, McAndrew NP, Hurvitz SA. Chemotherapy regimen choice and patient outcomes in early-stage triple-negative breast cancer: a retrospective analysis. Therapeutic Advances in Medical Oncology. 2022;14:17588359221085556.
37. Li A, Keck JM, Parmar S, Patterson J, Labrie M, Creason AL, et al. Characterizing advanced breast cancer heterogeneity and treatment resistance through serial biopsies and comprehensive analytics. NPJ Precis Oncol. 2021;5(1):28.
38. Hu XE, Yang P, Chen S, Wei G, Yuan L, Yang Z, et al. Clinical and biological heterogeneities in triple-negative breast cancer reveals a non-negligible role of HER2-low. Breast Cancer Res. 2023;25(1):34.

39. Immunohistochemistry: An Overview + Steps to Better IHC Staining [Available from: https://www.leicabiosystems.com/en-au/knowledge-pathway/immunohistochemistry-an-overview-steps-to-better-ihc-staining/.
40. Li L, Zhang F, Liu Z, Fan Z. Immunotherapy for Triple-Negative Breast Cancer: Combination Strategies to Improve Outcome. Cancers [Internet]. 2023; 15(1).
41. Petrucelli N, Daly MB, Pal T. BRCA1- and BRCA2-Associated Hereditary Breast and Ovarian Cancer. In: Adam MP, Feldman J, Mirzaa GM, Pagon RA, Wallace SE, Amemiya A, editors. GeneReviews(®). Seattle (WA): University of Washington, Seattle

42. .
43. Kuderer NM, Desai A, Lustberg MB, Lyman GH. Mitigating acute chemotherapy-associated adverse events in patients with cancer. Nature Reviews Clinical Oncology. 2022;19(11):681-97.
44. Mondal SB, Gao S, Zhu N, Liang R, Gruev V, Achilefu S. Real-time fluorescence image-guided oncologic surgery. Adv Cancer Res. 2014;124:171-211.
45. Wang Y, Shen J, Gu P, Wang Z. Recent advances progress in radiotherapy for breast cancer after breast-conserving surgery: a review. Front Oncol. 2023;13:1195266.
46. [Available from: https://www.mdanderson.org/cancerwise/triple-negative-breast-cancer-5-things-you-should-know.h00-158986656.html.
47. Mazonakis M, Kachris S, Damilakis J. SECOND CANCER RISK FROM RADIATION THERAPY FOR COMMON SOLID TUMORS DIAGNOSED IN REPRODUCTIVE-AGED FEMALES. Radiation Protection Dosimetry. 2018;182(2):208-14.
48. Heeke AL, Tan AR. Checkpoint inhibitor therapy for metastatic triple-negative breast cancer. Cancer Metastasis Rev. 2021;40(2):537-47.
49. Şimşek GÖ. Immunotherapy in the Treatment of Cancer: Today and Tomorrow. Current Molecular Biology Reports. 2024;10(3):54-64.
50. Bondar D, Karpichev Y. Poly(ADP-Ribose) Polymerase (PARP) Inhibitors for Cancer Therapy: Advances, Challenges, and Future Directions. Biomolecules [Internet]. 2024; 14(10).
51. Bouwman P, Jonkers J. Molecular pathways: how can BRCA-mutated tumors become resistant to PARP inhibitors? Clin Cancer Res. 2014;20(3):540-7.
52. Shaban N, Kamashev D, Emelianova A, Buzdin A. Targeted Inhibitors of EGFR: Structure, Biology, Biomarkers, and Clinical Applications. Cells. 2023;13(1).
53. Tao G, Chityala PK. Epidermal growth factor receptor inhibitor-induced diarrhea: clinical incidence, toxicological mechanism, and management. Toxicol Res (Camb). 2021;10(3):476-86.
54. Fabbrocini G, Panariello L, Caro G, Cacciapuoti S. Acneiform Rash Induced by EGFR Inhibitors: Review of the Literature and New Insights. Skin Appendage Disord. 2015;1(1):31-7.
55. Lopes-Coelho F, Martins F, Pereira SA, Serpa J. Anti-Angiogenic Therapy: Current Challenges and Future Perspectives. Int J Mol Sci. 2021;22(7).
56. Watson N, Al-Samkari H. Thrombotic and bleeding risk of angiogenesis inhibitors in patients with and without malignancy. Journal of Thrombosis and Haemostasis. 2021;19(8):1852-63.
57. Pettinato MC. Introduction to Antibody-Drug Conjugates. Antibodies (Basel). 2021;10(4).
58. Parit S, Manchare A, Gholap AD, Mundhe P, Hatvate N, Rojekar S, Patravale V. Antibody-Drug Conjugates: A promising breakthrough in cancer therapy. International Journal of Pharmaceutics. 2024;659:124211.

59. Bardia A, Mayer IA, Vahdat LT, Tolaney SM, Isakoff SJ, Diamond JR, et al. Sacituzumab Govitecan-hziy in Refractory Metastatic Triple-Negative Breast Cancer. New England Journal of Medicine. 2019;380(8):741-51.
60. Kanugo A, Gautam RK, Kamal MA. Recent Advances of Nanotechnology in the Diagnosis and Therapy of Triple- Negative Breast Cancer (TNBC). Curr Pharm Biotechnol. 2022;23(13):1581-95.
61. Chehelgerdi M, Chehelgerdi M, Allela OQB, Pecho RDC, Jayasankar N, Rao DP, et al. Progressing nanotechnology to improve targeted cancer treatment: overcoming hurdles in its clinical implementation. Molecular Cancer. 2023;22(1):169.
62. Peng X, Fang J, Lou C, Yang L, Shan S, Wang Z, et al. Engineered nanoparticles for precise targeted drug delivery and enhanced therapeutic efficacy in cancer immunotherapy. Acta Pharm Sin B. 2024;14(8):3432-56.
63. Manocha S, Dhiman S, Grewal AS, Guarve K. Nanotechnology: An approach to overcome bioavailability challenges of nutraceuticals. Journal of Drug Delivery Science and Technology. 2022;72:103418.
64. Najdian A, Beiki D, Abbasi M, Gholamrezanezhad A, Ahmadzadehfar H, Amani AM, et al. Exploring innovative strides in radiolabeled nanoparticle progress for multimodality cancer imaging and theranostic applications. Cancer Imaging. 2024;24(1):127.
65. Shinde VR, Revi N, Murugappan S, Singh SP, Rengan AK. Enhanced permeability and retention effect: A key facilitator for solid tumor targeting by nanoparticles. Photodiagnosis and Photodynamic Therapy. 2022;39:102915.
66. Sun L, Liu H, Ye Y, Lei Y, Islam R, Tan S, et al. Smart nanoparticles for cancer therapy. Signal Transduction and Targeted Therapy. 2023;8(1):418.
67. Deepak KGK, Vempati R, Nagaraju GP, Dasari VR, S N, Rao DN, Malla RR. Tumor microenvironment: Challenges and opportunities in targeting metastasis of triple negative breast cancer. Pharmacol Res. 2020;153:104683.
68. Liu J, Liu Z, Pang Y, Zhou H. The interaction between nanoparticles and immune system: application in the treatment of inflammatory diseases. J Nanobiotechnology. 2022;20(1):127.
69. Hu A, Sun L, Lin H, Liao Y, Yang H, Mao Y. Harnessing innate immune pathways for therapeutic advancement in cancer. Signal Transduction and Targeted Therapy. 2024;9(1):68.
70. Sun Z, Zhao H, Ma L, Shi Y, Ji M, Sun X, et al. The quest for nanoparticle-powered vaccines in cancer immunotherapy. Journal of Nanobiotechnology. 2024;22(1):61.
71. Zhang J, Li Y, Zeng F, Mu C, Liu C, Wang L, et al. Virus-like structures for combination antigen protein mRNA vaccination. Nature Nanotechnology. 2024;19(8):1224-33.
72. Yi W, Xiao P, Liu X, Zhao Z, Sun X, Wang J, et al. Recent advances in developing active targeting and multi-functional drug delivery systems via bioorthogonal chemistry. Signal Transduction and Targeted Therapy. 2022;7(1):386.
73. Gurunathan S, Kang MH, Qasim M, Kim JH. Nanoparticle-Mediated Combination Therapy: Two-in-One Approach for Cancer. Int J Mol Sci. 2018;19(10).
74. Mehta S, Shah V, Patel G, Conte-Junior CA, Joshi N. A holistic review of recent advances in nano-based drug delivery systems for the treatment of triple-negative breast cancer (TNBC). Journal of Nanoparticle Research. 2024;26(5):87.
75. Elumalai K, Srinivasan S, Shanmugam A. Review of the efficacy of nanoparticle-based drug delivery systems for cancer treatment. Biomedical Technology. 2024;5:109-22.
76. Begines B, Ortiz T, Pérez-Aranda M, Martínez G, Merinero M, Argüelles-Arias F, Alcudia A. Polymeric Nanoparticles for Drug Delivery: Recent Developments and Future Prospects. Nanomaterials (Basel). 2020;10(7).

77. Kumalasari MR, Alfanaar R, Andreani AS. Gold nanoparticles (AuNPs): A versatile material for biosensor application. Talanta Open. 2024;9:100327.
78. Xu B, Li S, Shi R, Liu H. Multifunctional mesoporous silica nanoparticles for biomedical applications. Signal Transduction and Targeted Therapy. 2023;8(1):435.
79. Materón EM, Miyazaki CM, Carr O, Joshi N, Picciani PHS, Dalmaschio CJ, et al. Magnetic nanoparticles in biomedical applications: A review. Applied Surface Science Advances. 2021;6:100163.
80. Qi K, Sun B, Liu S-y, Zhang M. Research progress on carbon materials in tumor photothermal therapy. Biomedicine & Pharmacotherapy. 2023;165:115070.
81. Farahbakhsh J, Shakori S, Najafi M, Delnavaz M, Khiadani M, Vatanpour V, et al. Functionalised carbon nanotube thin film nanocomposite membranes: A comparison study on the role of backbone monomers and hydraulic pressure on membrane's performance and fouling. Process Safety and Environmental Protection. 2024;190:1028-39.
82. Dr. Diana Díaz-García DMD-S, Dr. Javier Álvarez-Conde, Prof. Santiago Gómez-Ruiz. Emergence of Quantum Dots as Innovative Tools for Early Diagnosis and Advanced Treatment of Breast Cancer. ChemMedChem.
83. Sarode RJ, Mahajan HS. Dendrimers for drug delivery: An overview of its classes, synthesis, and applications. Journal of Drug Delivery Science and Technology. 2024;98:105896.
84. Rahnama M, Heidari M, Poursalehi Z, Golchin A. Global Trends of Exosomes Application in Clinical Trials: A Scoping Review. Stem Cell Reviews and Reports. 2024.
85. Zhao Y, Alakhova DY, Zhao X, Band V, Batrakova EV, Kabanov AV. Eradication of cancer stem cells in triple negative breast cancer using doxorubicin/pluronic polymeric micelles. Nanomedicine: Nanotechnology, Biology and Medicine. 2020;24:102124.
86. Mansoori-Kermani A, Khalighi S, Akbarzadeh I, Niavol FR, Motasadizadeh H, Mahdieh A, et al. Engineered hyaluronic acid-decorated niosomal nanoparticles for controlled and targeted delivery of epirubicin to treat breast cancer. Materials Today Bio. 2022;16:100349.
87. Moammeri A, Chegeni MM, Sahrayi H, Ghafelehbashi R, Memarzadeh F, Mansouri A, et al. Current advances in niosomes applications for drug delivery and cancer treatment. Mater Today Bio. 2023;23:100837.
88. Ghezzi M, Pescina S, Padula C, Santi P, Del Favero E, Cantù L, Nicoli S. Polymeric micelles in drug delivery: An insight of the techniques for their characterization and assessment in biorelevant conditions. Journal of Controlled Release. 2021;332:312-36.
89. Bastakoti BP, Liu Z. Chapter 10 - Multifunctional polymeric micelles as therapeutic nanostructures: targeting, imaging, and triggered release. In: Ficai A, Grumezescu AM, editors. Nanostructures for Cancer Therapy: Elsevier; 2017. p. 261-83.
90. Padarthi P, V K, Challa RR, Vallamkonda B, Grandhe N, Dogiparthi LK, Kaliyaperumal R. Non-Ionic Surfactant Vesicles (Niosomes): Structure, Functions, Classification and its Advances in Enhanced Drug Delivery. Recent Adv Drug Deliv Formul. 2024.
91. Saharkhiz S, Zarepour A, Nasri N, Cordani M, Zarrabi A. A comparison study between doxorubicin and curcumin co-administration and co-loading in a smart niosomal formulation for MCF-7 breast cancer therapy. European Journal of Pharmaceutical Sciences. 2023;191:106600.
92. Tian H, Ma D, Tan X, Yan W, Wu X, He C, et al. Platinum and Taxane Based Adjuvant and Neoadjuvant Chemotherapy in Early Triple-Negative Breast Cancer: A Narrative Review. Front Pharmacol. 2021;12:770663.
93. Li M, Guo T, Lin J, Huang X, Ke Q, Wu Y, et al. Curcumin inhibits the invasion and metastasis of triple negative breast cancer via Hedgehog/Gli1 signaling pathway. Journal of Ethnopharmacology. 2022;283:114689.

94. El-Saadony MT, Yang T, Korma SA, Sitohy M, Abd El-Mageed TA, Selim S, et al. Impacts of turmeric and its principal bioactive curcumin on human health: Pharmaceutical, medicinal, and food applications: A comprehensive review. Front Nutr. 2022;9:1040259.
95. Lin L, Lee K-H. Structure-Activity Relationships of Curcumin and Its Analogs with Different Biological Activities††Antitumor Agents 241. In: Atta ur R, editor. Studies in Natural Products Chemistry. 33: Elsevier; 2006. p. 785-812.
96. Aghajanpour S, Yousefi Jordehi S, Farmoudeh A, Negarandeh R, Lam M, Ebrahimnejad P, Nokhodchi A. Applying liquisolid technique to enhance curcumin solubility: a central composite design study. Chemical Papers. 2024;78(17):9257-71.
97. Zhang HA, Pratap-Singh A, Kitts DD. Effect of pulsed light on curcumin chemical stability and antioxidant capacity. PLoS One. 2023;18(9):e0291000.
98. Paul S, & Sa, G. . Curcumin as an Adjuvant to Cancer Immunotherapy. Frontiers in Oncology. 2021;11.
99. Zoi V, Galani V, Lianos GD, Voulgaris S, Kyritsis AP, Alexiou GA. The Role of Curcumin in Cancer Treatment. Biomedicines. 2021;9(9).
100. Amaroli A, Panfoli I, Bozzo M, Ferrando S, Candiani S, Ravera S. The Bright Side of Curcumin: A Narrative Review of Its Therapeutic Potential in Cancer Management. Cancers. 2024;16(14):2580.
101. Shakori Poshteh S, Alipour S, Varamini P. Harnessing curcumin and nanotechnology for enhanced treatment of breast cancer bone metastasis. Discover Nano. 2024;19(1):177.
102. Kaya M, Abuaisha A, Suer I, Emiroglu S, Abanoz F, Palanduz S, et al. Turmeric Inhibits MDA-MB-231 Cancer Cell Proliferation, Altering miR-638-5p and Its Potential Targets. Eur J Breast Health. 2024;20(2):102-9.
103. Chen Z, Lu P, Li M, Zhang Q, He T, Gan L. Curcumin suppresses metastasis of triple-negative breast cancer cells by modulating EMT signaling pathways: An integrated study of bioinformatics analysis. Medicine. 2024;103(8).
104. Suer I, Abuaisha A, Kaya M, Abanoz F, Cefle K, Palanduz S, Ozturk S. Curcumin suppresses cell viability in breast cancer cell line by affecting the expression of miR-15a-5p. Turkish Journal of Biochemistry. 2024;49(5):656-65.
105. Ameer SF, Mohamed, M. Y., Elzubair, Q. A., Sharif, E. A., & Ibrahim, W. N. (2024). Curcumin as a novel therapeutic candidate for cancer: Can this natural compound revolutionize cancer treatment? . Frontiers in Oncology, 14, 1438040 2024.
106. Zhou Y, Gong J, Deng X, Shen L, Wu S, Fan H, Liu L. Curcumin and nanodelivery systems: New directions for targeted therapy and diagnosis of breast cancer. Biomedicine & Pharmacotherapy. 2024;180:117404.
107. Zoghi M, Pourmadadi M, Yazdian F, Nigjeh MN, Rashedi H, Sahraeian R. Synthesis and characterization of chitosan/carbon quantum dots/Fe2O3 nanocomposite comprising curcumin for targeted drug delivery in breast cancer therapy. International Journal of Biological Macromolecules. 2023;249:125788.
108. Alves RC, Quijia CR, Bento da Silva P, Faria RS, Cabral Morais AA, Vasconcelos Morais JA, et al. Folic acid-conjugated curcumin-loaded bioMOF-101 for breast cancer therapy. Journal of Drug Delivery Science and Technology. 2023;86:104702.
109. Zhu J, Li Q, Wu Z, Xu Y, Jiang R. Curcumin for Treating Breast Cancer: A Review of Molecular Mechanisms, Combinations with Anticancer Drugs, and Nanosystems. Pharmaceutics [Internet]. 2024; 16(1).
110. Tondro G, Darvishi MH, Sahab-Negah S, Rajabzadeh G, Mohammadi A, Khaksar Z, Moradi HR. Comparative Effects of Curcumin Nano-Niosomes and Free Curcumin on Apoptosis, Intracellular ROS, and STAT3/NF-κB Signaling Pathway in A549 Lung Cancer Cells.

111. Cheng L, Yu J, Hao T, Wang W, Wei M, Li G. Advances in Polymeric Micelles: Responsive and Targeting Approaches for Cancer Immunotherapy in the Tumor Microenvironment. Pharmaceutics. 2023;15(11).
112. Moon DO. Curcumin in Cancer and Inflammation: An In-Depth Exploration of Molecular Interactions, Therapeutic Potentials, and the Role in Disease Management. Int J Mol Sci. 2024;25(5).
113. Hu A, Huang JJ, Zhang JF, Dai WJ, Li RL, Lu ZY, et al. Curcumin induces G2/M cell cycle arrest and apoptosis of head and neck squamous cell carcinoma in vitro and in vivo through ATM/Chk2/p53-dependent pathway. Oncotarget. 2017;8(31):50747-60.
114. Li W, Zhou, Y., Yang, J., Li, H., Zhang, H., Zheng, P. Curcumin induces apoptotic cell death and protective autophagy in human gastric cancer cells. Oncology

Reports. May 11, 2017 37(16).
115. Ligeret H, Barthelemy S, Zini R, Tillement J-P, Labidalle S, Morin D. Effects of curcumin and curcumin derivatives on mitochondrial permeability transition pore. Free Radical Biology and Medicine. 2004;36(7):919-29.
116. Tuorkey MJ. Curcumin a potent cancer preventive agent: Mechanisms of cancer cell killing. Interv Med Appl Sci. 2014;6(4):139-46.
117. Shishodia S. Molecular mechanisms of curcumin action: gene expression. Biofactors. 2013;39(1):37-55.
118. Fu Z, Chen X, Guan S, Yan Y, Lin H, Hua ZC. Curcumin inhibits angiogenesis and improves defective hematopoiesis induced by tumor-derived VEGF in tumor model through modulating VEGF-VEGFR2 signaling pathway. Oncotarget. 2015;6(23):19469-82.
119. Bhatia M, Bhalerao M, Cruz-Martins N, Kumar D. Curcumin and cancer biology: Focusing regulatory effects in different signalling pathways. Phytother Res. 2021;35(9):4913-29.
120. Lopes-Rodrigues V, Sousa E, Vasconcelos MH. Curcumin as a Modulator of P-Glycoprotein in Cancer: Challenges and Perspectives. Pharmaceuticals (Basel). 2016;9(4).
121. Shadnoush M, Momenan M, Seidel V, Tierling S, Fatemi N, Nazemalhosseini-Mojarad E, et al. A comprehensive update on the potential of curcumin to enhance chemosensitivity in colorectal cancer. Pharmacological Reports. 2024.
122. Volak LP, Ghirmai S, Cashman JR, Court MH. Curcuminoids inhibit multiple human cytochromes P450, UDP-glucuronosyltransferase, and sulfotransferase enzymes, whereas piperine is a relatively selective CYP3A4 inhibitor. Drug Metab Dispos. 2008;36(8):1594-605.
123. Bisht A, Avinash D, Sahu KK, Patel P, Das Gupta G, Kurmi BD. A comprehensive review on doxorubicin: mechanisms, toxicity, clinical trials, combination therapies and nanoformulations in breast cancer. Drug Delivery and Translational Research. 2025;15(1):102-33.
124. Janthima Methaneethorn KT, Nattawut Leelakanok, Rowan AlEjielat. Population pharmacokinetics of doxorubicin: A systematic review. Wiley Online Library. 12 April 2022;19(1).
125. Becker DE. Pharmacokinetic considerations for moderate and deep sedation. Anesth Prog. 2011;58(4):166-72; quiz 73.
126. Shi S, Chen Y, Luo Z, Nie G, Dai Y. Role of oxidative stress and inflammation-related signaling pathways in doxorubicin-induced cardiomyopathy. Cell Communication and Signaling. 2023;21(1):61.
127. Ciocan-Cartita CA, Jurj A, Zanoaga O, Cojocneanu R, Pop L-A, Moldovan A, et al. New insights in gene expression alteration as effect of doxorubicin drug resistance in triple negative breast cancer cells. Journal of Experimental & Clinical Cancer Research. 2020;39(1):241.
128. Mehraj U, Mir IA, Hussain MU, Alkhanani M, Wani NA, Mir MA. Adapalene and Doxorubicin Synergistically Promote Apoptosis of TNBC Cells by Hyperactivation of the ERK1/2 Pathway Through ROS Induction. Front Oncol. 2022;12:938052.

129. Paramanantham A, Jung EJ, Kim HJ, Jeong BK, Jung JM, Kim GS, et al. Doxorubicin-Resistant TNBC Cells Exhibit Rapid Growth with Cancer Stem Cell-like Properties and EMT Phenotype, Which Can Be Transferred to Parental Cells through Autocrine Signaling. Int J Mol Sci. 2021;22(22).
130. Haryanti S, Zulfin UM, Salsabila IA, Wulandari F, Meiyanto E. The Cytotoxic and Anti-Migratory Properties of Caesalpinia sappan and Ficus septica, in Combination with Doxorubicin on 4T1 TNBC Cells with Nephroprotective Potential. Asian Pac J Cancer Prev. 2022;23(2):743-52.
131. Attia Y, Hakeem A, Samir R, Mohammed A, Elsayed A, Khallaf A, et al. Harnessing adrenergic blockade in stress-promoted TNBC in vitro and solid tumor in vivo: disrupting HIF-1α and GSK-3β/β-catenin driven resistance to doxorubicin. Front Pharmacol. 2024;15:1362675.
132. Mabrouk N, Racoeur C, Shan J, Massot A, Ghione S, Privat M, et al. GTN Enhances Antitumor Effects of Doxorubicin in TNBC by Targeting the Immunosuppressive Activity of PMN-MDSC. Cancers (Basel). 2023;15(12).
133. Zhang J, Liu Y, Tan J, Zhang Y, Wong C-W, Lin Z, et al. Necroptotic virotherapy of oncolytic alphavirus M1 cooperated with Doxorubicin displays promising therapeutic efficacy in TNBC. Oncogene. 2021;40(29):4783-95.
134. Wang X, Chen T, Li C, Li W, Zhou X, Li Y, et al. CircRNA-CREIT inhibits stress granule assembly and overcomes doxorubicin resistance in TNBC by destabilizing PKR. J Hematol Oncol. 2022;15(1):122.
135. Zeng W, Luo Y, Gan D, Zhang Y, Deng H, Liu G. Advances in Doxorubicin-based nano-drug delivery system in triple negative breast cancer. Front Bioeng Biotechnol. 2023;11:1271420.
136. Zhang X, Chen W, Bai J, Jin L, Kang X, Zhang H, Wang Z. Pluronic P123 modified nano micelles loaded with doxorubicin enhanced tumor-suppressing effect on drug-resistant breast cancer cells. Aging (Albany NY). 2020;12(9):8289-300.
137. Tohidi M, Allahyari A, Ataei Azimi S, Alimi H, Elyasi S, Qoorchi Moheb Seraj F, Mehrad-Majd H. "The protective effect of nano curcumin supplementation on doxorubicin induced cardiotoxicity in breast cancer patients; a randomized, double-blind clinical trial". J Oncol Pharm Pract. 2024:10781552241277958.
138. Ray PD, Huang BW, Tsuji Y. Reactive oxygen species (ROS) homeostasis and redox regulation in cellular signaling. Cell Signal. 2012;24(5):981-90.
139. Pfitzer L, Moser C, Gegenfurtner F, Arner A, Foerster F, Atzberger C, et al. Targeting actin inhibits repair of doxorubicin-induced DNA damage: a novel therapeutic approach for combination therapy. Cell Death & Disease. 2019;10(4):302.
140. Kim HS, Lee YS, Kim DK. Doxorubicin exerts cytotoxic effects through cell cycle arrest and Fas-mediated cell death. Pharmacology. 2009;84(5):300-9.
141. Liu Z-L, Chen H-H, Zheng L-L, Sun L-P, Shi L. Angiogenic signaling pathways and anti-angiogenic therapy for cancer. Signal Transduction and Targeted Therapy. 2023;8(1):198.
142. Brian MO. Hypoxia-inducible factor in cancer: from pathway regulation to therapeutic opportunity. BMJ Oncology. 2024;3(1):e000154.
143. Halder J, Pradhan D, Kar B, Ghosh G, Rath G. Nanotherapeutics approaches to overcome P-glycoprotein-mediated multi-drug resistance in cancer. Nanomedicine: Nanotechnology, Biology and Medicine. 2022;40:102494.
144. Saharkhiz S, Zarepour A, Zarrabi A. Empowering Cancer Therapy: Comparing PEGylated and Non-PEGylated Niosomes Loaded with Curcumin and Doxorubicin on MCF-7 Cell Line. Bioengineering [Internet]. 2023; 10(10).
145. Bashkeran T, Kamaruddin AH, Ngo TX, Suda K, Umakoshi H, Watanabe N, Nadzir MM. Niosomes in cancer treatment: A focus on curcumin encapsulation. Heliyon. 2023;9(8).

146. Firouzi Amandi A, Jokar E, Eslami M, Dadashpour M, Rezaie M, Yazdani Y, Nejati B. Enhanced anti-cancer effect of artemisinin- and curcumin-loaded niosomal nanoparticles against human colon cancer cells. Medical Oncology. 2023;40(6):170.
147. Nurjis F, Sarwar U, Ali JS, Fayyaz M. Doxorubicin and Curcumin-Loaded Nanomicelles Targeting Multidrug Resistance in Cancer. BioNanoScience. 2024;14(3):2159-69.
148. Momekova DB, Gugleva VE, Petrov PD. Nanoarchitectonics of multifunctional niosomes for advanced drug delivery. ACS omega. 2021;6(49):33265-73.
149. Obeid MA, Alsaadi M, Aljabali AA. Recent updates in curcumin delivery. Journal of Liposome Research. 2023;33(1):53-64.
150. Pourmadadi M, Abbasi P, Eshaghi MM, Bakhshi A, Ezra Manicum A-L, Rahdar A, et al. Curcumin delivery and co-delivery based on nanomaterials as an effective approach for cancer therapy. Journal of Drug Delivery Science and Technology. 2022;78:103982.
151. Pourmadadi M, Abbasi P, Eshaghi MM, Bakhshi A, Manicum A-LE, Rahdar A, et al. Curcumin delivery and co-delivery based on nanomaterials as an effective approach for cancer therapy. Journal of Drug Delivery Science and Technology. 2022;78:103982.
152. Kaniuk M. Combined nanochemotherapy using doxorubicin and curcumin as an example. Biotechnologia Acta. 2023;16(1):5-20.
153. Bhardwaj P, Tripathi P, Gupta R, Pandey S. Niosomes: A review on niosomal research in the last decade. Journal of Drug Delivery Science and Technology. 2020;56:101581.
154. Park M, Kim D, Ko S, Kim A, Mo K, Yoon H. Breast Cancer Metastasis: Mechanisms and Therapeutic Implications. Int J Mol Sci. 2022;23(12).
155. Breast Cancer Surgery: Mastectomy, Lumpectomy, Lymph Node Removal & Breast Forms [Available from: https://www.mskcc.org/cancer-conditions/breast-cancer/surgery-for-breast-cancer.
156. Kumar S, Gupta S, Chandra Gupta S. Targeting triple negative breast cancer by natural compounds. Frontiers in Pharmacology. 2023;14:1172245.
157. Deng Z, Chen G, Shi Y, Lin Y, Ou J, Zhu H, et al. Curcumin and its nano-formulations: Defining triple-negative breast cancer targets through network pharmacology, molecular docking, and experimental verification. Frontiers in Pharmacology. 2022;13:920514.
158. Rupesh K. Gautam DAaSG. Pre-Clinical/Animal Studies Conducted on Turmeric and Curcumin and Their Formulations2019.
159. Urošević M, Nikolić L, Gajić I, Nikolić V, Dinić A, Miljković V. Curcumin: Biological Activities and Modern Pharmaceutical Forms. Antibiotics (Basel). 2022;11(2).
160. Guneydas G, Topcul MR. Antiproliferative Effects of Curcumin Different Types of Breast Cancer. Asian Pac J Cancer Prev. 2022;23(3):911-7.
161. Farghadani R, Naidu R. Curcumin as an enhancer of therapeutic efficiency of chemotherapy drugs in breast cancer. International Journal of Molecular Sciences. 2022;23(4):2144.
162. Dong S, Alahari SK. Combination treatment of bicalutamide and curcumin has a strong therapeutic effect on androgen receptor-positive triple-negative breast cancers. Anti-Cancer Drugs. 2020;31(4):359-67.
163. Hegde M, Girisa S, BharathwajChetty B, Vishwa R, Kunnumakkara AB. Curcumin formulations for better bioavailability: what we learned from clinical trials thus far? ACS omega. 2023;8(12):10713-46.
164. Sahu A, Kasoju N, Goswami P, Bora U. Encapsulation of curcumin in Pluronic block copolymer micelles for drug delivery applications. J Biomater Appl. 2011;25(6):619-39.
165. Bose A, Roy Burman D, Sikdar B, Patra P. Nanomicelles: Types, properties and applications in drug delivery. IET Nanobiotechnol. 2021;15(1):19-27.
166. Engel JB, Schally AV. Drug Insight: clinical use of agonists and antagonists of luteinizing-hormone-releasing hormone. Nat Clin Pract Endocrinol Metab. 2007;3(2):157-67.

167. Schally AV, Comaru-Schally AM, Nagy A, Kovacs M, Szepeshazi K, Plonowski A, et al. Hypothalamic hormones and cancer. Front Neuroendocrinol. 2001;22(4):248-91.
168. Keller G, Schally AV, Gaiser T, Nagy A, Baker B, Halmos G, Engel JB. Receptors for luteinizing hormone releasing hormone expressed on human renal cell carcinomas can be used for targeted chemotherapy with cytotoxic luteinizing hormone releasing hormone analogues. Clinical cancer research : an official journal of the American Association for Cancer Research. 2005;11(15):5549-57.
169. Schally AV, Halmos G, Rékási Z, Arencibia-Jimenez JM, editors. The actions of luteinizing hormone-releasing hormone agonists, antagonists, and cytotoxic analogues on the luteinizing hormone-releasing hormone receptors on the pituitary and tumors2001.
170. Targeting to Peptide Receptors [Internet]. Wiley Online Library. Available from: https://doi.org/10.1002/9783527634057.ch38.
171. Seitz S, Buchholz S, Schally AV, Weber F, Klinkhammer-Schalke M, Inwald EC, et al. Triple negative breast cancers express receptors for LHRH and are potential therapeutic targets for cytotoxic LHRH-analogs, AEZS 108 and AEZS 125. BMC Cancer. 2014;14:847.
172. Obayemi JD, Salifu AA, Eluu SC, Uzonwanne VO, Jusu SM, Nwazojie CC, et al. LHRH-Conjugated Drugs as Targeted Therapeutic Agents for the Specific Targeting and Localized Treatment of Triple Negative Breast Cancer. Scientific Reports. 2020;10(1):8212.
173. Khaliq NU, Lee J, Kim S, Sung D, Kim H. Pluronic F-68 and F-127 Based Nanomedicines for Advancing Combination Cancer Therapy. Pharmaceutics. 2023;15(8).
174. Bhalodi K, Kothari C, Butani S. Next-generation cancer nanotherapeutics: Pluronic® F127 based mixed micelles for enhanced drug delivery. Naunyn-Schmiedeberg's Archives of Pharmacology. 2024.
175. Moradi SV, Mansfeld FM, Toth I. Synthesis and in vitro evaluation of glycosyl derivatives of luteinizing hormone-releasing hormone (LHRH). Bioorg Med Chem. 2013;21(14):4259-65.
176. Alewood P, Alewood D, Miranda L, Love S, Meutermans W, Wilson D. Rapid in situ neutralization protocols for Boc and Fmoc solid-phase chemistries. Methods Enzymol. 1997;289:14-29.
177. Varamini P, Mansfeld FM, Giddam AK, Steyn F, Toth I. New gonadotropin-releasing hormone glycolipids with direct antiproliferative activity and gonadotropin-releasing potency. Int J Pharm. 2017;521(1-2):327-36.
178. Moradi SV, Varamini P, Toth I. Evaluation of the Biological Properties and the Enzymatic Stability of Glycosylated Luteinizing Hormone-Releasing Hormone Analogs. Aaps j. 2015;17(5):1135-43.
179. Kamble S, Varamini P, Müllner M, Pelras T, Rohanizadeh R. Bisphosphonate-functionalized micelles for targeted delivery of curcumin to metastatic bone cancer. Pharm Dev Technol. 2020;25(9):1118-26.
180. Ahmad N. LHRH-Receptor Mediated Targeting of Cancer Cells Using Curcumin Nano-micelle Formulation 2018.
181. Gera M, Sharma N, Ghosh M, Huynh DL, Lee SJ, Min T, et al. Nanoformulations of curcumin: an emerging paradigm for improved remedial application. Oncotarget. 2017;8(39):66680-98.
182. Aysola K, Desai A, Welch C, Xu J, Qin Y, Reddy V, et al. Triple negative breast cancer–an overview. Hereditary genetics: current research. 2013;2013(Suppl 2).
183. Almansour NM. Triple-negative breast cancer: a brief review about epidemiology, risk factors, signaling pathways, treatment and role of artificial intelligence. Frontiers in Molecular Biosciences. 2022;9:836417.
184. Ciocan-Cartita CA, Jurj A, Zanoaga O, Cojocneanu R, Pop L-A, Moldovan A, et al. New insights in gene expression alteration as effect of doxorubicin drug resistance in triple negative breast cancer cells. Journal of Experimental & Clinical Cancer Research. 2020;39:1-16.
185. Wooten J, Mavingire N, Damar K, Loaiza-Perez A, Brantley E. Triumphs and challenges in exploiting poly (ADP-ribose) polymerase inhibition to combat triple-negative breast cancer. Journal of Cellular Physiology. 2023;238(8):1625-40.

186. Cheng T-C, Sayseng JO, Tu S-H, Juan T-C, Fang C-L, Liao Y-C, et al. Curcumin-induced antitumor effects on triple-negative breast cancer patient-derived xenograft tumor mice through inhibiting salt-induced kinase-3 protein. Journal of Food and Drug Analysis. 2021;29(4):622.
187. Khaliq NU, Lee J, Kim S, Sung D, Kim H. Pluronic F-68 and F-127 based nanomedicines for advancing combination cancer therapy. Pharmaceutics. 2023;15(8):2102.
188. Vaidya FU, Sharma R, Shaikh S, Ray D, Aswal VK, Pathak C. Pluronic micelles encapsulated curcumin manifests apoptotic cell death and inhibits pro-inflammatory cytokines in human breast adenocarcinoma cells. Cancer Reports. 2019;2(1):e1133.
189. Shamsi S. Development and evaluation of curcumin-loaded Pluronic F127 nanoformulation. 2015.
190. Hering I, Eilebrecht E, Parnham MJ, Günday-Türeli N, Türeli AE, Weiler M, et al. Evaluation of potential environmental toxicity of polymeric nanomaterials and surfactants. Environmental toxicology and pharmacology. 2020;76:103353.
191. de Castro KC, Coco JC, Dos Santos ÉM, Ataide JA, Martinez RM, do Nascimento MHM, et al. Pluronic® triblock copolymer-based nanoformulations for cancer therapy: A 10-year overview. Journal of Controlled Release. 2023;353:802-22.
192. Sripetthong S, Nalinbenjapun S, Basit A, Surassmo S, Sajomsang W, Ovatlarnporn C. Preparation of Self-Assembled, Curcumin-Loaded Nano-Micelles Using Quarternized Chitosan–Vanillin Imine (QCS-Vani Imine) Conjugate and Evaluation of Synergistic Anticancer Effect with Cisplatin. Journal of Functional Biomaterials. 2023;14(10):525.
193. Klahan B, O'Reilly N, Sigurdsson HH, Chauhan A, Mering S, Fitzhenry L. Pluronic F127 micelles as a carrier for the topical ocular delivery of curcumin. Investigative Ophthalmology & Visual Science. 2023;64(8):1297-.
194. Kulkarni AS, Tapase SR, Kodam KM, Shinde VS. Thermoresponsive Pluronic based microgels for controlled release of curcumin against breast cancer cell line. Colloids and Surfaces B: Biointerfaces. 2021;205:111834.
195. Sung Y, Choi Y, Kim ES, Ryu JH, Kwon IC. Receptor-ligand interactions for optimized endocytosis in targeted therapies. Journal of Controlled Release. 2025;380:524-38.
196. Li X, Taratula O, Taratula O, Schumann C, Minko T. LHRH-Targeted Drug Delivery Systems for Cancer Therapy. Mini Rev Med Chem. 2017;17(3):258-67.
197. Bajracharya R, Song JG, Patil BR, Lee SH, Noh HM, Kim DH, et al. Functional ligands for improving anticancer drug therapy: current status and applications to drug delivery systems. Drug Deliv. 2022;29(1):1959-70.
198. Bisht A, Avinash D, Sahu KK, Patel P, Das Gupta G, Kurmi BD. A comprehensive review on doxorubicin: mechanisms, toxicity, clinical trials, combination therapies and nanoformulations in breast cancer. Drug Delivery and Translational Research. 2024.
199. Dhariwal R JM, Mir YR, Singh A, Jain B, Kumar P, Tariq M, Verma D, Deshmukh K, Yadav VK and Malik T. Targeted drug delivery in neurodegenerative diseases: the role of nanotechnology. 2025.
200. Moammeri A, Chegeni MM, Sahrayi H, Ghafelehbashi R, Memarzadeh F, Mansouri A, et al. Current advances in niosomes applications for drug delivery and cancer treatment. Materials Today Bio. 2023;23:100837.
201. Pirojiya H, Dudhat K. Niosomes: A Revolution in Sustainable and Targeted Drug Delivery-Green Synthesis, Precision Medicine, and Beyond. Regenerative Engineering and Translational Medicine. 2024.
202. Basheer HA, Alkilani AZ, Alhusban MA, Abo-Zour H, Alshaer W. Evaluating Niosomes Cytotoxicity on Fibroblast Cells: A Preliminary Step Towards Cancer Cell Assessment Using Telaglenastat as a Model Drug. BioNanoScience. 2024;15(1):35.
203. Deo A, Sleeman JP, Shaked Y. The role of host response to chemotherapy: resistance, metastasis and clinical implications. Clinical & Experimental Metastasis. 2024;41(4):495-507.

204. Zolghadri S, Asad AG, Farzi F, Ghajarzadeh F, Habibi Z, Rahban M, et al. Span 60/Cholesterol Niosomal Formulation as a Suitable Vehicle for Gallic Acid Delivery with Potent In Vitro Antibacterial, Antimelanoma, and Anti-Tyrosinase Activity. Pharmaceuticals (Basel). 2023;16(12).
205. Span 60 [Available from: https://www.atamanchemicals.com/span-60_u26797/.
206. Biochemistry of Cholesterol: Functions, Metabolism, and Clinical Significance [Available from: https://www.dovemed.com/health-topics/focused-health-topics/biochemistry-cholesterol-functions-metabolism-and-clinical-significance.
207. Mall J, Naseem N, Haider MF, Rahman MA, Khan S, Siddiqui SN. Nanostructured lipid carriers as a drug delivery system: A comprehensive review with therapeutic applications. Intelligent Pharmacy. 2024.
208. Liga S, Paul C, Moacă EA, Péter F. Niosomes: Composition, Formulation Techniques, and Recent Progress as Delivery Systems in Cancer Therapy. Pharmaceutics. 2024;16(2).
209. Marianecci C, Di Marzio L, Rinaldi F, Celia C, Paolino D, Alhaique F, et al. Niosomes from 80s to present: the state of the art. Advances in colloid and interface science. 2014;205:187-206.
210. Kumar GP, Rajeshwarrao P. Nonionic surfactant vesicular systems for effective drug delivery—an overview. Acta pharmaceutica sinica B. 2011;1(4):208-19.
211. Farrell KB, Karpeisky A, Thamm DH, Zinnen S. Bisphosphonate conjugation for bone specific drug targeting. Bone Rep. 2018;9:47-60.
212. Ruiz-Cruz M, Roa J, Tena-Sempere M. Gonadotropin-releasing hormone. Trends in Endocrinology & Metabolism.
213. Ndinguri M, Middleton L, Unrine J, Lui S, Rollins J, Nienaber E, et al. Therapeutic dosing and targeting efficacy of Pt-Mal-LHRH towards triple negative breast cancer. PLoS One. 2023;18(10):e0287151.
214. Ghanghoria R, Kesharwani P, Tekade RK, Jain NK. Targeting luteinizing hormone-releasing hormone: A potential therapeutics to treat gynecological and other cancers. Journal of Controlled Release. 2018;269:277-301.
215. Alaei MS, Ganji F, Shaki H. In vitro Preparation and Evaluation of Alendronate-modified Hyaluronic acid-based Nanomicelles as a Bone-Targeted Drug delivery system. Journal of Drug Delivery Science and Technology. 2024;101:106256.
216. Gui L, Ye Q, Yu L, Dou G, Zhou Y, Liu Y, et al. Bone-Targeting Peptide and RNF146 Modified Apoptotic Extracellular Vesicles Alleviate Osteoporosis. Int J Nanomedicine. 2024;19:471-88.
217. Wang R, Xiao R, Zeng Z, Xu L, Wang J. Application of poly(ethylene glycol)-distearoylphosphatidylethanolamine (PEG-DSPE) block copolymers and their derivatives as nanomaterials in drug delivery. Int J Nanomedicine. 2012;7:4185-98.
218. Owens DE, Peppas NA. Opsonization, biodistribution, and pharmacokinetics of polymeric nanoparticles. International Journal of Pharmaceutics. 2006;307(1):93-102.
219. Gref R, Lück M, Quellec P, Marchand M, Dellacherie E, Harnisch S, et al. 'Stealth' corona-core nanoparticles surface modified by polyethylene glycol (PEG): influences of the corona (PEG chain length and surface density) and of the core composition on phagocytic uptake and plasma protein adsorption. Colloids and Surfaces B: Biointerfaces. 2000;18(3):301-13.
220. Jia G, Jiang Y, Li X. Targeted drug conjugates in cancer therapy: Challenges and opportunities. Pharmaceutical Science Advances. 2024;2:100048.
221. Akbarzadeh I, Shayan M, Bourbour M, Moghtaderi M, Noorbazargan H, Eshrati Yeganeh F, et al. Preparation, Optimization and In-Vitro Evaluation of Curcumin-Loaded Niosome@calcium Alginate Nanocarrier as a New Approach for Breast Cancer Treatment. Biology. 2021;10(3):173.
222. Targhi AA, Moammeri A, Jamshidifar E, Abbaspour K, Sadeghi S, Lamakani L, Akbarzadeh I. Synergistic effect of curcumin-Cu and curcumin-Ag nanoparticle loaded niosome: Enhanced antibacterial and anti-biofilm activities. Bioorganic Chemistry. 2021;115:105116.

223. Chen S, Hanning S, Falconer J, Locke M, Wen J. Recent advances in non-ionic surfactant vesicles (niosomes): Fabrication, characterization, pharmaceutical and cosmetic applications. European Journal of Pharmaceutics and Biopharmaceutics. 2019;144:18-39.
224. Alakhov V, Klinski E, Li S, Pietrzynski G, Venne A, Batrakova E, et al. Block copolymer-based formulation of doxorubicin. From cell screen to clinical trials. Colloids Surf, B. 1999;16:113.
225. Mukherjee B, Patra B, Layek B, Mukherjee A. Sustained release of acyclovir from nano-liposomes and nano-niosomes: an in vitro study. Int J Nanomedicine. 2007;2(2):213-25.
226. Jin Y, Wen J, Garg S, Liu D, Zhou Y, Teng L, Zhang W. Development of a novel niosomal system for oral delivery of Ginkgo biloba extract. Int J Nanomedicine. 2013;8:421-30.
227. Shreya AB, Pandey A, Kulkarni S, Bhaskar KV, Parekh HS, Mutalik S. Exploring peptide dendrimers for intestinal lymphatic targeting: formulation and evaluation of peptide dendrimer conjugated liposomes for enhancing the oral bioavailability of Asenapine maleate. Scientific Reports. 2024;14(1):28225.
228. Ca coated plate catalog [Available from: https://www.cosmobiousa.com/products/bone-resorption-assay-kit.
229. Jayanta Kumar Patra K-HB. Green Nanobiotechnology: Factors Affecting Synthesis and Characterization Techniques. Journal of Nanomaterials. 2014.
230. Alex Murray ab PKcaMIG. Trehalose in cryopreservation. Applications, mechanisms and intracellular delivery opportunities. The Royal Society of Chemistry 2024. 2024.
231. Shrestha S, Wang B, Dutta P. Nanoparticle processing: Understanding and controlling aggregation. Advances in Colloid and Interface Science. 2020;279:102162.
232. Boedtkjer E, Pedersen SF. The Acidic Tumor Microenvironment as a Driver of Cancer. Annu Rev Physiol. 2020;82:103-26.
233. Pang C, Song C, Li Y, Wang Q, Zhu X, Wu J, et al. The Establishment and Application Studies on Precise Lysosome pH Indicator Based on Self-Decomposable Nanoparticles. Nanoscale Res Lett. 2020;15(1):143.
234. Brock DJ, Kondow-McConaghy HM, Hager EC, Pellois JP. Endosomal Escape and Cytosolic Penetration of Macromolecules Mediated by Synthetic Delivery Agents. Bioconjug Chem. 2019;30(2):293-304.
235. Bone Metastases and Metastatic Breast Cancer 2025 [Available from: https://www.komen.org/breast-cancer/metastatic/bones/.
236. Battistini L, Bugatti K, Sartori A, Curti C, Zanardi F. RGD Peptide-Drug Conjugates as Effective Dual Targeting Platforms: Recent Advances. European Journal of Organic Chemistry. 2021;2021(17):2506-28.
237. Chauhan VM, Zhang H, Dalby PA, Aylott JW. Advancements in the co-formulation of biologic therapeutics. Journal of Controlled Release. 2020;327:397-405.

Chapter 6. Appendices

6.1 Appendix 1. IncuCyte SX5 live cell imaging videos

This appendix includes representative time-lapse videos captured using the IncuCyte SX5 system, demonstrating the morphological changes and viability of MDA-MB-231 spheroids over time following treatment with various nanoparticle formulations. The videos correspond to the treatment groups discussed in the results section: PBS (control), void, free-Cur, free-Dox, and the optimized CDFN formulation. These recordings visually support the experimental findings described in section **3.4.2.3**and illustrate the extent of spheroid disintegration induced by each treatment.

Table 6-1. IncuCyte® SX5 live cell imaging videos

Video 1	IncuCyte® live cell imaging videos of PBS (control)
Video 2	IncuCyte® live cell imaging videos of void
Video 3	IncuCyte® live cell imaging videos of free-Cur
Video 4	IncuCyte® live cell imaging videos of free-Dox
Video 5	IncuCyte® live cell imaging videos of CDFN

6.2 Appendix 2. CDFN niosome stability under various storage conditions

Table 6-2 Stability Assessment of CDFN Niosomes Under Different Storage Conditions over 28 days.

Time point	Storage	PDI	Size
0		0.314±0.05	244.6±20.2
3 days	Fridge	0.385±0.03	383.3±18.2
3 days	Room	0.418±0.04	391.6±14.8
7 days	Fridge	0.436±0.03	1114±203
7 days	Room	0.645±0.06	1560±312
14 days	Fridge	0.536±0.04	1431±110
21 days	Fridge	0.843±0.01	6312±500
28 days	Fridge	1.000	1849

6.3 Appendix 3. Published literature review

Discover Nano

Review

Harnessing curcumin and nanotechnology for enhanced treatment of breast cancer bone metastasis

Shiva Shakori Poshteh[1] · Shohreh Alipour[2,3] · Pegah Varamini[1,4]

Received: 15 December 2023 / Accepted: 14 October 2024
Published online: 11 November 2024

Abstract
Breast cancer (BC) bone metastasis poses a significant clinical challenge due to its impact on patient prognosis and quality of life. Curcumin (CUR), a natural polyphenol compound found in turmeric, has shown potential in cancer therapy due to its anti-inflammatory, antioxidant, and anticancer properties. However, its metabolic instability and hydrophobicity have hindered its clinical applications, leading to a short plasma half-life, poor absorption, and low bioavailability. To enhance the drug-like properties of CUR, nanotechnology-based delivery strategies have been employed, utilizing polymeric, lipidic, and inorganic nanoparticles (NPs). These approaches have effectively overcome CUR's inherent limitations by enhancing its stability and cellular bioavailability both in vitro and in vivo. Moreover, targeting molecules with high selectivity towards bone metastasized breast cancer cells can be used for site specific delivery of curcumin. Alendronate (ALN), a bone-seeking bisphosphonate, is one such moiety with high selectivity towards bone and thus can be effectively used for targeted delivery of curcumin loaded nanocarriers. This review will detail the process of bone metastasis in BC, elucidate the mechanism of action of CUR, and assess the efficacy of nanotechnology-based strategies for CUR delivery. Specifically, it will focus on how these strategies enhance CUR's stability and improve targeted delivery approaches in the treatment of BC bone metastasis.

Keywords Alendronate · Curcumin · Breast cancer · Bone metastasis · Bisphosphonates · Drug delivery

Abbreviations

BC	Breast cancer
ALN	Alendronate
CUR	Curcumin
EMT	Epithelial-to-mesenchymal transition
MMPs	Matrix metalloproteinases
CTCs	Circulating tumor cells
DTCs	Disseminated tumor cells
MDR	Multidrug resistance
TME	Tumor microenvironment
FPPS	Farnesyl pyrophosphate synthase

✉ Shohreh Alipour, Shohreh.alipour@gmail.com; ✉ Pegah Varamini, pegah.varamini@sydney.edu.au; Shiva Shakori Poshteh, ssha7834@uni.sydney.edu.au | [1]School of Pharmacy, Faculty of Medicine and Health, University of Sydney, Sydney, NSW 2006, Australia. [2]Faculty of Pharmacy, Pharmaceutical Sciences Research Center, Shiraz University of Medical Sciences, Shiraz, Iran. [3]Department of Drug and Food Control, Faculty of Pharmacy, Shiraz University of Medical Sciences, Shiraz, Iran. [4]The University of Sydney Nano Institute, University of Sydney, Sydney, NSW 2006, Australia.

Discover Nano (2024) 19:177 | https://doi.org/10.1186/s11671-024-04126-1

1 Introduction

In recent years, breast cancer (BC) has surpassed lung tumors as the most diagnosed cancer, with the Global Cancer Observatory reporting around 2.3 million new cases in 2020, accounting for 11.7% of all cancer cases [1, 2]. Propensities for metastasis vary in different subtypes of BC. For example, patients are at higher risk of metastasis in HER2-positive

breast cancer (HER + BC) and triple-negative breast cancer (TNBC) [3]. In approximately 70% of individuals with metastatic BC [4], cancer often spreads to the bone [5, 6]. Hence, among the various organs susceptible to metastasis, the bone is the most frequently affected, whereas the brain is the least affected [3, 7]. BC bone metastasis occurs when cancer cells originating from the primary breast tumor invade the bones, marking an advanced stage of the cancer. This intricate process involves multiple steps, including invasion, migration, adhesion, and the survival of tumor cells at the metastatic sites [8]. Through the bloodstream or lymphatic system, these malignant cells navigate their way and establish secondary tumors within the bone structure [9, 10]. During metastasis processes, following extravasation, tumor cells often tend to colonize highly vascularized regions of the bone, including the sternum, pelvis, ribs, and vertebrae, where it disrupts not only the physiology of the bones but also hematopoiesis and the immune system [11, 12]. BC bone metastasis significantly impacts patient prognosis and quality of life, with poorer outcomes and decreased survival rates compared to patients without bone involvement [13]. The treatment of BC bone metastasis involves a comprehensive approach to control cancer spread, relieve symptoms, and improve the quality of life of the patients [14]. It involves systemic therapies like chemotherapy, hormone therapy, targeted therapies, and immunotherapy, local interventions like radiation therapy, bone-targeted therapies like bisphosphonates, and supportive care measures like pain management. Due to the complexities of the patient's circumstances, multidisciplinary collaboration is crucial for effective treatment decisions [13–19]. Nanotechnology-based delivery systems have emerged as a promising solution for tackling the complexities associated with managing BC bone metastasis by providing various benefits in comparison with conventional approaches to manage this com [13].

Curcumin (CUR), derived from the plant *Curcuma longa* (commonly known as turmeric) [20, 21], has demonstrated a range of advantageous biological properties. These include antiviral, antibacterial, anticancer, antioxidant activities, and anti-inflammatory. Notably, CUR has been shown to possess both preventive and therapeutic effects in diverse cancer types, including BC [22–26]. Nevertheless, the clinical utility of CUR is hindered by several factors, including its hydrophobic nature, instability, low bioavailability, short plasma half-life, and inadequate absorption [27]. To enhance CUR's drug-like properties, various nanotechnology-based strategies for CUR delivery have been explored, underscoring the impact of nanotechnology in cancer therapy. Additionally, some of these strategies have shown potential in overcoming drug resistance and achieving synergistic anticancer effects when used with CUR [28–33].

In this review, we first provided an introduction to breast cancer bone metastasis, outlining the steps involved, conventional treatments available, and treatment challenges. Following this, we delved into the promising therapeutic potential of CUR, specifically focusing on its effects on breast cancer bone metastasis. We discussed the molecular mechanisms and supporting studies of CUR's anti-metastatic effects, addressing the bioavailability issues that have limited its clinical use. To overcome these challenges, we examined nanotechnology-based delivery systems, including liposomes, polymeric nanoparticles, dendrimers, and micelles, which enhance CUR's solubility, stability, and targeted delivery. By reviewing recent advancements and outcomes in CUR nanoformulations, we provided a comprehensive perspective on using

nanotechnology to improve CUR's therapeutic efficacy in breast cancer bone metastasis, highlighting future directions and clinical applications.

2 Understanding breast cancer bone metastasis

Bone metastasis in BC is characterized by the dissemination of cancer cells from the primary tumor location to the bones, resulting in the formation of secondary tumors [34, 35] and giving rise to various complications, such as pain, fractures, and other associated issues [36]. Typical indications of bone metastasis encompass exacerbated bone pain that intensifies during movement or while at rest, as well as increased vulnerability of the bones, rendering them prone to fractures. Additionally, spinal cord compression can arise as a consequence of bone metastasis, leading to severe back pain, weakness, and numbness [6].

2.1 Breast cancer bone metastasis steps

The process of BC metastasis involves a series of intricate stages, namely invasion, migration, adhesion, and the survival of tumor cells at the metastatic sites. In 1889, the "seed and soil" hypothesis was first mentioned. This indicates that interactions between "seeds", which stand in for the tumor cells, and "soil", which denotes the prospective metastatic site's microenvironment, are what cause cancer to spread [8].

2.1.1 Invasion

In the formation of metastasis, BC cells at the primary tumor site initiate the process of generating new blood vessels to ensure a sufficient supply of nutrients for their proliferation known as angiogenesis. Subsequently, the tumor cells must navigate through these newly formed blood vessels to enter the bloodstream and lymphatic systems [37, 38]. The similarity between BC cells and healthy epithelial tissue cells hinders cell invasion and migration. Thus, to shed some of their epithelial characteristics, the BC cells must go through an epithelial-to-mesenchymal transition (EMT) [39]. Follow- ing that, within the primary tumor site, BC cells induce the synthesis of a significant group of enzymes known as matrix metalloproteinases (MMPs), which play a crucial role in tumor cell invasion. Facilitated by MMPs, the tumor cells degrade the extracellular matrix and breach the cell walls, allowing them to infiltrate the surrounding healthy tissues [40].

2.1.2 Migration

Following the invasion, the tumor cells transform into circulating tumor cells (CTCs), which then move to the bone through lymphatic or blood vessels. The CTCs might travel alone or in groups of several cells. Until the CTCs come into contact with small-caliber capillaries, these aggregates may keep moving. It is important to remember that most CTCs can be promptly cleared from the body. However, clusters of CTCs can traverse microvessels by retaining their sticky connections to create a single-cell chain [41]. The CTCs then dissolve the vascular basement membrane to get through the bone and into the blood artery, where they eventually reach the parenchymal tissue. The CTCs in the bone micro-environment then develop into the disseminated tumor cells (DTCs). The bone microenvironment changes by altering the biological phenotype of DTCs. DTCs in tissue parenchyma, for example, may withstand degradation and last for a long period. DTCs can survive by expressing the tyrosine kinase receptor TrkBor non-canonical WNT signaling, which can help them withstand anoikis [42].

2.1.3 Adhesion

When bone metastasis occurs, DTCs typically adhere to the favorable metastatic microenvironment, which is the bone marrow [43]. Integrin and cadherin play a key role in mediating this stage. Particularly αvβ3 integrin, which controls cell migration to trabecular bone, integrin, a transmembrane glycoprotein family member, facilitates BC cell attachment to the extracellular matrix. E-cadherin is an essential transmembrane glycoprotein for maintaining epithelial shape and cell-cell adhesion [44]. It facilitates cell–cell communication between bone marrow stromal cells and BC cells, enhancing cell homing [45, 46]. Cadherin-11, overexpressed in brain, lung, and bone, plays a vital role in BC bone metastasis [47].

2.1.4 Survival

Following BC cell adhesion to the bone tissue, the metastatic process progresses to its final, most crucial step. Tumor cells require the "vicious cycle of bone metastasis" to survive. When bone marrow stromal cells release tumor growth factors and tumor cells secrete osteoclast-stimulating substances, a vicious cycle starts. BC cells first overexpress PTHrP, a protein related to parathyroid hormone, in the bone microenvironment. This causes RANKL expression to rise and OPG expression to be inhibited [48]. Osteoclast activity is increased when OPG and RANKL are out of balance, which causes bone resorption. In this instance, the release of growth factors including TGF-, VEGF, IGFs, BMPs, and calcium may have an impact on the operation of the osteogenic process [49].

TGF-β, a multifunctional cytokine, regulates tissue homeostasis, cellular apoptosis, proliferation, and differentiation. In metastasis progression, it suppresses E-cadherin expression and upregulates pre-osteolytic factors like PTHrP, with metastatic bone site BC cells expressing more PTHrP [48]. Factors like TGF-β, IGFs, BMPs, and calcium stimulate BC cell proliferation and remodel the bone microenvironment, making it more suitable for colonization. Overexpression of PTHrP leads to osteoclastic bone destruction, promoting TGF-β and IGF expression, increasing PTHrP production, and promoting bone resorption, and bone metastasis [50]. Figure 1 shows a schematic mechanism of BC bone metastasis.

3 Conventional treatments for breast cancer bone metastasis

Most often utilized conventional treatments for BC bone metastasis include surgery, chemotherapy, and radiation therapy; however, additional approaches can also be employed in specific circumstances, including tailored medicine, immunotherapy, hormone therapy, and bone marrow transplant.

3.1 Surgery

Surgery is a versatile treatment for localized tumor removal, with adjuvant therapy like radiation or chemotherapy that is often recommended to shrink tumor size and mitigate recurrence risk [51]. Two main surgical approaches are breast-conserving surgery (lumpectomy) and quadrantectomy (particular mastectomy). Lumpectomy is recommended for early-stage patients and is outpatient, taking about 1–2 h. Quadrantectomy removes one-quarter of breast tissues and chest wall muscles within a 2–3 cm (about 1.18 in) radius of the tumor. Mastectomy involves complete removal of the breast, typically for stage III and IV patients. In many cases, there are some limitations; for instance, radiation therapy

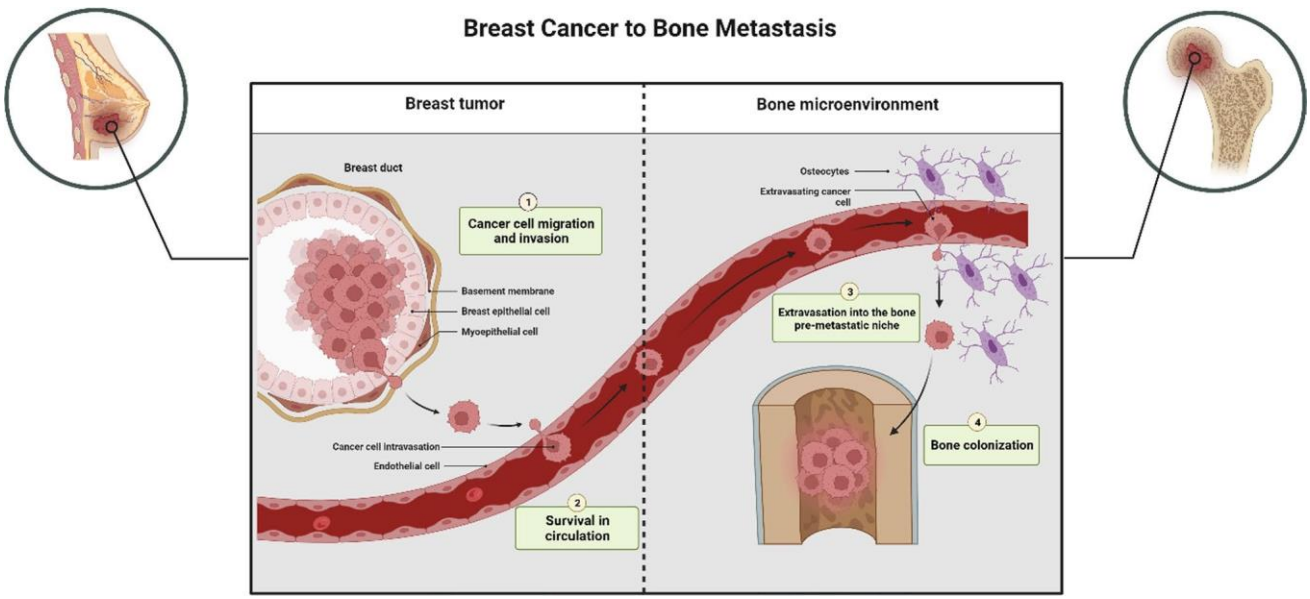

Fig. 1 Mechanism of BC bone metastasis. Bone metastasis in breast cancer encompasses a series of crucial steps, including migration, inva- sion, survival, extravasation, and colonization of cancer cells. Initially, these cells detach from the primary tumor, infiltrate neighboring tis- sues, and subsequently engage with the endothelial cells within the bone microenvironment

is recommended after post-surgical breast-conserving surgery to reduce recurrence risks. Additionally, the surgical approach to BC has limitations such as calcification formation, negative margin tumor removal, high recurrence risk, and invasiveness, necessitating additional reconstructive surgeries [52, 53].

3.2 Chemotherapy

Chemotherapy is the less invasive method which uses anticancer medications to target and eradicate BC cells. It may be given intravenously or orally, and it may be combined with other treatments like radiation, surgery, or hormone therapy [54]. Neo-adjuvant chemotherapy, also known as preoperative chemotherapy, is a treatment approach employed in breast cancer patients to reduce the size of tumors before surgery. This therapeutic strategy is particularly recommended for HER2-positive, triple-negative, inflammatory, lymph node-metastasized, and advanced-stage breast cancers. In cases where the cancer has progressed to the advanced stage with metastasis to other organs, chemotherapy is typically the preferred initial treatment option [55].

The studies conducted by the Early Breast Cancer Trialists' Collaborative Group (EBCTCG) indicated that the use of adjuvant or combined chemotherapy played a significant role in reducing mortality rates and the risk of recurrence in BC patients, particularly those under the age of 50. Specifically, drugs such as cyclophosphamide, methotrexate, and 5-fluorouracil have demonstrated effectiveness in treating node-positive tumors in premenopausal patients. Addition- ally, anthracyclines and chemo-endocrine therapy have also shown efficacy in the treatment of BC. A common regimen in the US is doxorubicin (Dox) and cyclophosphamide [56].

Despite that, its clinical significance is limited by poor selectivity, multidrug resistance (MDR), low availability, and adverse effects like alopecia, cognitive and sexual dysfunction, nausea, and pain. These limitations also affect patient compliance and the effectiveness of chemotherapy in treating advanced-stage BC [57–59].

3.3 Radiation therapy

Radiation therapy uses high doses of ionizing radiation to target cancerous tissues or cells, often combined with other conventional treatments. It reduces tumor size, decreases recurrence risks, and improves patient quality of life. Conventional radiotherapy requires 25–30 sessions, while hypofractionation therapy has 13–16 sessions but higher doses [60]. Radiation therapy is crucial for cancer treatment, but it can cause damage to non-cancerous tissues, chromosomal abnormalities, structural changes, skin irritation, dermatitis, swelling, discoloration, and lymph edema. Patients with medical conditions like scleroderma may also experience skin sensitivity issues [61].

In light of the inefficiencies of conventional therapies, the development of targeted and safe technology-based treatments has become imperative in addressing breast cancer bone metastases. Recent advancements have highlighted the potential of targeted drug delivery methods and nanotechnology in this regard. Various nanotechnology-based approaches have been explored to deliver therapeutic drugs and anticancer agents, such as curcumin, to metastatic lesions, aiming to achieve enhanced specificity and mitigate side effects. These strategies hold promise in facilitating disease identification, therapy, and prevention [6]. Specifically, advanced targeted drug delivery systems (DDSs), such as nanoparticles, have been investigated to modify drug solubility, reduce metabolism, and promote increased perme- ability and retention (EPR) effects in cancerous tissues. Notably, nanoparticles smaller than 200 nm exhibit the ability to traverse mucus barriers undetected by the immune system, thereby enabling precise medication delivery to bone metastases [62]. Consequently, the subsequent sections delve into the utilization of curcumin and nanotechnology to augment the efficacy of treating breast cancer bone metastases.

4 Curcumin (CUR)

Curcumin (CUR), a hydrophobic polyphenol from turmeric, has been extensively researched for its biomedical applications in treating various ailments with a range of properties including anticancer [63], wound healing [64–66], anti-inflammatory [67], antimicrobial [68], antioxidant, antipyretic, and anti-bone resorptive effects, among others. A core 1,6-heptadiene-3,5-dione with two terminal phenolic rings makes up the CUR structure. Curcumin's antioxidant properties are attributed to its o-methoxyphenol group and methylenic hydrogen. Additionally, CUR's antioxidant mechanism involves donating an electron or hydrogen atom to neutralize reactive oxygen species (ROS), thus preventing them from causing cell damage. This chemical interaction reduces oxidative stress in cells, which is linked to various inflammatory

diseases and age-related conditions [69]. In addition to its conventional use for the treatment of numerous medical diseases, CUR has demonstrated remarkable anticancer potential against several cancers, including BC bone metastasis [70]. CUR is a potentially effective anticancer agent that may be used alone or in combination with other traditional anticancer treatments including radiation [71, 72], surgery, [73], or chemotherapy [74]. CUR, when combined with radiotherapy enhanced radiotherapy's effectiveness, and reduced tumor size. Its anticancer effects include suppression of proliferation, migration, invasion, and inhibition of Ki-67, proliferating cell nuclear antigen (PCNA), Bcl-2, and P-53 mRNA expression [70, 75, 76].

CUR uses both covalent and non-covalent binding to interact with many biomolecules. Its biological action is attributed to hydrogen bonding, hydrophobicity, and the flexibility of the linker group, which result from its aromatic and tautomeric structures. CUR's hydrophobicity and structure–function connection are tightly connected. Its hydrophobic properties enable it to interact with proteins' hydrophobic regions, which inhibits protein aggregation and modifies protein function [77].

Nonetheless, CUR's anticancer potential as a pharmaceutical agent is hindered by low solubility, chemical instability, photo-degradability, bioavailability [78], rapid metabolism [79], short-plasma half-life, and auto-oxidation vulnerability [80, 81].

4.1 CUR mechanisms of action

CUR has demonstrated potential in both the treatment and prevention of BC through various mechanisms (Fig. 2). It exerts anti-inflammatory effects, reduces chronic inflammation, and exhibits antioxidant activity, protecting against oxidative stress. CUR modulates cell signaling pathways such as MAPK, JAK/STAT, PI3K/Akt, NF-κB, and Wnt/ß-catenin, inhibiting survival and proliferation signals in cancer cells. It induces apoptosis, or programmed cell death, in BC cells and inhibits angiogenesis, limiting the formation of new blood vessels that support tumor growth. These multifaceted actions of CUR collectively contribute to its ability to suppress tumor growth and metastasis, making it a promising

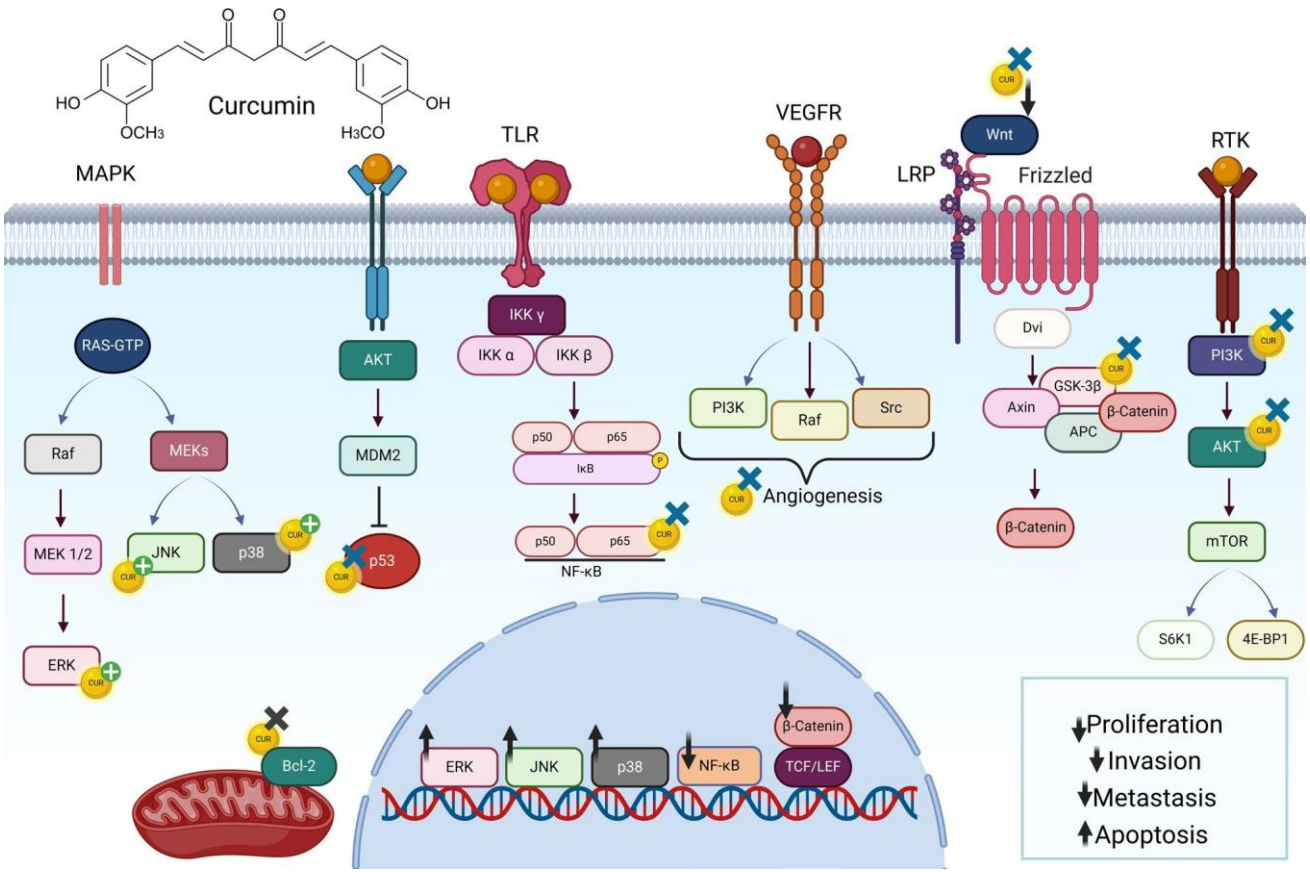

Fig. 2 Various signal transduction pathways by which curcumin modulates cancer progression

candidate for BC treatment and prevention [80–82]. Some important mechanisms by which CUR can affect BC cells are illustrated in Fig. 2 [83, 84].

4.1.1 Oncogene proteins of apoptosis and proliferation influenced by CUR

CUR as a vital player in cancer progression exhibits anticancer effects that are mainly mediated through regulation of multiple cellular signaling cascades including including nuclear factor-κB (NF-κB) pathway, Wnt/β-catenin signaling, phosphoinositide 3-kinase (PI3K)/protein kinase B (Akt) pathway, Janus kinase signal transducer and activator of transcription (JAK/STAT) signaling pathway, mitogen-activated protein kinase (MAPK) pathway, p53 signaling. Lately, CUR has been found to target oncogenic and tumor-suppressive miRNAs. Consequently, CUR is able to modify multiple signaling pathways and cellular targets and thus may affect cancer cell growth, apoptosis, invasion and metastasis [83]. CUR inhibits tumor cell proliferation in culture and protects animals against carcinogen-induced cancer. In Ortho-transplant animal models or xenotransplants, CUR suppresses human malignancies.According to Banerjee et al. [85], CUR caused death in MCF-7 cells and G2/M arrest, decreased cell growth by impairing the dynamics of microtubule assembly, and further activated the mitotic checkpoint. Furthermore, it was observed that CUR treatment led to cell accumulation in the G1 phase of the cell cycle. This effect was accompanied by the inhibition of Zeste homolog 2 (EZH2) gene expression. Mechanistically, CUR activated three crucial enzymes in the mitogen-activated protein kinase (MAPK) pathway, namely c-Jun NH2-terminal kinase (JNK), extracellular signal-regulated kinase (ERK), and p38 kinase [86].

CUR has been identified as a potent inhibitor of tumor cell growth, primarily through the promotion of apoptosis. Additionally, CUR effectively suppresses the expression of key markers associated with cell proliferation, such as Ki-67 and proliferating cell nuclear antigen (PCNA), as well as p53 mRNA levels in BC cells. Furthermore, CUR demonstrates the ability to down-regulate Bax mRNA expression [87]. Notably, in human mammary epithelial cells, CUR exerts a down- regulatory effect on p21 mRNA expression. These findings underline the multifaceted molecular mechanisms through which CUR exerts its anticancer effects in BC and highlight its potential as a therapeutic agent in the management of this disease.

Maspin, which is known as a serine protease inhibitor, reduces tumor motility and invasion in vitro as well as tumor development and metastasis in vivo. A study by Prasad et al. revealed that CUR boosted the expression of the Maspin gene in MCF-7 cells while up-regulating the p53 protein and down-regulating Bcl-2 [88]. In a separate study, it was discovered that CUR treatment resulted in increased expression of miR-16 and miR-15a in MCF-7 cells. This upregulation led to a decrease in the expression of Bcl-2 protein. Moreover, other studies have demonstrated that CUR effectively inhibits the proliferation of MDA-MB-231 cells by either upregulating p21 expression or modulating the Bax to Bcl-2 ratio [89]. Additionally, CUR down-regulates the AIP-1/Alix protein, an inhibitor of paraptosis, in malignant BC cells. Furthermore, CUR inhibits cell motility and invasion by targeting the function of α6β4 integrin. These findings collectively highlight the diverse molecular mechanisms employed by CUR in suppressing BC progression, making it a promising therapeutic candidate for combating this disease [90].

4.1.2 CUR's impacts on nuclear factor-κB (NF-κB)

Nuclear factor κB is a pro-inflammatory transcription factor with a critical role in the cancer progression signaling pathway since it is responsible for regulating tumor promotion genes. Even though the NF-κB signaling pathway must be activated for the immune system to combat infections, constitutive NF-κB activation will facilitate carcinogenesis by inhibiting apoptosis and promoting the growth of malignancies. Considering the key role of inflammatory pathways in cancer development, materials such as CUR with immunomodulatory ability can interact with several immune mediators, hence exhibit anticancer properties, thus CUR anti-cancer efficacy is related to inducing apoptosis by reducing NF-κB level [91, 92].

CUR activity which leads to apoptosis induction and cell death through disruption of the NF-κB pathway was reported in different cell lines including MCF-7 breast cancer cells, SGC-7901 and BGC-823 gastric cancer cells, MIAPaCa-E, MIAPaCa- M, and BxPC-3 Human pancreatic cancer cells, Oral squamous cell carcinoma cell, A549 human lung cancer cell lines, HT-29 colon cells, SUM159, MDA-MB-468 and MDA-MB-231 breast cancer cell lines [92, 93]. NF-κB is one of the main transcription factors that controls the genes responsible for cell survival and proliferation [94]. In between 15 and 25% of BC patients, the oncoprotein HER2 is overexpressed. In both SK-BR-3-h and BT-474 cells, CUR reduced the expression of NF-κB, Akt, and MAPK as well as the HER2 oncoprotein [95]. Additionally, CUR adapted p65-NF-κB-p300 crosstalk in favor of p53-p300 for BC, increasing the effectiveness of chemotherapy [96]. Thus, CUR exhibits a potential therapeutic

effect in preventing the invasion of BC cells mediated by Receptor'd Origin Nantais (RON) tyrosine kinase by influencing the expression and transcriptional activity of p65 protein through NF-κB [97].

Overall, CUR has shown promise in its ability to inhibit or down-regulate the activation of NF-κB, a transcription factor involved in cell proliferation and survival. By interfering with NF-κB signaling, CUR can down-regulate the expression of genes related to cell cycle progression, angiogenesis, and metastasis, which are important processes in cancer growth and spread, particularly BC. Additionally, CUR can induce apoptosis, a programmed cell death process, by counteracting NF-κB's anti-apoptotic effects. These combined effects make CUR a potentially useful compound in preventing tumor invasion and metastasis. However, more research is needed to fully understand its efficacy and potential applications in BC bone metastasis treatment.

4.1.3 CUR's impacts on endothelial growth factor

CUR has been found to suppress the production of vascular endothelial growth factor (VEGF) in tumor cells. It achieves this by blocking the induction of VEGF expression caused by osteoponin or medroxyprogesterone acetate. As a result, CUR has the potential to reduce angiogenesis in BC [76]. Notably, CUR exerts its suppressive effects on α6β4 signaling and activities by inducing changes in the intracellular localization of α6β4. This alteration prevents α6β4 from interact- ing with crucial signaling receptors such as Akt and the epidermal growth factor receptor (EGFR), thereby inhibiting their downstream signaling pathways [98]. Additionally, both in vitro and in vivo models of ER-BC show promise for the combination of CUR and epi gallo catechin gallate (EGCG). Thus, the anticancer actions in these processes may be significantly influenced by the control of VEGFR-1 [99].

4.1.4 CUR's impacts on Wnt/β-catenin signaling pathway

CUR has been shown to regulate the Wnt/β-catenin signaling pathway, a key pathway involved in essential cellular processes such as differentiation, development, and cell proliferation. The development and progression of BC have been linked to dysregulation of this pathway.

CUR can suppress the expression of Wnt ligands, which are the signaling molecules that initiate the pathway. By reducing the availability of Wnt ligands, CUR can limit the activation of the pathway [100]. Furthermore, CUR can directly target the key components of the Wnt/β-catenin pathway. It has been reported to inhibit the activity of glycogen synthase kinase-3β (GSK-3β) [101, 102], an enzyme that phosphorylates β-catenin. Phosphorylation of β-catenin leads to its degradation, preventing its accumulation and subsequent activation of the Wnt/β-catenin pathway. By inhibiting GSK-3β, CUR can stabilize β-catenin and decrease its translocation to the nucleus, thereby attenuating Wnt signaling [102–104]. Curcumin exerted an inhibitory effect through the Wnt/β-catenin pathway while inhibiting the nonsmall cell lung cancer cells, colon cancer, and medulloblastoma cells proliferation by obviously suppressing the β-catenin and p-glycogen synthase kinase-3β (GSK-3β) expression [83].

In addition to its direct effects on Wnt/β-catenin signaling components, CUR can also influence other regulatory proteins involved in the pathway. For example, it can down-regulate the expression of transcription factors such as T-cell factor/lymphoid enhancer factor (TCF/LEF), which interact with β-catenin to activate target genes [100, 105]. It is important to note that the effects of CUR on the Wnt/β-catenin pathway can vary depending on the specific cellular context and the characteristics of the BC subtype. Further research is needed to elucidate the precise mechanisms and optimize the potential therapeutic applications of CUR in BC bone metastasis treatment.

4.1.5 CUR's impacts on PI3K/Akt pathway

CUR has been shown to affect the PI3K/Akt pathway, which plays a pivotal role in cell growth, survival, and proliferation. In BC, dysregulation of this pathway was common and contributed to tumor progression and therapy resistance. CUR inhibits the PI3K/Akt pathway through multiple mechanisms. It directly inhibits the activity of PI3K, blocking the activation of Akt [106, 107].CUR also reduces the expression of growth factor receptors like EGFR and HER2, limiting PI3K/Akt activation induced by these receptors [22, 108]. Additional studies have shown that targeting CUR with other therapeutic agents in the PI3K/Akt pathway may enhance the efficacy of treatment and overcome resistance mechanisms in BC bone metastasis. Further research is required to fully understand CUR mechanisms and optimize their therapeutic application in BC treatment.

4.1.6 CUR's impacts on JAK/STAT

The JAK/STAT signaling pathway persuades the expression of various critical mediators of cancer and inflammation. This pathway regulates a wide range of cellular processes, including cell growth, proliferation, differentiation, and apoptosis. It has been shown that CUR exerts inhibitory effects on STAT3 which leads to apoptosis induction in human glioblastoma and squamous carcinoma cells and melanoma cells [109]. CUR by acting on the JAK2/STAT3 signaling pathway revealed the therapeutic effects on human lung cancer cell lines A549 [92]. CUR antiproliferative effect by STAT3-dependent pathways exerts a significant role in the inhibition of glioblastoma (GBM) [110].

5 CUR and nanotechnology

Nanotechnology has been used in the production of CUR's product to overcome these obstacles, and the results have led to a revolutionary advance in CUR's physicochemical qualities such as water solubility, chemical and metabolic stability, bioavailability, controlled release, targeted delivery and enhanced efficacy for the treatment of BC bone metastasis [111–113]. Liposomal CUR, polymeric nanoparticles, solid lipid nanoparticles (SLNs), dendrimers, gold nanoparticles, and magnetic nanoparticles are some of the approaches being explored [113–115]. Preclinical studies have shown promising results from nanobased DDSs regarding their anticancer activity, including inhibition of tumor growth, induction of apoptosis, and inhibition of angiogenesis [113, 116]. For instance, liposomal CUR utilizes lipid vesicles to improve solubility and protect against degradation [117]. Some CUR-based DDSs that have been investigated have potential to allow early diagnosis and treatment of diseases like BC bone metastasis by [118–122].

A comprehensive understanding of the physicochemical attributes of CUR-based nanoparticles, including size, zeta potential, thermodynamics, shape, and colloidal stability, is crucial for optimizing their pharmacokinetic properties and maximizing their anticancer effectiveness. For instance, the Scherrer equation from the X-ray powder diffraction spectrographs was used to determine the particle size of CUR nanoparticles. CUR's particle size (range of micrometers, for example 30 μm) was bigger than that of nano curcumin (47.4–98.7 nm), increasing its biological activity by giving it a greater surface area to interact with biomolecules [111]. The functional groups of curcumin and nano curcumin have been characterized using Fourier-transform infrared analysis [123]. It was discovered that the nano curcumin spectra showed the infrared vibrational bands corresponding to the respective positions of the curcumin functional groups but with some modifications at the molecular level during the synthesis process. Curcumin's crystallinity may be increased by nanotechnology, as evidenced by the X-ray diffraction (XRD) research, which revealed that the manufactured curcumin nanoparticles were more crystalline than the original pure curcumin [123]. When the zeta potential of nano curcumin was also examined, it was discovered to be negative and comparatively high, meaning that the particles were stable and dispersed uniformly [124].

Indeed, by exerting control over these characteristics, the potential for enhancing the pharmacokinetic profile and overall therapeutic activity of CUR-based nanoparticles can be significantly enhanced [118, 120]. Nanoencapsulation of CUR improves cell uptake and internalization, and anticancer efficacy against BC bone metastasis [125]. However, one of the key drawbacks of these nanoparticles is the absence of specific targeting, which might lead to adverse effects and lowered efficacy. To address this problem, many modifications have been made to the design of nanoparticles, enhancing their potential to target the tumor microenvironment (TME) and tumor cells. In this regard, passive targeting refers to the phenomenon where nanoparticles demonstrate a preference for accumulating in cancerous tissues due to leaky blood vessels and increased permeability and retention (EPR) [126]. This process can be further improved by optimiz- ing the physicochemical characteristics of the nanoparticles. Parameters ()hieving an ultrafine particle size (≤ 200 nm), developing a hydrophilic exterior, ensuring an optimal zeta potential, and incorporating surface modifications with diverse hydrophilic moieties contribute to the passive accumulation of nanoparticles within the TME. Additionally, the leaky vasculature observed in tumor tissues, arising from the irregular arrangement of endothelial cells in newly formed blood vessels as a consequence of abnormal angiogenesis, plays a significant role in facilitating the passive targeting of CUR-nanoparticles into the TME [127, 128]. The leaky vasculature observed in cancerous tissues is a consequence of the rapid growth of cancer cells, resulting in an imbalance between nutrient supply and demand. This increased demand leads to heightened permeability and vascular leakage within the TME. Consequently, the leaky vasculature facilitates the transportation of CUR nanoparticles to tumor tissues through the bloodstream. Moreover, the immature and mispositioned endothelial cells, combined with the abnormal structure and function of the tumor vasculature, promote the accumulation and penetration of CUR nanoparticles within the tumor site. Additionally, the retention of

CUR- nanoparticles in cancerous tissues is prolonged due to inadequate clearance through the lymphatic system. This extended retention increases the exposure of cancer cells to the therapeutic effects of CUR-nanoparticles, potentially enhancing their effectiveness against the disease [32].

The targeted delivery of drugs to certain bodily cells or areas is known as active targeting. To do this, the surface of CUR-nanoparticles can be coupled with a range of targeted ligands, including folic acid, antibodies, hyaluronic acid, peptides, etc. As a result, it is simpler to identify the specific substrate receptors that tumor cells overexpress on their surfaces, such as folate, CD44, transferrin receptors, etc. Notably, the precise engagement between nanoparticles adorned with targeting ligands and cancer cells expressing specific receptors results in the discerning accumulation of CUR-nanopar- ticles within the desired cancer cells and tissues. This phenomenon effectively impedes the undesired accumulation of chemotherapeutic cargo in non-target areas [129].

5.1 Nanotechnology-based strategies for CUR delivery

Nano-drug delivery systems have been developed to improve therapeutic agents' properties to treat diseases. Nanocarriers containing CUR exhibited remarkable anticancer effects against different cancer cells, especially BC. Studies showed successful encapsulation of CUR using various nano-based delivery strategies [130]. However, these platforms might also face challenges in in vivo settings, limiting their clinical application. Hence, further research and clinical trials are needed to determine the safety, efficacy, and optimal application of these delivery strategies in humans (Fig. 3).

To improve the pharmacokinetic profile, tumor biodistribution, and anticancer activity of CUR-based nanocarriers against BC and BC bone metastasis, various strategies have been developed, including functionalization and targeting

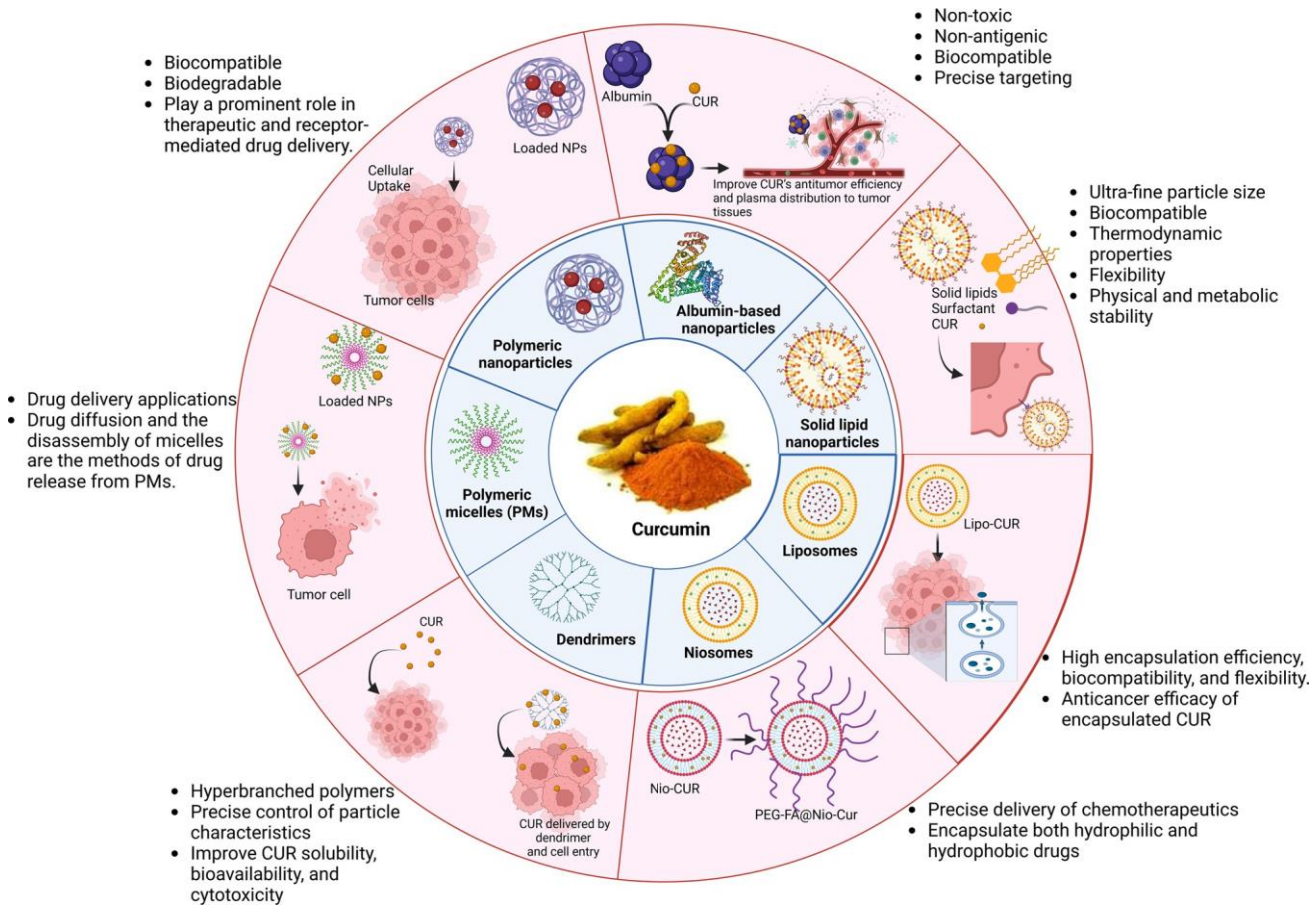

Fig. 3 Representation of nanotechnology-based strategies for CUR delivery. Some key nanotechnology-based delivery systems for CUR include liposomes, polymeric nanoparticles, solid lipid nanoparticles, albumin-based NPs, polymeric micelles, niosomes, and dendrimers. These systems have shown promising results in improving the biological activities of CUR

of the nanocarriers with different agents. Over the rest of this review, some important strategies that have been used to deliver CUR targeted with other drugs in BC and BC bone metastasis will be presented.

5.1.1 Liposomes

Liposomes, spherical nanovesicles with a lipid bilayer structure resembling biological membranes, have emerged as versatile drug nanocarriers for various medications [131]. Their utilization as a drug delivery system has gained significant attention owing to their advantageous characteristics such as high encapsulation efficiency, biocompatibility, and flexibility. Liposomes can effectively enhance the aqueous solubility, absorption, bioavailability, biodistribution, and anticancer efficacy of encapsulated CUR. Recent advancements in liposome technology, such as active targeting, PEGylation, and the incorporation of pH-sensitive linkers, such as IM-Chol, Glycyrrhetinic Acid-Polyethylene Glycol-Schiff Bond-Cholesterol (GPSC), and Polyacrylic Acid (pI-pAA), have further improved the effectiveness of CUR as a therapeu- tic agent. These developments hold immense promise for optimizing the delivery and therapeutic potential of CUR in diverse applications [132–134].

CUR-encapsulated liposomes, showed a dose-dependent escalation in cytotoxicity against breast cancer cells (MCF- 7). The liposomes were selective for BC cells and showed anticancer effectiveness due to increased ROS production and damage to vital cell structures [135]. The study revealed that surface functionalization of CUR-liposomes with salmon's lecithin significantly enhanced the NPs anticancer efficacy, suggesting further enhancement of their anticancer properties and oral bioavailability [136, 137].

Research on functionalizing liposomes with folic acid (FA) has demonstrated specific cell uptake efficiency in TNBC cells, demonstrating selective targetability due to overexpressed FA receptors [138]. The LD50 of CUR-liposomes in MDA-MB-321 was reported to be 19 μM, lower than against normal breast cells, MCF-12A, suggesting that FA-conjugation could enhance their anticancer effectiveness in targeting BC tumors [139]. Likewise, Luiz and colleagues studied FA-functionalized CUR-liposomes' selective targeting capabilities; found FA-functionalized CUR-liposomes improved cytotoxicity, cell uptake efficiency, and anticancer efficacy against BC cells (MCF-7) compared to unfunctionalized CUR-liposomes [140]. Curcumin encapsulated in ZHER2:342 affibody-conjugated liposomes were designed to specifically target HER-2 receptors in MCF-7 and SKBR3 cell lines. ZHER2:342 molecule was used as the affibody to be covalently conjugated to the liposomes via its C-terminal cysteine residue. The CUR-loaded liposomes enhanced cytotoxicity, anticancer effectiveness, and cell uptake efficiency [141].

Likewise, Ruttala et al. introduced a novel approach by developing a hybrid liposome system that was PEGylated and encapsulated with paclitaxel (PTX)-loaded albumin nanoparticles as well as CUR. This innovative formulation enables the simultaneous delivery of multiple chemotherapeutic agents, offering potential synergistic effects and enhanced therapeutic outcomes, whereby they showed improvement in the anti-metastatic and anti-proliferative efficacy of this method in treating BC [142]. Also, In vitro antitumor efficacy and increase plasma concentration-time curve, mean residence time, and biological half-life time of CUR- docetaxol loaded liposomes rather than free drugs suggesting a promising drug delivery system for the synergistic treatment of BC [143].

5.1.2 Solid lipid nanoparticles (SLNs)

The SLNs can enhance anticancer drug delivery owing to their composition, ultrafine particle size, biocompatibility, thermodynamic properties, flexibility, and physical and metabolic stability. Drugs are effectively protected from chemical deterioration when are encapsulated in SLNs, which increases their stability in storage [144]. The biodistribution to target tissues, pharmacokinetic profile, and therapeutic efficacy of SLNs have been shown to be improved by prolonging blood circulation time [145, 146].

The choice of lipid ingredient used in SLNs significantly impacts their stability, physicochemical properties, and transcellular permeation. Wang and coworkers [146] developed CUR-encapsulated SLNs using stearic acid and lecithin, showing good thermodynamic stability. The cytotoxicity data showed an enhanced anti-proliferative efficacy of CUR-loaded SLNs. Minafra et al. proposed a synergistic therapeutic approach combining radiotherapy with CUR-SLNs to enhance BC treatment efficacy. This approach demonstrated stronger cytotoxic effects due to increased radio-sensitization and potent antioxidant activity of CUR-SLNs. Using increasing concentrations of vehicled curcumin Cur-SLN, the DMFs (Dose Modifying Factor) values, determined at the isoeffect of SF = 50%, demonstrated that the Luminal A MCF7 was sensitive to the combination treatments (DMF: 1,78 with 10 μM Cur-SLN.) Rather,

MDA-MB-231 cells that were triple negative showed a greater sensitivity to free-Cur. However, these cells also experienced a radiosensitization effect when combined with Cur-SLN (DMF: 1.38 when using 10 μM Cur-SLN) [147].

The development of SLNs not only enabled the active targeting technique of certain BC cells and tissues but also offer versatil advantages including low toxicity, stability, and easy production by several mechanisms such as passive targeting, surface modification, and improving solubility [148]. Transferrin receptors are overexpressed on cancer cell surfaces, including BC cells. In a study, Mulik et al. engineered transferrin-conjugated SLNs as a targeted delivery system for CUR-SLNs into BC cells. The transferrin-conjugated SLNs exhibited favorable characteristics, including ultra-small particle size (194 ± 2.89 nm and zeta potential of 12.43 ± 1.58 mV), efficient encapsulation of CUR-SLNs (percent drug entrapment of 77.27 ± 2.34%) sustained release of the drug (84.3 ± 4.1% after 48 h), and enhanced cellular uptake. These findings highlight the potential of transferrin-conjugated SLNs as an effective strategy for targeted delivery of CUR-SLNs in BC therapy, offering improved drug delivery and potential therapeutic benefits [149].

To make them immune-compatible and biocompatible, Pawar et al. designed SLNs for the simultaneous administration of CUR and docetaxel (DTX) that were functionalized with FA and coated with polyethylene glycol. The FA-conjugated CUR/DTX-SLNs demonstrated increased BC cell cytotoxicity and cell uptake efficiency. Additionally, the results demonstrated improved pharmacokinetic and biodistribution profiles and greater tumor penetration [150]. The findings suggest that surface functionalization of CUR-SLNs through PEGylation or conjugation with targeted ligands leads to improved efficiency in cell uptake, enhanced cytotoxicity, favorable pharmacokinetic profiles, optimized biodistribution, and increased anticancer activity against BC.

5.1.3 Albumin-based NPs

The albumin NPs have been widely utilized for treating many diseases, including BC, due to their biocompatibility and non-antigenicity since albumin is a plasma-circulating protein. The physicochemical characteristics of albumin- based NPs, such as stablity at room and body temperatures, improving the bioavailability of poorly soluble drugs, and enhancing the permeability and retention of drugs, are crucial for their biodistribution, transmembrane permeability, and precise targeting of the TME. Albumin-based NPs characteristics including particle size (less than 200 nm), surface chemistry (as positive surface charge agent acts as a dysopsonin, protecting circulating NPs from recognition and clearance), entrapment potential (33.36%-94.57%), shape (Doughnut Shapes or Non-Spherical Shapes**)**, and colloidal stability (stored for several months without significant changes in particle size) are important in drug delivery. To improve CUR's antitumor efficiency and plasma distribution to tumor tissues, Jithan et al. devel- oped albumin-NPs that were nano-scaled (228.7 nm) and showed a prolonged release profile for at least 1 month. These CUR-loaded albumin-NPs' demonstrated increased cytotoxicity against MDA-MB-231 cells and enhanced pharmacokinetic profile via their increased dissolution rate and aqueous solubility [151].

Similarly, researchers have modified CUR-loaded albumin-NPs with PDL-1 binding peptide to enhance their selective targeting and anticancer efficacy against programmed death ligand 1 (PDL1) expressing cells. The PDL-1 binding peptide-functionalized CUR-loaded albumin-NPs (P-HAS/CUR-NPs) showed a powerful cytotoxic response against BC cells, with a fourfold lower IC50 than free CUR [152].

Additionally, Thadakapally et al. proposed PEGylation of CUR-loaded albumin-NPs to increase passive accumulation in BC cells, lengthen the plasma circulation period, and decrease hepatic clearance. PEGylation is known to speed up plasma circulation, promote preferential accumulation inside BC cells, and increase the effectiveness of treatments for cancer. Compared to free CUR and albumin-CUR-NPs that had not been functionalized with PEG, the produced PEG-CUR-albumin-NPs had a greater absorption efficiency in MD-MB-231 cells [153].

Recently, Hiremath et al. established a brand-new design for co-delivering CUR and 5-flurouracil against BC cells, referred to as "multi-functionalized NPs". For targeted delivery and providing stealth effect, albumin and citrate were added to these NPs as coating agents. The NPs demonstrated an extremely small particle size (10–15 nm), excellent anionic zeta potential (− 49.1 mV), colloidal stability, and sustained release at PH:7.4. The study demonstrated the best internalization and most cytotoxicity in BC cells, pointing to multifunctionalization as an effective approach for the treatment of cancer [154].

5.1.4 Polymeric NPs

Polymeric NPs have garnered extensive research attention as nano-delivery systems, owing to their inherent characteristics including particle size, colloidal stability, shape, entrapment efficiency, biocompatibility, biodegradability, and the versatility for functionalization. These features contribute to the wide exploration and comprehensive study of polymeric NPs in various applications [155, 156]. Furthermore, high rates of organ invasion and metastasis in BC patients are two main factors contributing to their high mortality rate. BC cells can travel from primary tumor sites to other body regions, causing inflammation and metastasis. While CUR, is potent anti-inflammatory agent and can be used to prevent metastasis and inflammation, due to its hydrophobicity and low stability it has poor bioavailability and minimal adsorption. To overcome these challenges, various functionalized polymeric NPs have been developed [157]

Polymeric NPs can be categorized into (a) nanospheres and (b) nano-capsules based on their architectural characteristics [158]. The drugs adhere to the surfaces of the polymeric nanospheres, while they are predominantly encapsulated within the inner core of the polymeric nano-capsules, which are enveloped by a solid polymer matrix. The type of polymer utilized to create them has a significant impact on the physicochemical properties of polymeric NPs [158, 159]. The polymeric NPs are fabricated utilizing a wide range of polymers, including synthetic, natural, and semi-synthetic polymers [119, 160]. Most polymeric NPs are studied for drug-drug or drug-gene co-encapsulation [130, 161, 162].

Pawar et al. developed poly (lactic-co-glycolic acid) nanoparticles (PLGA-NPs) for the co-delivery of DTX and CUR. The results demonstrated enhanced cytotoxicity, increased cell uptake, and improved pharmacokinetic profiles in male Wistar rats. The PLGA-NPs exhibited ultrafine particle size (219 nm), narrow polydispersity index (PDI), and biphasic release kinetics, highlighting their potential for enhanced anticancer efficacy against BC cells [163]. Moreover, Sampath et al. developed PLGA-NPs for optimal cell uptake efficiency into BC cells (MCF7). The PLGA-NPs were functionalized with various agents such as Chitosan, Dextran, and PEG, resulting in ultrafine particles, storage stability, high loading capac- ity, and smooth morphology. Among all, TPGS-CCUR-PLGA-NPs showed the highest cytotoxicity and internalization in MCF-7 cells [164]. PEG-CUR-PLGA-NPs upregulate ROS-induced apoptosis, alleviate angiogenesis, reduce proliferative properties, and have anti-metastatic potential.

PLGA-NPs face challenges in drug delivery due to recognition by the reticuloendothelial system (RES) [157, 165], which leads to their metabolism and excretion. To overcome these challenges, surface functionalization strategies, such as forming a hydrophilic layer around the exterior surface, have been employed. These strategies have improved plasma circulation time by reducing NP recognition by the RES and have enhanced the pharmacokinetic profile by decreasing NP clearance by the RES. Additionally, these modifications have improved biodistribution, cell uptake efficiency, and anticancer efficacy through the use of targeting ligands on the surface of the NPs.

To make CUR-PLGA-NPs hydrophobic and improve their uptake and permeability into MDA-MB-231 cells Palange and co-researchers proposed another technique of functionalizing NPs. This method involves coating the NPs' surfaces with lipids. Long-circulating, lipid-coated CUR-loaded PLGA NPs have demonstrated higher cytotoxicity in head and neck squamous cell carcinoma (HNSCC). This suggests that lipid coating can enhance the penetrability and anticancer efficacy of polymeric nanoparticles by increasing drug loading and encapsulation efficiency, improving stability and biocompatibility, enhancing cellular uptake and tumor penetration, controlling drug release, and providing synergistic anticancer effects [166].

Functionalized PLGA-NPs with transferrin for selective targeting and receptor-mediator endocytosis were prepared in a study. Transferrin-conjugated PLGA-NPs showed higher cell uptake into BC cells due to transferrin receptor-mediated endocytosis, resulting in higher cytotoxicity [167]. Similarly, engineered CUR-paclitaxel co loaded nano-formulations with the aim of selectively targeting BC cells. The optimized formulation, exhibited several advantageous properties, including ultrafine particle size (70.3 ± 7.6 nm and zeta potential of − 18.9 ± 1.5 mV), smooth morphology, high encapsulation efficiency, and sustained release profile with notably superior cell uptake efficiency and significant anti-proliferative efficacy against BC cells which highlighting their potential as an effective targeted therapeutic approach [168].

Ranjan et al. developed a functionalized approach by utilizing CUR-PLGA-NPs with Annexin A2 (AnxA2) antibody [169]. This strategy led to increased cell uptake efficiency and reduced proliferation of MDA-MB-231 cells. The optimized CUR-PLGA-NPs exhibited promising potential for selective targeting of BC cells and tissues. Additionally, the researchers introduced a novel hybrid nano curcumin formulation, where CUR was enclosed within a nanoshell. This hybrid design demonstrated improved bioavailability and enhanced anticancer efficacy, further highlighting its potential as a valuable therapeutic approach [170].

5.1.5 Polymeric micelles (PMs)

PMs have recently been exploited as targeted drug delivery systems for a variety of therapies, especially for poorly water-soluble compounds [171]. Multi-drug resistance (MDR) is a challenge in cancer treatment; hence, various targeted therapies have been developed to overcome this [172, 173]. Hyaluronic acid-vitamin E succinate copolymer-based PMs have been developed for simultaneous delivery of CUR and doxorubicin (DOX). These PMs have nanoscale dimensions, high encapsulation efficiency, and exhibit rapid release in acidic environments. In vivo studies showed that (Dox-CUR)-PMs could suppress tumor growth rate and show no cardiotoxicity or hepatotoxicity which is associated with Dox therapy, making them promising nanocarriers for co-encapsulation of two chemotherapeutics [174]. Xie et al. proposed a func- tionalized CUR-PMs, by incorporating methotrexate (MTX) in a prodrug conjugate (DSPE-PEG-Imine-MTX) for a dual role leading to self-assembled MTX-Imine-M-CUR micelles. MTX showed moderate targeting efficiency and fair anticancer efficacy for tumor cells with overexpressed FA receptors. The study found that MTX-Imine-M-CUR, demonstrated superior uptake efficiency, cytotoxicity, and anticancer efficacy in BC cells and tumor-bearing animals [175].

Curcumin loaded on the poly (sulfobetaine methacrylate), which formed CUR-PMs, prepared through the process of ultrasonication, have been awarded a Chinese patent for their application in the treatment of breast cancer, specifically MCF-7 cells. These CUR-loaded-PMs exhibited desirable characteristics, including small particle size, efficient CUR encapsulation, high efficacy results, and the ability to protect against photo-oxidation [176].

5.1.6 Niosomes

Noisomes, innovative nanovesicles, have been extensively utilized for the precise delivery of chemotherapeutics [177]. These vesicular delivery systems effectively address various challenges associated with therapeutic compounds [178]. Noisomes, as versatile drug delivery carriers, effectively encapsulate both hydrophilic and hydrophobic drugs, providing protection against degradation and enabling controlled release. These nanovesicles mimic biological membranes, making them suitable for addressing challenges such as low oral bioavailability. Additionally, noisomes hold promise for targeted delivery to BC cells [179]. For instance, a hybrid model, lipo-noisome, has demonstrated anticancer efficacy against various cancer cells by simultaneously delivering hydrophilic and hydrophobic drugs, including CUR and Dox [180]. Alemi et al. designed a PEG-functionalized noisome loaded with both CUR and PTX. These noisomes were specifically developed to improve uptake into BC cells, specifically MCF-7 cells. The researchers observed that the PEG-functionalized niosomes exhibited ultrafine vesicle size (90 nm), efficient encapsulation of the drugs, optimal zeta potential, and pH-responsive release behavior [181].

Akbarzadeh et al. proposed a novel functionalization strategy for treating BC using calcium alginate-shelled CUR-noisome (CA-CUR-noisome). The study evaluated their anticancer efficacy against various BC cells and normal breast cells. The CA-CUR-noisome, characterized by its small size (163.4–358.4 nm), efficient encapsulation, and stable colloidal properties, exhibited promising capabilities in targeting and suppressing cancer cells, particularly breast cancer cell lines. Additionally, the results demonstrated the ability to promote apoptotic pathways, further highlighting their potential as an effective therapeutic approach [182].

5.1.7 Dendrimers

Dendrimers are branching polymeric macromolecules with large molecular weight and a high degree of organization. Dendrimers are highly regarded as effective drug delivery systems for a wide range of medications, genes, proteins, and RNAs due to their compact architecture, low polydispersity, and unique properties. Their well-defined structure and controlled size enable precise control over drug release and targeting, making them versatile carriers for therapeutic applications [183, 184].

CUR loaded in Dendrimers exhibited improveed solubility, bioavailability, and cytotoxicity, thereby enhancing its anticancer effects against BC cells through the induction of apoptotic cell death [185]. Likewise, in another study., CUR-loaded dimer and poly(amidoamine) (PAMAM) dendrimers were developed (CUR-dendrimers). This functionalization led to improved aqueous solubility of the dendrimers and pH-responsive release of CUR. The CUR-dendrimers demonstrated a significant increase in cell uptake efficiency specifically in BC cells, which can be attributed to receptor-mediated endocytosis. The functionalization of dendrimers holds promise as an approach to enhance the specific targeting and anticancer effectiveness of CUR-nanoparticles against BC [186]. Various nanocarriers investigated for targeted drug delivery of curcumin against breast cancer bone metastases are listed in Table 1.

Table 1 Nanocarriers explored for targeted delivery of curcumin in breast cancer bone metastases

Nanocarrier type	Drug	Target/cell line	Description	References
Liposome	CUR-encapsulated liposomes	MCF-7	Dose-dependent escalation in cytotoxicity against breast cancer cells due to increased ROS production and damage to vital cell structures	[135]
	Folic acid conjugated CUR-liposomes	FA receptors/MDA-MB-321 and MCF-12A cell lines	Improved cytotoxicity, cell uptake efficiency, and anticancer efficacy against	[139]
	CUR- encapsulated in ZHER2:342 Affibody-decorated liposomes	HER-2 receptors/MCF-7 and SKBR3 cell lines		[187]
Solid lipid nanoparticles (SLNs)	CUR-encapsulated stearic acid and lecithin	SKBR3 cells	Good thermodynamic stability and efficiency	[188]
	Transferrin-conjugated SLNs	Transferrin receptor	Exhibited favorable characteristics, including ultra-small particle size efficient encapsulation of CUR-SLNs, sustained release of the drug, and enhanced cellular uptake	[149]
	FA-conjugated CUR/DTX-SLNs	MCF-7 and MDA-MB-231 cell lines	Increased BC cell cytotoxicity and cell uptake efficiency Improved pharmacokinetic and biodistribution profiles and greater tumor penetration	[189]
Albumin-based NP	Albumin-conjugated CUR	MDA-MB-231 cells	Increased cytotoxicity and pharmacokinetic profile	[190]
	P-HAS/CUR-NPs	PDL-1 receptor	Showed a powerful cytotoxic response against BC cells, with a fourfold lower IC50 than free CUR	[152]
	PEGylated CUR-loaded albumin-NPs	MD-MB-231 cell line	Increased passive accumulation in BC cells, lengthen the plasma circulation period, and decreased hepatic clearance	[153]
Polymeric NPs	Poly (lactic-co-glycolic acid) nanoparticles TPGS-CCUR-PLGA-NPs	MCF7 and Xenograft wistar rats	Used for co-delivery of DTX and CUR Demonstrated enhanced cytotoxicity, increased cell uptake, and improved pharmacokinetic profiles in male Wistar rats Showed the highest cytotoxicity and internalization in MCF-7 cells	[163]
	PEG-CUR-PLGA-NPs		Upregulate ROS-induced apoptosis, alleviate angiogenesis, reduce proliferative properties, and have anti-metastatic potential	[164]
	CUR-PLGA-NPs with Annexin A2 (AnxA2)	MB-231 cell line	Exhibited promising potential for selective targeting of BC cells and tissues	[170]
Polymeric micelles (PMs)	DSPE-PEG-Imine-MTX	BC cells	MTX showed moderate targeting efficiency and fair anticancer efficacy for tumor cells with overexpressed FA receptors	[191]

Table 1 (continued)

Nanocarrier type	Drug	Target/cell line	Description	References
Niosomes	PEG-functionalized noisome loaded with both CUR and PTX	MCF7	Exhibited ultrafine vesicle size (90 nm), efficient encapsulation of the drugs, optimal zeta potential, and pH-responsive release behavior	[192]
	CA-CUR-noisome	Various BC cells and normal breast cells	Demonstrated the ability to promote apoptotic pathways	[193]
Dendrimers	PAMAM	BC cells	Demonstrated a significant increase in cell uptake efficiency specifically	[194]

Discover Nano (2024) 19:177 | https://doi.org/10.1186/s11671-024-04126-1

5.2 Bisphosphonates-conjugated CUR nanosystems targeting BC bone metastasis

A class of chemical substances known as bisphosphonates has a strong affinity for the hydroxyapatite crystals that are frequently seen in bones and teeth. This strong affinity is caused by the ability of bisphosphonates to produce tridentate or bidentate chelation with the calcium ion on hydroxyapatite [195]. After intravenous or oral administration, the bisphosphonates can swiftly localize to tissues where hydroxyapatite is present. As a result, a promising method of targeting the bone particularly is provided by conjugating bisphosphonates to drug delivery systems [196] Additionally, bisphosphonates are frequently used to treat diseases that result in bone resorption. It was shown that osteoclasts can take up specific bisphosphonates [197]. The osteoclasts can concurrently play the targeted role and have supplementary therapeutic effects on skeletal-related events by inactivating osteoclasts, such as enhancing bone density, reducing fracture risk, and treating bone pain at metastatic locations [198]. Furthermore, bisphosphonates may have direct and indirect antitumor effects on various tumors, including prostate, lung, and melanoma cancer cells, in vitro. The possibility that bisphosphonates could mediate apoptosis and cell cycle arrest is a plausible mechanism for these antitumor activities, which supports synergistic therapeutic effects with anticancer drugs [199]. ALN is the bisphosphonate analog that is most frequently utilized as a targeting agent in nano-based DDSs. This bisphosphonate analog is a second-generation bisphosphonate, that has been approved by the FDA for the treatment of postmenopausal osteoporosis, Paget disease of the bones, male osteoporosis, and steroid-induced osteoporosis [200, 201]. ALN, when bound to hydroxyapatite crystals in bone, reduces osteoclast-mediated bone reabsorption and bone matrix breakdown, thereby regulating mineral reabsorption and turnover [200, 202]. Furthermore, ALN has been employed as a bone-targeting drug in the treatment of BC [203], metastatic bone cancer, primary bone cancer [204], and metastatic lung cancer [205]. A study by Rouach et al. revealed that a history of oral ALN use in postmenopausal patients with early BC was associated with a decreased risk of bone metastases [203].

Notably, the utilization of ALN has been widely implemented to functionalize nanoparticles, enabling diverse strategies for achieving targeted delivery specifically to the bone. Numerous nanotherapeutic systems coated with ALN have various chemotherapy medications added to them. Of these, the most important have been Zn [206], folic acid [207], Dox [208], and CUR [209].

The mechanisms of ALN in cancer therapy are multifaceted some of which are summarized as follows:

1. *Bone resorption inhibition* ALN preferentially targets areas of high bone turnover, binding to hydroxyapatite on bone surfaces to inhibit osteoclast-mediated bone resorption. This disruption of the "vicious cycle", where tumor cells pro- mote bone resorption which in turn releases growth factors that enhance tumor development, is crucial in halting the progression of bone metastases [210].
2. *Impairment of tumor cell dynamics* Studies have shown that ALN inhibits breast cancer cells from adhering to, migrat- ing through, and invading the bone matrix, thus interrupting a critical phase in the metastatic cascade [211].
3. *Induction of apoptosis* ALN has been demonstrated to induce apoptosis in cultured breast cancer cells, reducing their ability to proliferate and spread [212].
4. *Premetastatic niche inhibition* ALN may also prevent the formation of the "premetastatic niche", environments in distant organs that support the growth of incoming metastases. It has been observed to hinder cancer cell invasion into the stroma, thereby potentially disrupting the TME and further preventing cancer cell migration into these areas [213, 214]. Additionally, ALN combined with a bisphosphonate-glucomannan conjugate significantly reduces tumor-associated macrophages (TAMs) infiltration and polarization, suggesting a role in modifying the TME [215].

Furthermore, ALN inhibits the enzyme farnesyl pyrophosphate synthase (FPPS) [216], disrupting the mevalonate pathway, and interfering with the prenylation of small GTPases involved in osteoclast signaling. To illustrate in detail, ALN exerts its effects on bones by inhibiting FPPS, an enzyme involved in the mevalonate pathway. The mevalonate pathway is responsible for producing isoprenoid compounds, including farnesyl pyrophosphate (FPP), which is essen- tial for the proper functioning of small GTPases. These GTPases, such as Ras, Rac, Rho, and Cdc42, play crucial roles in intracellular signaling pathways involved in osteoclast differentiation, activation, and bone resorption [217].

By inhibiting FPPS, ALN disrupts the synthesis of FPP and subsequently impairs the prenylation process. Prenylation is a post-translational modification that involves the addition of farnesyl and geranylgeranyl groups to small GTPases, enabling their proper localization and activation. However, when ALN inhibits FPPS, the prenylation of small GTPases is disrupted, compromising their normal function [218].

Notably, the impaired function of small GTPases, resulting from the inhibition of FPPS by ALN, has significant downstream effects. For example, Ras GTPases are involved in activating the mitogen-activated protein kinase (MAPK) pathway, which influences osteoclast survival, differentiation, and cytoskeletal organization. Rho GTPases regulate cytoskeletal dynamics, crucial for osteoclast attachment, migration, and resorption activity. Thus, by disrupting the function of small GTPases, ALN reduces osteoclast-mediated bone resorption, which in turn leads to a decrease in the breakdown of bone tissue, resulting in increased bone mineral density, and a decreased risk of fractures [218, 219].

Moreover, ALN disrupts osteoclast attachment to the bone surface, impairing their ability to create a sealed microenvironment necessary for bone resorption [220]. Additionally, ALN has been shown to induce osteoclast apoptosis, which in turn leads to reducing their numbers and activity. It also inhibits the release of enzymes and acids involved in bone breakdown, further decreasing bone resorption [221, 222]. For instance, ALN affects the enzymes involved in bone breakdown, including cathepsin K and matrix metalloproteinases (MMPs) [223]. Cathepsin K is an enzyme produced by osteoclasts that degrades the organic components of bone, and MMPs are a group of enzymes that contribute to the degradation of proteins in the extracellular matrix of bone. ALN inhibits the release and activity of these enzymes, which leads to reducing their ability to break down the organic components of bone [224].

In addition to the processes, ALN exerts its effects on bone health by modulating the signaling of receptor activators of nuclear factor kappa-B ligand (RANKL). RANKL is a crucial cytokine involved in osteoclast differentiation and activa- tion. ALN reduces the production of RANKL by osteoblasts, thereby limiting the availability of this cytokine for binding to its receptor, RANK, on osteoclast precursor cells. Thus, by reducing bone resorption and promoting a more favorable balance between bone formation and breakdown, ALN enhances bone mineralization, leading to increased bone density and strength [225–227].

6 ALN and CUR: evidence for targeted and combination therapy

6.1 Examples for targeted therapies of BC bone metastasis

CUR provides benefits over potent cytotoxic agents due to its safety profile and potential synergistic effects with other chemotherapeutic drugs like doxorubicin [157]. Moreover, the broad radical-scavenging action of curcumin is advantageous due to its proton-transfer-dissociation mechanism, which is intricately linked to its ability to neutralize a wide range of radicals, thereby mitigating oxidative stress and potentially offering therapeutic benefits in various disease conditions including cancer [228].

Dong et al. developed redox-sensitive CUR-loaded micelles targeted with ALN, which inhibited MDA-MB-231 tumor growth in vitro and in vivo. These stimuli-responsive nanoparticles bind to CD44 receptors of tumor necrosis factor-beta cells, releasing drugs proportionally. This formulation has been studied for its potential to improve osteosarcoma therapy and alleviation of bone resorption in metastatic BC [209]. Based on the findings of this study, it is possible that the mechanism of action of CUR-loaded micelles with ALN in bone cancer cells involves targeted delivery of CUR to the cancer cells in bone tissue, sustained release of CUR, and higher cytotoxic activity against cancer cells compared to free CUR. The versatility of micelles, capable of being conjugated with various moieties, renders them ideal for CD44 receptor-targeting and bone-targeting effects. Additionally, those micelles with reduction-responsive properties enable controlled release of CUR in response to the TME [229, 230]. It should be noted that micelles have the potential to provide benefits over other DDSs when it comes to the delivery of CUR for metastatic malignancies. These benefits include improved drug solubility, protection against inactivation in the biological environment, increased drug bioavailability, and less side effects [231]. Furthermore, micelles can be engineered to release their therapeutic payloads in a controlled manner, allowing for optimal drug concentrations at the target site for an extended period. Additionally, micelles can be targeted to certain receptors by targeting moieties. One such receptor that can be targeted specifically is the CD44 receptor, which is frequently overexpressed in cancer cells that cen be easily targeted by hyaluronic acid micelles [232]. Moreover, it is possible to modify the responsiveness of micelles to certain stimuli, including alterations in pH, redox potential, or the presence of particular enzymes, enabling regulated release in reaction to the TME [233].

In a study, researchers have developed an innovative approach for targeted delivery of CUR using ALN-hyaluronic acid-octadecanoic acid (ALN-HA-C18) micelles. These nano micelles exhibited exceptional characteristics, including a high capacity for drug loading, sustained release, and a strong binding affinity with hydroxyapatite, a key component of bone. The results of this investigation suggest that CUR-loaded NPs targeted with ALN-HA-C18 hold tremendous promise for bone-related applications, particularly due to their dual targeting mechanism involving the significant affinity for

bone tissue, making them an ideal carrier for targeted drug delivery. Additionally, these micelles exhibited significantly enhanced cytotoxic activity against MG-63 cells and effectively impeded the growth of tumors in mice with osteosarcoma. These exciting findings strongly support the potential of CUR NPs targeted with ALN-HA-C18 as a highly effective and promising therapeutic strategy for targeting osteosarcoma [230].

Furthermore, a team of researchers has successfully engineered a nano micelle called CUR-loaded ALN-oHA-S-S-CUR, which possesses reduction-responsive properties and targets both the CD44 receptor and bone tissue. In an in vivo experiment, these nano micelles exhibited remarkable efficacy in inhibiting tumor growth. This breakthrough holds substantial promise for the development of an effective drug delivery system specifically designed for bone tumor therapy, especially in cases where cancers prone to bone metastasis, such as BC, are involved [229].

6.2 Examples for CUR and ALN combination therapy

A clinical trial evaluated the effects of the combination of CUR with ALN on bone mineral density (BMD) and bone turnover markers in postmenopausal women with osteoporosis, highlighting aging-related bone fragility. The study found that postmenopausal women with estrogen deficiency experienced increased bone turnover markers like BALP and CTx, while osteocalcin decreased. Notably, BMD indices also were shown to be decreased. ALN is a well-known therapeutic agent in patients going through hormone replacement therapy (HRT). It could effectively reduce bone turnover markers and increase osteocalcin. Thus, ALN can help to prevent osteoporosis in postmenopausal women, even more effectively than HRT without its associated side effects like atrial fibrillation. It has been shown to reduce atypical diaphyseal femoral fracture, or jaw osteonecrosis in these patients [234].

Likewise, in a different investigation, it was discovered that a combination therapy involving high doses of CUR and standard doses of ALN presented notable advantages compared to monotherapy with either CUR or ALN alone. Specifically, the combination therapy exhibited a synergistic antiresorptive effect on bone remodeling and resulted in improved bone mechanical strength. The group receiving the combination therapy demonstrated reduced concentrations of CTX-1 and ALP, increased BMD, and a higher maximal load value, indicating enhanced bone health and resilience [235]. These studies found that CUR and ALN improved densitometric status and bone remodeling markers in postmenopausal women, with higher results in combined use compared to alone use. Yet, further clinical trials should be explored to reach a convergent conclusion.

7 Conclusions and future perspectives

CUR has shown promising anticancer properties against BC, but its clinical evidence is limited due to low bioavailability, hydrophobicity, poor absorption, instability, and a short plasma half-life. Due to CUR's fast metabolism and limited water solubility, nanotechnology has been utilized to increase its bioavailability and therapeutic potential. Through increased cellular absorption, localization to specific regions, and higher bioavailability, nanotechnology-based DDSs have demonstrated the potential to augment the anticancer effects of CUR. CUR nanoparticles have the potential to be used in the treatment of breast cancer, as demonstrated by in vivo studies that indicate a considerable reduction in tumor volume in breast cancer models. However, challenges like recognition by the reticuloendothelial system, non-specific accumulation, and multidrug resistance hinder CUR nanoparticles' clinical significance using these platforms. Future advancements in CUR-based therapeutics via nanocarriers aim to overcome some limitations. Nanotechnology-based delivery systems can incorporate other strategies, including targeted therapies and combinations with other drugs, development of prodrugs and analogs integration with medical imaging techniques, and personalized medicine approaches. Among all targeting agents, ALN, a bone-seeker drug, has potential benefits for treating bone metastasis, particularly when combined with CUR. Therefore, CUR NPs targeted with ALN have been developed which have shown an enhanced therapeutic efficacy and potential inhibition of BC cell spread to the bone and preserving bone integrity, in addition to improving CUR's bioavailability through delivery in nanosystems. However, despite the promising results observed in in vivo experiments, the translation of drug delivery nanosystems modified with bone-targeting moieties into clinical applications remains uncommon. This is due to various factors including the rate of drug loading into the nanosystem, stability during storage, drug release capability, blood flow, and in vivo metabolism, all of which necessitate further investigation [62]. Despite minimal toxicity observed in most nanomaterials, only a small number of nanomedicines have received FDA approval for marketing, underscoring the need for more research to ensure their long-term safety and clinical efficacy. Future studies should focus on enhancing drug loading and release mechanisms, investigating the effects of nanoparticles on

cells comprehensively, and identifying more precise targeting ligands. Well-designed clinical trials and evidence-based data are essential for establishing the safety, efficacy, and optimal use of CUR-based therapies, with the potential to maximize their therapeutic benefits and broaden their applications in disease treatment, including cancer. Collaboration between researchers and surgeons, particularly orthopedic surgeons, is crucial for developing nanosystems tailored to clinical needs..

Acknowledgements Not applicable.

Author contributions The manuscript was developed through the collaborative efforts of SS (conceptualization, writing—original draft prepara- tion, writing, review and editing, visualization), SA (writing—review and editing), and PV (conceptualization, writing, supervision of SS, critical review, and editing of the manuscript). All authors have thoroughly read and approved the final version of the manuscript for publication.

Funding This study did not receive any specific grants from funding agencies in the public, commercial, or not-for-profit sectors.

Data availability All data and materials are included within the paper.

6.4 Declarations

Ethics approval and consent to participate There was no need for this research because it was a review, and no volunteers were involved.

Consent for publication All authors have consented to publish this work in Discover Nano journal.

Competing interests The authors declare that they have no competing interests.

References

1. Sung H, Ferlay J, Siegel RL, Laversanne M, Soerjomataram I, Jemal A, Bray F. Global cancer statistics 2020: GLOBOCAN estimates of inci- dence and mortality worldwide for 36 cancers in 185 countries. CA Cancer J Clin. 2021;71(3):209–49.
2. Yiallourou A. Hereditary Breast Cancer Syndromes Breast cancer represents the most common type of cancer affect-ing the female population worldwide. According to the most recent data from the Global Cancer Observatory (GLOBOCAN), breast cancer has surpassed lung cancer as the leading cause of. Breast Cancer Manag Surg Exam Guide. 2023:79.
3. Wang H, Zhang C, Zhang J, Kong L, Zhu H, Yu J. The prognosis analysis of different metastasis pattern in patients with different breast cancer subtypes: a SEER based study. Oncotarget. 2017;8(16):26368.
4. Nagini S. Breast cancer: current molecular therapeutic targets and new players. Anti-cancer Agents Med Chem Former Curr Med Chem Anti-cancer Agents. 2017;17(2):152–63.
5. Pang L, Gan C, Xu J, Jia Y, Chai J, Huang R, Li A, Ge H, Yu S, Cheng H. Bone metastasis of breast cancer: molecular mechanisms and thera- peutic strategies. Cancers. 2022;14(23):5727.
6. Shao H, Varamini P. Breast cancer bone metastasis: a narrative review of emerging targeted drug delivery systems. Cells. 2022;11(3):388.
7. Clézardin P, Coleman R, Puppo M, Ottewell P, Bonnelye E, Paycha F, Confavreux CB, Holen I. Bone metastasis: mechanisms, therapies, and biomarkers. Physiol Rev. 2021;101(3):797–855.
8. Peinado H, Zhang H, Matei IR, Costa-Silva B, Hoshino A, Rodrigues G, Psaila B, Kaplan RN, Bromberg JF, Kang Y. Pre-metastatic niches: organ-specific homes for metastases. Nat Rev Cancer. 2017;17(5):302–17.
9. Soni S, Torvund M, Mandal CC. Molecular insights into the interplay between adiposity, breast cancer and bone metastasis. Clin Exp Metastasis. 2021;38(2):119–38.
10. Xu Y, Zhang S, Liao X, Li M, Chen S, Li X, Wu X, Yang M, Tang M, Hu Y, et al. Circular RNA circIKBKB promotes breast cancer bone metastasis through sustaining NF-κB/bone remodeling factors signaling. Mol Cancer. 2021;20(1):98.
11. Adam MA, Mohamed NM, Othman A, Gasmalla A, Mansour WA. Frequency distribution of bone metastasis in breast cancer: a retrospec- tive study in Khartoum Oncology Hospital 2019. Int J Orthop Res. 2020;3:123–8.
12. Ban J, Fock V, Aryee DN, Kovar H. Mechanisms, diagnosis and treatment of bone metastases. Cells. 2021;10(11):2944.
13. Shao H, Varamini P. Breast cancer bone metastasis: a narrative review of emerging targeted drug delivery systems. Cells. 2022;11(3):388.
14. Waks AG, Winer EP. Breast cancer treatment: a review. JAMA. 2019;321(3):288–300.
15. Kent CL, McDuff SG, Salama JK. Oligometastatic breast cancer: where are we now and where are we headed? A narrative review. Ann Palliat Med.

2021;10(5):5954–68.

16. Leto G. Current status and future directions in the treatment of bone metastases from breast cancer. Clin Exp Pharmacol Physiol. 2019;46(10):968–71.
17. Marazzi F, Orlandi A, Manfrida S, Masiello V, Di Leone A, Massaccesi M, Moschella F, Franceschini G, Bria E, Gambacorta MA. Diagnosis and treatment of bone metastases in breast cancer: radiotherapy, local approach and systemic therapy in a guide for clinicians. Cancers. 2020;12(9):2390.
18. Inotai A, Ágh T, Maris R, Erdősi D, Kovács S, Kaló Z, Senkus E. Systematic review of real-world studies evaluating the impact of medica- tion non-adherence to endocrine therapies on hard clinical endpoints in patients with non-metastatic breast cancer. Cancer Treat Rev. 2021;100:102264.
19. Terret C, Russo C. Pharmacotherapeutic management of breast cancer in elderly patients: the promise of novel agents. Drugs Aging. 2018;35:93–115.
20. Hewlings SJ, Kalman DS. Curcumin: a review of its effects on human health. Foods. 2017;6(10):92.
21. Razavi BM, Ghasemzadeh Rahbardar M, Hosseinzadeh H. A review of therapeutic potentials of turmeric (*Curcuma longa*) and its active constituent, curcumin, on inflammatory disorders, pain, and their related patents. Phytother Res. 2021;35(12):6489–513.
22. Farghadani R, Naidu R. Curcumin: modulator of key molecular signaling pathways in hormone-independent breast cancer. Cancers. 2021;13(14):3427.
23. Farghadani R, Naidu R. Curcumin as an enhancer of therapeutic efficiency of chemotherapy drugs in breast cancer. Int J Mol Sci. 2022;23(4):2144.
24. Sinha D, Biswas J, Sung B, Aggarwal B, Bishayee A. Chemopreventive and chemotherapeutic potential of curcumin in breast cancer. Curr Drug Targets. 2012;13(14):1799–819.
25. Song X, Zhang M, Dai E, Luo Y. Molecular targets of curcumin in breast cancer. Mol Med Rep. 2019;19(1):23–9.
26. Witika BA, Makoni PA, Matafwali SK, Mweetwa LL, Shandele GC, Walker RB. Enhancement of biological and pharmacological properties of an encapsulated polyphenol: curcumin. Molecules. 2021;26(14):4244.
27. Ombredane AS, Silva VR, Andrade LR, Pinheiro WO, Simonelly M, Oliveira JV, Pinheiro AC, Goncalves GF, Felice GJ, Garcia MP. In vivo efficacy and toxicity of curcumin nanoparticles in breast cancer treatment: a systematic review. Front Oncol. 2021;11:612903.
28. Afshari AR, Sanati M, Kesharwani P, Sahebkar A. Recent advances in curcumin-based combination nanomedicines for cancer therapy. J Funct Biomater. 2023;14(8):408.
29. Lu KH, Lu PW, Lu EW, Lin CW, Yang SF. Curcumin and its analogs and carriers: potential therapeutic strategies for human osteosarcoma. Int J Biol Sci. 2023;19(4):1241–65.
30. Tagde P, Najda A, Nagpal K, Kulkarni GT, Shah M, Ullah O, Balant S, Rahman MH. Nanomedicine-based delivery strategies for breast cancer treatment and management. Int J Mol Sci. 2022;23:2856.
31. Valentino A, Di Cristo F, Bosetti M, Amaghnouje A, Bousta D, Conte R, Calarco A. Bioactivity and delivery strategies of phytochemical compounds in bone tissue regeneration. Appl Sci. 2021;11:5122.
32. Zhang J, Sun J, Li C, Qiao H, Hussain Z. Functionalization of curcumin nanomedicines: a recent promising adaptation to maximize phar- macokinetic profile, specific cell internalization and anticancer efficacy against breast cancer. J Nanobiotechnol. 2023;21(1):106.
33. Hegde M, Girisa S, BharathwajChetty B, Vishwa R, Kunnumakkara AB. Curcumin formulations for better bioavailability: What we learned from clinical trials thus far? ACS Omega. 2023;8(12):10713–46.
34. Ban J, Fock V, Aryee DNT, Kovar H. Mechanisms, diagnosis and treatment of bone metastases. Cells. 2021;10:2944.
35. Monteran L, Ershaid N, Sabah I, Fahoum I, Zait Y, Shani O, Cohen N, Eldar-Boock A, Satchi-Fainaro R, Erez N. Bone metastasis is associated with acquisition of mesenchymal phenotype and immune suppression in a model of spontaneous breast cancer metastasis. Sci Rep. 2020;10(1):13838.
36. Confavreux CB, Follet H, Mitton D, Pialat JB, Clezardin P. Fracture risk evaluation of bone metastases: a burning issue. Cancers. 2021;13(22):5711.
37. Al-Ostoot FH, Salah S, Khamees HA, Khanum SA. Tumor angiogenesis: current challenges and therapeutic opportunities. Cancer Treat Res Commun. 2021;28:100422.
38. Moriwaki K, Wada M, Kuwabara H, Ayani Y, Terada T, Higashino M, Kawata R, Asahi M. BDNF/TRKB axis provokes EMT progression to induce cell aggressiveness via crosstalk with cancer-associated fibroblasts in human parotid gland cancer. Sci Rep. 2022;12(1):17553.
39. D'Oronzo S, Silvestris E, Paradiso A, Cives M, Tucci M. Role of bone targeting agents in the prevention of bone metastases from breast cancer. Int J Mol Sci. 2020;21(8):3022.
40. Mareel M, Leroy A. Clinical, cellular, and molecular aspects of cancer invasion. Physiol Rev. 2003;83(2):337–76.
41. Au SH, Storey BD, Moore JC, Tang Q, Chen YL, Javaid S, Sarioglu AF, Sullivan R, Madden MW, O'Keefe R, et al. Clusters of circulating tumor cells traverse capillary-sized vessels. Proc Natl Acad Sci U S A. 2016;113(18):4947–52.
42. Lambert AW, Pattabiraman DR, Weinberg RA. Emerging biological principles of metastasis. Cell. 2017;168(4):670–91.
43. Sai B, Xiang J. Disseminated tumour cells in bone marrow are the source of cancer relapse after therapy. J Cell Mol Med. 2018;22(12):5776–86.
44. Bandzerewicz A, Gadomska-Gajadhur A. Into the tissues: Extracellular matrix and its artificial substitutes: cell signalling mechanisms. Cells. 2022;11(5):914.
45. Kaszak I, Witkowska-Piłaszewicz O, Niewiadomska Z, Dworecka-Kaszak B, Ngosa Toka F, Jurka P. Role of cadherins in cancer—a review. Int J Mol Sci. 2020;21(20):7624.
46. Izaguirre MF, Casco VH. E-cadherin roles in animal biology: a perspective on thyroid hormone-influence. Cell Commun Signal. 2016;14:1–16.
47. Satriyo PB, Bamodu OA, Chen JH, Aryandono T, Haryana SM, Yeh CT, Chao TY. Cadherin 11 inhibition downregulates β-catenin, deactivates the canonical WNT signalling pathway and suppresses the cancer stem cell-like phenotype of triple negative breast cancer. J Clin Med. 2019;8(2):148.
48. Taverna S, Giusti I, D'Ascenzo S, Pizzorno L, Dolo V. Breast cancer derived extracellular vesicles in bone metastasis induction and their clinical implications as biomarkers. Int J Mol Sci. 2020;21(10):3573.
49. Waning DL, Guise TA, Mohammad KS. A "Connexin" responsible for the fatal attraction of cancer to bone. Cell Metab. 2019;29(1):6–8.

50. Le Pape F, Vargas G, Clézardin P. The role of osteoclasts in breast cancer bone metastasis. J Bone Oncol. 2016;5(3):93–5.
51. Admoun C, Mayrovitz H, Mayrovitz HN. Choosing mastectomy vs. lumpectomy-with-radiation: experiences of breast cancer survivors. Cureus. 2021;13(10):e18433.
52. Gonzalez-Angulo AM, Morales-Vasquez F, Hortobagyi GN. Overview of resistance to systemic therapy in patients with breast cancer. Breast Cancer Chemosensit. 2007:1–22.
53. Riis M. Future perspectives of surgical treatment of breast cancer. Ann Med Surg. 2020;59:93–5.
54. Moo TA, Sanford R, Dang C, Morrow M. Overview of breast cancer therapy. PET Clin. 2018;13(3):339–54.
55. Korde LA, Somerfield MR, Carey LA, Crews JR, Denduluri N, Hwang ES, Khan SA, Loibl S, Morris EA, Perez A. Neoadjuvant chemotherapy, endocrine therapy, and targeted therapy for breast cancer: ASCO guideline. J Clin Oncol. 2021;39(13):1485.
56. Franceschini G, Di Leone A, Natale M, Sanchez MA, Masett R. Conservative surgery after neoadjuvant chemotherapy in patients with operable breast cancer. Ann Ital Chir. 2018;89:290–290.
57. Galizia D, Milani A, Geuna E, Martinello R, Cagnazzo C, Foresto M, Longo V, Berchialla P, Solinas G, Calori A. Self-evaluation of duration of adjuvant chemotherapy side effects in breast cancer patients: a prospective study. Cancer Med. 2018;7(9):4339–44.
58. Montemurro F, Mittica G, Cagnazzo C, Longo V, Berchialla P, Solinas G, Culotta P, Martinello R, Foresto M, Gallizioli S. Self-evaluation of adjuvant chemotherapy-related adverse effects by patients with breast cancer. JAMA Oncol. 2016;2(4):445–52.
59. Pearce A, Haas M, Viney R, Pearson S-A, Haywood P, Brown C, Ward R. Incidence and severity of self-reported chemotherapy side effects in routine care: a prospective cohort study. PLoS ONE. 2017;12(10):e0184360.
60. Jain N, Sharma R, Sachdeva K, Kaur A, Sudan M. Conventional versus different hypofractionated radiotherapy dosage schedules in postmastectomy advanced breast cancer. J Med Phys. 2022;47(2):141–4.
61. Borrelli MR, Shen AH, Lee GK, Momeni A, Longaker MT, Wan DC. Radiation-induced skin fibrosis: pathogenesis, current treatment options, and emerging therapeutics. Ann Plast Surg. 2019;83(4S):S59–64.
62. Chen Y, Wu X, Li J, Jiang Y, Xu K, Su J. Bone-targeted nanoparticle drug delivery system: an emerging strategy for bone-related disease. Front Pharmacol. 2022;13:909408.
63. Tomeh MA, Hadianamrei R, Zhao X. A review of curcumin and its derivatives as anticancer agents. Int J Mol Sci. 2019;20(5):1033.
64. Akbik D, Ghadiri M, Chrzanowski W, Rohanizadeh R. Curcumin as a wound healing agent. Life Sci. 2014;116(1):1–7.
65. Tejada S, Manayi A, Daglia M, Nabavi SF, Sureda A, Hajheydari Z, Gortzi O, Pazoki-Toroudi H, Nabavi SM. Wound healing effects of cur- cumin: a short review. Curr Pharm Biotechnol. 2016;17(11):1002–7.
66. Kumari A, Raina N, Wahi A, Goh K, Sharma P, Nagpal R, Jain A, Ming L, Gupta M. Wound-healing effects of curcumin and its nanoformula- tions: a comprehensive review. Pharmaceutics. 2022;14:2288.
67. Peng Y, Ao M, Dong B, Jiang Y, Yu L, Chen Z, Hu C, Xu R. Anti-inflammatory effects of curcumin in the inflammatory diseases: status, limitations and countermeasures. Drug Des Dev Ther. 2021;15:4503–25.
68. Gunes H, Gulen D, Mutlu R, Gumus A, Tas T, Topkaya AE. Antibacterial effects of curcumin: an in vitro minimum inhibitory concentration study. Toxicol Ind Health. 2016;32(2):246–50.
69. Urošević M, Nikolić L, Gajić I, Nikolić V, Dinić A, Miljković V. Curcumin: biological activities and modern pharmaceutical forms. Antibiotics. 2022;11(2):135.
70. Liu D, Chen Z. The effect of curcumin on breast cancer cells. J Breast Cancer. 2013;16(2):133–7.
71. Verma V. Relationship and interactions of curcumin with radiation therapy. World J Clin Oncol. 2016;7(3):275–83.
72. Zoi V, Galani V, Tsekeris P, Kyritsis AP, Alexiou GA. Radiosensitization and radioprotection by curcumin in glioblastoma and other cancers. Biomedicines. 2022;10(2):312.
73. Mansouri K, Rasoulpoor S, Daneshkhah A, Abolfathi S, Salari N, Mohammadi M, Rasoulpoor S, Shabani S. Clinical effects of curcumin in enhancing cancer therapy: a systematic review. BMC Cancer. 2020;20(1):791.
74. Tan BL, Norhaizan ME. Curcumin combination chemotherapy: the implication and efficacy in cancer. Molecules. 2019;24(14):2527.
75. Coker-Gurkan A, Celik M, Ugur M, Arisan ED, Obakan-Yerlikaya P, Durdu ZB, Palavan-Unsal N. Curcumin inhibits autocrine growth hor- mone-mediated invasion and metastasis by targeting NF-κB signaling and polyamine metabolism in breast cancer cells. Amino Acids. 2018;50(8):1045–69.
76. Saberi-Karimian M, Katsiki N, Caraglia M, Boccellino M, Majeed M, Sahebkar A. Vascular endothelial growth factor: an important molecular target of curcumin. Crit Rev Food Sci Nutr. 2019;59(2):299–312.
77. Wang Z-Y, Sreenivasmurthy SG, Song J-X, Liu J-Y, Li M. Strategies for brain-targeting liposomal delivery of small hydrophobic molecules in the treatment of neurodegenerative diseases. Drug Discov Today. 2019;24(2):595–605.
78. Jurenka JS. Anti-inflammatory properties of curcumin, a major constituent of *Curcuma longa*: a review of preclinical and clinical research. Altern Med Rev. 2009;14(2):141–53.
79. Yallapu MM, Jaggi M, Chauhan SC. Curcumin nanomedicine: a road to cancer therapeutics. Curr Pharm Des. 2013;19(11):1994–2010.
80. Adamczak A, Ożarowski M, Karpiński TM. Curcumin, a natural antimicrobial agent with strain-specific activity. Pharmaceuticals. 2020;13(7):153.
81. Dai C, Lin J, Li H, Shen Z, Wang Y, Velkov T, Shen J. The natural product curcumin as an antibacterial agent: current achievements and problems. Antioxidants. 2022;11(3):459.
82. Sadeghi M, Dehnavi S, Asadirad A, Xu S, Majeed M, Jamialahmadi T, Johnston TP, Sahebkar A. Curcumin and chemokines: mechanism of action and therapeutic potential in inflammatory diseases. Inflammopharmacology. 2023;31(3):1069–93.
83. Wang M, Jiang S, Zhou L, Yu F, Ding H, Li P, Zhou M, Wang K. Potential mechanisms of action of curcumin for cancer prevention: focus on cellular signaling pathways and miRNAs. Int J Biol Sci. 2019;15(6):1200.
84. Yi D, Elise V, Ramin R. Molecular mechanisms of anti-metastatic activity of curcumin. Anticancer Res. 2016;36(11):5639.
85. Banerjee M, Singh P, Panda D. Curcumin suppresses the dynamic instability of microtubules, activates the mitotic checkpoint and induces apoptosis in MCF-7 cells. Febs j. 2010;277(16):3437–48.
86. Hua WF, Fu YS, Liao YJ, Xia WJ, Chen YC, Zeng YX, Kung HF, Xie D. Curcumin induces down-regulation of EZH2 expression through the MAPK pathway in MDA-MB-435 human breast cancer cells. Eur J Pharmacol. 2010;637(1–3):16–21.

87. Elbassiouni FE, El-Kholy WM, Elhabibi E-SM, Albogami S, Fayad E. Comparative study between curcumin and nanocurcumin loaded PLGA on colon carcinogenesis induced mice. Nanomaterials. 2022;12(3):324.
88. Ismail NI, Othman I, Abas F, Lajis NH, Naidu R. Mechanism of apoptosis induced by curcumin in colorectal cancer. Int J Mol Sci. 2019;20(10):2454.
89. Yang J, Cao Y, Sun J, Zhang Y. Curcumin reduces the expression of Bcl-2 by upregulating miR-15a and miR-16 in MCF-7 cells. Med Oncol. 2010;27(4):1114–8.
90. Wang Y, Wen X, Zhang N, Wang L, Hao D, Jiang X, He G. Small-molecule compounds target paraptosis to improve cancer therapy. Biomed Pharmacother. 2019;118:109203.
91. Radzka J, Łapińska Z, Szwedowicz U, Gajewska-Naryniecka A, Gizak A, Kulbacka J. Alternations of NF-κB signaling by natural compounds in muscle-derived cancers. Int J Mol Sci. 2023;24(15):11900.
92. Giordano A, Tommonaro G. Curcumin and cancer. Nutrients. 2019;11(10):2376.
93. Liu T, Long T, Li H. Curcumin suppresses the proliferation of oral squamous cell carcinoma through a specificity protein 1/nuclear factor- κB-dependent pathway. Exp Ther Med. 2021;21(3):1–1.
94. Fan Y, Mao R, Yang J. NF-κB and STAT3 signaling pathways collaboratively link inflammation to cancer. Protein Cell. 2013;4(3):176–85.
95. Lai HW, Chien SY, Kuo SJ, Tseng LM, Lin HY, Chi CW, Chen DR. The potential utility of curcumin in the treatment of HER-2-overexpressed breast cancer: an in vitro and in vivo comparison study with herceptin. Evid Based Complement Alternat Med. 2012;2012:486568.
96. Sen GS, Mohanty S, Hossain DMS, Bhattacharyya S, Banerjee S, Chakraborty J, Saha S, Ray P, Bhattacharjee P, Mandal D, et al. Cur- cumin enhances the efficacy of chemotherapy by tailoring p65NFκB-p300 cross-talk in favor of p53–p300 in breast cancer. J Biol Chem. 2011;286(49):42232–47.
97. Narasimhan M, Ammanamanchi S. Curcumin blocks RON tyrosine kinase-mediated invasion of breast carcinoma cells. Cancer Res. 2008;68(13):5185–92.
98. Li W, Wang Z, Xiao X, Han L, Wu Z, Ma Q, Cao L. Curcumin attenuates hyperglycemia-driven EGF-induced invasive and migratory abilities of pancreatic cancer via suppression of the ERK and AKT pathways. Oncol Rep. 2019;41(1):650–8.
99. Somers-Edgar TJ, Scandlyn MJ, Stuart EC, Le Nedelec MJ, Valentine SP, Rosengren RJ. The combination of epigallocatechin gallate and curcumin suppresses ER alpha-breast cancer cell growth in vitro and in vivo. Int J Cancer. 2008;122(9):1966–71.
100. Ahn J, Lee H, Kim S, Ha T. Curcumin-induced suppression of adipogenic differentiation is accompanied by activation of Wnt/beta-catenin signaling. Am J Physiol Cell Physiol. 2010;298(6):C1510-1516.
101. Jeong CW, Yoo KY, Lee SH, Jeong HJ, Lee CS, Kim SJ. Curcumin protects against regional myocardial ischemia/reperfusion injury through activation of RISK/GSK-3β and inhibition of p38 MAPK and JNK. J Cardiovasc Pharmacol Ther. 2012;17(4):387–94.
102. Vallée A. Curcumin and Wnt/β-catenin signaling in exudative age-related macular degeneration. Int J Mol Med. 2022;49(6):1–13.
103. Song HC, Chen Y, Chen Y, Park J, Zheng M, Surh YJ, Kim UH, Park JW, Yu R, Chung HT, et al. GSK-3β inhibition by curcumin mitigates amyloidogenesis via TFEB activation and anti-oxidative activity in human neuroblastoma cells. Free Radic Res. 2020;54(11–12):918–30.
104. Yun JH, Park YG, Lee KM, Kim J, Nho CW. Curcumin induces apoptotic cell death via Oct4 inhibition and GSK-3β activation in NCCIT cells. Mol Nutr Food Res. 2015;59(6):1053–62.
105. Hamdy MM, Antar A, El-Mesery ME, El-Shafey M, Ali AN, Abbas KM, Abulseoud OA, Hussein AM. Curcumin offsets PTZ-induced epilepsy: involving inhibition of apoptosis, wnt/β-catenin, and autophagy pathways. Egypt J Basic Appl Sci. 2020;7:240–51.
106. Borges GA, Elias ST, Amorim B, de Lima CL, Coletta RD, Castilho RM, Squarize CH, Guerra ENS. Curcumin downregulates the PI3K-AKT- mTOR pathway and inhibits growth and progression in head and neck cancer cells. Phytother Res. 2020;34(12):3311–24.
107. Jin H, Qiao F, Wang Y, Xu Y, Shang Y. Curcumin inhibits cell proliferation and induces apoptosis of human non-small cell lung cancer cells through the upregulation of miR-192-5p and suppression of PI3K/Akt signaling pathway. Oncol Rep. 2015;34(5):2782–9.
108. Vadukoot AK, Mottemmal S, Vekaria PH, Vadukoot AK. Curcumin as a potential therapeutic agent in certain cancer types. Cureus. 2022;14(3):e22825.
109. Hu X, Li J, Fu M, Zhao X, Wang W. The JAK/STAT signaling pathway: from bench to clinic. Signal Transduct Target Ther. 2021;6(1):402.
110. Mishra AP, Swetanshu, Singh P, Yadav S, Nigam M, Seidel V, Rodrigues CF. Role of the dietary phytochemical curcumin in targeting cancer cell signalling pathways. Plants. 2023;12(9):1782.
111. Elanthendral G, Shobana N, Meena R, Prakash P, Samrot AV. Utilizing pharmacological properties of polyphenolic curcumin in nanotech- nology. Biocatal Agric Biotechnol. 2021;38:102212.
112. Amekyeh H, Alkhader E, Sabra R, Billa N. Prospects of curcumin nanoformulations in cancer management. Molecules. 2022;27(2):361.
113. Hafez Ghoran S, Calcaterra A, Abbasi M, Taktaz F, Nieselt K, Babaei E. Curcumin-based nanoformulations: a promising adjuvant towards cancer treatment. Molecules. 2022;27(16):5236.
114. Montaseri H, Alipour S, Vakilinezhad MA. Development, evaluation and optimization of superparamagnetite nanoparticles prepared by co-precipitation method. Res Pharm Sci. 2017;12(4):274–82.
115. Mundekkad D, Cho WC. Applications of curcumin and its nanoforms in the treatment of cancer. Pharmaceutics. 2023;15:2223.
116. Harakeh S, Saber SH, Al-Raddadi R, Alamri T, Al-Jaouni S, Qari M, Qari Y, Haque S, Zawawi A, Ali SS, et al. Novel curcumin nanoformulation induces apoptosis, and reduces migration and angiogenesis in liver cancer cells. Artif Cells Nanomed Biotechnol. 2023;51(1):361–70.
117. Battista S, Maggi MA, Bellio P, Galantini L, D'Archivio AA, Celenza G, Colaiezzi R, Giansanti L. Curcuminoids-loaded liposomes: influence of lipid composition on their physicochemical properties and efficacy as delivery systems. Colloids Surf A. 2020;597:124759.
118. Hussain Z, Arooj M, Malik A, Hussain F, Safdar H, Khan S, Sohail M, Pandey M, Choudhury H, Ei Thu H. Nanomedicines as emerging platform for simultaneous delivery of cancer therapeutics: new developments in overcoming drug resistance and optimizing anticancer efficacy. Artif Cells Nanomed Biotechnol. 2018;46(sup2):1015–24.
119. Hussain Z, Pandey M, Thu HE, Kaur T, Jia GW, Ying PC, Xian TM, Abourehab MAS. Hyaluronic acid functionalization improves dermal targeting of polymeric nanoparticles for management of burn wounds: in vitro, ex vivo and in vivo evaluations. Biomed Pharmacother. 2022;150:112992.
120. Hussain Z, Thu HE, Amjad MW, Hussain F, Ahmed TA, Khan S. Exploring recent developments to improve antioxidant, anti-inflammatory and antimicrobial efficacy of curcumin: a review of new trends and future perspectives. Mater Sci Eng C Mater Biol Appl. 2017;77:1316–26.

121. Hussain Z, Thu HE, Ng SF, Khan S, Katas H. Nanoencapsulation, an efficient and promising approach to maximize wound healing efficacy of curcumin: a review of new trends and state-of-the-art. Colloids Surf B Biointerfaces. 2017;150:223–41.
122. Shah SA, Sohail M, Minhas MU, Khan S, Hussain Z, Mahmood A, Kousar M, Thu HE, Abbasi M, Kashif MUR. Curcumin-laden hyaluronic acid-co-Pullulan-based biomaterials as a potential platform to synergistically enhance the diabetic wound repair. Int J Biol Macromol. 2021;185:350–68.
123. Kanwal Q, Ahmed M, Hamza M, Ahmad M, Yousaf N, Javaid A, Anwar A, Khan IH, Muddassar M. Curcumin nanoparticles: phys- icochemical fabrication, characterization, antioxidant, enzyme inhibition, molecular docking and simulation studies. RSC Adv. 2023;13(32):22268–80.
124. Rageh MM, Abdelmoneam EA, Sharaky M, Mohamad EA. Physico-chemical properties of curcumin nanoparticles and its efficacy against Ehrlich ascites carcinoma. Sci Rep. 2023;13(1):20637.
125. Khan S, Imran M, Butt TT, Ali Shah SW, Sohail M, Malik A, Das S, Thu HE, Adam A, Hussain Z. Curcumin based nanomedicines as efficient nanoplatform for treatment of cancer: New developments in reversing cancer drug resistance, rapid internalization, and improved anticancer efficacy. Trends Food Sci Technol. 2018;80:8–22.
126. Hussain Z, Khan S, Imran M, Sohail M, Shah SWA, de Matas M. PEGylation: a promising strategy to overcome challenges to cancer-targeted nanomedicines: a review of challenges to clinical transition and promising resolution. Drug Deliv Transl Res. 2019;9(3):721–34.
127. Dessale M, Mengistu G, Mengist HM. Nanotechnology: a promising approach for cancer diagnosis, therapeutics and theragnosis. Int J Nanomed. 2022;17:3735.
128. Gavas S, Quazi S, Karpiński TM. Nanoparticles for cancer therapy: current progress and challenges. Nanoscale Res Lett. 2021;16(1):173.
129. Fang G, Zhang Q, Pang Y, Thu HE, Hussain Z. Nanomedicines for improved targetability to inflamed synovium for treatment of rheumatoid arthritis: multi-functionalization as an emerging strategy to optimize therapeutic efficacy. J Control Release. 2019;303:181–208.
130. Vakilinezhad MA, Amini A, Dara T, Alipour S. Methotrexate and Curcumin co-encapsulated PLGA nanoparticles as a potential breast cancer therapeutic system: In vitro and in vivo evaluation. Colloids Surf B Biointerfaces. 2019;184:110515.
131. Ong JC, Sun F, Chan E. Development of stealth liposome coencapsulating doxorubicin and fluoxetine. J Liposome Res. 2011;21(4):261–71.
132. Fulton MD, Najahi-Missaoui W. Liposomes in cancer therapy: how did we start and where are we now. Int J Mol Sci. 2023;24(7):6615.
133. Wang S, Chen Y, Guo J, Huang Q. Liposomes for tumor targeted therapy: a review. Int J Mol Sci. 2023;24(3):2643.
134. Feng T, Wei Y, Lee RJ, Zhao L. Liposomal curcumin and its application in cancer. Int J Nanomed. 2017;12:6027–44.
135. Prathyusha E, Prabakaran A, Ahmed H, Dethe MR, Agrawal M, Gangipangi V, Sudhagar S, Krishna KV, Dubey SK, Pemmaraju DB. Investi- gation of ROS generating capacity of curcumin-loaded liposomes and its in vitro cytotoxicity on MCF-7 cell lines using photodynamic therapy. Photodiagn Photodyn Ther. 2022;40:103091.
136. Hasan M, Elkhoury K, Belhaj N, Kahn C, Tamayol A, Barberi-Heyob M, Arab-Tehrany E, Linder M. Growth-inhibitory effect of chitosan- coated liposomes encapsulating curcumin on MCF-7 breast cancer cells. Mar Drugs. 2020;18(4):217.
137. Hasan M, Elkhoury K, Kahn CJF, Arab-Tehrany E, Linder M. Preparation, characterization, and release kinetics of chitosan-coated nanoli- posomes encapsulating curcumin in simulated environments. Molecules. 2019;24(10):2023.
138. Feng T, Wei Y, Lee RJ, Zhao L. Liposomal curcumin and its application in cancer. Int J Nanomed. 2017;12:6027–44.
139. Jadia R, Kydd J, Piel B, Rai P. Liposomes aid curcumin's combat with cancer in a breast tumor model. Oncomedicine. 2018;3:94–109.
140. Tavares Luiz M, Dutra JA, Ribeiro T, Carvalho G, Sábio R, Marchetti J, Chorilli M. Folic acid-modified curcumin-loaded liposomes for breast cancer therapy. Colloids Surf A. 2022;645:128935.
141. Moballegh-Nasery M, Mandegary A, Eslaminejad T, Zeinali M, Pardakhti A, Behnam B, Mohammadi M. Cytotoxicity evaluation of curcumin- loaded affibody-decorated liposomes against breast cancerous cell lines. J Liposome Res. 2021;31(2):189–94.
142. Ruttala HB, Ko YT. Liposomal co-delivery of curcumin and albumin/paclitaxel nanoparticle for enhanced synergistic antitumor efficacy. Colloids Surf B Biointerfaces. 2015;128:419–26.
143. Ye X, Chen X, He R, Meng W, Chen W, Wang F, Meng X. Enhanced anti-breast cancer efficacy of co-delivery liposomes of docetaxel and curcumin. Front Pharmacol. 2022;13:969611.
144. Rehman MU, Khan MA, Khan WS, Shafique M, Khan M. Fabrication of Niclosamide loaded solid lipid nanoparticles: in vitro characteriza- tion and comparative in vivo evaluation. Artif Cells Nanomed Biotechnol. 2018;46(8):1926–34.
145. Rudhrabatla VSA, Sudhakar B, Reddy KVN. In vitro and in vivo assessment of designed melphalan loaded stealth solid lipid nanoparticles for parenteral delivery. BioNanoScience. 2020;10:168–90.
146. Wang W, Chen T, Xu H, Ren B, Cheng X, Qi R, Liu H, Wang Y, Yan L, Chen S, et al. Curcumin-loaded solid lipid nanoparticles enhanced anticancer efficiency in breast cancer. Molecules. 2018;23(7):1578.
147. Minafra L, Porcino N, Bravatà V, Gaglio D, Bonanomi M, Amore E, Cammarata FP, Russo G, Militello C, Savoca G, et al. Radiosensitizing effect of curcumin-loaded lipid nanoparticles in breast cancer cells. Sci Rep. 2019;9(1):11134.
148. Bhagwat GS, Athawale RB, Gude RP, Md S, Alhakamy NA, Fahmy UA, Kesharwani P. Formulation and development of transferrin targeted solid lipid nanoparticles for breast cancer therapy. Front Pharmacol. 2020;11:614290.
149. Zhang J, Sun J, Li C, Qiao H, Hussain Z. Functionalization of curcumin nanomedicines: a recent promising adaptation to maximize phar- macokinetic profile, specific cell internalization and anticancer efficacy against breast cancer. J Nanobiotechnol. 2023;21(1):106.
150. Pawar H, Surapaneni SK, Tikoo K, Singh C, Burman R, Gill MS, Suresh S. Folic acid functionalized long-circulating co-encapsulated docetaxel and curcumin solid lipid nanoparticles: in vitro evaluation, pharmacokinetic and biodistribution in rats. Drug Deliv. 2016;23(4):1453–68.
151. Jithan A, Madhavi K, Madhavi M, Prabhakar K. Preparation and characterization of albumin nanoparticles encapsulating curcumin intended for the treatment of breast cancer. Int J Pharm Investig. 2011;1(2):119–25.
152. Hasanpoor Z, Mostafaie A, Nikokar I, Hassan ZM. Curcumin-human serum albumin nanoparticles decorated with PDL1 binding peptide for targeting PDL1-expressing breast cancer cells. Int J Biol Macromol. 2020;159:137–53.
153. Thadakapally R, Aafreen A, Aukunuru J, Habibuddin M, Jogala S. Preparation and characterization of PEG-albumin-curcumin nanopar- ticles intended to treat breast cancer. Indian J Pharm Sci. 2016;78(1):65–72.
154. Hiremath CG, Kariduraganavar MY, Hiremath MB. Synergistic delivery of 5-fluorouracil and curcumin using human serum albumin-coated iron oxide nanoparticles by folic acid targeting. Prog Biomater. 2018;7(4):297–306.
155. Rizi HAY, Shin DH, Rizi SY. Polymeric nanoparticles in cancer chemotherapy: a narrative review. Iran J Public Health. 2022;51(2):226.

156. Madej M, Kurowska N, Strzalka-Mrozik B. Polymeric nanoparticles—tools in a drug delivery system in selected cancer therapies. Appl Sci. 2022;12(19):9479.
157. Mundekkad D, Cho WC. Applications of curcumin and its nanoforms in the treatment of cancer. Pharmaceutics. 2023;15(9):2223.
158. Madawi EA, Al Jayoush AR, Rawas-Qalaji M, Thu HE, Khan S, Sohail M, Mahmood A, Hussain Z. Polymeric nanoparticles as tunable nano- carriers for targeted delivery of drugs to skin tissues for treatment of topical skin diseases. Pharmaceutics. 2023;15(2):657.
159. Syed MA, Aziz G, Jehangir MB, Tabish TA, Zahoor AF, Khalid SH, Khan IU, Hosny KM, Rizg WY, Hanif S, et al. Evaluating novel agarose-based buccal gels scaffold: mucoadhesive and pharmacokinetic profiling in healthy volunteers. Pharmaceutics. 2022;14(8):1592.
160. Hussain Z. Nanotechnology guided newer intervention for treatment of osteoporosis: efficient bone regeneration by up-regulation of proliferation, differentiation and mineralization of osteoblasts. Int J Polym Mater Polym Biomater. 2021;70(1):1–13.
161. Vakilinezhad M, Alipour S, Montaseri H. Fabrication and in vitro evaluation of magnetic PLGA nanoparticles as a potential Methotrexate delivery system for breast cancer. J Drug Deliv Sci Technol. 2018;44:467–74.
162. Alipour S, Shirazi H, Kazemi M, Dehshahri A, Ahmadi F. Synthesis and cytotoxicity evaluation of doxorubicin-polyethyleneimine conjugate as a potential carrier for dual delivery of drug and gene. J Drug Deliv Sci Technol. 2021;68:102994.
163. Pawar H, Wankhade SR, Yadav DK, Suresh S. Development and evaluation of co-formulated docetaxel and curcumin biodegradable nanoparticles for parenteral administration. Pharm Dev Technol. 2016;21(6):725–36.
164. Sampath M, Pichaimani A, Kumpati P, Sengottuvelan B. The remarkable role of emulsifier and chitosan, dextran and PEG as capping agents in the enhanced delivery of curcumin by nanoparticles in breast cancer cells. Int J Biol Macromol. 2020;162:748–61.
165. Tang Y, Wang X, Li J, Nie Y, Liao G, Yu Y, Li C. Overcoming the reticuloendothelial system barrier to drug delivery with a "don't-eat-us" strategy. ACS Nano. 2019;13(11):13015–26.
166. Roschenko V, Ayoub AM, Engelhardt K, Schäfer J, Amin MU, Preis E, Mandic R, Bakowsky U. Lipid-coated polymeric nanoparticles for the photodynamic therapy of head and neck squamous cell carcinomas. Pharmaceutics. 2023;15(10):2412.
167. Zheng Y, Yu B, Weecharangsan W, Piao L, Darby M, Mao Y, Koynova R, Yang X, Li H, Xu S, et al. Transferrin-conjugated lipid-coated PLGA nanoparticles for targeted delivery of aromatase inhibitor 7alpha-APTADD to breast cancer cells. Int J Pharm. 2010;390(2):234–41.
168. Hu H, Liao Z, Xu M, Wan S, Wu Y, Zou W, Wu J, Fan Q. Fabrication, optimization, and evaluation of paclitaxel and curcumin coloaded PLGA nanoparticles for improved antitumor activity. ACS Omega. 2022;8(1):976–86.
169. Ranjan AP, Mukerjee A, Vishwanatha JK, Helson L. Curcumin-er, a liposomal-PLGA sustained release nanocurcumin for minimizing QT prolongation for cancer therapy. In: Google Patents; 2015.
170. Ranjan AP, Mukerjee A, Vishwanatha JK. Solid in oil/water emulsion-diffusion-evaporation formulation for preparing curcumin-loaded PLGA nanoparticles. In: Google Patents; 2010.
171. Majumder N, Das NG, Das SK. Polymeric micelles for anticancer drug delivery. Ther Deliv. 2020;11(10):613–35.
172. Cagel M, Tesan FC, Bernabeu E, Salgueiro MJ, Zubillaga MB, Moretton MA, Chiappetta DA. Polymeric mixed micelles as nanomedicines: achievements and perspectives. Eur J Pharm Biopharm. 2017;113:211–28.
173. Zhang Y, Huang Y, Li S. Polymeric micelles: nanocarriers for cancer-targeted drug delivery. AAPS PharmSciTech. 2014;15(4):862–71.
174. Ma W, Guo Q, Li Y, Wang X, Wang J, Tu P. Co-assembly of doxorubicin and curcumin targeted micelles for synergistic delivery and improv- ing anti-tumor efficacy. Eur J Pharm Biopharm. 2017;112:209–23.
175. Xie J, Fan Z, Li Y, Zhang Y, Yu F, Su G, Xie L, Hou Z. Design of pH-sensitive methotrexate prodrug-targeted curcumin nanoparticles for efficient dual-drug delivery and combination cancer therapy. Int J Nanomed. 2018;13:1381–98.
176. Hafez Ghoran S, Calcaterra A, Abbasi M, Taktaz F, Nieselt K, Babaei E. Curcumin-based nanoformulations: a promising adjuvant towards cancer treatment. Molecules. 2022;27(16):5236.
177. Barani M, Mirzaei M, Torkzadeh-Mahani M, Adeli-Sardou M. Evaluation of carum-loaded niosomes on breast cancer cells: physicochemical properties, in vitro cytotoxicity, flow cytometric, DNA fragmentation and cell migration assay. Sci Rep. 2019;9(1):7139.
178. Obeid MA, Gany SAS, Gray AI, Young L, Igoli JO, Ferro VA. Niosome-encapsulated balanocarpol: compound isolation, characterisation, and cytotoxicity evaluation against human breast and ovarian cancer cell lines. Nanotechnology. 2020;31(19):195101.
179. Jamaludin R, Daud NM, Sulong RSR, Yaakob H, Aziz AA, Khamis S, Salleh LM. Andrographis paniculata-loaded niosome for wound healing application: characterisation and in vivo analyses. J Drug Deliv Sci Technol. 2021;63:102427.
180. Naderinezhad S, Amoabediny G, Haghiralsadat F. Co-delivery of hydrophilic and hydrophobic anticancer drugs using biocompatible pH-sensitive lipid-based nano-carriers for multidrug-resistant cancers. RSC Adv. 2017;7(48):30008–19.
181. Alemi A, Zavar Reza J, Haghiralsadat F, Zarei Jaliani H, Haghi Karamallah M, Hosseini SA, Haghi Karamallah S. Paclitaxel and curcumin coadministration in novel cationic PEGylated niosomal formulations exhibit enhanced synergistic antitumor efficacy. J Nanobiotechnol. 2018;16(1):28.
182. Akbarzadeh I, Shayan M, Bourbour M, Moghtaderi M, Noorbazargan H, Eshrati Yeganeh F, Saffar S, Tahriri M. Preparation, optimization and in-vitro evaluation of curcumin-loaded niosome@calcium alginate nanocarrier as a new approach for breast cancer treatment. Biology (Basel). 2021;10(3):173.
183. Pérez-Ferreiro M, Abelairas MA, Criado A, Gómez IJ, Mosquera J. Dendrimers: exploring their wide structural variety and applications. Polymers. 2023;15(22):4369.
184. Mittal P, Saharan A, Verma R, Altalbawy F, Alfaidi MA, Batiha GE-S, Akter W, Gautam RK, Uddin MS, Rahman MS. Dendrimers: a new race of pharmaceutical nanocarriers. BioMed Res Int. 2021;2021:8844030.
185. Alven S, Aderibigbe BA. The therapeutic efficacy of dendrimer and micelle formulations for breast cancer treatment. Pharmaceutics. 2020;12(12):1212.
186. Shi W, Dolai S, Rizk S, Hussain A, Tariq H, Averick S, L'Amoreaux W, El Idrissi A, Banerjee P, Raja K. Synthesis of monofunctional cur- cumin derivatives, clicked curcumin dimer, and a PAMAM dendrimer curcumin conjugate for therapeutic applications. Org Lett. 2007;9(26):5461–4.
187. Luiz MT, Dutra JAP, de Cássia RT, Carvalho GC, Sábio RM, Marchetti JM, Chorilli M. Folic acid-modified curcumin-loaded liposomes for breast cancer therapy. Colloids Surf A. 2022;645:128935.
188. Wang W, Chen T, Xu H, Ren B, Cheng X, Qi R, Liu H, Wang Y, Yan L, Chen S. Curcumin-loaded solid lipid nanoparticles enhanced anticancer efficiency in breast cancer. Molecules. 2018;23(7):1578.

189. Pawar H, Surapaneni SK, Tikoo K, Singh C, Burman R, Gill MS, Suresh S. Folic acid functionalized long-circulating co-encapsulated docetaxel and curcumin solid lipid nanoparticles: in vitro evaluation, pharmacokinetic and biodistribution in rats. Drug Deliv. 2016;23(4):1453–68.
190. Jithan A, Madhavi K, Madhavi M, Prabhakar K. Preparation and characterization of albumin nanoparticles encapsulating curcumin intended for the treatment of breast cancer. Int J Pharm Investig. 2011;1(2):119.
191. Xie J, Fan Z, Li Y, Zhang Y, Yu F, Su G, Xie L, Hou Z. Design of pH-sensitive methotrexate prodrug-targeted curcumin nanoparticles for efficient dual-drug delivery and combination cancer therapy. Int J Nanomed. 2018;13:1381–98.
192. Alemi A, Zavar Reza J, Haghiralsadat F, Zarei Jaliani H, Haghi Karamallah M, Hosseini SA, Haghi Karamallah S. Paclitaxel and curcumin coadministration in novel cationic PEGylated niosomal formulations exhibit enhanced synergistic antitumor efficacy. J Nanobiotechnol. 2018;16:1–20.
193. Akbarzadeh I, Shayan M, Bourbour M, Moghtaderi M, Noorbazargan H, Eshrati Yeganeh F, Saffar S, Tahriri M. Preparation, optimization and in-vitro evaluation of curcumin-loaded niosome@ calcium alginate nanocarrier as a new approach for breast cancer treatment. Biology. 2021;10(3):173.
194. Shi W, Dolai S, Rizk S, Hussain A, Tariq H, Averick S, L'Amoreaux W, El Idrissi A, Banerjee P, Raja K. Synthesis of monofunctional cur- cumin derivatives, clicked curcumin dimer, and a PAMAM dendrimer curcumin conjugate for therapeutic applications. Org Lett. 2007;9(26):5461–4.
195. Mbese Z, Aderibigbe BA. Bisphosphonate-based conjugates and derivatives as potential therapeutic agents in osteoporosis, bone cancer and metastatic bone cancer. Int J Mol Sci. 2021;22(13):6869.
196. Farrell KB, Karpeisky A, Thamm DH, Zinnen S. Bisphosphonate conjugation for bone specific drug targeting. Bone Rep. 2018;9:47–60.
197. Bai S-B, Liu D-Z, Cheng Y, Cui H, Liu M, Cui M-X, Mei Q-B, Zhou S-Y. Osteoclasts and tumor cells dual targeting nanoparticle to treat bone metastases of lung cancer. Nanomed Nanotechnol Biol Med. 2019;21:102054.
198. Celin MR, Simon JC, Krzak JJ, Fial AV, Kruger KM, Smith PA, Harris GF. Do bisphosphonates alleviate pain in children? A systematic review. Curr Osteoporos Rep. 2020;18:486–504.
199. Santini D, Stumbo L, Spoto C, D'Onofrio L, Pantano F, Iuliani M, Fioramonti M, Zoccoli A, Ribelli G, Virzì V. Bisphosphonates as anticancer agents in early breast cancer: preclinical and clinical evidence. Breast Cancer Res. 2015;17:1–7.
200. Wilkins Parker LR, Preuss CV. Alendronate. In: StatPearls. Treasure Island: StatPearls Publishing Copyright © 2023, StatPearls Publishing LLC.; 2023.
201. León Vázquez F, Herrero Hernández S, Cuerpo Triguero C, Andrés Prado MJ, Cabello Ballesteros L. Prescription of alendronate and rise- dronate in men: off-label use in a health area. Reumatol Clin. 2015;11(2):64–7.
202. Vrahnas C, Buenzli PR, Pearson TA, Pennypacker BL, Tobin MJ, Bambery KR, Duong LT, Sims NA. Differing effects of parathyroid hormone, alendronate, and odanacatib on bone formation and on the mineralization process in intracortical and endocortical bone of ovariecto- mized rabbits. Calcif Tissue Int. 2018;103(6):625–37.
203. Rouach V, Goldshtein I, Wolf I, Catane R, Chodick G, Iton A, Stern N, Cohen D. Exposure to alendronate is associated with a lower risk of bone metastases in osteoporotic women with early breast cancer. J Bone Oncol. 2018;12:91–5.
204. Rudnick-Glick S, Corem-Salkmon E, Grinberg I, Margel S. Targeted drug delivery of near IR fluorescent doxorubicin-conjugated poly (ethylene glycol) bisphosphonate nanoparticles for diagnosis and therapy of primary and metastatic bone cancer in a mouse model. J Nanobiotechnol. 2016;14(1):1–11.
205. Bai S-B, Cheng Y, Liu D-Z, Ji Q-F, Liu M, Zhang B-L, Mei Q-B, Zhou S-Y. Bone-targeted PAMAM nanoparticle to treat bone metastases of lung cancer. Nanomedicine. 2020;15(9):833–49.
206. He Y, Huang Y, Huang Z, Jiang Y, Sun X, Shen Y, Chu W, Zhao C. Bisphosphonate-functionalized coordination polymer nanoparticles for the treatment of bone metastatic breast cancer. J Control Release. 2017;264:76–88.
207. Chen S-H, Liu T-I, Chuang C-L, Chen H-H, Chiang W-H, Chiu H-C. Alendronate/folic acid-decorated polymeric nanoparticles for hierarchi- cally targetable chemotherapy against bone metastatic breast cancer. J Mater Chem B. 2020;8(17):3789–800.
208. Kang N-W, Lee J-Y, Kim D-D. Hydroxyapatite-binding albumin nanoclusters for enhancing bone tumor chemotherapy. J Control Release. 2022;342:111–21.
209. Dong X, Zou S, Guo C, Wang K, Zhao F, Fan H, Yin J, Chen D. Multifunctional redox-responsive and CD44 receptor targeting polymer-drug nanomedicine based curcumin and alendronate: synthesis, characterization and in vitro evaluation. Artif Cells Nanomed Biotechnol. 2018;46(sup1):168–77.
210. Shi C, Wu T, He Y, Zhang Y, Fu D. Recent advances in bone-targeted therapy. Pharmacol Ther. 2020;207:107473.
211. Şen Ö, Emanet M, Ciofani G. Nanotechnology-based strategies to evaluate and counteract cancer metastasis and neoangiogenesis. Adv Healthc Mater. 2021;10(10):2002163.
212. Xing L, Ebetino FH, Boeckman RK Jr, Srinivasan V, Tao J, Sawyer TK, Li J, Yao Z, Boyce BF. Targeting anti-cancer agents to bone using bisphosphonates. Bone. 2020;138:115492.
213. Cavalluzzi MM, Viale M, Rotondo NP, Ferraro V, Lentini G. Drug repositioning for ovarian cancer treatment: an update. Anti-cancer Agents Med Chem Former Curr Med Chem Anti-cancer Agents. 2024;24(8):637–47.
214. Islam MR, Patel J, Back PI, Shmeeda H, Kallem RR, Shudde C, Markiewski M, Putnam WC, Gabizon AA, La-Beck NM. Pegylated lipo- somal alendronate biodistribution, immune modulation, and tumor growth inhibition in a murine melanoma model. Biomolecules. 2023;13(9):1309.
215. Zhan X, Jia L, Niu Y, Qi H, Chen X, Zhang Q, Zhang J, Wang Y, Dong L, Wang C. Targeted depletion of tumour-associated macrophages by an alendronate–glucomannan conjugate for cancer immunotherapy. Biomaterials. 2014;35(38):10046–57.
216. Cremers S, Drake MT, Ebetino FH, Bilezikian JP, Russell RGG. Pharmacology of bisphosphonates. Br J Clin Pharmacol. 2019;85(6):1052–62.
217. Han S-Y, Kim J-h, Jo EH, Kim Y-K: Eleutherococcus sessiliflorus inhibits receptor activator of nuclear factor Kappa-B ligand (RANKL)-induced osteoclast differentiation and prevents ovariectomy (OVX)-induced bone loss; 2021.
218. Park J, Pandya VR, Ezekiel SJ, Berghuis AM. Phosphonate and bisphosphonate inhibitors of farnesyl pyrophosphate synthases: a structure- guided perspective. Front Chem. 2020;8:612728.
219. Sharma R, Wu X, Rhodes SD, Chen S, He Y, Yuan J, Li J, Yang X, Li X, Jiang L, et al. Hyperactive Ras/MAPK signaling is critical for tibial nonunion fracture in neurofibromin-deficient mice. Hum Mol Genet. 2013;22(23):4818–28.

220. Koyama C, Hirota M, Okamoto Y, Iwai T, Ogawa T, Hayakawa T, Mitsudo K. A nitrogen-containing bisphosphonate inhibits osteoblast attachment and impairs bone healing in bone-compatible scaffold. J Mech Behav Biomed Mater. 2020;104:103635.
221. Krüger TB, Syversen U, Herlofson BB, Lian AM, Reseland JE. Targeting a therapeutically relevant concentration of alendronate for in vitro studies on osteoblasts. Acta Odontol Scand. 2022;80(8):619–25.
222. Hedvičáková V, Žižková R, Buzgo M, Rampichová M, Filová E. The effect of alendronate on osteoclastogenesis in different combinations of M-CSF and RANKL growth factors. Biomolecules. 2021;11(3):438.
223. Bautista-Carbajal A, Villanueva-Arriaga RE, Páez-Arenas A, Massó-Rojas F, Frechero Molina N, García-López S. Nitrogen-containing bisphosphonates downregulate cathepsin K and upregulate annexin V in osteoclasts cultured in vitro. Int J Dent. 2023;2023:2960941.
224. Mijanović O, Jakovleva A, Branković A, Zdravkova K, Pualic M, Belozerskaya TA, Nikitkina AI, Parodi A, Zamyatnin AA Jr. Cathepsin K in pathological conditions and new therapeutic and diagnostic perspectives. Int J Mol Sci. 2022;23(22):13762.
225. Han SY, Kim YK. Yukmijihwang-Tang suppresses receptor activator of nuclear factor kappa-B ligand (RANKL)-induced osteoclast differ- entiation and prevents ovariectomy (OVX)-mediated bone loss. Molecules. 2021;26(24):7579.
226. Rong-hua Z. Effects of exercise combined with alendronate sodium tablets on RANKL/OPG balance and MAPK signaling pathways in ovariectomized rats. Acad J Second Mil Med Univ 2013.
227. Trouvin AP, Goëb V. Receptor activator of nuclear factor-κB ligand and osteoprotegerin: maintaining the balance to prevent bone loss. Clin Interv Aging. 2010;5:345–54.
228. Huang M, Zhai B-T, Fan Y, Sun J, Shi Y-J, Zhang X-F, Zou J-B, Wang J-W, Guo D-Y. Targeted drug delivery systems for curcumin in breast cancer therapy. Int J Nanomed. 2023;18:4275–311.
229. Wang K, Guo C, Dong X, Yu Y, Wang B, Liu W, Chen D. In vivo evaluation of reduction-responsive alendronate-hyaluronan-curcumin polymer-drug conjugates for targeted therapy of bone metastatic breast cancer. Mol Pharm. 2018;15(7):2764–9.
230. Xi Y, Jiang T, Yu Y, Yu J, Xue M, Xu N, Wen J, Wang W, He H, Shen Y. Dual targeting curcumin loaded alendronate-hyaluronan-octadecanoic acid micelles for improving osteosarcoma therapy. Int J Nanomed. 2019;14:6425–37.
231. Kuru MM, Dalgakiran EA, Kacar G. Investigation of morphology, micelle properties, drug encapsulation and release behavior of self-assembled PEG-PLA-PEG block copolymers: a coarse-grained molecular simulations study. Colloids Surf A. 2021;629:127445.
232. Jarak I, Pereira-Silva M, Santos AC, Veiga F, Cabral H, Figueiras A. Multifunctional polymeric micelle-based nucleic acid delivery: current advances and future perspectives. Appl Mater Today. 2021;25:101217.
233. Peng S, Xiao F, Chen M, Gao H. Tumor-microenvironment-responsive nanomedicine for enhanced cancer immunotherapy. Adv Sci. 2022;9(1):2103836.
234. Khanizadeh F, Rahmani A, Asadollahi K, Ahmadi MRH. Combination therapy of curcumin and alendronate modulates bone turnover markers and enhances bone mineral density in postmenopausal women with osteoporosis. Arch Endocrinol Metab. 2018;62(4):438–45.
235. Cho D-C, Kim K-T, Jeon Y, Sung J-K. A synergistic bone sparing effect of curcumin and alendronate in ovariectomized rat. Acta Neurochir. 2012;154:2215–23.